# LATE QUATERNARY SEDIMENTARY AND PALEOCLIMATIC EVOLUTIONOF KORDOFAN, SUDAN

Ahmed Dawelbeit Mohammedahmed Eltahir

Communauté
UNIVERSITÉ Grenoble Alpes

# THÈSE

Pour obtenir le grade de

**DOCTEUR DE LA COMMUNAUTE UNIVERSITE GRENOBLE ALPES**

Spécialité : **Terre Solide**

Arrêté ministériel : 25 mai 2016

Présentée par


## Ahmed DAWELBEIT


Thèse dirigée par **Etienne JAILLARD**, DR IRD, ISTerre,
et codirigée par **Ali EISAWI**, Prof., Université d'Al Neelain, Soudan

préparée au sein du **Laboratoire Institut des Sciences de la Terre**
è **l'École Doctorale Terre, Univers, Environnement**

# EVOLUTION SEDIMENTAIRE ET CLIMATIQUE DU KORDOFAN (SOUDAN) AU QUATERNAIRE SUPERIEUR

Thèse soutenue publiquement le **5 octobre 2018**,
devant le jury composé de :

**Dr. Marie REVEL**
Maître de conférences, Sophia-Antipolis, Rapporteur
**Dr. Florence SYLVESTRE**
Directeur de Recherche IRD, CEREGE, Rapporteur
**Dr. Fabienne GIRAUD**
Maître de conférences, Grenoble Alpes, Examinateur
**Dr. David WILLIAMSON**
Directeur de Recherche IRD, Examinateur
**Pr. Christophe BASILE**
Professeur, Grenoble Alpes, Président du jury
**Dr. Etienne JAILLARD**
Directeur de Recherche IRD, ISTerre, directeur de thèse
**Pr. Ali EISAWI**
Professeur, Al Neelain Khartoum, co-directeur, invité

Communauté
UNIVERSITÉ Grenoble Alpes

# LATE QUATERNARY SEDIMENTARY AND PALEOCLIMATIC EVOLUTION OF KORDOFAN, SUDAN

**Dissertation for the doctorate degree of the Université Grenoble Alpes, France**

**prepared at the Institut des Sciences de la Terre (ISTerre)**

**Submitted by Ahmed DAWELBEIT**
**on October the 5th, 2018**

**Defense committee**

**Dr. Marie REVEL**
Lecturer, University Sophia-Antipolis, Rapporteur
**Dr. Florence SYLVESTRE**
Director of Research IRD, CEREGE, Rapporteur
**Dr. Fabienne GIRAUD**
Lecturer, University Grenoble Alpes, Examiner
**Dr. David WILLIAMSON**
Director of Research IRD, LOCEAN, Examiner
**Pr. Christophe BASILE**
Professor, University Grenoble Alpes, Head of the jury
**Dr. Etienne JAILLARD**
Director of Research IRD, ISTerre, Grenoble, supervisor
**Pr. Ali EISAWI**
Professor, Al Neelain, Khartoum, co-supervisor, invited

**Grenoble, 2018**

***DEDICATION***

*to*

*My wife Makka , my daughters Mawahib and Masajid , and to my little baby Moyeiad*

# *ACKNOWLEDGEMENTS*

I would like to take this space to express my thanks to all of the people who contributed to the successful completion of my PhD.

First of all, I would like to thank my supervisor Prof. Etienne Jaillard for initiating this fantastic research project within the ISTerre and École doctorale : Terre, Univers, Environnement (TUE), of the Université Grenoble Alpes. His broad knowledge and special way to look at data from an interdisciplinary point of view was most inspiring. I really appreciate his efficient work during all stages of this project, significantly improving whatever I wrote and always within an incredible short time. This efficiency was extremely helpful during the last months while my thesis was developing.

I would like to express my thanks to my co-supervisor Prof. Ali Eisawi from Al-Neelain University, Sudan, for his worthy support and guidance when writing the proposal of this project and encouraging to go forward in this field of research. His broad knowledge in palynology was very helpful for me to understand the basic principles of this field.

I owe a lot of thanks to the members of my thesis committee : Prof. Christophe Basile and Dr. Julien Carcaillet for their annual evaluation and valuable advices and suggestions.

Great thanks to those who provided limitless help in the practical work : Dr. Dirk Vandamme (Ghent University, Belgium) for identification of the gastropod shells, Mr. Shaaedeen Ahmed (PLRS, Khartoum, Sudan) for help in the palynomorphs identification, Dr. Howeida M. Adam (Khartoum University, Sudan) for her help in the identification of the archeological remnants, Dr. Nathaniel Findling and Dr. Bruno Lanson (ISTerre) for their help in the explanation of the basic principles of XRD for clay mineralogy (theoretically and practically), Valérie Magnin and Martine Lanson (ISTerre) for help in the practically in XRF explanation, Dr. Catherine Chauvel (ISTerre) for her help in the preparation of samples for isotope analysis, to Dr. Christophe Griggo (EDyTeM, Chambéry) for the determination of numerous vertebrate bones of the Sodari and El Ga'ah paleolakes, and to Mr. Badr-Eddeen En Nour (Univ. Kordofan) for help in granulometric analysis test.

Really, I appreciated and thanks very much the institutions and people who welcomed us generously during our field works, to stay at their house guest or personal homes. Appreciation and thanks to : house guest of the University of Kordofan (El Obeid), house guest of the University of Dilling (Dilling), house guest of the University of west Kordofan (Abu Zabad and En Nahud), my brother Eltahir (El Fula), my father "Dawelbeit" (El Khowei), Mr. Adam Husain "leader of El Ga'ah area" (El Ga'ah village), and house guest of the Sodari locality (Sodari).

I would like to express my special thanks to our excellent and patient driver Mr. Elghali Khaleel Ahmed Gorami, who joined us during our two seasons of field work.

Unlimited thanks to my colleagues Dr. Hassan Abdelsalam and Ms. Einas Mohammed Salama for joining us during our second season of field work and many thanks to my colleague Badr-Eddeen En Nour, who joined me in my final field trip to north Bara.

Thanks should be extended to all colleagues and staff in ISTerre, Université Grenoble Alpes, France, especially Hugo Sanchez, Eleanor Bakker, Melanie Balvay and Hafid Bouchafa.

Without financial support everything is difficult to achieve. Thanks are due to the bilateral – Sudanese-French – agreements represented by the Sudanese Ministry of Higher Education and Scientific Research and the French Embassy in Khartoum, which gave the opportunity of a doctoral grant, and to the French Ministry of foreign affairs (PHC "Napata" project) for providing support for fruitful travels between our countries. Thanks also to the ISTerre laboratory and the Institut de Recherche pour le Développement (IRD) for offering the financial costs of the analysis.

Finally and most importantly, thanks to all my family for their unconditional support and encouragement throughout all ! And kept praying for me to success in this research project, and very special thanks to my brother Eltyeib for his unlimited different kinds of support.

# *ABSTRACT*

This study is conducted in the Kordofan region, central-southern Sudan. The study area is bounded by longitudes 28° 00' and 31° 00' E, and latitudes 11° 30' and 15°00' N and covers an area of about 125835 $km^2$. The Kordofan region is located at the southern end of the present-day Sahara. Late Pleistocene-Holocene deposits in Kordofan, recorded sedimentary discontinuities that probably reflect climatic fluctuations during the latest Quaternary. $^{14}C$ dating and some archeological findings have been used to date the latest Pleistocene-Holocene succession. In the investigated sections, four stratigraphic units have been recognized, which exhibit eight sedimentological facies.

The first unit is older that ≈ 10 ky BP and is formed of mottled sandstone or siltstone facies of aeolian origin. The second unit (≈ 10 to 6 ky BP) comprises palustrine and lacustrine facies in the central and northern parts, and fluviatile facies in the South. The third unit ranges from ≈ 6 to 3 ky BP and is restricted to the southern part; it is made of aeolian deposits intercalated with fluviatile or flood plain facies. The fourth unit is younger than 1000 y BP, and is dominated by aeolian red sandstone in the North, and by flood plain facies to the South. Between ≈ 6 and 1 ky BP in the North and between ≈ 3 and 1 ky BP in the South, no deposits are recorded. This hiatus is marked by deflation surfaces in the North, and is interpreted as a period of strong aeolian activity, which prevented deposition, or even eroded part of the sediments deposited between 6 and 3 ky BP.

Several proxies (sedimentology, gastropod sub-fossil shells, pollens, stable isotopes, major element chemistry, clay mineralogy and paleohydrology) have been used to reconstruct the climatic evolution of the region for the past 13 ky, which can be correlated to the well-known evolution of Eastern Sahara during this time-span. Our results indicate that the region has been subjected to arid climate prior to 10 ky BP as evidenced by thick aeolian deposits. Between 10 and 6 ky BP, the region experienced a wet climate as evidenced by the development of pedogenetic calcareous nodules, local deposition of palustrine and lacustrine limestone, abundance of aquatic and semi-aquatic gastropods, high lake levels, and depleted $\delta^{18}O$ values from gastropod shells and calcareous nodules. After ≈ 6 ky BP, climate evolved to dry conditions in the northern part of the region as indicated by an strong aeolian activity recorded by erosion features, sedimentary hiatus and deflation surfaces, while its southern part remained more humid, as shown by channel and flood plain deposits, and tropical and aquatic pollen taxa. From 1000 yr BP to Present, and probably after 3 ka BP, the region became arid as evidenced by aeolian deposits, the predominance of arid indicator pollens and the enrichment in $^{18}O$ of land snail shells.

# *RÉSUMÉ*

Cette étude concerne la région du Kordofan, dans le centre-Sud du Soudan. La région étudiée est comprise entre les méridiens 28°00' et 31°00' E, et les latitudes 11°30' et 15°00' N, et couvre une surface d'environ 125 835 $km^2$. Le Kordofan est situé en bordure Sud du Sahara actuel. Les dépôts du Pléistocène supérieur-Holocène du Kordofan, ont enregistré des discontinuités sédimentaires qui reflètent des fluctuations climatiques au cours du Quaternaire terminal. Des datations au $^{14}C$ et des collectes archéologiques ont permis de dater la série étudiée. Quatre unités stratigraphiques ont été identifiées, qui comprennent huit faciès sédimentaires.

La première unité est antérieure à ≈ 10 ka BP et est formée de sables ou silts marmorisés d'origine éolienne. La deuxième unité (≈ 10 à 6 ka BP) comprend des faciès palustres et lacustres au Nord et au centre, et des faciès fluviatiles au Sud. La troisième unité, d'âge ≈ 6 à 3 ka BP, n'est présente qu'au Sud; elle est faite de dépôts éoliens intercalés de faciès fluviatiles ou de plaine d'inondation. La quatrième unité est plus jeune que 1000 ans BP, et est dominée par des sables rouges éoliens au Nord, et par des dépôts de plaine d'inondation au Sud. Entre ≈ 6 et 1 ka BP au Nord et entre ≈ 3 et 1 ka BP au Sud, un hiatus est marqué par une surface de déflation au Nord, et est interprété comme une période de forte activité éolienne, qui a empêché le dépôt et a même érodé une partie des sédiments déposés entre 6 et 3 ka BP.

Plusieurs indicateurs (sédimentologie, gastéropodes, pollens, isotopes stables, géochimie des majeurs, minéralogie des argiles et paléo-hydrologie) ont servi à reconstituer l'évolution climatique de la région depuis 13000 ans, qui est cohérente avec l'évolution paléo-climatique de l'Afrique nord-orientale à la même époque. Nos résultats montrent que la région a connu un climat aride avant 10 ka BP, matérialisé par d'épais dépôts éoliens. Entre 10 et 6 ka BP, un climat humide est démontré par le développement de nodules calcaires pédogénétiques, le dépôt local de calcaires palustres et lacustres, l'abondance de gastéropodes aquatiques et semi-aquatiques, le haut niveau de lacs, et les valeurs très négatives du $\delta^{18}O$ des coquilles d'escargots et des nodules calcaires. Après ≈ 6 ka BP, le climat s'assèche dans le Nord de la région étudiée comme le suggèrent la forte activité éolienne enregistrée par un hiatus sédimentaire, des érosions et surfaces de déflation, alors que le Sud reste plus humide, comme le montrent des dépôts fluviatiles (chenaux et plaine d'inondation), et les pollens tropicaux et aquatiques. Après 1000 ans BP, et plus probablement après 3 ka BP, la région devient aride comme en témoignent les dépôts éoliens, la prédominance de pollens de milieu aride et l'enrichissement en $^{18}O$ des coquilles d'escargots terrestres.

# *TABLE OF CONTENTS*

# *LIST OF TABLES*

# *LIST OF FIGURES*

# *LIST OF PLATES*

# I. INTRODUCTION

## 1.1. Preface

The Quaternary period covers the last two and an half million years of the Earth history and is well known as the period of ice ages. The Quaternary is characterized by repeated cycles of cold – warm climatic oscillations as the Earth's climate was submitted to alternating glacial and interglacial modes. Associated with the climatic fluctuations and advancing and retreating continental ice sheets, there were dramatic responses of the biota, rivers, lakes, oceans and other natural systems. More than 30 glacial – interglacial cycles are recorded in deep-sea sediment records spanning the last 2.6 my. The Quaternary period is divided into two epochs, the Pleistocene (2600 ka BP) and the Holocene (11.7 ka BP to Present). The late Pleistocene-Holocene epoch is marked by rapid short climatic fluctuations. As a result, the complex Late Quaternary environment (500 ka – Present) recorded rapid sedimentation changes. Therefore, the Quaternary sediments are considered a very important archive to determine environmental and climatic information.

## 1.2. Location

The study area is situated in central-southern Sudan, in the Kordofan Region, East of the White Nile valley and SW of Khartoum. It is bounded by longitudes 28°00' and 31°00'E, and latitudes 11°30' and 15°00'N and covers an area of about 125,835 $km^2$ (Fig. 1.1).

## 1.3. Climate

According to the classification of climates by Rodis (1968), Kordofan contains three climatic belts, which correspond to three major north-south zones in the sub-Saharan region of Africa, where the amount of rainfall and the duration of the rainy season increase toward the equator. The northern part of the region is a low-latitude desert, which merges southward into a belt of tropical steppe. Still farther south is a belt of tropical savanna. Figure 1.2 shows the regional climatic zones around Sudan.

The present-day climate of Kordofan region is variable from North to South. It varies between sub-tropical in Southern Kordofan, and poor savanna to arid in Northern part.

The rainy season in Southern Kordofan is longer than in Northern Kordofan. In Southern Kordofan, it begins in April and continues up to October with varying annual rainfall from 800 mm in the South to 400 mm in the North, while in Northern Kordofan the rainy season usually starts at the end of June and continues till October (92% of the total year precipitation in June-September in El Obeid), with approximate annual rainfall of 320 mm per year in El Obeid. The average annual rainfall increases southward, from approximately 200 mm per year in the northern part and approximately 600 mm per year in the southern part of the study area (Fig. 1.3).

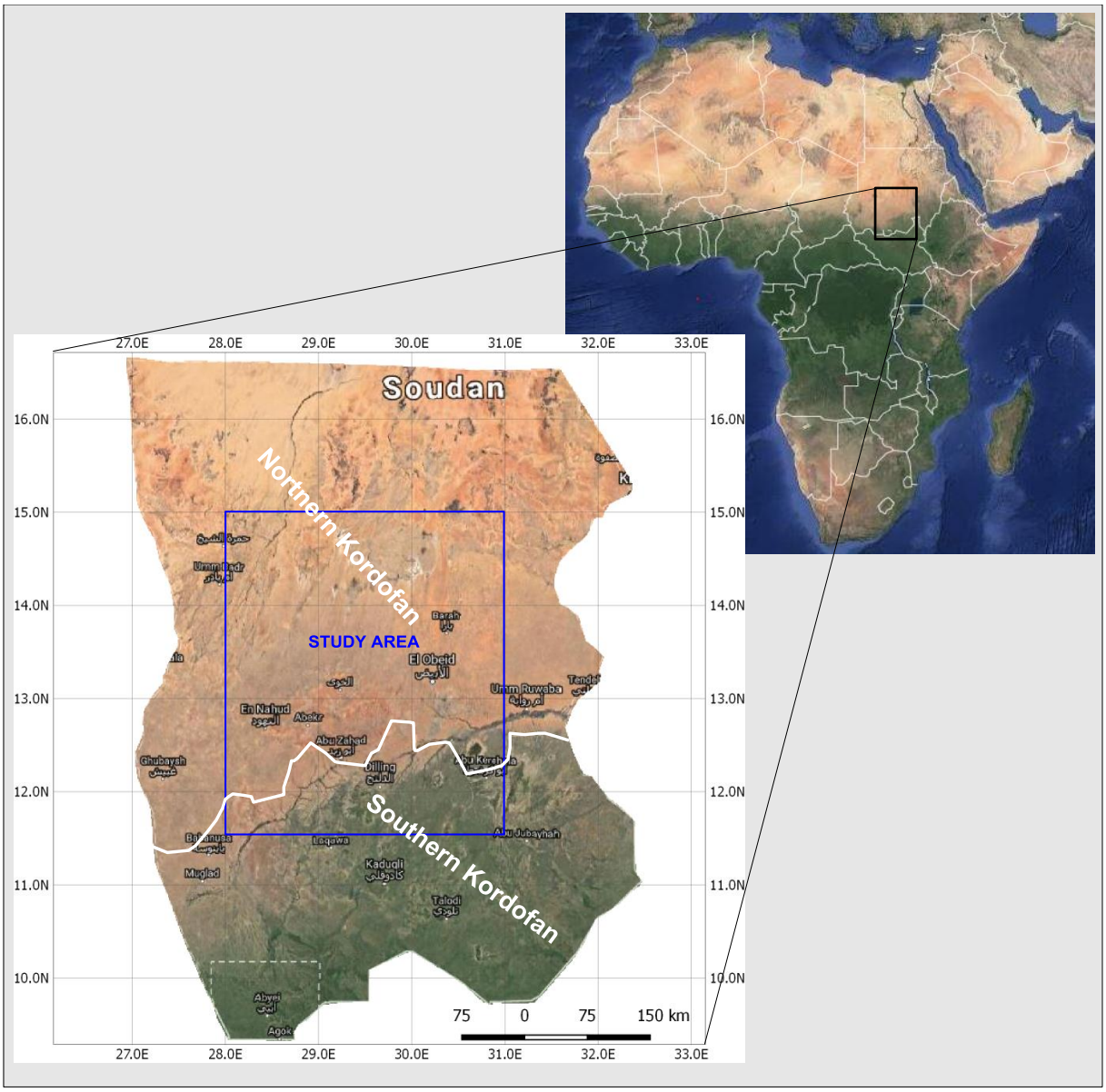


*Fig. 1.1: Location map of the study area.*

The difference between North and South is also reflected in the wind directions, with northerly and southerly winds dominating for six months each in Southern Kordofan, while the northerly winds dominate increasingly northward.

The mean annual air temperature of the province is 27°C (80°F), and temperature extremes of 10°C (50°F) and 46°C (115°F) are common to most areas. The monthly average temperature fluctuates between 40°C in summer and 22°C in winter. The mean relative humidity averages about 21% in the dry season, and 75% during the rainy season. The prevailing winds in the winter are from the north, but during the rainy season they are from the southwest. Wind velocities are usually less than 8 kilometers per hour (5 miles per hr) and frequent calms are not uncommon.

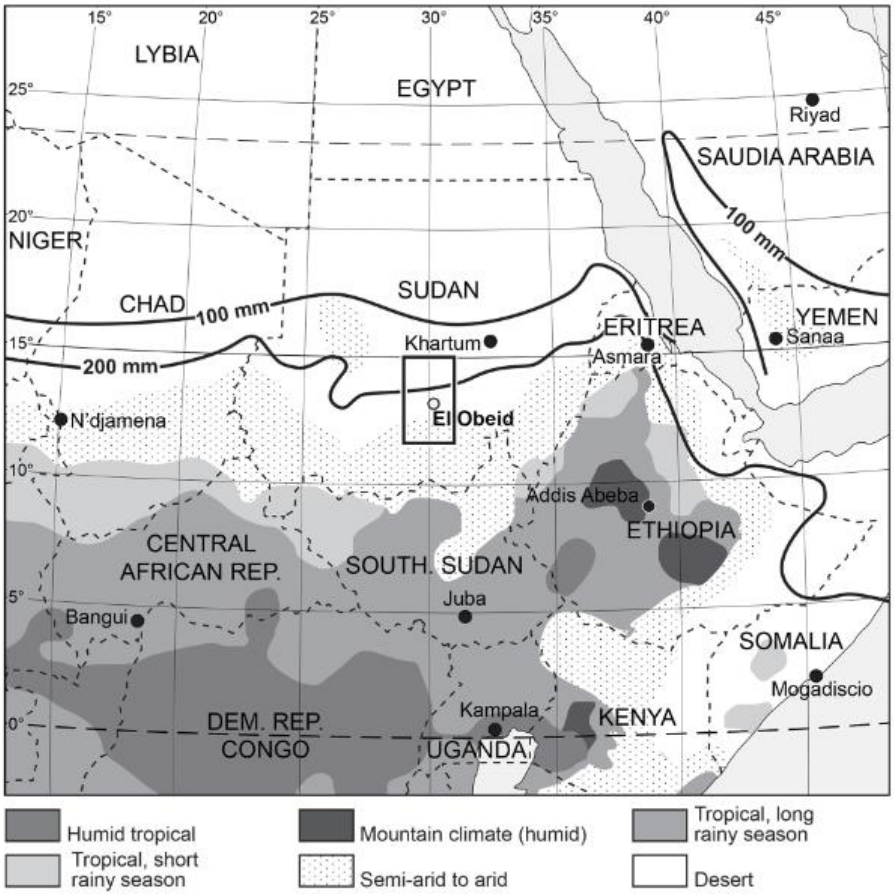


*Fig. 1.2: Regional climatic zones around Sudan, and location of the study area.*

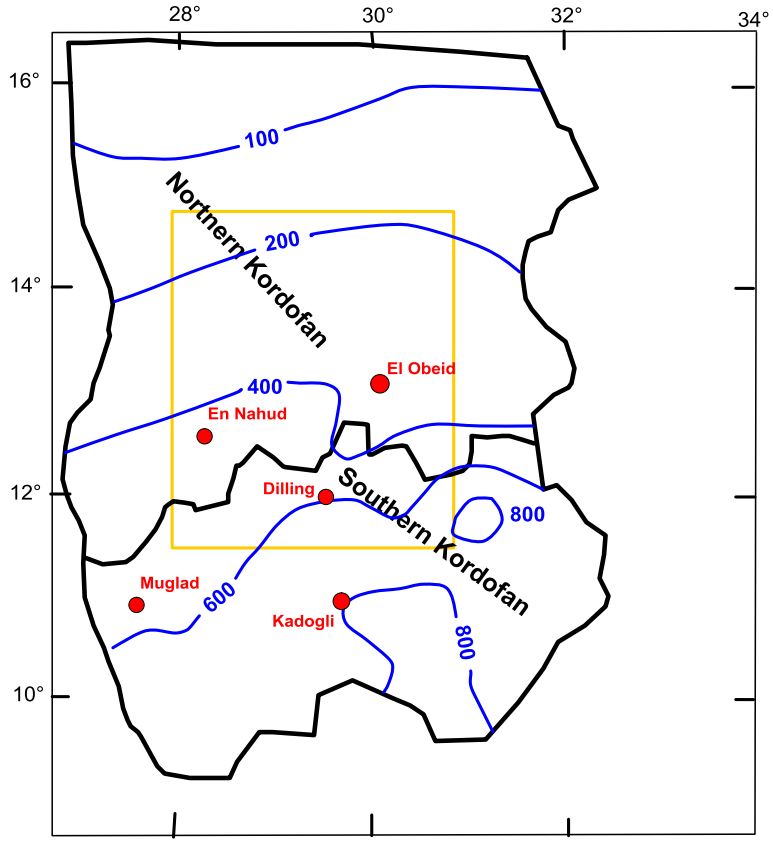


*Fig. 1.3: Mean annual rainfall across the Kordofan Region (Rodis et al., 1968).*

## 1.4. Physiography

The physiographic features are variable in the study area, regarding topography, relief, drainage, soils and vegetation. Figure 1.4 summarizes the geomorphologic features in the study area with some extension to the East to include the White Nile. The climate and geology are the most important factors controlling this physiographic variabilities.

### 1.4.1. Topography

Figure 1.5. is a general digital elevation model of the Kordofan region, while Fig.1.6 provides more details on the study area. The northern part of the study area is characterized by a low lying, gently undulating surface topography, with few scattered, little elevated but sharp inselbergs mostly made of Paleogene rocks. This terrain is covered by extensive qoz (stabilized sand dunes), sand sheets, and N-S orientated sand dunes and stabilized sand dunes. The sand dunes decrease in size and abundance toward the south (Fig. 1.4).

The southern part is characterized by scattered steep massifs and inselbergs made of basement rocks, some of which are as high as 1300 m above sea level (J. Ed Dair). The plains are formed of dark-grey soils locally intercalated with some sands and sand dunes further north.

### 1.4.2. Relief and drainage system

The study area presents variable relief shapes. The northern part is dominated by topographic depressions of interdunes located between up to 15 m high sand dunes. The size of these interdunes differs according to differences in the dune amplitudes. In the Sodari and El Ga'ah areas, the sand dunes are large and this results in large interdunes, whereas around Bara, as well as north and east of El Obeid, the sand dunes are thinner and result in narrower interdunes, compared to those of Sodari-El Ga'ah area (Fig. 1.7). These dune and iterdune fields are surrounded by sand sheets.

The central part of the study area is generally marked by its flatness. Reliefs are dominated by smooth V-shaped valleys in the El Khowei-En Nahud, while to the East as well as around Khour Abu Habil, the relief is marked by wide wadies. The southern part is marked by deep V-shaped valleys and by some saddles between the mountains.

These variations in the relief result from variation in the drainage system. The Kordofan region lies within the drainage basin of the White Nile River. The northern part of the study area shows a poor drainage system due to the development of the north-south sand dunes forming barriers or dams crosscutting the ancient rivers (Figs. 1.4 and 1.7). Therefore, seasonal rivers (wadies) are quite rare and may form seasonal lakes behind the sand dunes, or vanish rapidly due to the infiltration of the running water in the sand dunes.

The dominance of sand dunes and sheets in the central part of the study area (En Nahud-El Khowei), results in a coarse dendritic drainage system (Elmansour, 2017), with intensive infiltration. The surface water of this area is drained to the South through the El Fula area down to its delta around Muglad.

In the eastern part of the study area, surface water is drained through Khor Abu Habil to the White Nile. The southern part is marked by a well-marked drainage pattern due to more abundant rainfalls and to the clayey soils. Small wadies of this southern part form the tributaries of Khor Abu Habil, or flow southward toward the Sudd area.

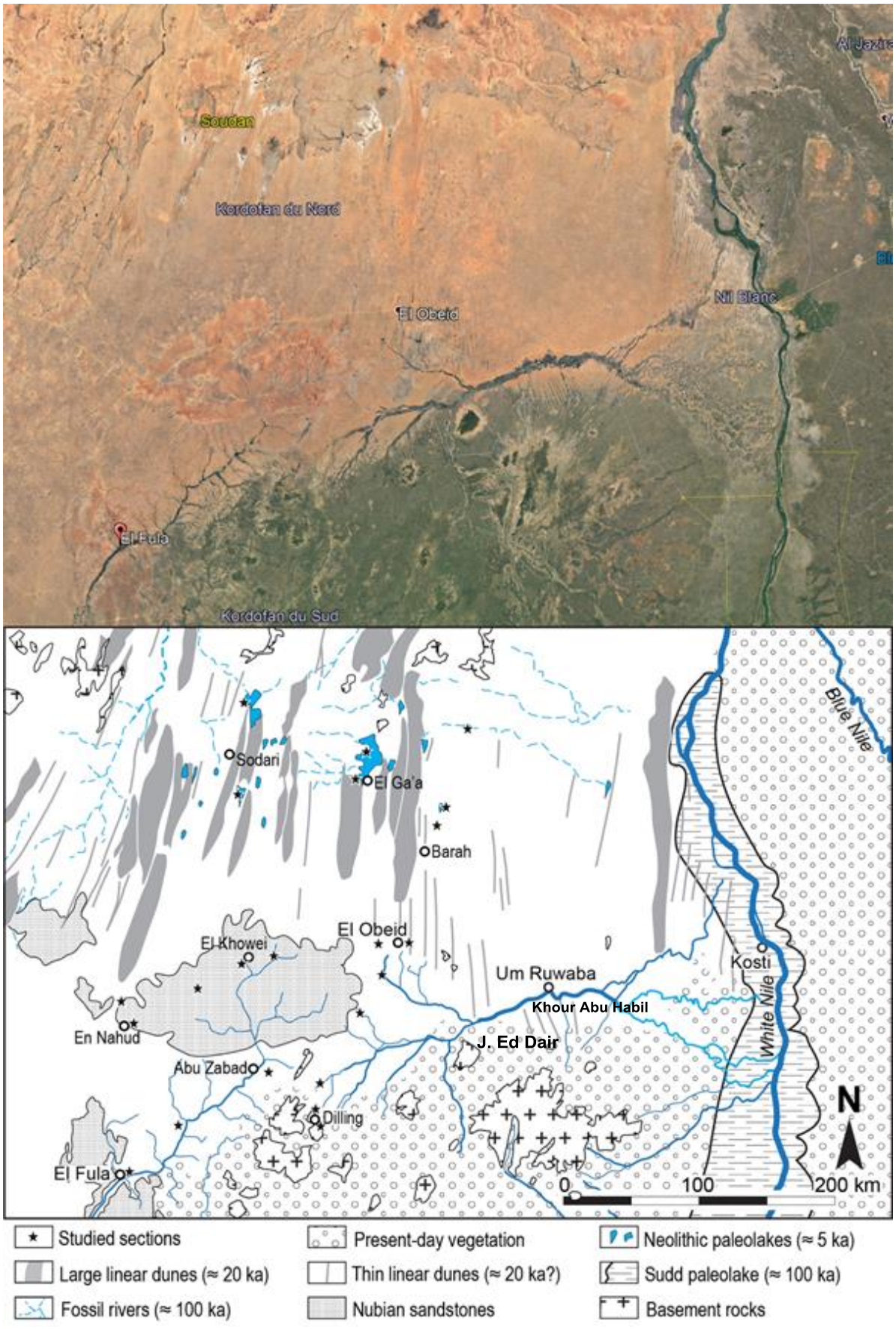


*Fig. 1.4: Geomorphological map of the study area.*

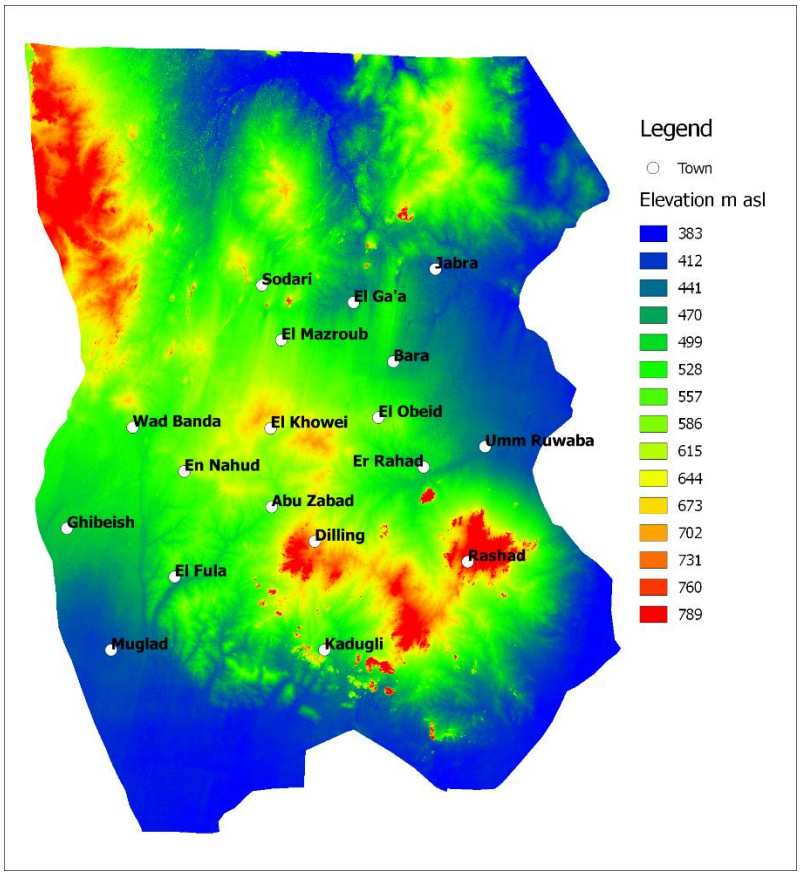


*Fig. 1.5. Digital elevation model of the Kordofan Region.*

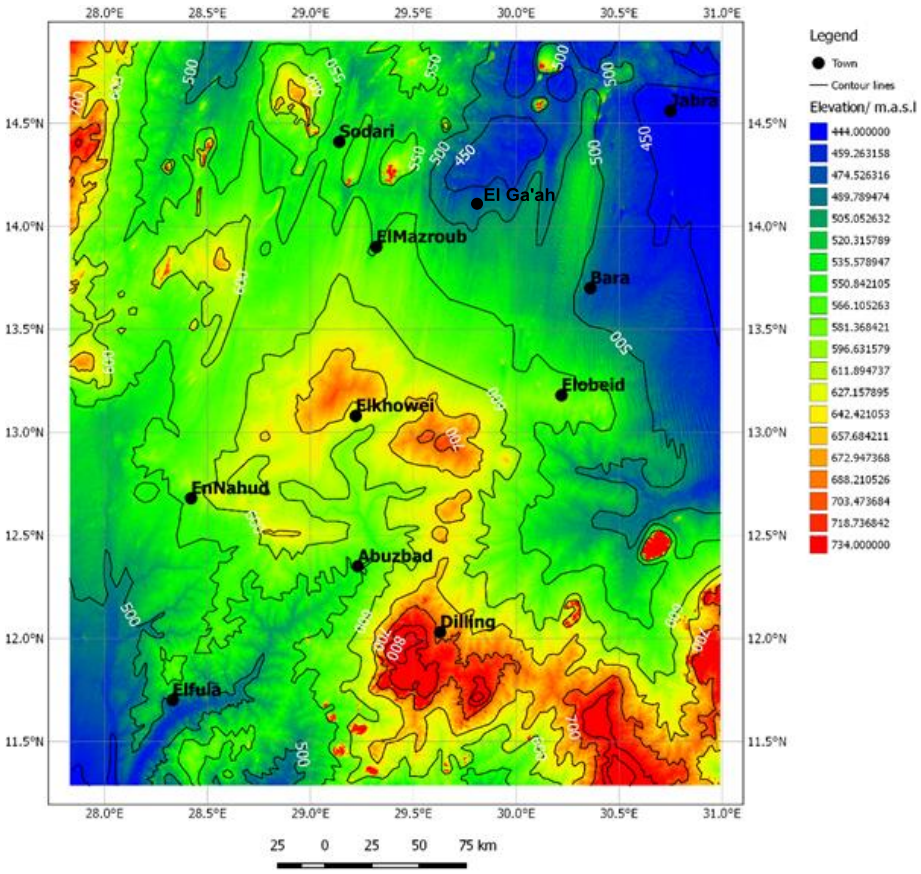


*Fig. 1.6. Detailed digital elevation model of the study area.*

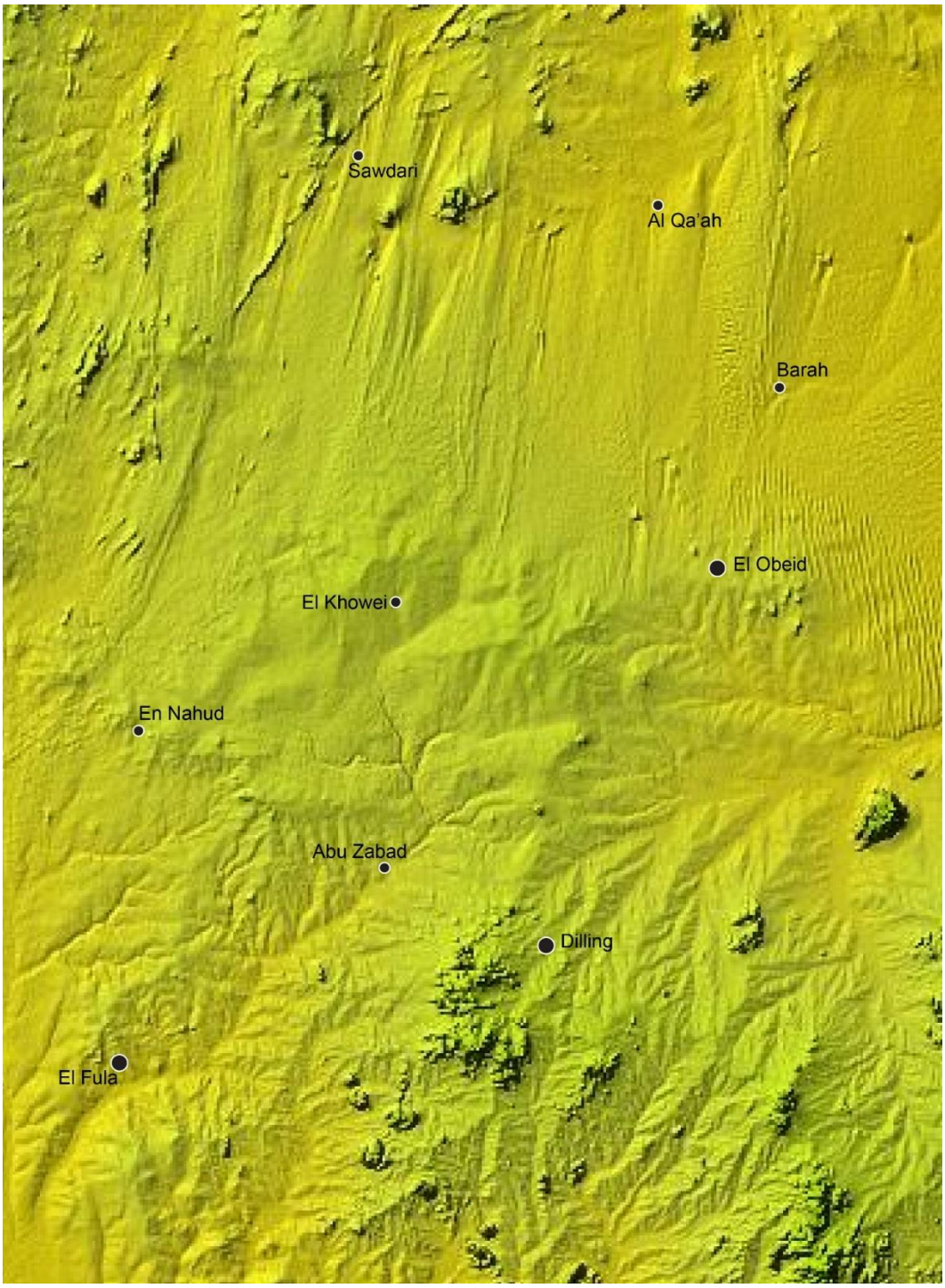


*Fig. 1.7. Relief of the study area.*

### 1.4.3. Vegetation cover

In a general way, the vegetation type is determined by the climate, relief and type of soil. The variation in rainfall and soil nature from North to South resulted in varied types and density of the vegetation cover. The relief also leads to remarkable variations in the vegetation cover density, since vegetation is denser along the course of the wadies or the depression zones.

In the northern part of the study area, the vegetation cover ranges from sparse growth, drought-resistant grasses and dwarf scrub. The central part is covered by acacia and baobab trees; grassland and bushland are scattered mainly around wadies and khors, and form the bushland-woodland transition. The southern part is mostly covered by edaphic grassland mosaics with trees.

## 1.5. Geology

### 1.5.1. Background

Rodis et al. (1968) provided a general summary of the geologic units in the Kordofan region. Among the rocks underlying Kordofan, these authors distinguished the basement complex of Precambrian age, the Nawa Series of Late Paleozoic age, the Nubian Series of Mesozoic age (recently renamed Cretaceous sediments), laterite of Early to Middle Paleogene/Neogene age, the Um Ruwaba Series of Pliocene to Pleistocene age, and surficial deposits of Quaternary age.

The oldest rocks in the region that now constitute the basement complex were formed in Precambrian times. Following the emplacement of these rocks the region was subjected to a period of prolonged erosion that apparently lasted through most of Paleozoic times. Shallow seas invaded parts of the region in the Late Paleozoic and deposited the sediments of the Nawa Series. Before the close of Paleozoic times, however, the region was uplifted and most of the Nawa sediments were removed by erosion. Only a few isolated remnants of the Nawa Series are now left in Kordofan as evidences of this once-extensive geologic unit.

Deposition of rock-forming materials in the area did not take place again until Mesozoic time when shallow continental seas covered much, if not all, the Province. During this time the clastic sediments of the Nubian Series were laid in continental or nearshore marine environments and over the eroded basement. Near the close of Mesozoic times, the sea receded as the region was again uplifted and then subjected to prolonged subaerial erosion that apparently lasted until Pliocene time. During this interval of erosion most of the Nubian rocks were stripped away and only those occupying the deeper basins in the basement rock surface were preserved. Extensive laterization of the Cretaceous sediments and possibly older rocks occurred during Peleogene time when climatic conditions favorable to laterite formation prevailed in much of the region. Tectonic movements in eastern Africa, probably during Neogene time, resulted in the formation of several structural basins in the Nubian and basement rocks of the Kordofan Province. During Pliocene and early Pleistocene times, these basins were filled with fluvial and lacustrine deposits that now make up the clastic Umm Ruwaba Formation. According to El Shafie et al. (2011), the Um Ruwaba Formation ranges from the Pliocene to Pleistocene.

Following deposition of the Umm Ruwaba Formation, several types of surficial deposits were laid down that now form a virtually continuous mantle over the Umm Ruwaba Formation and older rocks of Kordofan. In late Pleistocene time, the southern part of the Province (now Southern Kordofan State), was subjected to widespread and recurrent flooding. The floods, probably emanating from the Nile headwaters to the south, brought clay and silt and deposited these over most of the southern part of the region. Concurrent with flooding in the south, strong northerly winds prevailed in the northern part of the region (Northern Kordofan State now), and

denuded the land surface of much of its residual soil cover. A considerable part of the eroded material was deposited as sand dunes over the central part of the region. The residual soils in the north, stabilized sand dunes (Qoz) in the central part of the Province, and clay-plains deposits in the South remain today as evidence of the climatic conditions since late Pleistocene time (Rodis et al., 1968).

### 1.5.2. Geological units in the study area

#### 1.5.2.1. Basement Complex

The name Basement Complex is used to include those igneous, metamorphic and sedimentary rocks that are overlain by horizontal and sub-horizontal, Paleozoic or Mesozoic sedimentary or igneous rocks (Rodis et al., 1968). It is considered the most extensive formation in Sudan, excluding the superficial deposits (Whiteman, 1971).

Although the basement rocks cover a great part of the study area, they are poorly exposed in the northern parts, while they crop out more extensively in the southern part. The basement outcrops comprise a variety of rock types. Gneisses and migmatites, amphibolites, various types of schists, marbles and calc-silicate rocks, gabbros, syn- to late-tectonic granites, acid volcanic rocks and post-tectonic intrusions are distributed in scattered outcrops (Abdel Galil, 2008). Some isolated outcrops of gneiss and chlorite schist, granite, granodiorite, graphitic schist and syenite are observed in the western parts of the study area (Dawelbeit, 2011; Ginaya, 2011; Ginaya et al., 2013). Gneisses and migmatites, sericite-graphite schists, chlorite schists, slates and meta-quartzites, granite and granodiorite, schists, slates and quartzites crop out in some small isolated outcrops in the southwestern part of the area (Strojexport, 1976).

#### 1.5.2.2. Nawa Series (Upper Paleozoic)

The Nawa Series is the least extensive of the sedimentary rock units and has been identified only in the east-central part of Kordofan, south of El Obeid and northeast of Dilling. The series includes well-consolidated micaceous and non-micaceous sandstone, arkose, shale, mudstone, and thin-bedded limestone (Rodis et al., 1968). In absence of fossil evidence the Nawa Formation is best classed as Palaeozoic–Mesozoic undifferentiated (Whiteman, 1971).

#### 1.5.2.3. Cretaceous sediments

Cretaceous sediments at first were known as Nubian Sandstone or Nubian Formation. The latter term is applied to those bedded and usually flat-lying conglomerates, grits, sandstones, sandy mudstones and mudstones that rest unconformably on the Basement Complex and Paleozoic sandstone formation (Karakanis 1965). Rodis et al. (1968) and Whiteman (1971) assumed that the Nubian Formation is of continental and/or nearshore marine origin.

In the study area the Nubian Formation is found in some isolated basins in the northeastern, northwestern and central-western parts (Fig. 1.8) with variable thicknesses. The thickness of the Nubian Formation depends on the paleo-relief of the Basement Complex, the thickest deposits being deposited in the depressions (Geotechnika, 1985). Borehole data and geophysics in En Nuhud outlier show a maximum thickness for the Nubian Formation of about 1000-1200 m (Elmansour and Omer, 2017).

Karakanis (1965) divided the Nubian Sandstone Group in Western Kordofan and Darfur into a basal, middle and upper series. The basal series consists of coarse silicified sandstone and

conglomerates. The middle series is composed of mudstone and sandstone (mudstones dominate over sandstones). The upper series is composed of poorly sorted sandstone.

In the study area, the Nubian Formation has been subdivided into three lithological facies: (I) Psephitic facies: conglomerates, with predominant grain size > 4.0 mm, (II) Psammitic facies: sandstones and gravely sandstone (0.05 mm < grain size < 4.0 mm, and (III) Pelitic facies: claystone, mudstone and siltstone (grain size < 0.05 mm) (Ginaya, 2011).

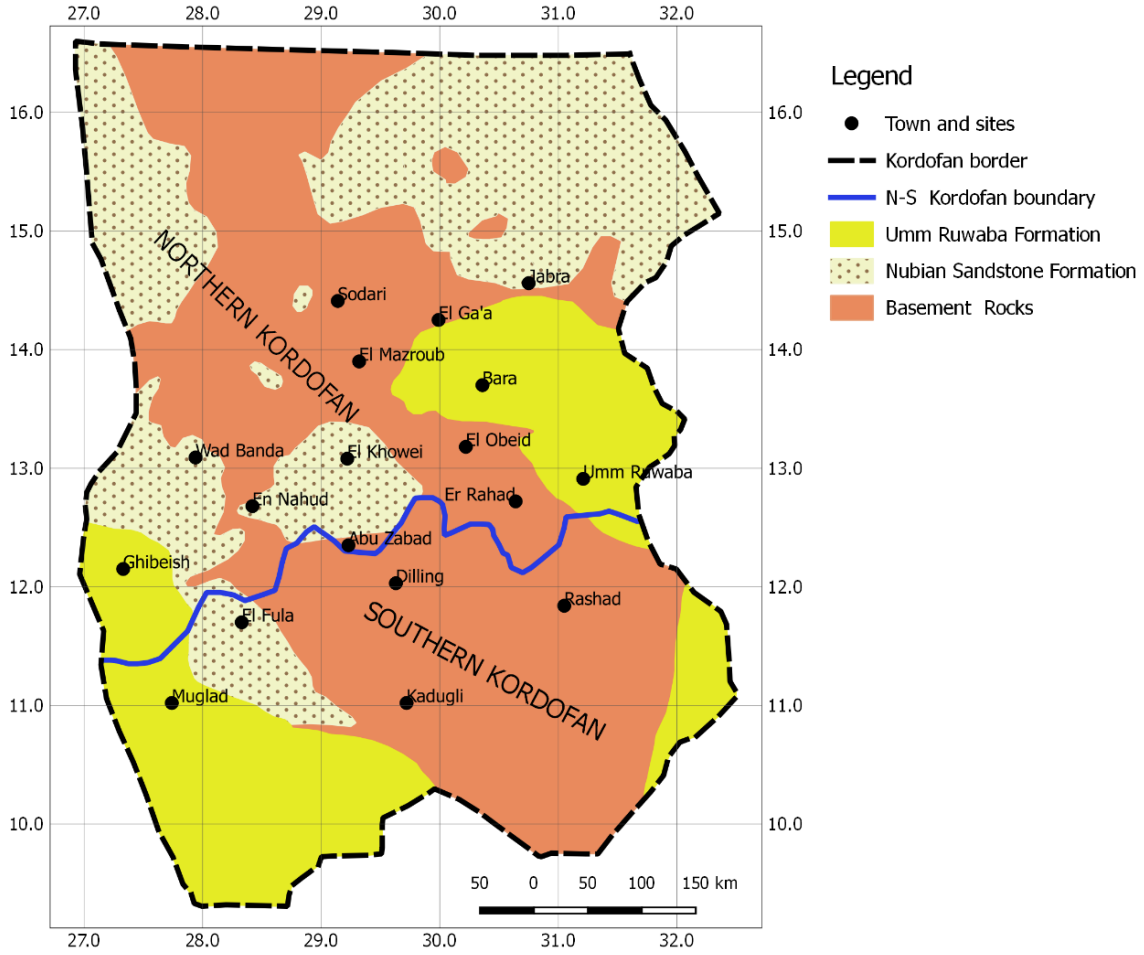


*Fig. 1.8: Distribution of pre-Quaternary gelogical units in the Kordofan Region (from Rodis et al., 1968; Elhag et al., 2014).*

### 1.5.2.4. Laterite (Late Paleogene)

Laterite or ironstone was apparently developed extensively on Nubian sandstones over much of the Kordofan Province during Early and Middle Tertiary time and corresponds to a prolonged period of deep in-place weathering of the host rock under tropical climatic conditions of alternating wet and dry seasons. Erosional remnants of this once extensive laterite deposit occur east and southeast of En Nahud and north of El Fula but are small outcrops. The laterite consists of a highly ferruginous layer of hematitic and limonitic ironstone that locally has an oolitic or vermicular texture. In places, the laterite is hardly distinguishable from the underlying ferruginous Nubian mudstone (Rodis et al., 1968).

#### 1.5.2.5. Umm Ruwaba Formation (Paleogene-Neogene)

The Umm Ruwaba Series consists of lacustrine and fluviatile deposits that, in east-central Kordofan, rest largely on the irregular surface of the basement rocks. In the southwestern part of the Province, however, the deposits are underlain largely by rocks of the Nubian Formation from which in places, they are hardly distinguishable. Outcrops of Umm Ruwaba strata are rare because they are covered in most places by a thin but almost continuous veneer of surficial deposits (Rodis et al., 1968). The Umm Ruwaba Formation is composed mostly of mudstone, sandstone and conglomerate. Facies and bedding changes within relatively short distances are very common, the conglomerates are often silty and the mudstones are sandy (Rodis et al., 1968).

#### 1.5.2.6. Quaternary deposits (Pleistocene to Recent)

The terms surficial or superficial deposit are the most used in the previous studies to describe the Quaternary deposits.

Rodis et al. (1968) provided a powerful summary of the Quaternary sediments, indicating that the Kordofan Province is covered by a mantle of unconsolidated surficial deposits. In the northern two-fifths of the Province, this cover consists of coarse residual desert soils and active sand dunes. Adjoining these deposits to the South and extending over most of the central part of the Province is the Qoz sand (largely stabilized sand dunes), sometimes also called the Kordofan sands. Covering the southern part of Kordofan and in places interfingered with the Qoz sand, are the clay-plains deposits (Fig. 1.9). Alluvium in the channels of wadis and khors and slope-wash deposits around the footslopes of the jebels occur locally throughout the Province. Because of their limited areal extent, alluvium and slope-wash deposits are not indicated in Figure 1.9.

Residual desert soils in the north derive from the weathering of the parent rock and are the most extensive of the surficial deposits in the northern part of Kordofan. These materials are unconsolidated, generally less than 7 m thick, and consist largely of unsorted angular and sub-angular rock fragments ranging in size from sand to boulders. Most of the finer rock material in this area was apparently removed by strong northerly winds and deposited as sand in the central part of the Province (Rodis et al., 1968).

The Qoz sand deposits, or Kordofan sand (Edmond, 1942), are characteristically red (Rodis et al., 1968), or varying from pale buff to deep red (Edmond, 1942), and marked by their gently undulating surface (Rodis et al., 1968), which may indicate typical wind deposited sand (Edmond, 1942). These Qoz sands are composed of fine to medium sand (Ginaya, 2011) made of well-rounded quartz grains (Edmond, 1942). The Kordofan sand is assumed to represent the southern limit of the windblown sands (Elmansour, 2017). The Kordofan sand covers large areas in central Sudan, west of the White Nile, especially in the province of Kordofan (Elmansour, 2017), but are less common east of the Nile. This would be related to the distribution of the Nubian Formation, which is much more limited on the right bank (Salama, 1976).

The clay-plains deposits consist of laminated, loosely compacted clay, silt, sandy clay, and sandy silt formed during successive floods of extensive areas, chiefly in southern Kordofan (Rodis et al., 1968).

Regarding the origin of superficial deposits, Grabham (*in* Whiteman, 1971) assumes that the sands were transported by wind from desert areas floored by granitic rocks, while Andrew (*in* Whiteman, 1971) accepts their local origin. Edmond (1942) proposed the Qoz sands are a product of weathering of the Nubian Formation. Rodis et al. (1968) believe that their reddish color and their gently undulating surface reflects their aeolian origin.

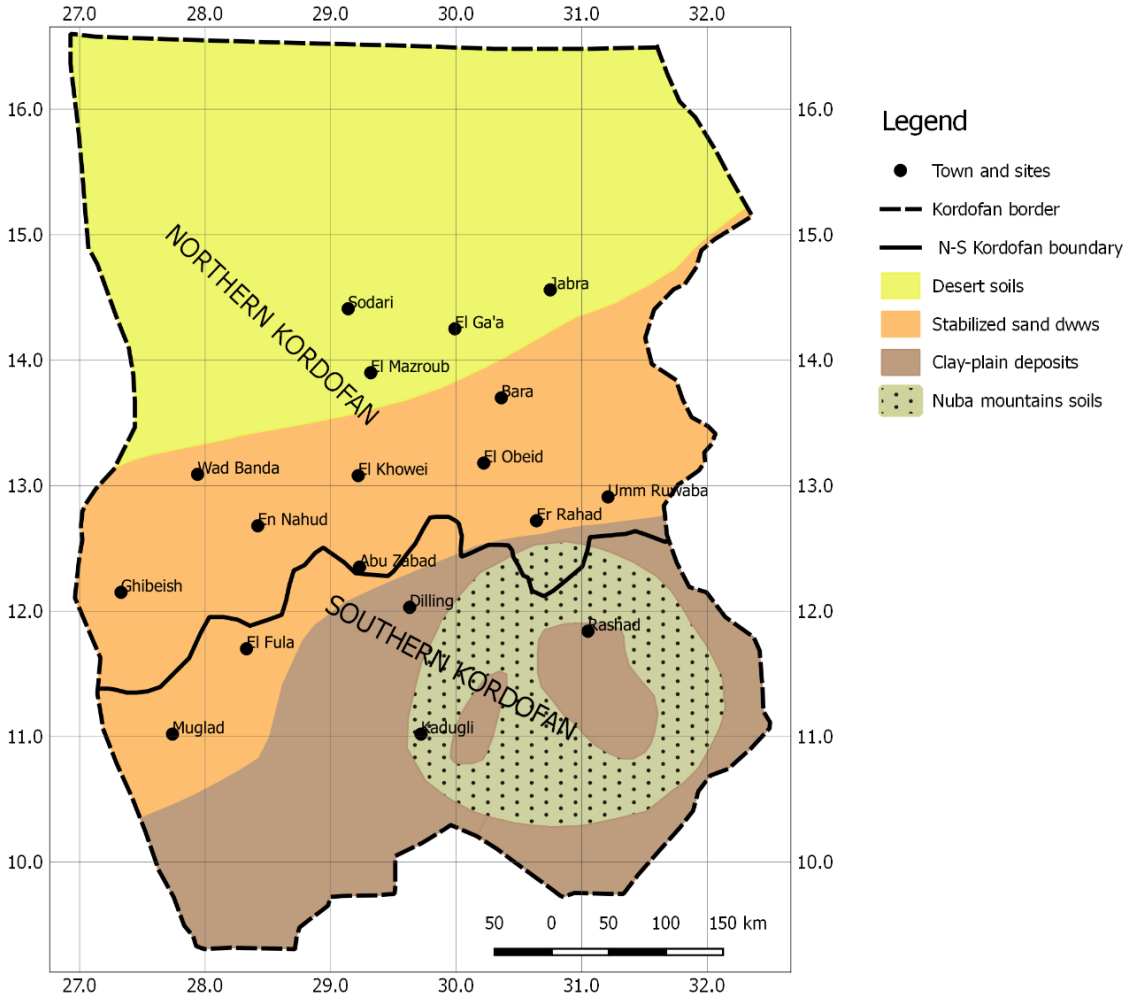


*Fig. 1.9: General distribution of surficial deposits in the Kordofan Region (after Rodis et al., 1968).*

### 1.6. Present-day climate of Africa

Because Africa is such an enormous landmass, stretching from about 35°N to 35°S, the climate differs according to location within the continent (Collier et al., 2008). Therefore, Africa can broadly be divided into four climatic zones based on a combination of temperature, precipitation (ppt) and evapotranspiration (Ngaira, 2007) (Fig. 1.10). The zones are:

i) Arid and semi-arid (Sahel region, Kalahari and Namib deserts).
ii) Tropical Savanna grasslands (Sub-Saharan Africa and Central Southern Africa).
iii) Equatorial (the Congo region and the East African highlands).

iv) Temperate (the South Eastern tip of South Africa) (Ngaira, 2007).

The African climates depend on low altitude pressure and winds over the continent, which are the surface expression of the upper air circulation (Gasse, 2000). One of the most important zone of the air circulation is the Congo Basin in Central Africa, which represents the biggest water catchment in Africa. As a consequence, Central Africa is one of the most important climatic regions in the world. During the rainy seasons, the Congo is the wettest place on Earth, and adds 3.5 mm to global sea level each year (Beighley et al., 2011). Seasonal variations in the position of the Inter tropical Convergence Zone (ITCZ) exert a significant control on the seasonal pattern of precipitation maxima across much of Africa. Figure 1.9 shows the major climatic zones and atmospheric circulation regimes for average conditions in July/August and January that allows understanding climatic variability (Nicholson, 2000). Distinct atmospheric circulation systems affect North Africa, West and Central Africa, East Africa, and southern Africa; they are separated in large part by the ITCZ (Gasse, 2000). Moreover, the Atlantic and Indian oceans play an important role in shaping the regional climate. During the southern hemisphere summer, differences in surface air pressure between the two oceans drive an east-west air circulation cell which makes the rainfall more variable over southern Central Africa. The transport of low-level water vapor from the Atlantic Ocean brings clouds and rain to central Africa throughout the year (Creese and Pokam, 2016).

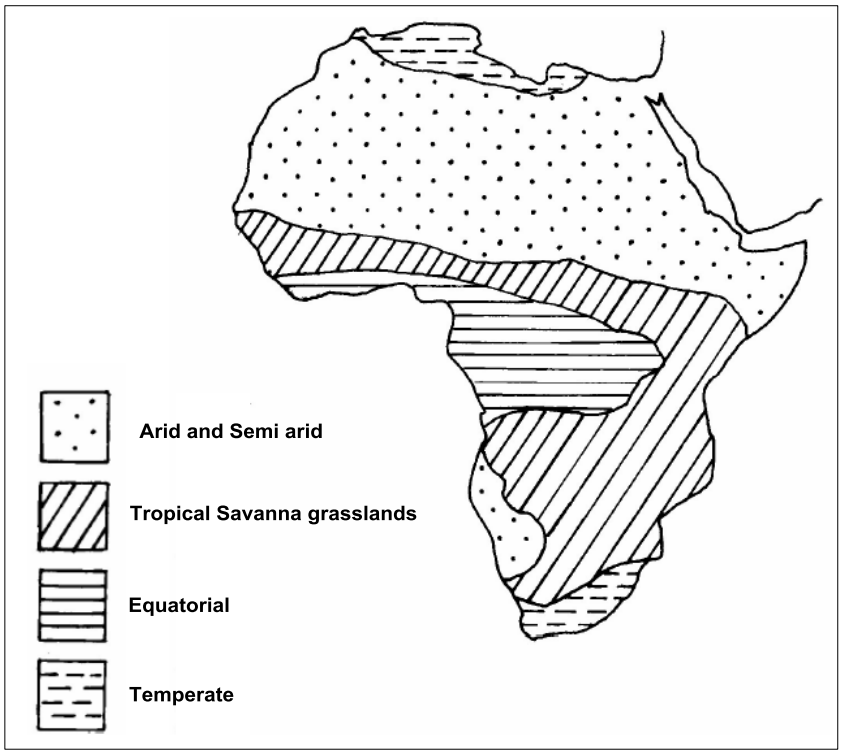


*Fig. 1.10: Current climatic zones of Africa (after Ngaira, 2007).*

### 1.7. Late Quaternary hydrology of Eastern and Western Sahara

Several important studies either focused on paleohydrology, or related to hydrology, provide good references. These are the study of the paleohydrology of tropical Africa (Gasse, 2000), the study of the White Nile valley (Williams et al., 2000), the White Nile and Lake Albert

(Williams, et at., 2006) and the Nile Basin (Williams, 2009), as well as some other studies carried out in paleolakes of Eastern Sahara (e.g., Pachur and Kröpelin, 1987; Pachur and Hoelzmann, 1991; Hoelzmann et al., 2001; 2010; Bouchette et al., 2010).

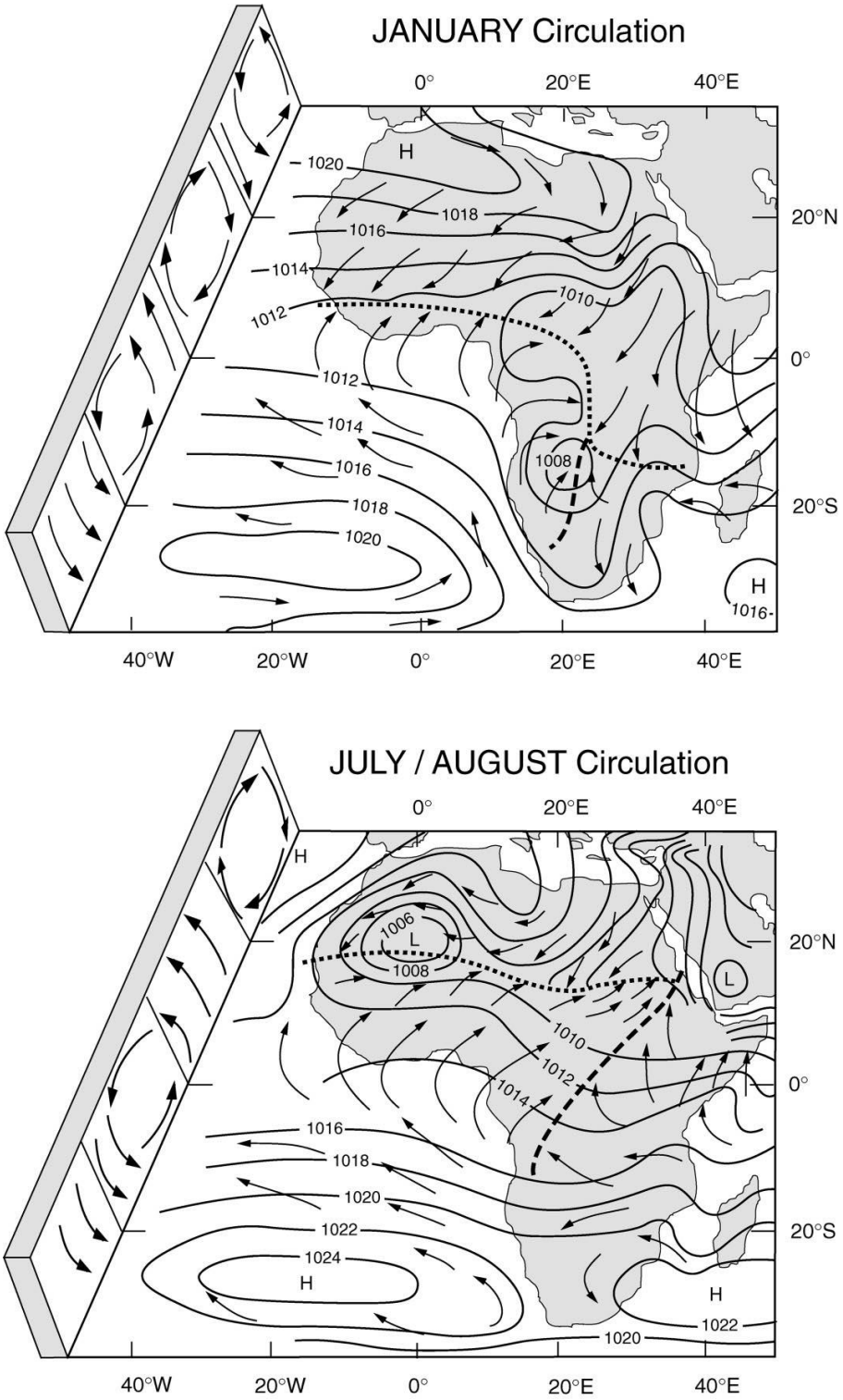


*Fig. 1.11: Sketches of the general patterns of winds and pressure over Africa. Dotted lines indicate the Intertropical Convergence Zone (ITCZ), dashed lines indicate the Congo Air Boundary (after Nicholson, 1996, in: Gasse, 2000).*

At a regional scale, Gasse (2000) summarized the major hydrological features of Africa based on the general climate, topography and geological features. These features are: (i) large internal drainage basins (e.g., Lake Chad basin) and enormous groundwater reservoirs (e.g., geological formations of the Continental Intercalaire in the Sahara); (ii) large exoreic rivers (Congo, Nile and Niger rivers) and associated wetlands, which have their headwaters in the humid equatorial belt; (iii) great East African Rift lakes that play a significant role in regional climate through water recycling; (iv) other permanent waterbodies concentrated in, or depending on, the equatorial zone (e.g., Lake Chad through the Chari river), or on highlands (e.g., the Ethiopian lakes Ziway-Shala and Abhé) (Gasse, 2000). Depending on that, the study of paleohydrology and its implication in the paleoclimatic studies, requires great attention to the lake level fluctuations, record of the flood events in rivers and fluctuation of the groundwater levels.

Holocene Mega-lake Chad (ca. 10°N to 18°N; 12°E to 20°E) was the largest late Quaternary water body in Africa with maximum surface area during the Holocene exceeding 350,000 $km^2$. The development of this giant paleo-lake is related to a northward shift of the isohyets interpreted as evidence for an enhanced Monsoon during the African Humid Period (Bouchette et al., 2010). The water depth of this giant Mega-Lake was exceeding 150 m at its deepest part in the central northern sub-basin. The lowest elevation point at this lake is less than 200 m asl, while the maximum determined water lake level is 330 m asl (Bouchette et al., 2010).

Although the River Nile and its two main branches (White and Blue Nile) represent the main and most important hydrological feature in Sudan, there are other more local features. These are represented by some paleolakes west of the White Nile, some active seasonal rivers and wadies, and other fossil rivers and wadies. The most important and already investigated paleolakes are: the West Nubian Lake in NW Sudan (Pachur and Hoelzmann, 1991; Hoelzmann, et al., 2001), Selima in north Sudan (Abell and Hoelzmann, 2000), and some small lakes along Wadi Howar in NW Sudan (Pachur and Kröpelin, 1987).

The West Nubia Paleolake is considered the largest hydrographic evidence in Eastern Sahara of the early to mid-Holocene wet phase that affected northern Africa (Hoelzmann et al., 2001) and its basin represents an area of about 20,000 $km^2$ (Pachur and Hoelzmann, 1991). The maximum water depth estimated in the the West Nubia Paleolake between 9400 and 7500 $^{14}C$ yr BP was 15 m (Hoelzmann et al., 2001).

Moreover, beside these paleolakes, paleoclimatic and paleohydrological research undertaken in Eastern Sahara revealed the existence of two major late Pleistocene to mid-Holocene drainage networks that once interrupted the state of internal drainage of this vast region. One network is an about 800 km long watercourse in eastern Libya (Pachur, 1974), and the second network is the about 400 km long Wadi Howar in northwestern Sudan, which linked the mountains of Western Sudan to the Nile (Pachur and Kröpelin, 1987). Beside, some other wadies are known in southern Libya with present rainfall of 20 mm/year (Pachur, 1974). From about 9500 to 4500 years ago, the lower Wadi Howar flowed through an environment characterized by numerous ground water outlets and freshwater lakes (Pachur and Kröpelin, 1987). Wadi Howar constituted the largest tributary to the Nile from the Sahara between the Mediterranean Sea and the Atbara River, and it drained a 400 km wide area linking the present extremely arid northern Sudan (present rainfall, 25 mm/year) to the Nile (Pachur and Kröpelin, 1987).

### 1.8. Latest Quaternary climate of Northeastern Africa

The continental deposits often provide more detailed information about short-term (high frequency) change of climate than most marine records (Bradley, 1989). The Sahara sediments in particular, represent an important archive for the climate variabilities and consequently the development of the Sahara during the late Pleistocene-Holocene period. Since 1980, the Sahara was the site of important development in paleoclimatology researches throughout a variety of climate proxies that have been recorded in this continental sediments. Most of these researches have focused on the last glacial maximum (LGM)-Holocene period, and very special attention was paid for terminal Pleistocene-Holocene (the last 12 ka) (Nicholson and Flohn, 1980; Pachur and Kröpelin, 1987; Rodrigues et al., 2000; Gasse, 2000; DeMenocal et al., 2000; Williams et al., 2000; Abell and Hoelzmann, 2000; Hoelzmann et al., 2001; Kuper and Kröpelin, 2006; Woodward et al., 2007; Hamann et al., 2009; DeMenocal Williams, 2009; Hoelzmann et al., 2010; Tierney et al., 2011b; Tierney, 2012; Williams, 2014).

The period between 20 and 12 ka BP is well documented as a period of dune building in the central Sahara, the Nile basin and East Africa (Nicholson and Flohn, 1980; Woodward et al., 2007; Tierney et al., 2011b; Williams et al., 2000; Williams, 2009; 2014). This hyper arid phase had great effects and influence on the geomorphology and landscape features of the Sahara region.

The dune building period is followed by a humid phase that extended between ≈ 12 and 6 ky BP. This humid phase is well known as the African Humid Period (AHP) (DeMenocal et al., 2000; Hamann et al., 2009; DeMenocal and Tierney, 2012) or lacustrine period (Williams, 2014). The AHP is well-characterized by numerous large and small lakes (Bakker and Maley, 1977; Flohn, 1980; Szabo et al., 1995; DdeMenocal et al., 2000; Cole et al., 2009) (Fig. 1.12). Some of the small lakes are the Dry Selima lake (northern Sudan), the West Nubian Palaeolake (NW Sudan; Pachur and Hoelzmann, 1991; Kröpelin and Soulié-Märsche, 1991; Abell and Hoelzmann, 2000; Hoelzmann et al., 2010), Lake Challa in Ethiopia (Tierney et al., 2011b), Lake Tilo in the Ethiopian highlands (Telford and Lamb, 1999) and Lake Yao in Chad (Lézine et al., 2011). Other palaeolakes formed along the Wadi Howar (Pachur and Kröpelin, 1987). Some lake basins in North Africa were exceptionally large; these so-called megalakes include the Megalake Fezzan (Libya), Megalake Chad, Chotts Megalakes (Algeria) and Megalakes Turkana and Kenya to the southeast (DeMenocal and Tierney, 2012).

Moreover, the AHP is also well documented through the archeological evidences that linked the development of these lakes and the Nile valley. Eastern Sahara (which includes partially Libya, Chad, Egypt and Sudan) represents an important archive for the Holocene climate through the existence of this early to mid-Holocene lakes and development of the human occupation evolution. This human occupation history is well documented over Eastern Sahara in general (Kuper and Kröpelin, 2006), in the West Nubia Palaeolake (Hoelzmann et al., 2001), west of the Nile across the Sahara-Sahel Belt (Mohammed-Ali, 2003), in Egypt and northern Sudan (Nicoll, 2004), along Wadi Howar (Jesse, 2007), on the eastern margin of the Blue Nile (Lario et al., 1997), and in many other sites in northern and central Sudan. The timing and development of Holocene human occupation in the now hyperarid Sahara has major

implications for understanding links between climate change, demography and cultural adaptation (Manning and Timpson, 2014). In the Atlas, Eastern Sahara and Central Sahara regions, Manning and Timpson (2014) demonstrated synchronicity in the population increase and the start of the AHP. The compilation of radiocarbon dates from archeological sites showed that the older dates are in the North, while the bulk of younger dates is located in the South, clearly indicating a movement of prehistoric populations toward the present day Sahelian zone (Kuper and Kröpelin, 2006).

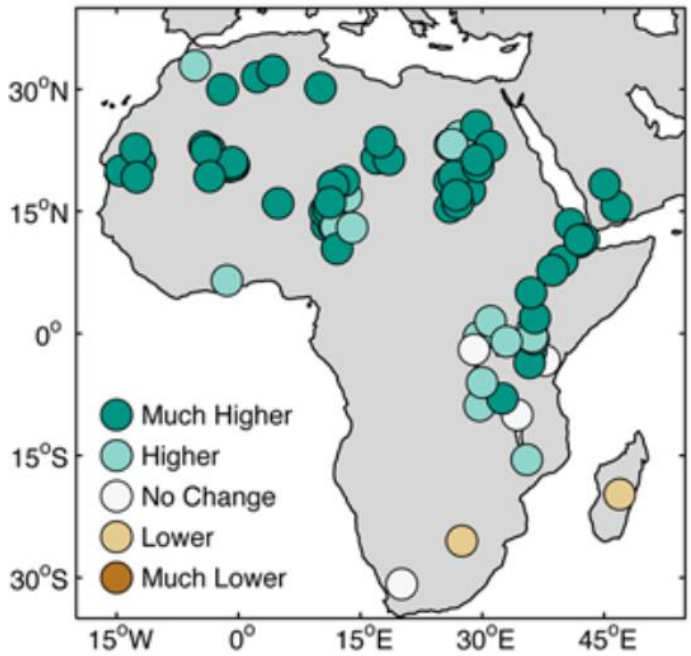


*Fig. 1.12: Distribution map of reconstructed lake levels across Africa, 9,000 years ago relative to today. Data from Oxford Lake Level Database (COHMAP members, 1988; Street-Perrott et al., 1989) updated with lake-level reconstructions generated in the last twenty years (deMenocal and Tierney, 2012).*

During the late Holocene period (≈ 6 ka BP to present), the Sahara recorded progressively drier condition, although the real start of this dry phase is different across the Sahara in particular, and the African continent in general. This aridification period is well documented in the Eastern Sahara (Tierney and deMenocal, 2013; Manning and Timpson, 2014) through a variety of evidences: northern Chad experienced a progressive drying in response to weakened insolation forcing of the African monsoon and abrupt hydrological change in the local aquatic ecosystem (Kröpelin et al., 2008); palynological evidences from Lake Yoa (Chad) indicate gradual shift from moist to arid conditions during the last 6000 yr (Lézine et al., 2011); and desertification and aeolian deflation are recorded during the Middle and Late Holocene in Egypt and northern Sudan (Nicoll, 2004). In some sites, this dry period has been detected earlier than 6 ka BP, where warm, dry phase between 7000 and 6800 BP has been recognized in the Blue Nile, from sedimentological, flooding and lake level data. This short dry phase in Blue Nile was interrupted by somehow wetter conditions than the present day ones, and continued about 4500 BP when the present arid to hyper-arid conditions commenced (Lario et al., 1997). In eastern Africa this dry phase has started later ≈ 4.5 ka BP (Telford and Lamb, 1999).

### 1.9. Statement of the problem and aim of this study

The present study is dealing with the late Quaternary deposits in the Kordofan region from sedimentological and climatic points of view. Most of the previous studies carried out in this region focused on the hydrogeology (Karkanis, 1966; Rodis et al., 1968; Salama, 1976; Strojexport, 1976; Ginaya, 2011; Dawelbeit, 2011; El Hadi, 2012; Elhag et al., 2013; Elhag et al., 2014; Elmansour, 2017), geology (Whiteman, 1971; Strojexport, 1975; Abdel Galil, 2008; Elhag and Elzien, 2013; Elmansour and Omer, 2017), and many other mineralogical investigation in the Nuba mountains, and hydrocarbon investigation south of El Fula. Very few attention has been paid for the Quaternary by those previous studies, due to less economical value of these sediments, and consequently, all the geophysical exploration and drilling reports describe the Quaternary units as superficial deposits with only very little information about their textural description. Edmond (1942) was the first to study in detail these late Quaternary deposits of Kordofan and paid special attention to the distribution of what is called the "Kordofan sand", the geomorphology of the dunes and the origin of the sand. Rodis et al. (1968) provided a map for the surficial deposits of the whole Kordofan region with valuable information about their physical and textural characteristics. However, the lithological variability of the late Quaternary units requires detailed studies, since the "Kordofan sand" is locally interbedded with important units of limestone that had never been mentioned by previous workers, and seems to have experienced intensive pedogenetic processes. Consequently, the sedimentological environment and paleogeographic distribution of these deposits need to be studied. Moreover, the real age of the Quaternary units is still unknown.

On the other hand, although intensive climatic studies have been carried out in the Sahara and especially in Eastern Sahara, the southern limit of the Sahara in Sudan (Kordofan region) has never been studied in order to document the climate evolution during the terminal Pleistocene-Holocene period. However, Late Pleistocene-Holocene deposits in the Kordofan region exhibit lithological discontinuities that probably reflect climatic fluctuations during the late Quaternary. In addition, there are clear lateral and/or vertical variations in the physical properties of the deposits (color, texture, grain size, fossil content …), which suggest large variability in sedimentary and climatic conditions during the late Quaternary.

The present study is focused on the sedimentary record of the climatic evolution of Central Kordofan through several climatic proxies. Therefore, the main objectives of this study are (1) to determine the age, areal extent and thickness of the Quaternary units, (2) to understand the processes that controlled the deposition and distribution of the Quaternary deposits, and (3) to reconstruct the late Quaternary paleoclimatic evolution of Kordofan region. The results of this study will help us to assess the relationships between climate and sedimentation. In this view, I hoped to address the following questions:

- What were the sedimentation processes of the Late-Quaternary deposits, are there any evidences of fluviatile, aeolian or lacustrine deposits ? If such different kinds of sediment exist; do they show any conformable and/or unconformable contacts ? And what is the age of these successive sedimentary units ?
- Do the lithological discontinuities and lateral and/or vertical variations in the sedimentary facies reflect any climatic variations ? If so, what was the role of regional Quaternary climate changes and monsoonal fluctuations, and their relations with the regional context ?

# II. METHODOLOGY

## 2.1. Introduction

In order to reconstruct the late-Quaternary sedimentary and climatic evolution of the Kordofan region, it is important to pay great attention in the field to sedimentological features and to know which climatic proxies should be used. Kordofan deposits incorporate and preserve multi-proxy evidences in a variety of sedimentary successions. This chapter outlines the approach taken for field observation, selection of representative sites, sample collection, and the practical laboratory investigations of selected paleoclimatic and paleoenvironmental proxies, namely: sedimentological, paleontological (palynology and gastropod sub-fossil shells), geochemical (stable isotopes, major elements and clay mineralogy), hydrological, archeological and carbon dating analyses.

## 2.2. Sites selection

Sites selection is the most important step in conducting such geological research. To investigate the sedimentological and stratigraphic succession in the Kordofan region, sites were selected across the study area depending on a preliminary short field works and *Google Earth* map survey that show some variations in the geomorphologic features (Fig. 1.4). These geomorphological features provided preliminary indicators of some morphological or lithological variation across the targeted area.

Sites selection was focused on the outcrops that likely contain: (1) well-preserved and well exposed sedimentary successions, (2) organic matter suitable for palynological analysis and carbon dating, although preserved organic matter is scarce in the greatest part of the area, (3) gastropod-rich successions for paleontological and paleobiological studies, (4) clastic sediments suitable for grain size analysis. The selected sites included: banks of wadies and khours (seasonal rivers) that expose sections up to 5 m thick, excavated sections along asphaltic roads up to 7 m deep, active or abandoned quarries and some other sites for surficial survey. In some cases, handmade wells have been caved to obtain adequate sections.

## 2.3. Field work

Two intensive field campaigns in November 2015 and November 2016, in addition to many other short complementary field works, have been carried out. The aims of the field work are to conduct sedimentological investigation (study, measurement and sampling of verical sedimentary profiles), in addition to some archeological and paleohydrological observations.

### 2.3.1. Sedimentological investigations

The purpose of the field work was to investigate in detail the sedimentary successions across the study area in order to document all the needed information. Tucker (2003) summarized the main aspects of sedimentary rocks to consider in the field, which should be recorded in as much detail as possible. These are:

1. The **lithology**, that is the composition and/or mineralogy of the sediment;

2. The **texture**, referring to the features, shape and arrangements of the grains in the sediment, of which the most important aspect to examine in the field is the grain-size;

3. The **sedimentary structures**, present on bedding surfaces and within beds, some of which record the palaeocurrents that deposited the sediments;

4. The **color** of the sediments;

5. The **geometry** and **relationships** of the beds or rock units, and their lateral and vertical changes; and

6. The nature, distribution and preservation of **fossils** contained within the sedimentary rocks.

The various attributes of a sedimentary rock are then combined to define a facies, which is the product of a particular depositional environment or of depositional process in that environment. Facies identification and analysis are the next steps after the field data have been collected (Tucker, 2003). In this study, facies identification provided preliminary indications on the climatic evolution, which required confirmations by other analytical climatic proxies.

### 2.3.2. Sampling

During field work, great attention was paid for samples collection. The collected samples included charcoal, bones and organic matter for carbon dating, organic-rich sediments for palynology, gastropod sub-fossil shells for paleontological investigation, in addition to *in situ* shells counting in some sections, clastic sediments collection for grain size analysis, clay mineralogy and major elements geochemistry, systematic gastropod sub-fossil shells and calcareous nodules sampling for oxygen and carbon stable isotopes analyses, and archeological remnants when present (Fig. 2.1).

#### 2.3.2.1. Carbon dating samping

Twenty-six samples for carbon dating were collected across the study area. These samples include: (1) eight samples of bones collected mostly from surficial outcrops of lake shorelines and only one of them collected from a section of wady or khour bank, (2) five charcoal pieces collected from sections of wady or khou banks, and (3) thirteen samples of organic-rich soils and paleosols from sections of wady or khou banks.

Many of these samples were collected randomly (not systematically) due to the lack of material suitable for dating in most parts of the sections.

#### 2.3.2.2. Palynology sampling

The palynological data obtained in this study proceed from twenty-nine samples from six sections. All samples are from the shaly parts of each section, with focus on the dark fine sediments. The sections rich in clayey strata have been sampled systematically with constant intervals, while those with rare shale levels have been sampled according to the potential suitability of the sediments.

#### 2.3.2.3. Paleontology sampling

Sampling for paleontology was focused on the collection of gastropod sub-fossil shells from different sites (surficial and in sections). The main purpose of the paleontological sampling was to identify the various observed sub-fossil shells, in order to determine their living environment, and thus, the depositional environment of the surrounding sediment.

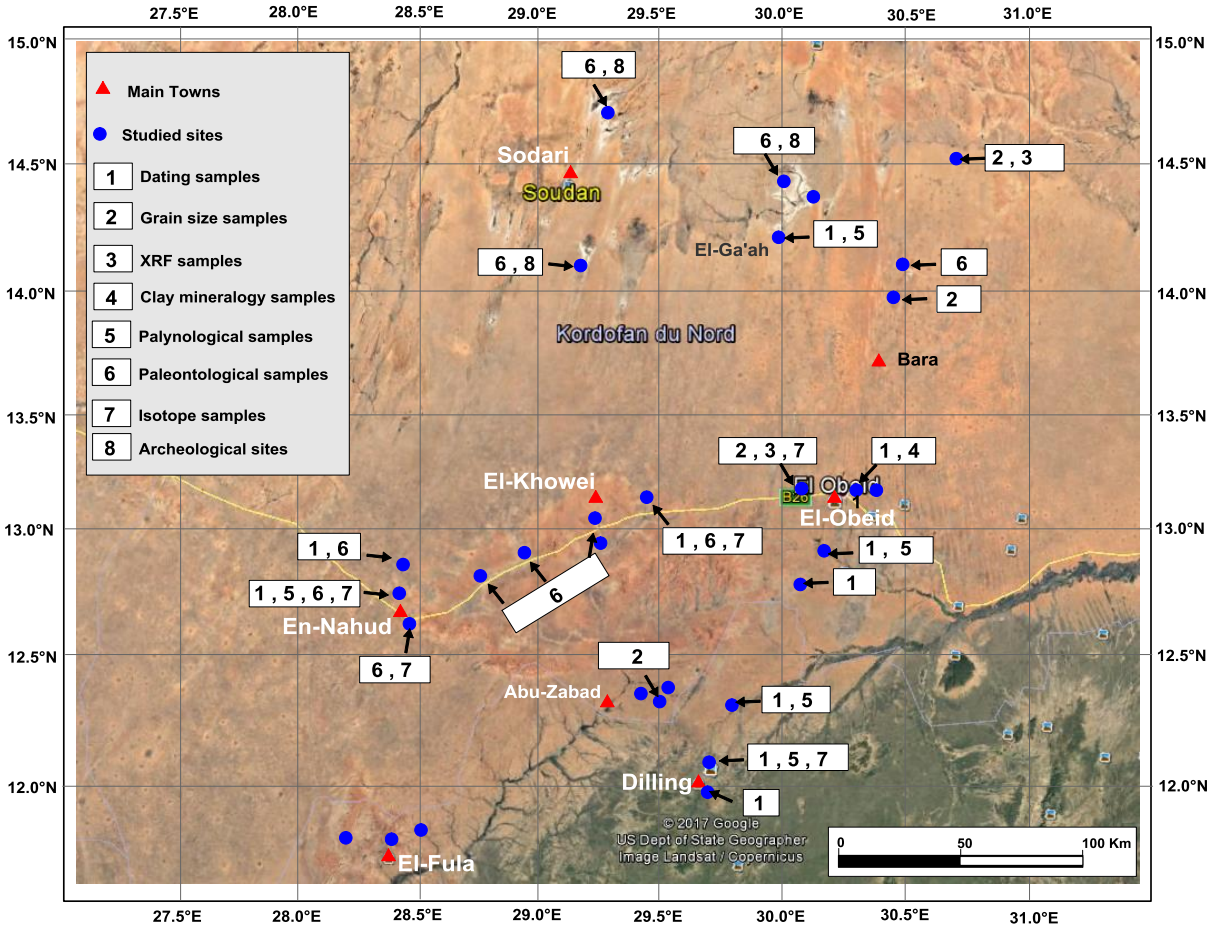


*Fig. 2.1. Sample location.*

### 2.3.2.4. Grain size and XRF samplings

Fourty-eight samples from four sections were systematically collected for grain size analysis. Among them, twenty-two samples from two sections were used for XRF analysis of major elements.

All sampled sections are composed of pedogenitized and non pedogenitized levels. From the pedogenitized parts, only the matrix have been collected after removing the pedogenitized features represented by calcareous nodules. Sediment samples range between 400 and 500 g.

### 2.3.2.5. Clay mineralogy sampling

Only eight samples were collected along one section, proceeding from different deposits. 300 g of sediments were originally sampled, reduced to a few grams after prepartion (see section 2.4.3.4.).

### 2.3.2.6. Stable isotopes sampling

Forty-nine samples were systematically collected from five sections: three sections yielded twenty-four gastropod sub-fossil shells from various species, while other samples are calcareous nodules from two other sections.

## 2.4. Laboratory analyses

### 2.4.1. Radiocarbon dating

#### 2.4.1.1. Overview

Radiocarbon $^{14}C$ is one of three isotopes of carbon, the others being $^{12}C$ and $^{13}C$. By far the most abundant of these is $^{12}C$, which comprises around 98.9% of all naturally occurring carbon atoms. $^{13}C$ forms around 1.1% and $^{14}C$ one part in $10^{10}$%. In other words, only about one among one million atoms of carbon is $^{14}C$. Both $^{12}C$ and $^{13}C$ are stable isotopes, but $^{14}C$ is not, and it 'decays' to a stable form of nitrogen, $^{14}N$, through the emission of beta (ß) particles. One ß particle is released from the nucleus for every atom of $^{14}C$ that decays (Walker, 2005).

Radiocarbon dating is the most widely applied dating technique for the Holocene and late Pleistocene period, providing reliable and accurate temporal controls for palaeoenvironmental studies. It was therefore applied to obtain absolute independent chronology of the studied samples.

Radiocarbon dating determines ages of carbonaceous materials using the radio-isotope $^{14}C$. $^{14}C$ is produced in the upper atmosphere mainly as the result of the interaction of cosmic ray neutrons with Nitrogen-14 atoms (Muscheler et al., 2004; Fairbanks et al., 2005). $^{14}C$ mixes rapidly throughout the atmosphere to form carbon dioxide and enters the global carbon cycle and is assimilated by plants through the photosynthesis process, and by animals through the ingestion of plant tissue (Walker, 2005). The majority of $^{14}C$ (more than 95%) is absorbed into the oceans as dissolved carbonate, which means that organisms that live in sea water (corals, molluscs, etc.) will also take up $^{14}C$ during the course of their life cycle. Although the $^{14}C$ in the terrestrial biosphere and in the oceans is constantly decaying, it is continuously replenished from the atmosphere. Hence, the amount of $^{14}C$ that is stored in plant and animal tissue and in the world's oceans, the global carbon reservoir, remains approximately constant through time (Walker, 2005).

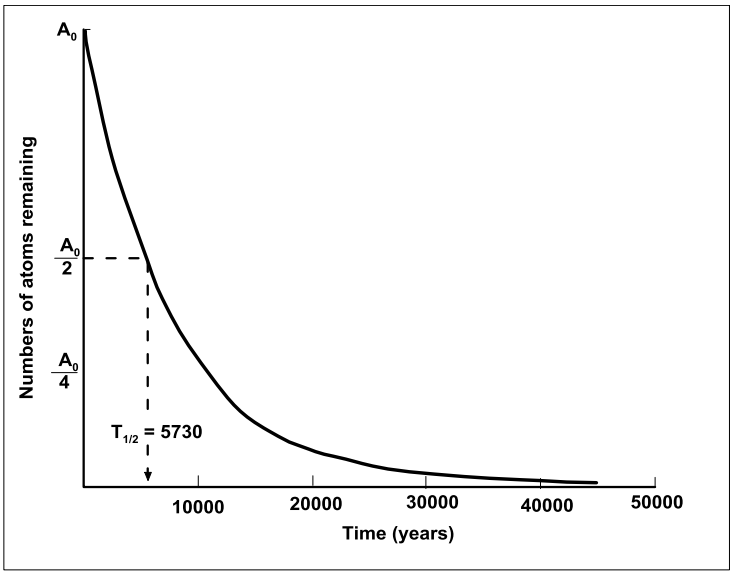


*Fig. 2.2. Decay curve of radiocarbon. This curve is exponential, not linear. A after each half-life the number of atoms remaining is halved. If there are $A_0$ atoms of radiocarbon at the beginning of the decay process, then after one half-life there will be $A_0/2$ atoms remaining; after two half-lives, there will be $A_0/4$, after three, $A_0/8$ and so on (after Bowman, 1990; in Walker, 2005).*

Once an organism dies, however, it becomes isolated from the $^{14}C$ sources, no further replenishment of $^{14}C$ can take place, and the 'radiocarbon clock' runs down by radioactive decay, which occurs in constant rate. Hence by measuring the amount of $^{14}C$ that remains in a sample of fossil materials (the residual $^{14}C$ content) and comparing this to modern $^{14}C$ in standard material, an age can be inferred since the death of the organism. However, the rate at which $^{14}C$ decays is needed to know the rate at which $^{14}C$ decays. Experimental results have shown that the decay rate of $^{14}C$ is 1% every 83 years. However, as with all radioactive isotopes, the decay curve is not linear but exponential (Fig. 2.2). This means that materials significantly older than this can still be dated. The half-life of a $^{14}C$ atom is 5730 years, and under normal circumstances, the limit of measurement of $^{14}C$ activity (i.e. decay rate) is eight half-lives. This translates into an upper age limit of around 45 000 years. Therefore, samples older than this are usually described as being 'infinite age' and are expressed, for example, as > 45 000 years (Walker, 2005).

$^{14}C$ dating of our samples have been carried out (1) at the Poznań Radiocarbon Laboratory, Poland, by Dr. Tomasz Goslar, and (2) at the Laboratoire des Sciences du Climat et de l'Environnement (LSCE), in Gif sur Yvette, France, by Dr. Jean Pascal Dumoulin, through the Institut de Recherche pour le Développement (IRD).

#### 2.4.1.2. Procedures of AMS $^{14}C$ dating used in the Poznań Radiocarbon Laboratory

Procedure of $^{14}C$ dating with the AMS technique, consists of a few stages: chemical pre-treatment, production of $CO_2$ and graphitisation, AMS $^{14}C$ measurement, calculation of $^{14}C$ age and calibration of $^{14}C$ age.

##### 2.4.1.2.1. Chemical pre-treatment

Methods of chemical pre-treatment generally follow those used in the Oxford Radiocarbon Accelerator Unit, as described by Brock et al. (2010, *Radiocarbon*, 52, 102-112).

- Samples of charcoal, wood or other plant remains (after mechanical removal of macroscopic contamination visible under binocular) are treated with 1M HCl (80°C, 20+ min), 0.025-0.2M NaOH (room temperature for fragile plant remains, 80°C for wood) and then 0.25M HCl (80°C, 1 hour). After treatment with each reagent, the samples are rinsed with deionised water (Millipore) until pH = 7. For the first HCl treatment, longer time (20+) is applied, if emanation of gas bubbles from sample is still visible. The step of NaOH treatment is repeated a few times, generally until no more coloration of the NaOH solution appears (coloration of solution is caused by humic acids dissolved in NaOH), but the NaOH treatment is interrupted if there is a danger of complete dissolution of the sample.

- Samples of sediments are usually treated with 1M HCl (room temperature overnight and then 80°C, 1+ hour), 0.2M NaOH (80°C, 10 min) and then 0.25M HCl (80°C, 1 hour). After treatment with each reagent, the samples are rinsed with deionised water (Millipore) until pH = 7. For the first HCl treatment, longer time (1+) is applied, if emanation of gas bubbles from a sample is still visible. The step of NaOH treatment is repeated a few times, generally until no more coloration of the NaOH solution appears (coloration of solution is caused by

humic acids dissolved in NaOH). In case where total organic carbon (TOC) is to be analysed, the procedure is limited to the first HCl treatment only.

- In case of bones, extraction of collagen is performed using the procedures originally described by Longin (1971, *Nature*, 230, 241-242), with further modifications (e.g. Piotrowska N., Goslar T., 2002, *Isotopes in Environmental and Health Studies*, 38, 1-9). Before extraction, degree of collagen degradation is checked by measuring content of nitrogen and carbon in bone, using analyser Flash EA 1112 Series (ThermoScientific). The samples are regarded suitable for collagen dating, if nitrogen content in bone is not lower than 0.6%, and ratio C/N is not higher than 5. Suitable bones are crushed mechanically to granulation <0.3 mm, the bone powder is then treated with 2M HCl (room temp., 20 min), and 0.1M NaOH (room temp., 1 h). After each step of treatment, the sample is centrifuged and the residuum is collected. Extraction of collagen is processed in HCl (pH = 3, 80°C, 10h), and after centrifugation, residuum is removed. The extracted collagen is then ultrafiltered on pre-cleaned Vivaspin 15 MWCO 30 kD filters (Bronk Ramsey et al. 2004, *Radiocarbon*, 46, 155-163). Quality of the collagen is ultimately assessed basing on C/N atomic ratio (interval of acceptance: 2.7-3.5) and collagen extraction yield (acceptance threshold: 0.5%). On demand, carbon and nitrogen stable isotopic composition of the collagen can be determined.

In cremated bones, where collagen is too degraded and not suitable for $^{14}C$ dating, and geological situation at the site of sample collection excludes precipitation of secondary carbonates, a fraction of structural carbonates is forwarded for dating, while organic fraction is removed by treating bones with 2% NaClO for 48 h and then in 8% $CH_3COOH$ for 48h (according to Lanting J.N., Van der Plicht J., 2001. *Radiocarbon*, 43, 249-254). Then the outer layer of carbonate grains is removed in 2% HCl (1 h) and additionally by quick rinsing with 36% HCl.

- Samples of shells (and other carbonate features) are checked and mechanically cleaned under binocular. The organic coating, if visible, is removed with $H_2O_2$ (15-30%) in an ultrasonic bath. Then the outer carbonate layer (ca. 30%) is removed in 0.5M HCl (if the sample is large enough), the remaining material is treated in 15% $H_2O_2$ again (for 10 min in an ultrasonic bath) and the remaining carbonate is leached with concentrated $H_3PO_4$ in a vacuum line.

#### 2.4.1.2.2. Production of $CO_2$ and graphitisation

In case of organic samples, $CO_2$ is produced by combusting the sample. Combustion of organic samples is performed in closed (sealed under vacuum) quartz tubes, together with CuO and Ag wool, in 900°C over 10 hours. $CO_2$ from carbonate samples is leached by treating with concentrated orto-phosphoric acid ($H_3PO_4$) in a vacuum line.

The obtained gas ($CO_2$ + water vapour) is then dried in a vacuum line, and reduced with hydrogen ($H_2$), using 2 mg of Fe powder as a catalyst. The obtained mixture of carbon and iron is then pressed into special aluminium holder, according to the description provided by Czernik J., Goslar T., 2001, *Radiocarbon*, 43, 283-291.

#### 2.4.1.2.3. Accelerator mass spectrometry (AMS) $^{14}C$ measurement

Measurements described in this point, are performed in the AMS $^{14}C$ Laboratory of the A. Mickiewicz University in Poznań. Cooperation between the Poznań Radiocarbon Laboratory

and the AMS $^{14}C$ Laboratory is regulated by the Agreement between Foundation of the A. Mickiewicz University and the A. Mickiewicz University.

Content of $^{14}C$ in a sample of carbon is measured using the spectrometer "Compact Carbon AMS" (produced by: National Electrostatics Corporation, USA) described in the paper: Goslar T., Czernik J., Goslar E., 2004, *Nuclear Instruments and Methods B*, 223-224, 5-11). The measurement is performed by comparing intensities of ionic beams of $^{14}C$, $^{13}C$ and $^{12}C$ measured for each sample and for standard samples (modern standard: "Oxalic Acid II" and standard of $^{14}C$-free carbon: "background"). In each AMS run, 30-33 samples of unknown age are measured, alternated with measurements of 3-4 samples of modern standard and 1-2 samples of background. In case, where organic samples are dated, the background is represented by coal, while in case of carbonate samples, the background is represented by the sample IAEA C1.

#### 2.4.1.2.4. Calculation of $^{14}C$ age

Conventional $^{14}C$ age is calculated using correction for isotopic fractionation (according to Stuiver, Polach 1977, *Radiocarbon* 19, 355), basing on ratio $^{13}C/^{12}C$ measured in the AMS spectrometer simultaneously with the ratio $^{14}C/^{12}C$ (note: the measured values of $\delta^{13}C$ depend on isotopic fractionation during $CO_2$ reduction and isotopic fractionation inside the AMS spectrometer, and as such, they cannot be compared with values of $\delta^{13}C$ determined with conventional mass spectrometers on gas samples). Uncertainty of calculated $^{14}C$ age is determined using uncertainty implied from counting statistics, and also spread (standard deviation) of partial $^{14}C/^{12}C$ results, whichever is bigger. Uncertainties of $^{14}C/^{12}C$ ratios measured on standard samples are additionally taken into account. The 1-sigma uncertainty of conventional $^{14}C$ age given in our reports, is the best estimate of the total uncertainty of measurement.

### 2.4.1.3. Procedures of AMS $^{14}C$ dating used in the Laboratoire des Sciences du Climat et de l'Environnement - Plateforme Nationale LMC14

#### 2.4.1.3.1. Chemistry of organic matter

Samples marked A are treated in an excess of 0.5N hydrochloric acid for several hours at 80°C to remove carbonates and then rinsed with ultrapure water to neutral pH.

Different amounts, depending on the TOC% of the samples, are taken in order to obtain, after combustion, a volume of $CO_2$ containing approximately 1 mg of carbon. The sample is burned in the presence of about 500 mg of copper oxide and silver wire for 5 hours at 835°C.

#### 2.4.1.3.2. Graphite reduction protocol

$CO_2$ is reduced by hydrogen in the presence of iron powder at 600°C. The mass of iron is equal to 3 times the mass of carbon with a minimum value of 1.5 mg and a maximum value of 4 mg. Carbon is deposit on the iron powder and the whole is then pressed into a support for measurement by AMS.

#### 2.4.1.3.3. Measurement and analysis protocol

The $^{14}C$ activity of the sample is calculated by comparing the intensities measured sequentially beams of $^{14}C$, $^{13}C$ and $^{12}C$ from each sample with those of $CO_2$ standards prepared from the

reference oxalic acid HOxII. It is expressed in pMC (percent Modern Carbon) normalized to a delta $^{13}C$ of -25 per thousand.

The radiocarbon ages are calculated according to Mook and Van der Plicht (Radiocarbon 14, 1999, p. 227) in correcting the $\delta^{13}C$ fractionation calculated from the $^{13}C/^{12}C$ ratio measured on ARTEMIS.

The $\delta^{13}C$ used includes fractionation occurring both during sample preparation only during SMA measurement. It is also dependent on the transmission of the installation, namely the $^{13}C/^{12}C$ measured at the output of the ARTEMIS mass spectrometer compared to the value of $^{13}C/^{12}C$ at source output. These values depend on the beam at injection, current and emission. The $\delta^{13}C$ measured by ARTEMIS can not be compared to the $\delta^{13}C$ measured on a spectrometer massive. Since $\delta^{13}C$ values are corrected to a standard, they do not affect the age measurement of $^{14}C$.

### 2.4.1.4. Calibration of $^{14}C$ age

In addition to natural variation, the atmospheric $^{14}C$ levels have been affected by human activity (Walker, 2005). Over the past 250 year, the burning of fossil fuels has liberated large quantities of $^{12}C$ into the atmosphere (Houghton et al., 2001, *in* Walker, 2005). These quantities of $^{12}C$ have diluted $^{14}C$ levels and cause some variations in the atmospheric $^{14}C$ concentration and consequently profound effects for radiocarbon dating (Walker, 2005). A comparison between $^{14}C$ and uranium-series dates on fossil coral, indicate that radiocarbon dates are around 3000 years younger than 'true' ages at 15 000 $^{14}C$ year BP, and around 4000 year younger at 20 000 $^{14}C$ year BP (Stuiver et al., 1998, *in* Walker, 2005). For this reason it is important to convert the radiocarbon date into calendar time or $^{14}C$ year BP.

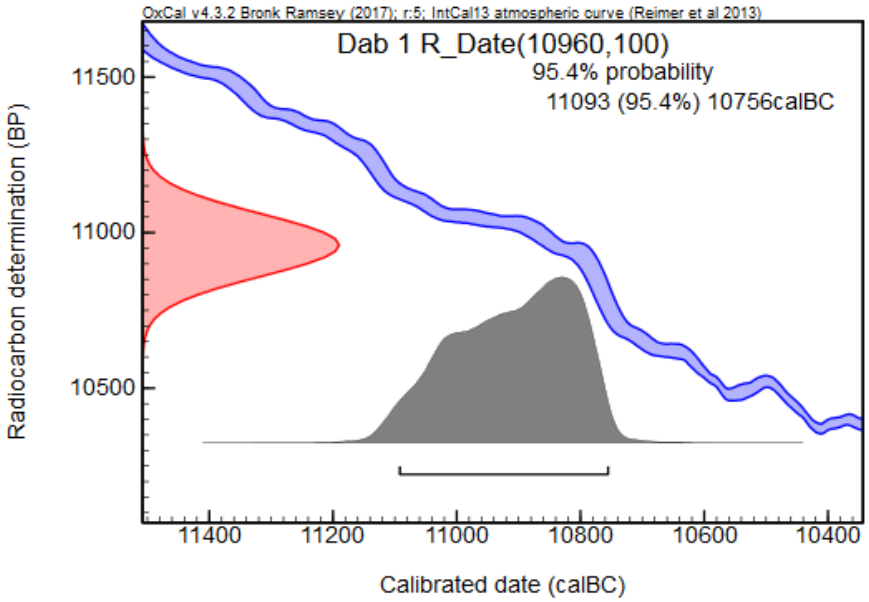


*Fig. 2.3. OxCal calibration curve showing one probability range - sample from East Abu Zabd. The sample code is Dab 1. $^{14}C$ date is 10960 ± 100 yr BP. The curve indicates only one probability (95.4%) with calendar age ranging between 11093 and 10756 yr **BC**. The average of this range is 10925 yr BC (equivalent to **12942 yr BP**).*

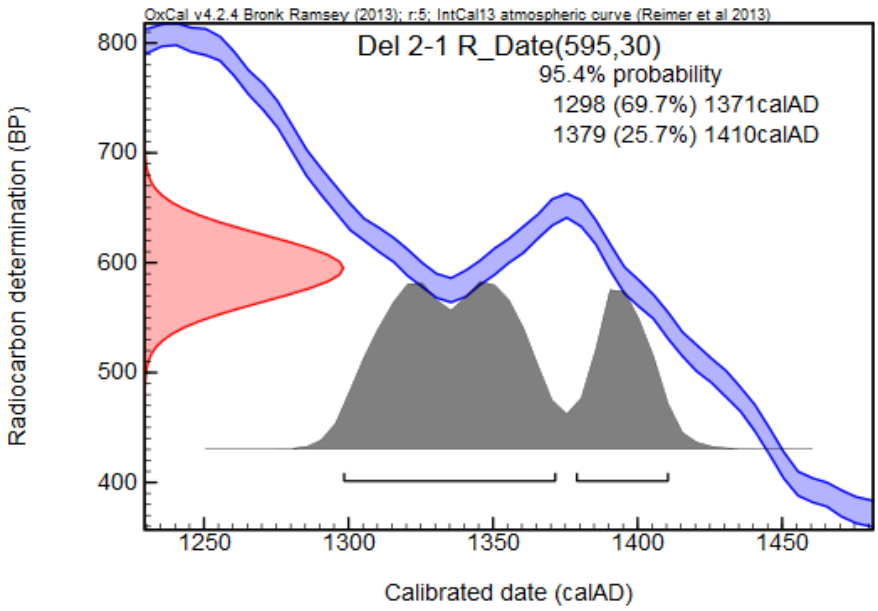


*Fig. 2.4. OxCal calibration curve showing two probability ranges - sample from Dilling. The sample code is Del 2-1. $^{14}C$ date is 595 ± 30 yr BP. The curve shows two probabilities (69.7 % and 25.7 %) with calendar age ranges of 1298 – 1371 and 1379 – 1410 yr **AD**. The average of these two ranges is calculated from the small value of the first probability (1298) and the big value of the second probability (1410) it is 1354 yr AD (equivalent to **663 yr BP**).*

Various methods and programs have been developed for the calibration of radiocarbon dates, of which the most important are: the Dendrochronological calibration method, INTCAL calibration program, and OxCal calibration program.

The online OxCal calibration program has been used in this study. The program is always developing through time, the present version of this program is 4.3 and works with IntCal13. Both, version 4.3 and the old one 4.2 have been used during this study. A variety of different chronological models can be included in the analysis. The information for such analysis can be entered using the user interface or in the form of text command files. The calibration output is usually given in term of probability. The accuracy of this program have maximum probability of 95.4% which may be represented in one probability or more. Each probability expresses the calibrated $^{14}C$ age in term of calendar age range either "*anno Domini*" **AD** or "*before Christ*" **BC** then the average of this range will consider the age of the sample. In turn, this average age can be converted into **BP** "*before present*" calendar age. Figures 2.3 and 2.4 show two calibrated ages for two samples among the analyzed samples for this study.

### 2.4.2. Grain size analysis

Grain size is the most fundamental property of sediment particles, affecting their environment, transport and deposition. Grain size analysis therefore provides important clues to the sediment provenance, transport history and depositional conditions (Folk and Ward, 1957).

The original aims of this grain size investigation is to determine the origin of the Kordofan sand (aeolian or fluviatile origin), to understand the transport direction, and to have an idea about the transportation mode(s).

Samples for grain size analysis were prepared using standard techniques as described by Folk (1974) to determine grain size distribution. The samples were dry-sieved at a sieve sets ranges from 2.83 to 0.074 mm opening for five minuts, the retained in each sieve is weighted using electronic balance of 0.1g sensitivity. Material smaller than 0.074 mm were not analyzed, instead, a single weight percent is given and plotted as one size then the curves completed according to their directions to include the percentages of the silt and clay contents (material < 0.063 mm) to help in the approximate evaluation of the percentages for all materials.

The cumulative curves of the samples were plotted manually using the free drawing computer program Surfer 11. Graphical statistical parameters (mean grain size M*Z*, sorting $\sigma_I$, skewness SK*I*, and kurtosis K*G*) were calculated for each sample following Folk and Ward (1957) (equations 2.1 – 2.4). Mean grain size represents the average grain size; sorting (as a standard deviation) refers to the uniformity of the sediment; and skewness measures the asymmetry of the size distribution curve Folk (1974).

$$M_Z + \frac{\emptyset_{16}+\emptyset_{50}+\emptyset_{84}}{3} \quad \text{..... (2.1)}$$

$$\sigma_I = \frac{\emptyset_{84}-\emptyset_{16}}{4} + \frac{\emptyset_{95}-\emptyset_5}{6.6} \quad \text{..... (2.2)}$$

$$SK_I = \frac{\emptyset_{16}+\emptyset_{84}-\emptyset_{50}}{2\,(\emptyset_{84}-\emptyset_{16})} + \frac{\emptyset_5+\emptyset_{95}-\emptyset_{50}}{2\,(\emptyset_{95}-\emptyset_5)} \quad \text{..... (2.3)}$$

$$K_G = \frac{\emptyset_{95}-\emptyset_5}{2.44\,(\emptyset_{75}-\emptyset_{25})} \quad \text{..... (2.4)}$$

Where: $\mathbf{M_Z}$ is the mean size; $\boldsymbol{\sigma_I}$ is the inclusive graphical standard deviation; $\mathbf{SK_I}$ is the inclusive graphic skewness; $\mathbf{K_G}$ is the graphic kurtosis; and $\boldsymbol{\emptyset_n}$ is the diameter where n% of the sample is greater than this diameter.

Description of sorting, skewness, and kurtosis after Folk (1974) has been used for better understanding of these graphical parameters.

The cumulative percentages of the grain size classification after Folk (1974), were calculated from each curve and plotted in vertical diagrams against their depths to understand their vertical distribution in each section and to have an idea about wind energy fluctuation through time. Horizontal diagrams were also plotted to understand the spatial variations in wind energy (from NE to SW). As a matter of fact, in areal studies of sand sheets it is useful to know which direction the sand is moving, and to this end an areal study of mean grain size would be of critical importance. One of the ways to proceed would be to lay a sampling grid over the dune field and see if there were any systematic regional changes in grain size (Folk 1974).

Log-probability curves have been prepared according to Visher (1969), in order to understand the mode(s) of sediments transportation (suspension, saltation, traction) in each sample, and therefore, in each part of the studied sections. Moreover, geographical profiles of the modes of transport across section were used to confirm the variability of the transport energy.

The grain size analysis hase been conducted at the Department of Geology, University of Kordofan, El Obeid, Sudan.

### 2.4.3. Analysis of paleoclimate proxies

### 2.4.3.1. Palynological analysis

Sporomorphs data are used for a variety of Quaternary applications including geochronology, biostratigraphy, palaeoecology, palaeoclimatology and archaeology (Traverse, 2008). Faegri and Iversen (1989) indicated that the reliability of palynology as a palaeoenvironmental tool is a function of :

• the robust preservation of pollen grains and their resistance to decay,

• the wide dispersal of pollen grains and their presence in a broad range of environments such as lakes, peat deposits, soils, colluvium, alluvium, estuarine deposits, ocean floor and faecal material,

• the abundant production of pollen grains,

• the relative ease of identification as a result of the distinctive structural pattern of the exine (the outer layer of the wall of a palynomorph), and

• the direct link between the identification of pollen grains and the parent plant (Quick, 2013).

It has been established that a combination of a few prominent "indicator" taxa can be characteristic of certain vegetation types and environmental conditions (Scott and Cooremans, 1992). The so-called indicator approach therefore uses the presence (or absence) of indicator taxa, whose modern ecological tolerances are well understood as a basis for reconstructing palaeoenvironments (Quick, 2013). This approach assumes that the limiting conditions in the past were the same as they are today, an assumption thet most probably holds for the time period in question "i.e. the late Pleistocene and Holocene periods" (Quick, 2013). At the beginning of sample preparation, at least tow samples per section were prepared to confirm the existence of palynomorphs and to decide the continuation of the preparation.

The samples have been analyzed using standard palynological preparation techniques established in the Petroleum Laboratories Research and Studies (PLRS), Khartoum, Sudan, by Mr. Abdelbasit Mustafa and Miss. Malaz Mohammed-Ali.

Chemical processing of palynological samples and preparation of slides were carried out at the Petroleum Laboratories Research and Studies (PLRS), Khartoum. The procedure followed in the preparation of palynological slides was largely adapted from the scheme established at PLRS. The following paragraphs outline the steps of this scheme:

Twenty grams of each sample were weighed and crushed to the size of about 2 mm. Samples were then placed in a plastic beaker and thoroughly washed under running water in order to get rid of mud additives and other surface contaminants.

Concentrated hydrochloric acid (35%) was carefully used to remove the carbonates. As there was an abundance of silica in the analyzed samples, about 60 ml of cold concentrated hydrofluoric acid (40%) was carefully added to dissolve the silica and the silicate minerals. Sometimes a mixture of HF and HCl acids in the ratio of 1:3, respectively, wazs used to remove the fluorides that might have formed during the HF treatment.

For quick removal of the acids, samples were placed in a centrifuge to achieve rapid settling of the organic residue. A further concentration of some residues was achieved by sieving using mesh widths between 10-15 μm. The residue was then placed in a clean 50 ml polythene

(polyethylene) centrifuge tube. Few drops of HCl were added followed by a solution of zinc chloride (Zn $Cl_2$) of density 2.2 g/cm the tube was then centrifuged at 2200 rotations/second for 15 minutes. The organic part of the residue appeared as a dark layer floating on the top, while the heavy minerals settled at the bottom of the tube. The floating layer was carefully pipetted and washed.

Two or three drops of residue, mixed with few drops of Polyvinyl alcohol (PVA) were evenly spread over a cover slip and placed on a hot plate for 15 minutes to dry. A drop of petropoxy was gently placed in the central portion of each slide and left for ten seconds to get rid of any bubble, which may have formed in the resin. A cover slip was gently lowered allowing the resin to flow to all edges of the slide. The slide was then left for 15 minutes on the hot plate to dry. Two sdes per each sample were made and labeled.

Two slides per samples have been scanned and the various palynomorph types are counted. The counted and identified palynomorphs were classified into major climatic groups and plotted in vertical evolution and geographic distribution, in order to understand the chronological and geographic climate evolution.

#### 2.4.3.2. Stable isotopes

The stable isotopes of many elements are fractionated during changes in their states of aggregation and by chemical reactions between compounds which the elements occur. The extent of fractionation of two isotopes of the same element is controlled primarily by the difference in their masses and by the temperature of the environment (Faure and Mensing, 2005).

Forty-nine samples from five sections were analyzed for oxygen and carbon isotopes. Samples of three sections are gastropod shells, while samples from two sections are calcareous nodules.

***Preparation of gastropod shells.*** Initial cleaning of the outer shell surface with normal water removed any adhering sediment and any other contaminations. Shells were then coarsely crushed and the internal surfaces cleaned using normal water followed by ultrasonic cleaning in distilled water for10 min. The ultrasonic cleaning step is repeated three times. Samples are then dried at 60°C for 24 hours. An agate mortar and pestle was used to powder samples and only 1 to 2 mg/sample sent to the laboratory to determine the carbonate mineralogy by X-ray diffraction.

***Preparation of calcareous nodules.*** Initial cleaning of the outer nodule surface with normal water to remove any adhering sediment and any other contaminants. Further advanced preparation was performed at the Institute of Mineralogy and Geochemistry, University of Lausanne by M. Jorge Spangenberg. During this advanced preparation, the calcareous nodule samples were meticulously examined under a binocular microscope to eliminate the organic matter or soil matrix components contaminating the samples, then samples were powdered using an agate mortar samples.

Isotopic analysis of carbon and oxygen was performed at Lausanne Laboratory (Switherlad) by M. Jorge Spangenberg. The stable carbon and oxygen isotope composition of the gastropod shells and calcareous nodules were determined using a Thermo Fisher GasBench II connected to a Delta Plus XL isotope ratiomass spectrometer (IRMS). The stable oxygen isotope ratios

are reported in the delta notation as the permil (‰) deviation relative to theVienna PeeDee Belemnite (VPDB) and Vienna Standard Mean Ocean Water standard (VSMOW), while the stable carbon isotope ratios are reported in the delta notation as the permil (‰) deviation relative to theVienna PeeDee Belemnite (VPDB).

#### 2.4.3.2.1. Oxygen isotopes

Oxygen (O) is the most abundant chemical element in the crust of the earth. It has three stable isotopes $^{16}O$, $^{17}O$, and $^{18}O$ with abundance of 99.726%, 0.038%, and 0.200%, respectively. $^{18}O$ is 12.5% heavier than $^{16}O$ (Faure and Mensing, 2005).

The isotopic composition of O and of all other elements whose isotopes are fractionated is usually expressed as the ratio R of the isotopic abundance of the heavy isotope divided by the abundance of the light isotope. Therefore, *R* is defined in terms of the numbers of atoms rather than in terms of the masses of the isotope. In the case of O, *R* is defined by the abundance (Equation 2.5).

$$R = \frac{^{18}O}{^{16}O} = \frac{0.200}{99.762} = 0.002004 \quad \text{..... (2.5)}$$

The isotope ratio of the oxygen is measured by mass spectrometry and is expressed relative to standard mean ocean water (SMOW) (Faure and Mensing, 2005). However, the standard used for the samples of this study is Vienna Pee Dee Belemnite (VPDB). The use of a standard reduces systematic errors in measurements made on different mass spectrometers and permits *R* value to be expressed in terms of parameter called delta (δ) as defined in equation (2.6).

$$\delta^{18}O = \left(\frac{R_{spl} - R_{std}}{R_{std}}\right) \times 10^3‰ \quad \text{..... (2.6)}$$

Where: $R_{spl} = {}^{18}O/{}^{16}O$ ratio of the sample; and $R_{std} = {}^{18}O/{}^{16}O$ ratio of the standard

$\Delta^{18}O$ is the difference between the *R* value of the sample and the standard expressed in terms of permille relative to the *R* value of the standard.

The $\delta^{18}O$ parameters may be positive, negative, or zero. A positive $\delta^{18}O$ value indicates that the sample has a higher $^{18}O/^{16}O$ ratio than the standard, which is expressed by stating that sample is enriched in $\delta^{18}O$ relative to the standard. A negative $\delta^{18}O$ value indicates that the sample has a lower $^{18}O/^{16}O$ ratio than the standard and that sample is depleted in $\delta^{18}O$ relative to the standard. In other words, the isotopic composition of the oxygen in the sample is always expressed in terms of enrichment or depletion of the heavy isotope ($^{18}O$).

Since the analyzed samples were collected systematically along sections, then the corresponding $\delta^{18}O$ values were plotted to show the vertical evolution of the oxygen $\delta^{18}O$, which may be then interpreted in terms of climatic evolution through time.

#### 2.4.3.2.2. Carbon isotopes

Carbon is the fourth in abundance among the elements of the solar system after H, He and O (Anders and Grevesse, 1989). Carbon has two stable isotopes: $^{12}C$ and $^{13}C$ with an abundance of 98.90% and 1.10%, respectively. Consequently, the $^{13}C/^{12}C$ ratio is 1.083612 and the atomic weight of C is 12.01103. The mass of $^{13}C$ is 8.36% greater than that of $^{12}C$, which causes the C isotopes to be fractionated by chemical and biological processes in nature (Faure and Mensing, 2005).

The isotopic composition of C is expressed by the $\delta^{13}C$ parameter (Equation 2.7).

$$\delta 13_C = \left( \frac{\left({}^{13C}/_{12C}\right)_{spl} - \left({}^{13C}/_{12C}\right)_{std}}{\left({}^{13C}/_{12C}\right)_{std}} \right) \times 10^3‰ \quad \text{..... (2.7)}$$

where the standard is **PDB**.

Therefore, positive $\delta^{13}C$ values signify that sample is enriched in $^{13}C$ relative to the standard, whereas negative $\delta^{13}C$ values imply depletion in $^{13}C$. The fractionation factor for C isotopes expressed in equation (2.8) as follows:

$$\alpha_b^a(13_C) = \frac{\mathrm{R_a}}{\mathrm{R_b}} \quad \text{..... (2.8)}$$

where ***a*** and ***b*** are C-bearing compounds or phase in isotopic equilibrium at a specified temperature and *R* is the isotopic $^{13}C/^{12}C$ ratio. However, the isotopic composition of C in biogenic carbonate and organic compounds is not a reliable recorder of the environmental temperature because these kinds of compounds do not achieve isotopic equilibrium with the major C reservoir on Earth. When green plants absorb $CO_2$ molecules during photosynthesis, they prefer $^{12}C$ over $^{13}C$, which explain why organic matter of photosynthesis plants and herbivorous and carnivorous animals has negative $\delta^{13}C$ values. On the other hand, the $\delta^{13}C$ values of marine calcite and aragonite are close to zero because the BDP standard is itself a marine carbonate (Faure and Mensing, 2005).

The obtained $\delta^{13}C$ values were plotted in vertical evolution along the targeted sections and then $\delta^{13}C$ was translated into environmental evolution through time.

### 2.4.3.3. Major elements geochemistry

Geochemical analysis of major elements has been applied in this study as a proxy for climate evolution in the study area. The chemical index of alteration (CIA) is the main Climofunction applied in this study. Nesbitt and Young (1982) proposed the use of chemical index of alteration (CIA) as a scale of the degree of rock weathering. It is calculated by taking the molar ratio of $Al_2O_3$ to $Al_2O_3$ + CaO + $Na_2O$ + $K_2O$ (alumina, lime, soda and potash) multiplying it by 100 (Equation 2.9). The CIA measures the degree of weathering in the source area of the analyzed sediment (Nesbitt and Young, 1982; Madhavaraju et al., 2016).

$$CIA = \frac{\mathrm{Al_2O_3}}{(\mathrm{Al_2O_3} + CaO^* + \mathrm{Na_2O} + \mathrm{K_2O})} \times 100 \quad \text{..... (2.9)}$$

where **CaO*** is the amount of CaO incorporated in the silicate fraction of the rock (Nesbitt and Young, 1982; Madhavaraju et al., 2016).

According to Madhavaraju et al. (2016), the CaO*content has been calculated using the following methods: a) if the content of CaO was less or equal to the $Na_2O$ content, CaO value will be compensated for further calculation, b) if the CaO content is higher, it will be substituted by $Na_2O$ value in the above equation.
According to Sheldon et al. (2002) the dgree of chemical weathrering in soil due to hydrolysis increases with available precipitation and temperature, the calculated CIA values plotted against corressonding sections.

Since the intensity of weathering depends, in part, on precipitation, Sheldon et al. (2002) developed an empirical relationship relating mean annual precipitation (MAP) to chemical

index of alteration without potassium (CIA-K) (Equation 2.10). Because diagenesis can yield elevated potassium (K) concentrations in paleosols, this chemical index omits K (Adams et al., 2011).

$$P = 221e^{0.0197(CIA-K)} \quad \text{..... (2.10)}$$

In order to have an idea about the temperature, the empirical relationship of Sheldon et al. (2002) between mean annual temperature (MAT) and molecular weathering ratio of $K_2O+Na_2O$ to $Al_2O_3$, have been applied (Equation 2.11).

$$T = -18.516(S) + 17.298 \quad \text{..... (2.11)}$$

where ***S*** is the molecular weathering ratio ($K_2O+Na_2O/Al_2O_3$).

X-ray fluorescence analysis carried out at the chemical laboratory of the Geological Research Authority of Sudan (GRAS), under supervision of the chief chemist Emtithal Ali.

***Samples preparation for X-ray fluorescence analysis***

The sediment samples are firstly air-dried, then each sample is sieved through a sieve of 63 µm size. The pressed powder method is applied for sample preparation. Pressed pellets are prepared by pressing loose powder of the sieved sample filled in a hard steel ring, very smooth inside, using a set of dies and pressing machine.

Pellets are generally pressed at 15 to 20 tons per square inch, which produces a flat smooth, dense sample for testing. Once the pellet is held at this pressure for about 30 seconds the pellet is carefully removed. The average thickness of the pellets is about 3 mm. The ring and set of dies are washed thoroughly with first tap water then ethanol acid, and dried to prevent contamination.

### 2.4.3.4. Clay mineralogy

Millot (1965) distinguished three principal processes to account for the genesis of clay minerals, which may occur at different points in the geochemical cycle including weathering or soil formation at the earth's surface. These processes are: (a) detrital inheritance whereby, for soils, clay minerals are inherited from pre-existing parent rock or weathered materials; (b) transformation where the essential silicate structure of the clay mineral is maintained to a large extent, but with major change in the interlayer region of the structure; and (c) neoformation, where the clay mineral forms through crystallization of gels or solutions (Wilson, 1999).

Inherited soil clays may be of an extremely diverse and complex nature, reflecting both the variety of the parent rock as well as the transformation and neoformation processes that may have occurred in previous weathering environments (Wilson, 1999). Therefore, the clay mineralogy has been used as climate proxy for the weathering experienced by the source area of the analyzed sediments.

The clay mineral assemblages are controlled by a number of factors (climate, time, parent material, topography, soil-profile type, transport processes, burial diagenesis) (Singer, 1984; Hillier, 1995, *in* Kemp et al., 2016).

The principle of using the clay mineralogy as a climate proxy is based on the fact that each clay mineral assemblage develops in a preferred environment (physico-chemical conditions), and that predominance of a specific assemblages reflects high degree of the required environmental

conditions, leading to climatic information and interpretation. For instance, kaolinite and smectite are considered indicators of humid conditions, possibly tropical climate (Kemp et al., 2016; Madhavaraju et al., 2016), smectite and illite indicate warm climate with alternating wet and dry seasons (Madhavaraju et al., 2016), the interstratified smectite illite (I-S) suggests seasonal tropical climate with a prolonged dry season (Kemp et al., 2016), and illite and chlorite form under physical weathering conditions (Madhavaraju et al., 2016).

In this study, the quantitative results of the clay mineralogy have been plotted in vertical evolution and translated into climatic information to describe the weathering conditions in the source area of the analyzed sediments.

Clay mineralogy analysis and interpretation has been performed in the ISTerre laboratory in Grenoble, France, with the priceless help of Dr. Nathaniel Findling and Dr. Bruno Lanson.

***Samples preparation and purification of clay.*** The objective of the treatment of the samples is to obtain a suspension of the desired size fraction. To do that, firstly the grain size of the samples is reduced by seaving them through sieve of 63 μm size. A suspension of 25-30 g/L is prepared in centrifuge bottles, each bottle being filled with pure water and placed in an ultrasonic bath to enhance particle disaggregation.

***Size fractionation by centrifugation with a swinging-bucket rotor***

- *Particules < 2 μm fraction.* To do so the clay suspension (25-30 g/L) is placed in a 500 ml centrifuge pot and centrifuged for 8 minutes at 700 rpm. The top 7 cm of the suspension are collected using a Pasteur pipette whose tip is curved and a water pump (or vacuum pump). This supernatant is kept in a 5 liters beaker. The remaining suspension is diluted with pure water. Centrifuge pots are shaken to put the remaining solid phase back in suspension. Then centrifuge the clay suspension again.

$CaCl_2$ 1M (10 ml per liter) is added to flocculate the particles. Decant left overnight. The next day the clear supernatant is removed by siphoning, and the remaining suspension is centrifuged at high speed (4300 rpm for 15 minutes). The clear supernatant is then removed and the < 2 μm clay fraction is resuspended in pure water and kept at 4°C.

- *Particules below 0.2 μm.* The suspension of the < 2 μm clay fraction (5 g/Lmax) is used in 500 ml centrifuge pots and placed on a shaking table for at least 2 days at 100 rpm. Then the suspension is centrifuged during 40 minutes at 4000 rpm. The top 7 cm of the suspension are collected using a Pasteur pipette and kept in a 5 liters beaker.

The remaining suspension is diluted with pure water. Centrifuge pots are shaken to put the remaining solid phase back in suspension. Ultrasonic bath is used when necessary. Then the clay suspension is centrifuged again for 40 minutes at 4000 rpm to collect again the top 7 cm.

$CaCl_2$ 1M (10ml per liter) is added to flocculate the particles. Decant left overnight. The next day the clear supernatant is removed by siphoning and the remaining suspension is centrifuged at high speed (4300 rpm for 15 minutes). The clear supernatant is then removed and the < 0.2 μm clay fraction is resuspended in pure water and kept at 4°C.

***Mineralogical purifications.*** This process includes carbonate removal and removal of organic matter. Sodium acetate buffer solution at pH = 5 is used to remove the carbonate, while Hydrogen peroxide ($H_2O_2$) is used to remove the organic matter.

***Preparation of homoionic clay separates ($Na^+$ or $Ca^{2+}$).*** Saturation of a clay separate with Na/Ca (or other cations) is achieved by washing cycles with the desired solutions NaCl. Centrifugation and removal of the supernatant. The first three cycles are performed for 24 h (room temperature) with concentrated solutions (0.5-1.0 M), and a minimum of three additional cycles are performed with a solution of the desired molarity. Samples are kept on a shaking table during the 24 h contact time so as to optimize the solid-solution contact.

# III. STRATIGRAPHY AND SEDIMENTOLOGY

## 3.1. Stratigraphy

A total of twenty-four sections of the Late Quaternary sediments, distributed over five sectors, has been studied in detail in order to build a general stratigraphic picture of the area. Surficial survey was carried out in some sites, where no suitable sections were available for study. The location of the studied sites and their geographic information are given in Figure 3.1 and Table 3.1. The sections will be analyzed according to five areas, corresponding to the Dilling area to the Southeast, the El Fula-Abu Zabad area to the Southwest, the En Nahud-El Khowei area to the West, the El Obeid-South El Obeid in the East, and the North Bara-Sodari sector to the North (Fig. 3.1).

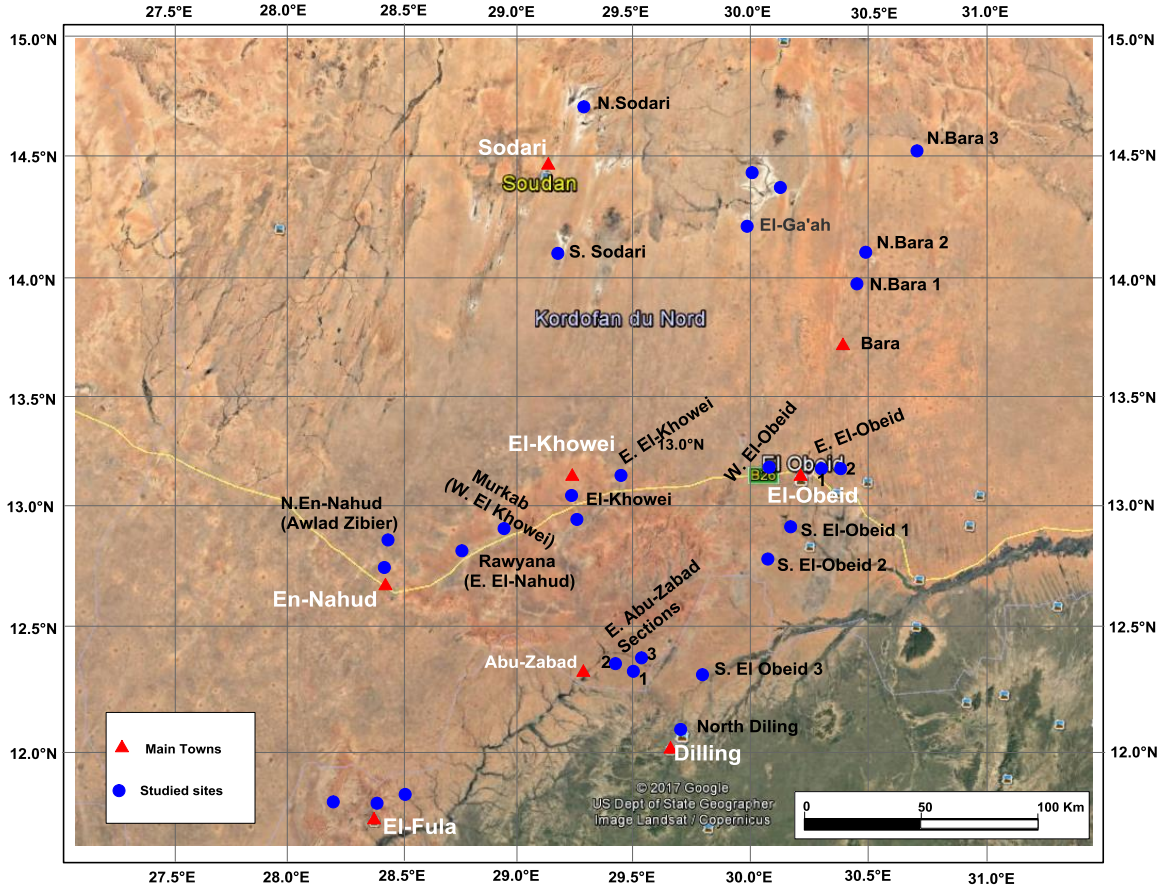


*Fig. 3.1. Location of the studied sections.*

Four stratigraphic units have been distinguished across the study area. The first unit is found in all areas, except in the Dilling sector. The second unit is found in the Dilling, El Khowei-En Nahud and North Bara-Sodari areas. The third unit crops out in the El Obeid-South El Obeid and Dilling sectors. The upper or fourth unit is detected in the whole area.

### 3.1.1. Stratigraphy of the Dilling area

Three sections have been studied in the Dilling area. These are the Dilling section in the main Khour Abu-Habil seasonal river bank, and two sections North of the Dilling town (North Dilling 1 and 2), along another branch of Khour Abu-Habil.

*Table 3.1: Geographical information on the studied sections.*

| Section | Longitude / deg.min.sec. | Latitude / deg.min.sec. | Elevation / m asl |
|---|---|---|---|
| Dilling | 29 39 22.5 | 12 02 23 | 680 |
| North Dilling1 | 29 39 26.2 | 12 05 0.9 | 670 |
| North Dilling2 | 29 39 46.5 | 12 05 3.96 | 669 |
| El Fula | 28 22 55 | 11 43 58 | 529 |
| East El Fula | 28 22 48.7 | 11 44 1.7 | 513 |
| West El Fula | 28 17 52.3 | 11 41 06 | 500 |
| East Abu Zabad1 | 29 28 16 | 12 20 49 | 617 |
| East Abu Zabad2 | 29 24 16 | 12 21 11 | 614 |
| East Abu Zabad3 | 29 28 47 | 12 20 59 | 611 |
| East El Obeid1 | 30 17 43.4 | 13 12 55.8 | 559 |
| East El Obeid2 | 30 18 21.4 | 13 12 06.1 | 564 |
| West El Obeid | 29 59 59.7 | 13 10 3.7 | 585 |
| South El Obeid1 | 30 08 31.2 | 12 56 44.4 | 536 |
| South El Obeid2 | 30 04 47.7 | 12 48 13.3 | 557 |
| South El Obeid3 | 29 45 45.4 | 12 19 24.4 | 595 |
| East El Khowei | 29 42 10.7 | 13 06 35.8 | 624 |
| El Khowei | 29 12 53.2 | 13 03 20.8 | 628 |
| West El Khowei | 28 54 15.9 | 12 55 34 | 625 |
| East En Nahud | 28 43 25.1 | 12 49 49 | 611 |
| North Bara1 | 30 25 55.3 | 13 51 58.5 | 484 |
| North Bara2 | 30 28 38.7 | 14 04 36.1 | 478 |
| North Bara3 | 30 45 13.1 | 14 30 48.3 | 455 |
| El Ga'ah well | 29 59 12.6 | 14 14 34 | 468 |

The succession in the Dilling area is composed of three main stratigraphic units (Fig. 3.2). Considering that the lower unit is missing in this sector, the second unit directly overlies the basement rocks, which crops out extensively in this area. The third unit overlies the second one with a conformable contact. The upper unit overlies the third one with an unconformable contact.

**Second unit**. This unit overlies unconformably foliated granitic rocks. It is formed of breccia or conglomerate comprising reworked rock fragments, as well as some reworked calcareous nodules. Its maximum measured thickness is ≈ 80 cm.

**Third unit.** The third unit is formed of dark grey, organic-rich, shaly, fine sand sediments, containing some gravels, and *in situ* developed calcareous nodules. The maximum measured thickness of this unit is ≈ 110 cm.

**Fourth unit**. The Upper unit overlies unconformably the third unit. A basal conglomerate bearing reworked calcareous nodules is overlain by sandy shales alternating with sand sediments beds, and containing locally calcareous nodules. The contacts between these beds are conformable, either abrupt or progressive. This unit has a maximum measured thickness of ≈ 375 cm.

**Age constraints**

The organic-rich shaly sand sediments bed of the third unit yielded $^{14}C$ ages of 4870 ± 30 and 4133 ± 30 cal. yr BP (Fig. 3.2). Charcoal fragment within the basal conglomerate/breccia of the

upper unit yielded a $^{14}C$ age of 7682 ± 110 cal. yr BP. Charcoal and wood fragments from the upper part of the Upper unit provided $^{14}C$ ages of 759 ± 30, 663 ± 30 and 246 ± 30 cal. yr. BP.

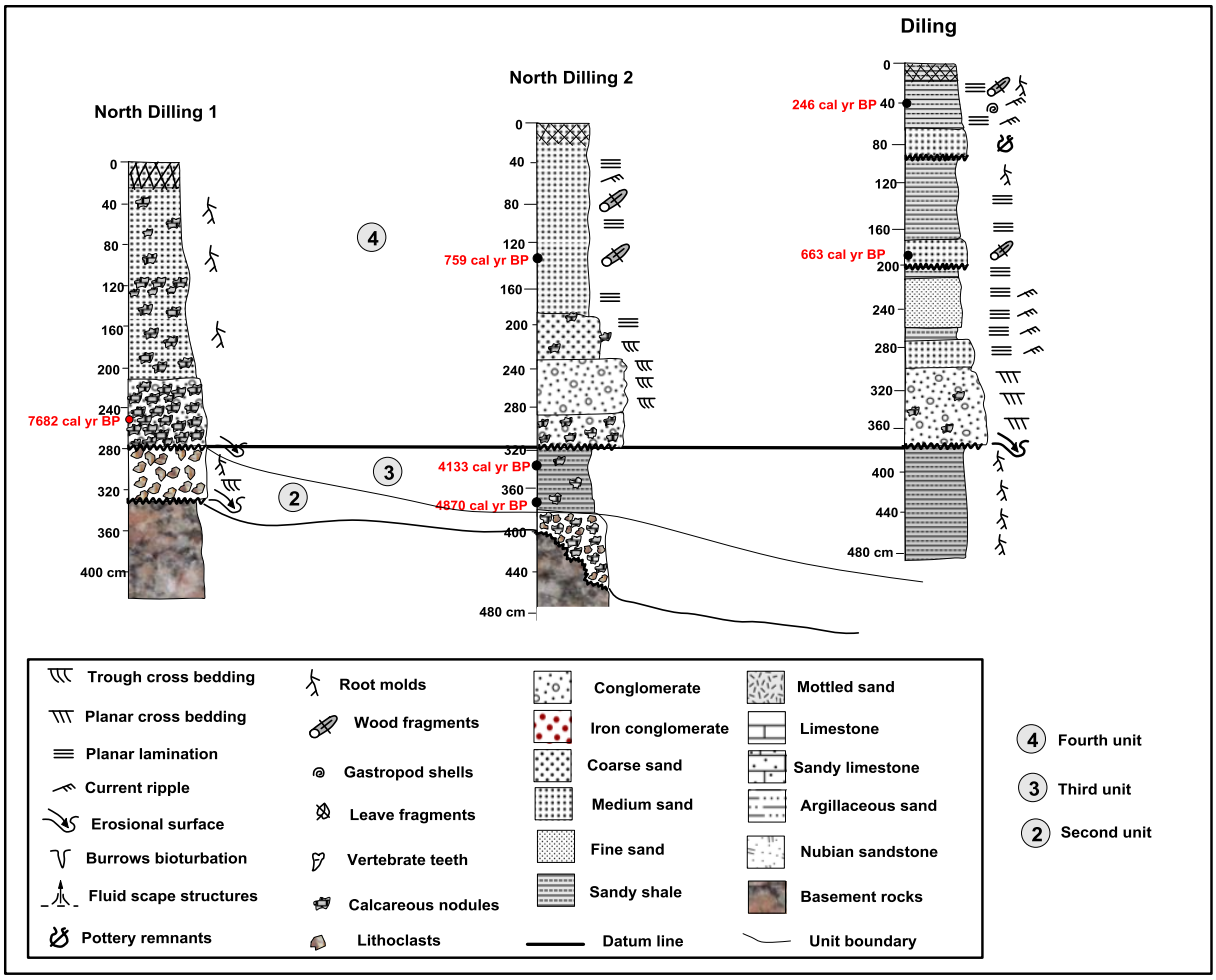


*Fig. 3.2: Stratigraphic units of the Dilling area.*

### 3.1.2. Stratigraphy of the Abu Zabad – El Fula sector

Six sections have been studied in this sector, among which three are located East of the Abu Zabad town, and three others around the El Fula town. In this sector, Late Quaternary sediments are composed of three main stratigraphic units (lower, third, and upper) (Fig. 3.3).

**Lower unit.** The Lower (first) unit overlies the Cretaceous Nubian Sandstone or the Basement rocks. The contact with the pre-Quaternary rocks is abrupt and unconformable, and is locally underlined by coarse grained conglomerate beds (East of El Fula, East of Abu Zabad). It exhibits mostly mottled silt or fine sand sediments, rich in calcareous nodules and locally in poorly sorted gravels. This unit locally includes conglomerates found either in thick beds (east of El Fula), or in thin lenses in mottled sand sediments (East of Abu Zabad). The maximum measured thickness of this unit is ≈ 450 cm.

**Third unit.** The third unit overlies the first one with a conformable contact. It exhibits mostly mottled silt or fine sand sediments, the difference with the lower mottled sand is the absence of the calcareous nodules. The maximum measured thickness of this unit is ≈ 120 cm.

**Upper unit.** This unit overlies conformably the Third unit. It is mostly formed of red, fine sand locally interbedded with sand sediment beds. The latter comprise interbedded layers of coarse sand with lithoclasts, medium sand, fine sandand sandy shale sediments. The contacts between these beds are conformable, either abrupt or progressive. The maximum measured thickness of this unit is ≈ 290 cm.

### Age constraints

Only one date have been obtained in this sector, from the lower part of the Lower Unit. The organic matter of this mottled silt sediments bed yielded a $^{14}C$ age of 12942 ± 100 cal. yr BP.

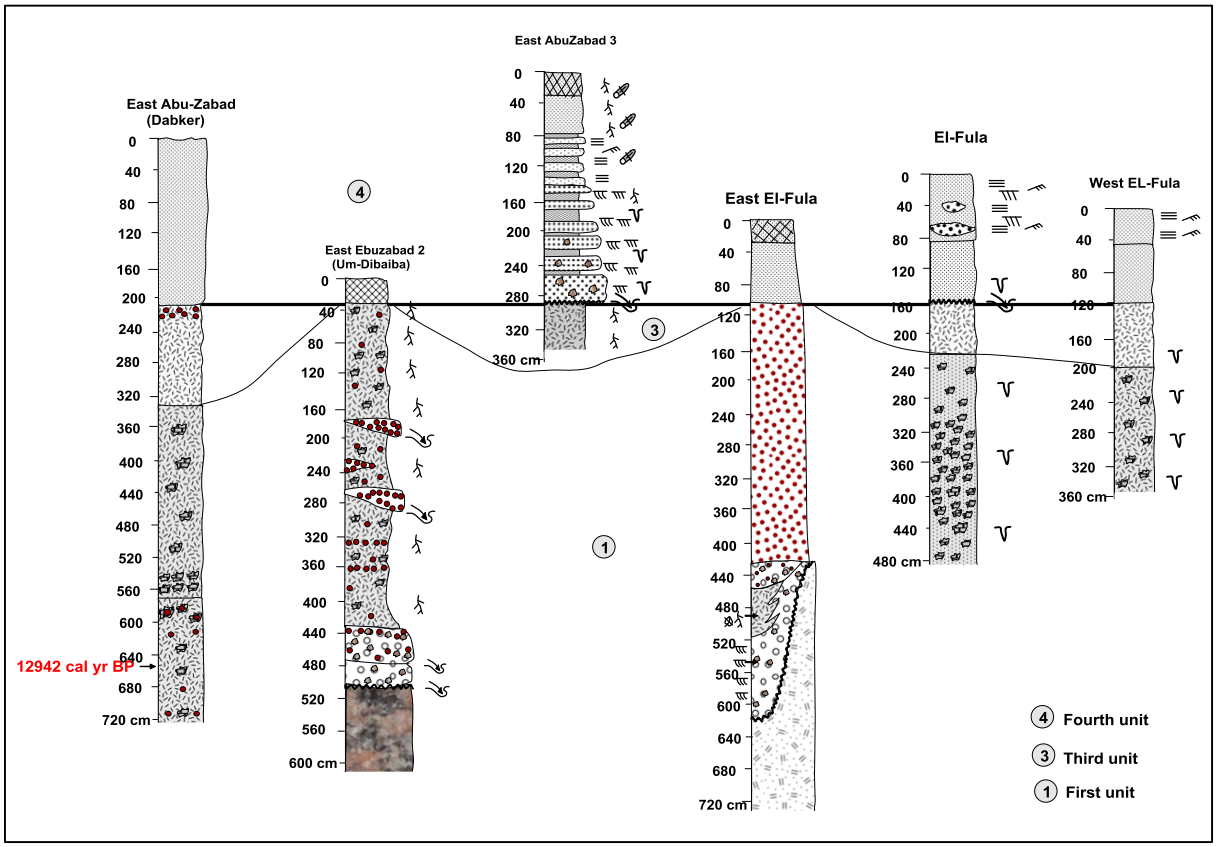


*Fig. 3.3: Stratigraphic units of the Abu Zabad – El Fula area. Legend in figure 3.2.*

### 3.1.3. Stratigraphy of the El Obeid – South El Obeid sector

This sector extends southward until Khour Es Sonjokaya (section South El Obeid3). Five sections have been studied. Three main stratigraphic units have been identified (lower, third, and upper unit) (Fig. 3.4).

**Lower unit.** This unit exhibits mostly mottled silt or fine sand sediments rich in calcareous nodules. Structureless beds of the sand sediments have been locally observed. The maximum measured thickness of this unit is ≈ 410 cm. The contact with the pre-Quaternary rocks is abrupt and unconformable, and has been observed only in west El Obeid.

**Third unit.** This unit also exhibits mostly mottled silt or fine sand and locally planar laminated sand sediments, but without calcareous nodules. Its contact on the Lower unit is conformable.

The maximum measured thickness of this unit is ≈ 390 cm, the thickness increases gradually southward.

**Upper unit**. The Upper unit unconformably overlies the Third unit in the east and south El Obeid sections, but in west El Obeid the Upper Unit directly overlies the Lower Unit. It is formed mostly of red fine sand sediments locally interbedded with coarser sand sediment beds. The grain size of the latter varies from coarse sand with lithoclasts, to sandy shale. The contacts between beds are conformable, either abrupt or gradual. The maximum thickness measured for this unit is ≈ 280 cm.

**Age constraints**

Organic matter from the third unit yielded $^{14}C$ ages of 3438 ± 30 and 3331± 35 cal. yr. BP, while charcoal fragments from the base and middle part of the Upper unit yielded $^{14}C$ ages of 1088 ± 30 and 905 ± 30 cal. yr. BP, respectively (Fig. 3.4).

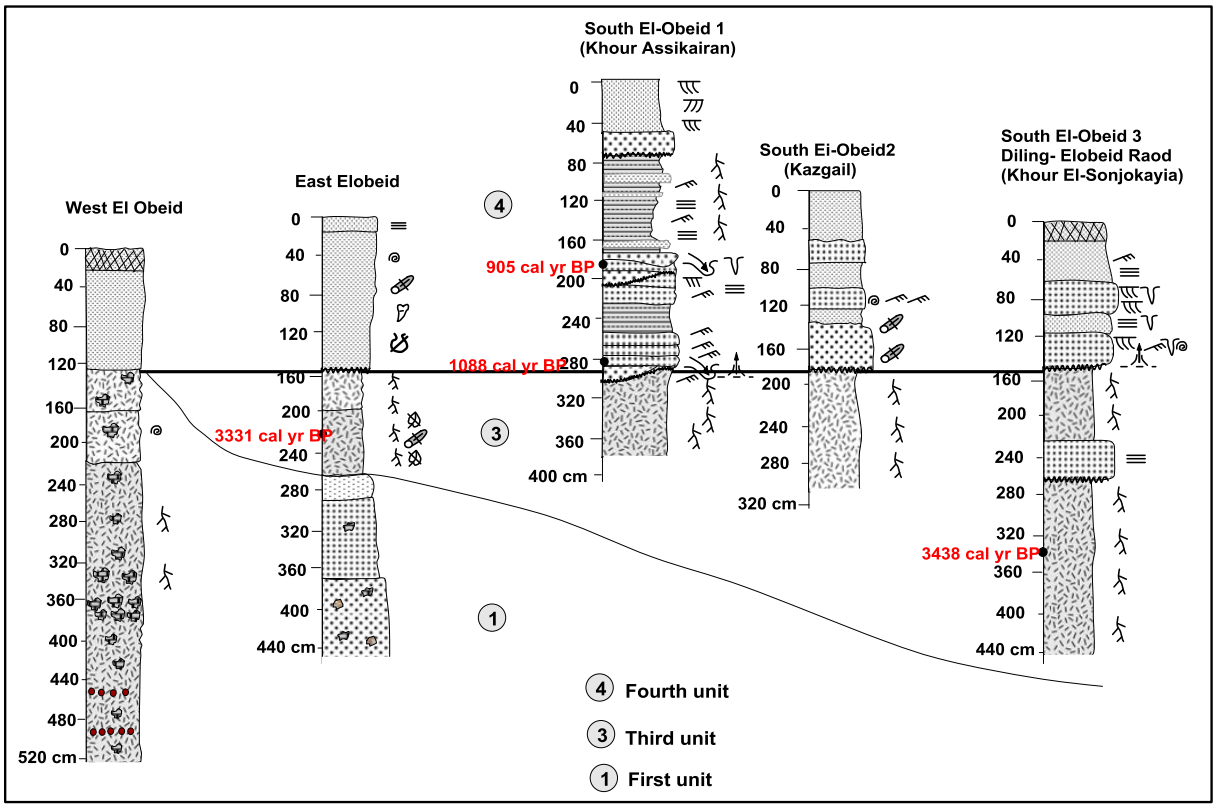


*Fig. 3.4: Stratigraphic units of the El Obeid – South El Obeid area. For the legend refer to figure 3.2.*

### 3.1.4. Stratigraphy of the En Nahud – El Khowei Sector

Four sections have been studied in this sector. There, the succession comprises three main stratigraphic units, separated by erosional contacts (Fig. 3.5).

**Lower unit.** This unit exhibits mostly mottled silt or fine sand sediments rich in calcareous nodules. Structureless beds of sand sediments have been observed locally. Its maximum measured thickness is ≈ 270 cm. Its lower contact has not been observed.

**Socond unit.** The second unit overlies conformably the Lower unit. It is a lime or sandy limestone bed, the thickness of which varies between ≈ 55 and ≈ 80 cm. The carbonate bed of

this unit is marked by the presence of gastropod shells. The lower contact of this unit is usually progressive, whereas the upper contact is abrupt.

**Upper unit.** The Upper unit unconformably overlies the second unit through an erosional contact. It is formed entirely of red fine sand sediments containing gastropod shells. Its maximum measured thickness is ≈ 155 cm.

**Age constraints**

Organic matter from the Lower unit yielded a $^{14}C$ age of 7968 ± 50 cal. yr BP (Fig. 3.5), while the gastropod-rich limestone bed from the second unit yielded $^{14}C$ ages of 9788 ± 80 and 6419 ± 35 cal. yr. BP in the En Nahud area. Both were collected from quarries, the older sample was collected ≈ 20 km north of the En Nahud town, while the younger one is from the southern part of the En Nahud city. The exact stratigraphic location of these samples are unknown, they may either represent the base and top of the limestone unit, or come from two or more distinct limestone levels. These ages are discussed below.

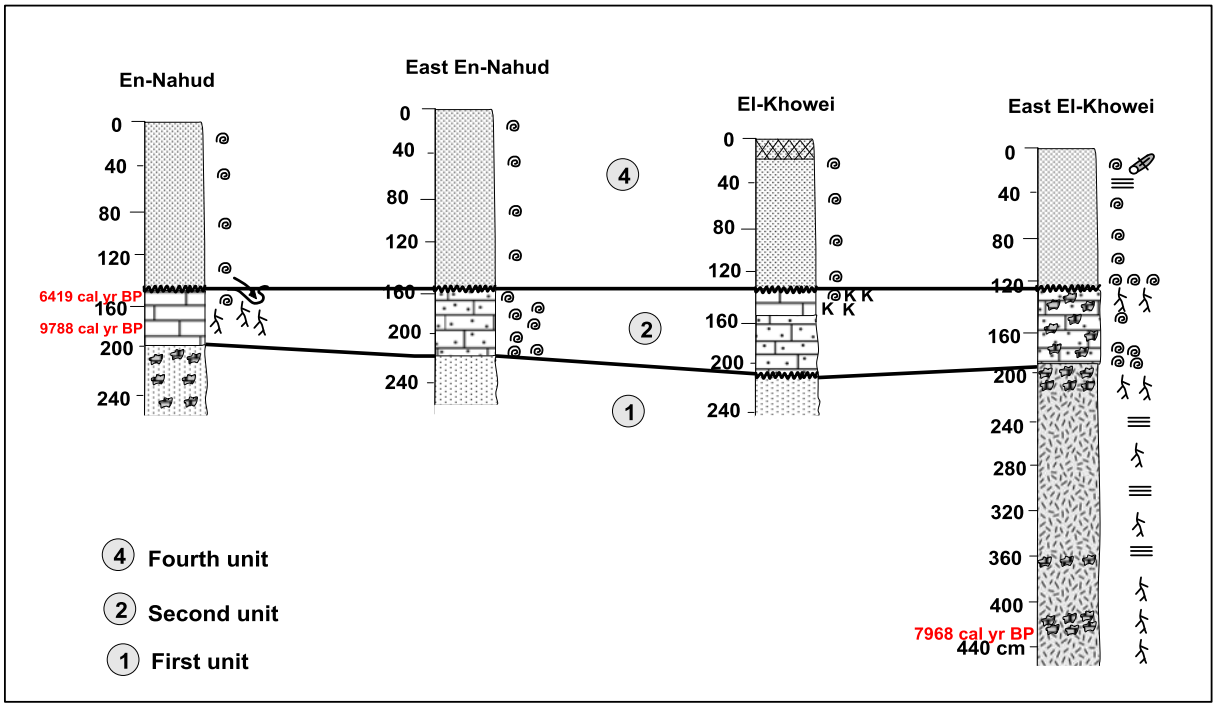


*Fig. 3.5: Stratigraphic units of the En Nahud – El Khowei area. Legend in figure 3.2.*

### 3.1.5. Stratigraphy of the North Bara – Sodari sector

In addition to the surficial survey in many sites in the El Ga'a and Sodari area, the stratigraphy of this sector has been defined according to four sections, three of them are located North of Bara, while the fourth one is a 4 meters deep well, caved in the El Ga'ah area. The Late Quaternary series of this sector comprises three stratigraphic units, separated locally by erosional contacts (Fig. 3.6).

**Lower unit**. The Lower unit is formed of mottled sand sediments. The sand grains are coarse to fine. The maximum measured thickness of this unit is ≈ 445 cm. Its basal contact has not been observed.

**Second unit.** This unit overlies unconformably the Lower unit. It is formed of alternating beds of limestone and argillaceous sand sediments. The upper surface of the limestone beds is karsted and/or eroded. The argillaceous sand beds may contain limestone clasts. The contact between the middle and lower units is generally abrupt and conformable, but an erosional, unconformable contact is observed locally in section North Bara 2. The thickness of this unit varies from 0 to ≈ 360 cm, according to the places (Fig. 3.6).

**Upper unit.** The Upper unit conformably overlies the second unit, or rests directly on the Lower unit through a conglomeratic bed made of iron concretions. It is entirely formed of coarse- to fine-grained red sand sediments. Its maximum measured thickness is ≈ 255 cm.

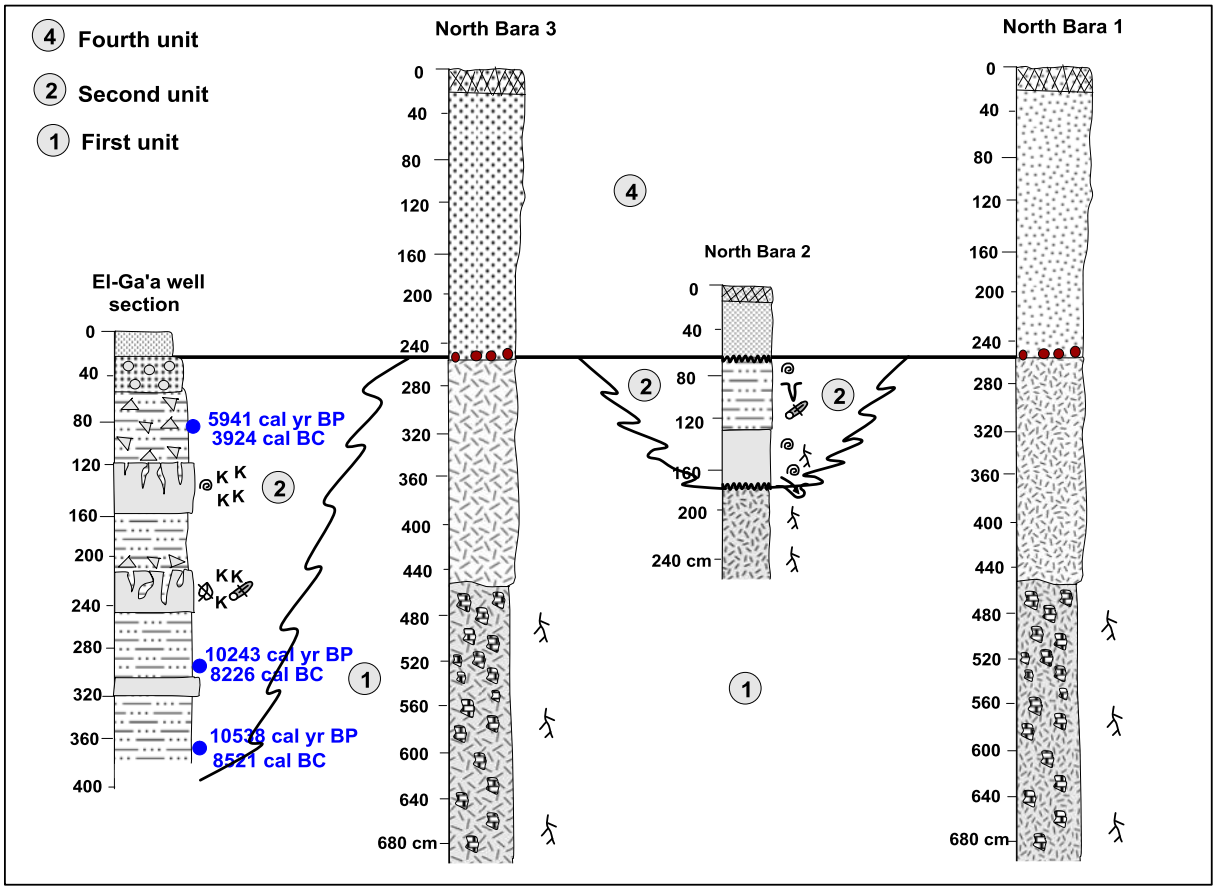


*Fig. 3.6: Stratigraphic units of the North Bara – Sodari area. Legend in figure 3.2.*

## Age constraints

Three samples of organic matters from organic-rich argillaceous sand sediment beds have been collected in the El Ga'ah well. They belong to the second unit and yielded $^{14}C$ ages of 10538 ± 45, 10243 ± 40 and 5941 ± 30 cal. yr BP, respectively. The oldest age has been obtained from the base of the second unit, while the youngest one is from the top of the same unit (Fig. 3.6). In addition, archeological potteries and bone samples have been collected from the paleo-shoreline of north El Ga'ah and north Sodari paleo-lakes, in order to obtain more dates. However, bone samples either were not suitable for dating (lack of collagen for five samples), or yielded very recent ages : 108.47 ± 0.36 yr BP North of El Ga'ah, and 107.86 ±

0.31 yr BP near Sodari. These two samples exhibit present modern carbon (PMC), which means that they are not even suitable for calibration.

Archeological pottery samples have been investigated at the university of Khartoum-Sudan, Archeology department, with the help of the archeologist Dr. Huweida. The collected potteries included the dotted wavy lines decorative, banded decorative, polished and thin, and polished and thick. The dotted wavy line potteries have been classified as Neolithic potteries, whereas other three forms have been determined as historic potteries (Merowetic and Islamic eras).

The dotted wavy line has a wide distribution west of the Nile across the Sahara-Sahel Belt (Mohammed-Ali, 2003) where it is observed in Wadi Howar (Jesse, 2000). Some sites of the Neolithic dotted wavy line ceramics have been dated as Middle Holocene. Radiocarbon dates obtained from Neolithic level in the Shaqadud Neolithic site provided ages of 6880 ± 180 BP (55–62 cm below datum) and 6430 ± 180 BP (85–90 cm below datum; Marks, 1991; Mohammed-Ali, 1991, *in* Mohammed-Ali, 2003). Radiocarbon dates, taken from bone or snails, place the Early Khartoum type ceramics in Wadi Howar in the 6$^{th}$ millennium BP (Jesse, 2000). Reappraisal of radiocarbon dates from central Sudan suggests the following culture succession: Early Khartoum is 9000-7000 BP, Early Neolithic Group is 6900-6450 BP, Middle Neolithic Group is 6400-5800 BP, Late Neolithic Group ages are 5500 to 4700 BP (Hassan, 1986). Therefore, the age indication of the potteries ornamented by dotted wavy lines (≈ 7000-6000 yr BP) is consistent with our $^{14}C$ ages from the Second unit.

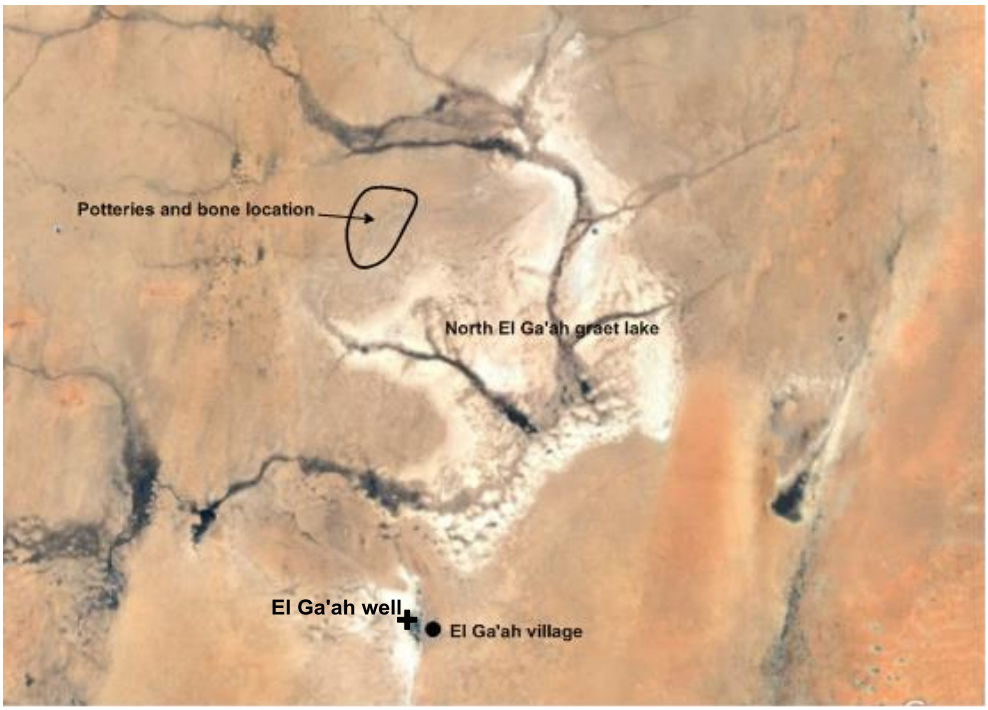


*Fig. 3.7: Location of the potteries and bones collected from the El Ga'ah paleolake shoreline.*

## 3.2. Carbon dating

### 3.2.1. Preview of Carbon dating

The lack or limitation of organic material makes it difficult to date all the stratigraphic units, especially those of light or reddish color. Among the twenty-six samples tested for carbon

dating (organic soils and/or paleosols, charcoal, bones; Table 3.2), only seventeen $^{14}C$ dates have been considered as dated points in the study area. The remaining nine samples either produced very recent ages, or were not suitable for dating. Among the rejected samples, eight are bones and only one is charcoal. The charcoal sample (Ka 1-1) produced a recent age due to its high percent modern carbon (pMC). The bone samples were rejected due to their high percentage of modern collagene and/or due their very low nitrogene content (< 0.1% N).

The stratigraphic position of the dated samples is given in Figures 3.8 – 3.15. The oldest date is 12 942 ± 100 cal. yr BP from the mottled, pale grey Lower unit of the East Abu-Zabad 1 section at depth 650 cm, and the youngest date is 246 ± 30 cal. yr BP from the Dilling section, at depth 40 cm.

### 3.2.2. Discussion of the $^{14}C$ dates

As shown in table 3.2, the dated material includes organic soil, charcoal and limestone. This kind of material, however, has some problems when being dated (Walker, 2005). Although all soils contain carbon and can theoretically be dated by radiocarbon, the dynamic nature of the soil system implies that it receives organic matter over a protracted time period, and thus, any radiocarbon date on a soil will be largely a measure of the mean residence time of the various organic fractions within the soil. Therefore, because of the continuous input of organic material into soil, measured radiocarbon ages of soil organic matter or its fractions are generally younger that the true ages of soil (Wang et al., 1996, *in* Walker, 2005). Among the samples we dated for this study, a sample from East El Khowei belonging to the Lower unit provided a ≈ 8 kyr BP age (Fig. 3.11), although it is located below the Second unit (limestone and sandy limestone), which yielded ages of ≈10 and ≈ 6 k yr BP around En Nahud and El Ga'ah (Figs. 3.12 and 3.15). This may be due to the contamination by younger material, such as deep roots, which may have introduced young organic matter into older horizons (Walker, 2005). Alternatively, deposition of the Second unit around the El Khowei town may have started later than in En Nahud, or the Second unit may correspond to some distinct, heterochronous carbonate beds, the age of which varies from ≈10 and ≈ 6 k cal. yr BP.

Lake sediments are extremely susceptible to contamination by older carbon residue and this leads to a dilution of the $^{14}C$ concentration, and hence, to dates that are older than the actual date of sediment deposition (Walker, 2005). The same problem is also found in the terrestrial organisms, which may ingest older carbonates (limestone or soil carbonate) during their life time and this older material can be integrated into their shell (Walker, 2005). On the other hand, bioturbation caused by organisms in pond or lake beds can lead to disturbance of the sediment sequence and the downward movement of younger sediments, and thus younger age can be recorded from older sediments (Walker, 2005).

The two dated samples from the En Nahud area were collected from excavated quarries. Therefore, they may represent the base and top of limestone horizon, or they may represent two distinct limestone horizons. We did not observe superimposed carbonate levels in the En Nahud and El Khowei areas, but several limestone beds were observed in the El Ga'ah well. On the other hand, since the samples were collected very close to the surface, one of them may have been contaminated by modern organic matter which may reduce its real age.

***Table 3.2: Carbon dating results***

| Lab Cod | Laboratory | Sample name | Section | Depth cm | analyzed material | Age $^{14}C$ BP | Error ±BP | Age cal yr (AD or BC) | Age cal yr BP | Remark |
|---|---|---|---|---|---|---|---|---|---|---|
| 49432 | LSCE | NDel 16-17 | North Dilling2 | 375 | Organic paleosols | 4055 | 30 | 2853 BC | **4870** | |
| 49433 | | NDel 16-18 | North Dilling2 | 337 | Organic paleosols | 3720 | 30 | 2116 BC | **4133** | |
| 49434 | | NDel 16-20 | North Dilling2 | 135 | Organic paleosols | 740 | 30 | 1258 AD | **759** | |
| 50046 | | NDel 16-2 | North Dilling1 | 250 | Charcoal | 6750 | 110 | 5665 BC | **7682** | |
| Poz-79741 | Poznan | Del 1-2 | Dilling | 40 | Charcoal | 165 | 30 | 1771 AD | **246** | |
| Poz-79743 | | Del 2-1 | Dilling | 185 | Charcoal | 595 | 30 | 1354 AD | **663** | |
| 50047 | LSCE | Ga 6-1 | El-Ga'ah | 360 | Organic Paleosol | 9195 | 45 | 8521 BC | **10538** | |
| 49435 | | Ga 6-3 | El-Ga'ah | 290 | Organic Paleosol | 9040 | 40 | 8226 BC | **10243** | |
| 49436 | | Ga 6-7 | El-Ga'ah | 85 | Organic Paleosol | 5095 | 30 | 3924 BC | **5941** | |
| Poz-79737 | Poznan | Kh 1-1 | South El Obeid1 | 185 | Charcoal | 910 | 30 | 1112 AD | **905** | |
| Poz-79739 | | Kh 1-2 | South El Obeid1 | 280 | Charcoal | 1120 | 30 | 929 AD | **1088** | |
| Poz-81611 | | En Nahud | En Nahud | * | Limestone | 5565 | 35 | 4402 BC | **6419** | |
| Poz-81229 | | AWZ1-4 | En Nahud | * | Limestone | 8680 | 80 | 7771 BC | **9788** | |
| 49437 | LSCE | Sonj 9 | Khour Es Sonjokaya | 340 | Organic paleosol | 3140 | 30 | 1421 BC | **3438** | |
| Poz-79736 | Poznan | KT 1-1 | East Elobeid1 | 220 | Organic paleosol | 3050 | 35 | 1314 BC | **3331** | |
| Poz-0 | | KT 4-2 | East El Obeid | 65 | bone | **>0** | | | | not suitable (<0,1%N 2.5%C) |
| Poz-79740 | | Ka 1-1 | South El Obeid3 | 30 | Charcoal | **132.87** | | | | Modern (0.35 pMC) |
| 50044 | LSCE | Dod 1 | East El Khowei | 440 | Organic paleosol | 6960 | 50 | 5951 BC | **7968** | |

| | | | | | | | | | | |
|---|---|---|---|---|---|---|---|---|---|---|
| 50045 | | Dab 1 | East Abu Zabad1 | 650 | Organic paleosol | 10960 | 100 | 10925 BC | **12942** | |
| Poz-0 | Poznan | Ga 4-3a | El Ga'ah | surficial | bone | **>0** | - | - | - | not suitable (<0,1%N 4%C) |
| Poz-93016 | | Ga-5 | El Ga'ah | surficial | bone | **108.47** | | | | Modern (9%collagene, 3,3%N 8,7%C) |
| Poz-0 | | S-Sod 1-2 | Sodari | surficial | bone | **>0** | | | | Not suitable (0,1%N 2,6%C) |
| Poz-0 | | Ga 4-3b | El Ga'ah | surficial | bone | **>0** | | | | Not suitable (<0,1%N 5.6%C) |
| Poz-0 | | Ga 4-3c | El Ga'ah | surficial | bone | **>0** | | | | Not suitable (<0,1%N 3.7%C) |
| Poz-93017 | | Sod 3-1 | Sodari | surficial | bone | **107.86** | | | | Modern 12.5%coll 2.8%N 8.7%C, |
| Poz-0 | | S Sod 3 | Sodari | surficial | bone | **>0** | | | | Not suitable (<0,1%N 3.3%C) |

*The * symbol in the En Nahud sample depths indicates that the samples were collected from surficial excavated material.*

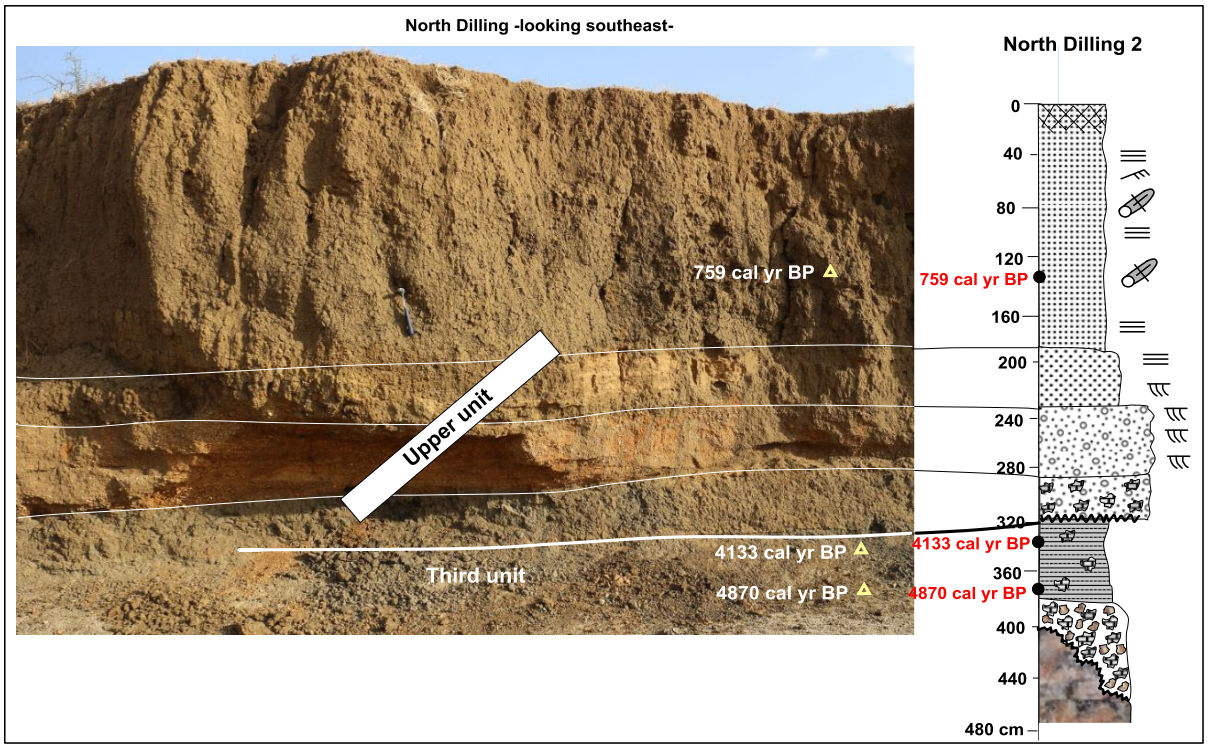


*Fig. 3.8: Position of dated samples in the North Dilling 2 section. Mean sedimentation rate for the lower unit is ≈ 0.52 mm/yr.*

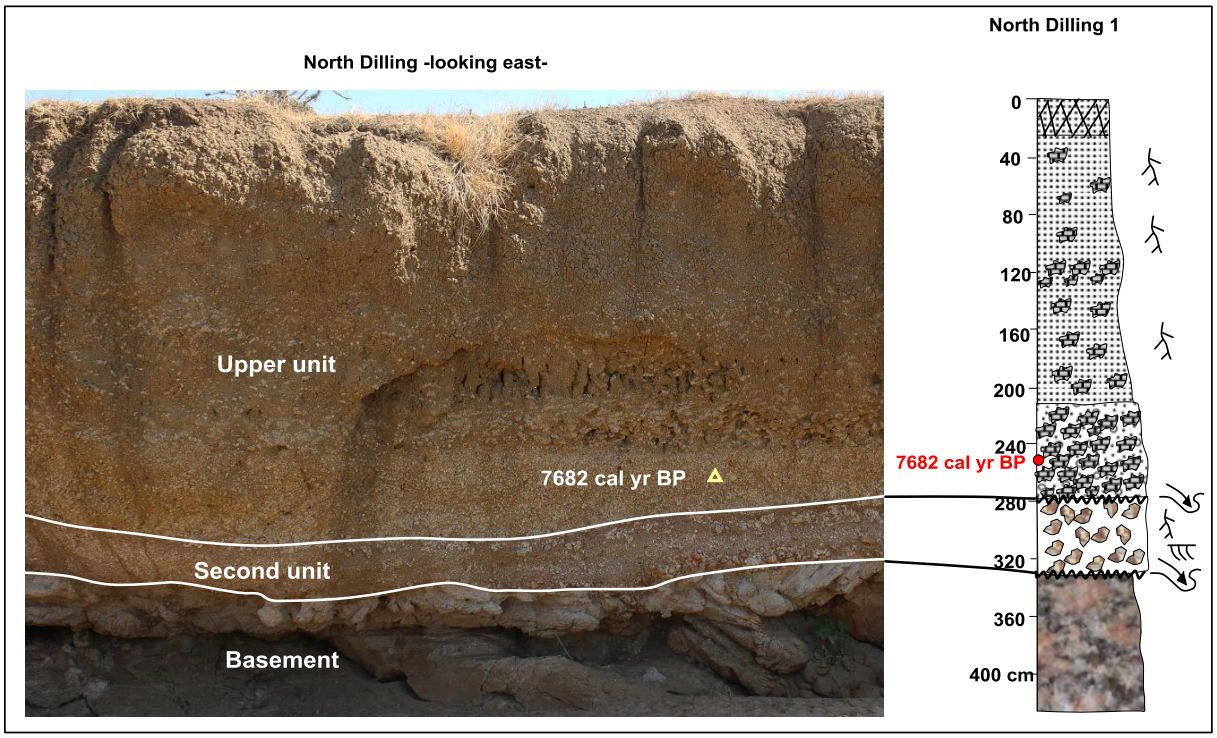


*Fig. 3.9: Position of dated sample in the North Dilling 1 section.*

The reworking of sediments may have some effects on the dated samples of charcoal materials. As a matter of fact, all charcoal samples were collected in fluviatile sediments. Therefore, this material is likely reworked from older deposits, and old dates may be obtained from younger sediments. This process may have affected the date obtained from the North Dilling1 section (Fig. 3.9), where a sample collected from the base of the Upper unit, yielded an age of ≈ 7700

yr BP, which is older than dates from the underlying unit of North Dilling2, dated at ≈ 4900 and ≈ 4100 yr BP (Fig. 3.8). Moreover, deposition may take place in channels caved in older sediment due to local erosion, and yielding young ages in depth. In the East El Obeid section, a sample collected at depth of ≈ 90 cm provided a $^{14}C$ age of 40 ± 30 yr. This date has been excluded from the samples presented in table 3.2.

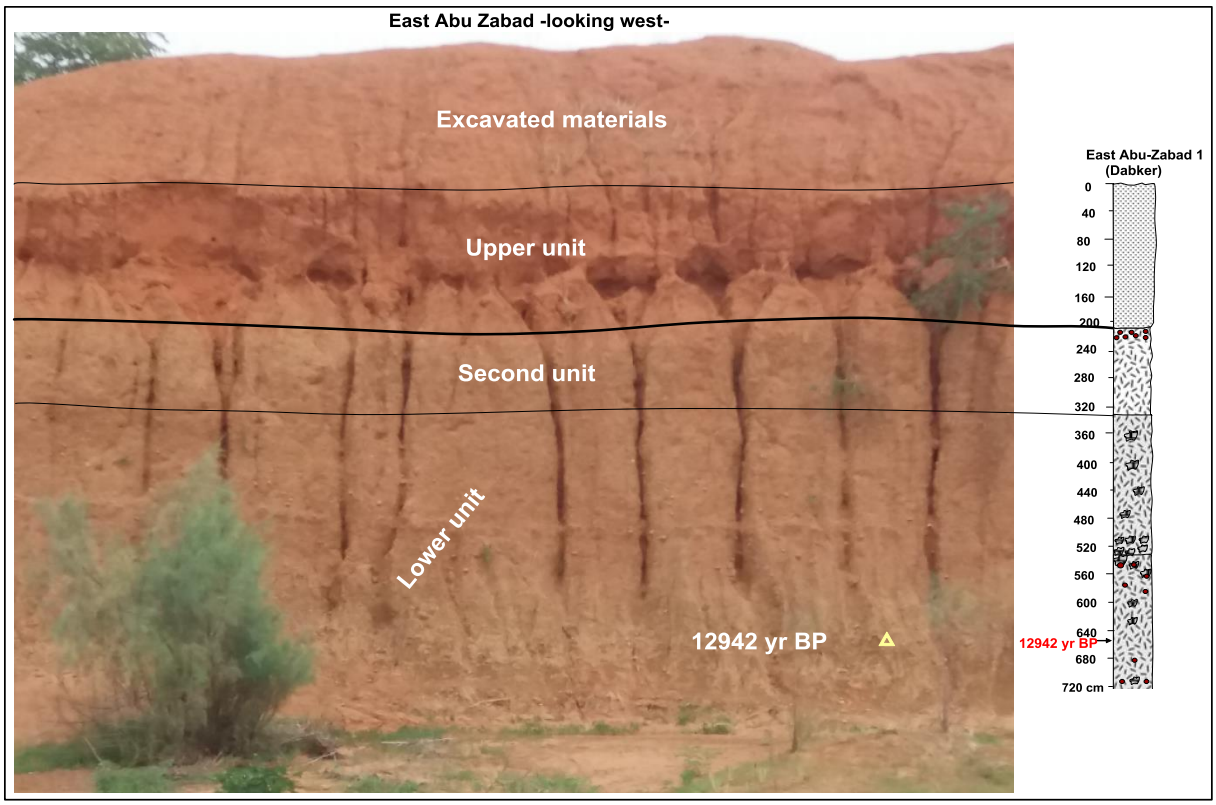


*Fig. 3.10: Position of dated samples in the East Abu Zabad section.*

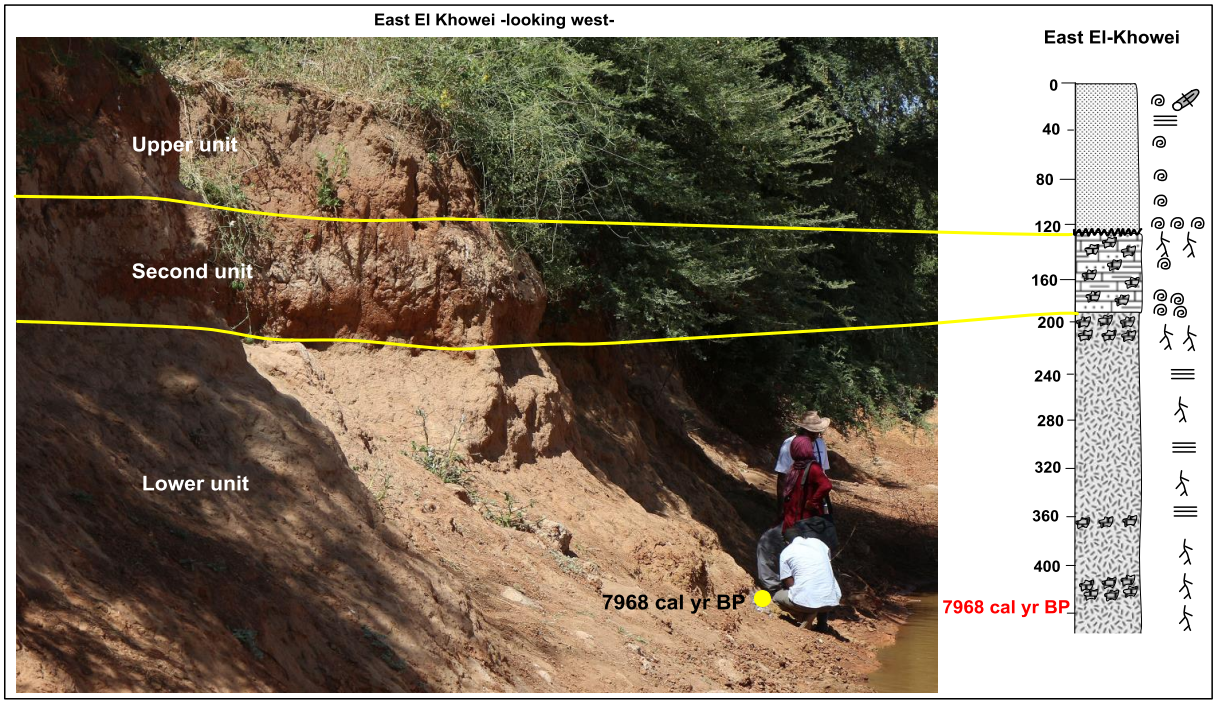


*Fig. 3.11: Position of dated samples in the East El Khowei section.*

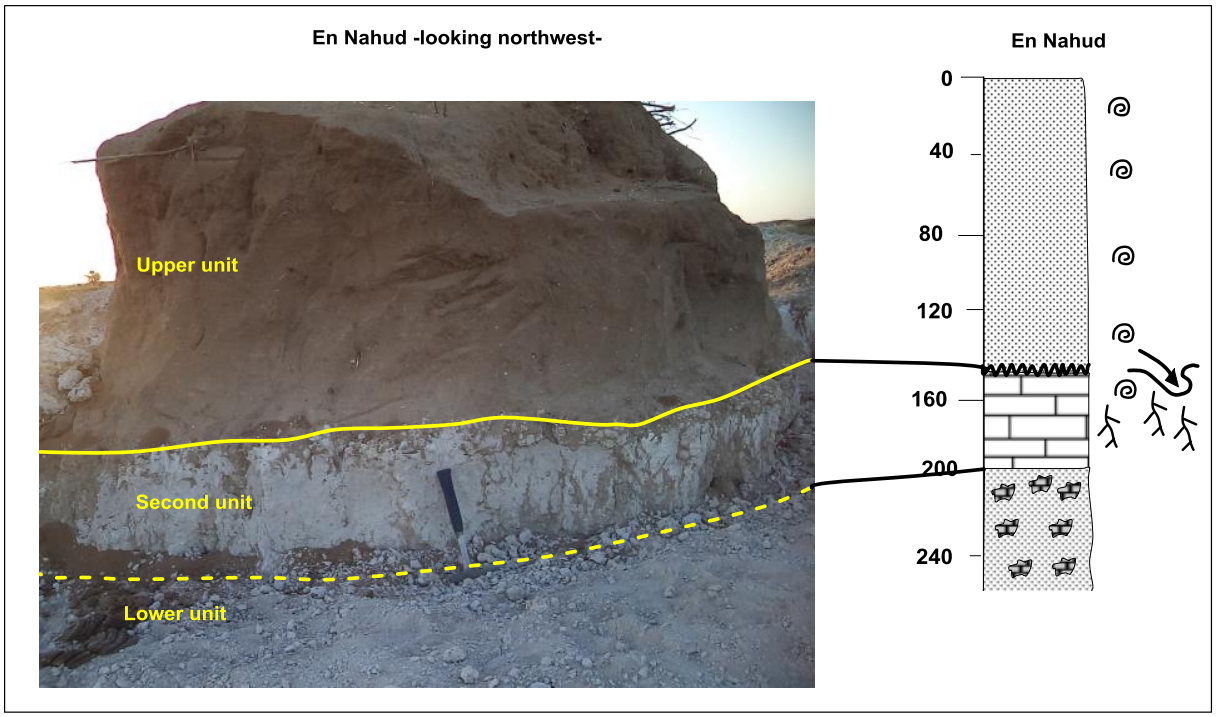


*Fig. 3.12: Section near En Nahud. Two $^{14}C$ ages for the Second unit were obtained from other two sites in En Nahud, and north En Nahud (Awlad Zibare village). They yielded ages of 6419 and 9788 cal yr BP, respectively.*

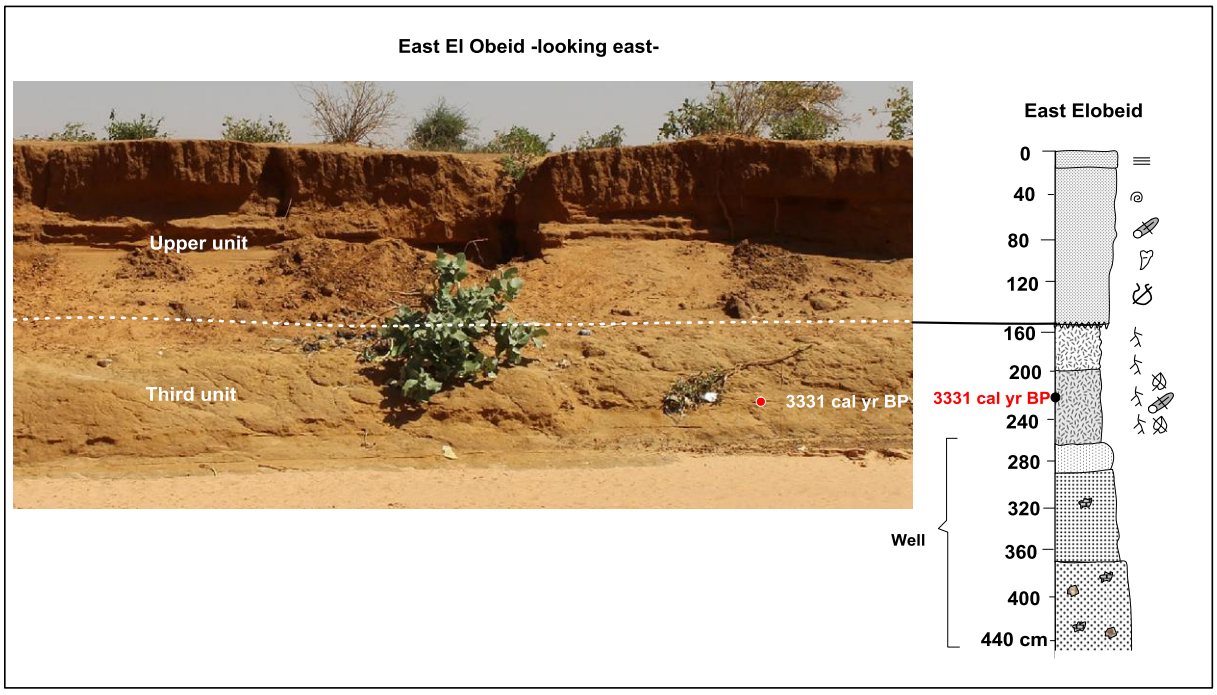


*Fig. 3.13: Position of dated samples in the East El Obeid section.*

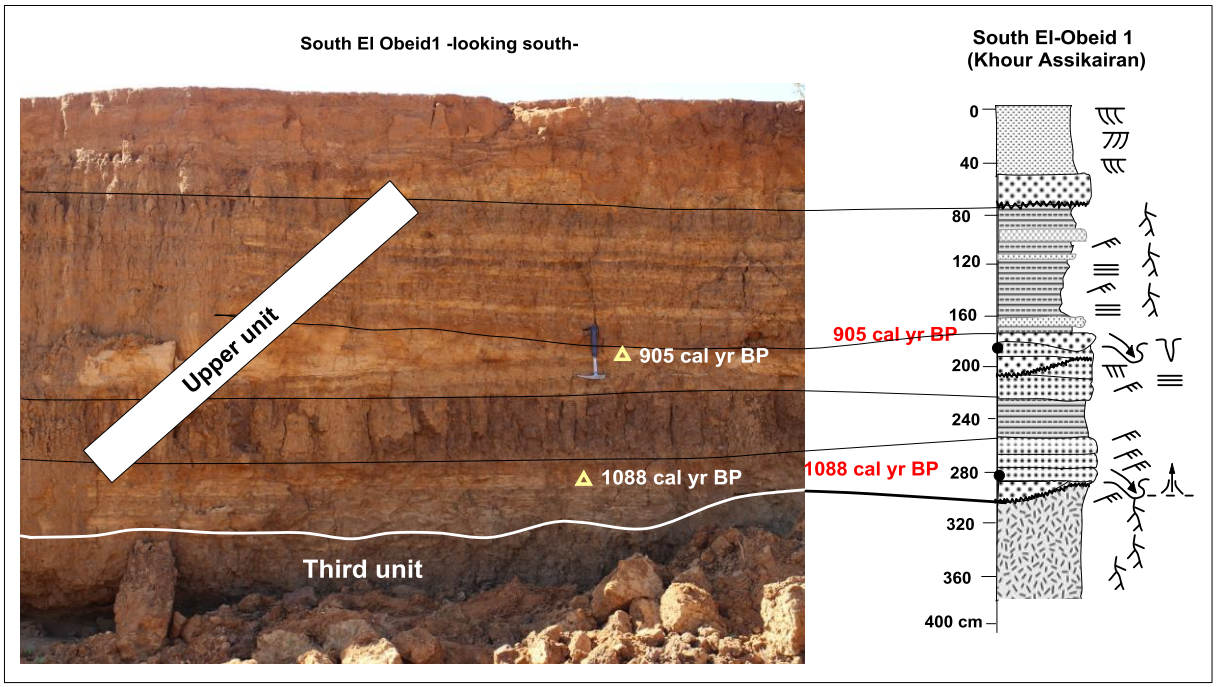


*Fig. 3.14: Position of dated samples in the south El Obeid1 section. The average accumulation rate of sediments for the Upper unit is 2.76 mm/yr (5.4 mm/yr between ≈ 1100 and 900 yr ago).*

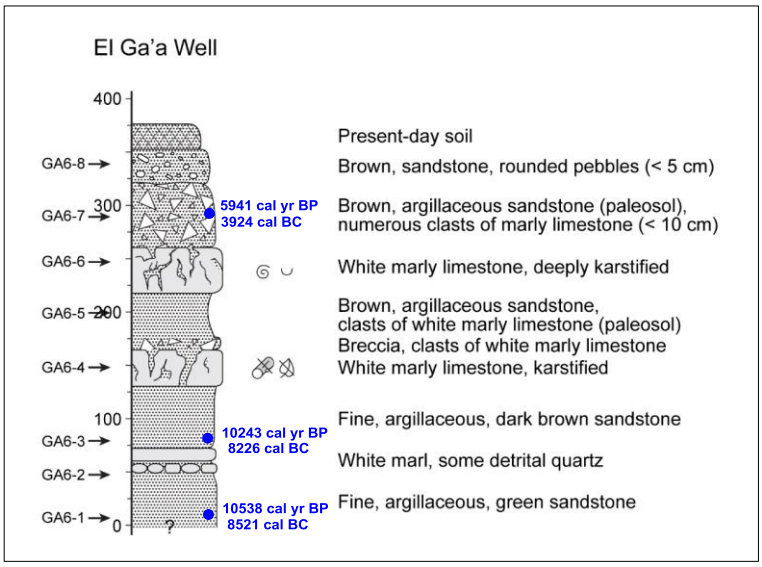


*Fig. 3.15: Position of dated samples in the El Ga'a well. The accumulation rate for lower part of the section is ≈ 2.4 mm/yr, and ≈ 0.47 mm/yr for the upper part.*

## 3.3. Stratigraphic correlations and synthesis

Although the concept of correlation goes back to the early history of stratigraphy, disagreement has persisted over the exact meaning of the term. Historically, two points of view have prevailed. One view rigidly restricts the meaning of correlation to demonstration of time equivalency, that is, to the demonstration that two bodies of rock were deposited during the same period of time (Dunbar and Rodgers, 1957; Rodgers, 1959). From this point of view, establishing the equivalence of two lithostratigraphic units on the basis of lithologic similarities

does not constitute a correlation. A broader interpretation of correlation allows that equivalency may be expressed in lithologic, paleontologic or chronologic terms (Krumbein and Sloss, 1963). In other words, two bodies of rock can be correlated as belonging to the same lithostratigraphic or biostratigraphic unit even though these units may be of different ages. From a practical point of view, most geologists today accept the latter, broader view of correlation. Petroleum geologists, for example, routinely correlate subsurface units based on lithology, on specific "signatures" recorded by instrumental well logs, or on reflection characteristics on seismic records (Boggs, 2006). When dealing with long-lasting units, or regional map surveying, this may be acceptable. In the present work, since (1) the age difference of the Lower unit would represent 70 to 90% of the studied period, (2) the targeted period is very short (mostly Holocene), and (3) the aim of this study is to reconstruct the time evolution of climate, this becomes unacceptable ! Therefore, we preferred to follow time correlation in this study.

According to the presented stratigraphic results in the different areas (Figs. 3.2 – 3.6), many areas comprise two stratigraphic units. However, a carbonate unit is present in the En Nahud-El Khowei and Bara-Sodari areas, and deposits younger than the limestone beds are evidenced by $^{14}C$ datings in the El Obeid area. Additionally, $^{14}C$ dates disclosed a sedimentary hiatus between the second or third unit, and the Upper unit, i.e. between ≈ 6 or 3 kyr BP, and ≈ 1 kyr BP. As a consequence, we drew three time-correlation profiles: an E-W trending El Fula – Dilling (southern part) profile, an E-W oriented En Nahud – El Obeid profile (central part of the study area), and a N-S trending El Ga'a – Dilling profile. Because of the scarcity of dates, these correlations are partly based on the lithological similarities of the units.

### 3.3.1. El Fula – Dilling transect

The southern profile joins the sections of the El-Fula and Dilling areas, through the Abu-Zabad sections, along a total distance of 180 km. In this area, the four stratigraphic units are recognized partially, since the second unit is missing along Abu Zabad El Fula sector (present in channel deposition lenses ?), and the lower (first) unit is missing in the Dilling area. The base of the lower unit is dated at ≈ 13 000 yr BP in Abu Zabad. The Second unit has not been dated in this transect. The Third unit is dated at ≈ 4900 yr BP in the Dilling area. In the latter area, the charcoal from the basal conglomerate of the Upper unit dated at ≈ 7700 yr BP is interpreted as reworked. The Upper unit in the Dilling area has been dated between ≈ 750 and ≈ 250 yr BP in its upper half part, while its lower part remained undated.

In the Abu Zabad and El Fula areas, the oldest and only available date is the ≈ 13 000 yr BP age obtained from the lower part of the Lower unit. The Third unit in the Abu Zabad and El Fula areas is tentatively correlated with the dated beds of the Dilling area. The Upper unit of the Abu Zabad – El Fula area is correlated with the Upper unit of the Dilling area. In this interpretation, this unit has a maximum age of ≈ 1000 yr BP (see below).

The sedimentary gap between the Lower and Upper unit extends from ≈ 4 to 1 kyr BP in the Dilling area. This gap is marked by erosions and therefore, is shown as a non-deposition and erosional hiatus in the correlation profile (Fig. 3.16).

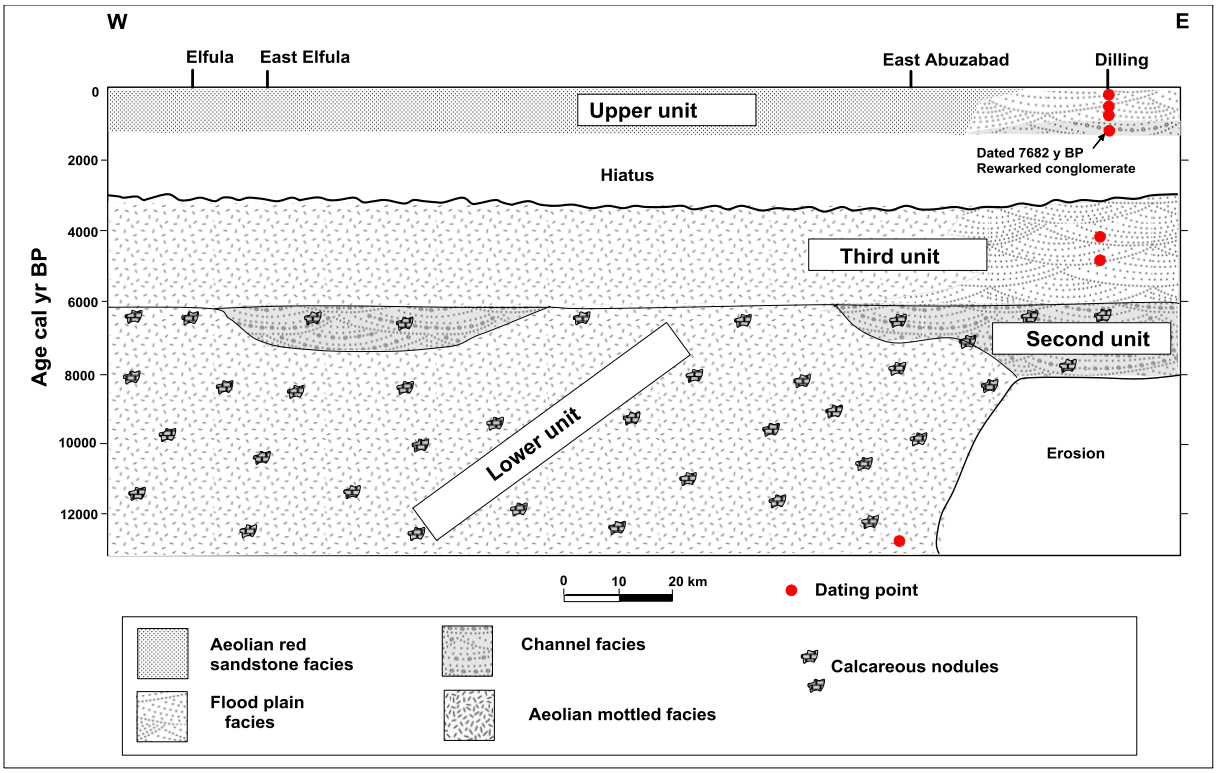


*Fig. 3.16: Time-correlation transect between El Fula and Dilling.*

### 3.3.2. En Nahud – El Obeid transect

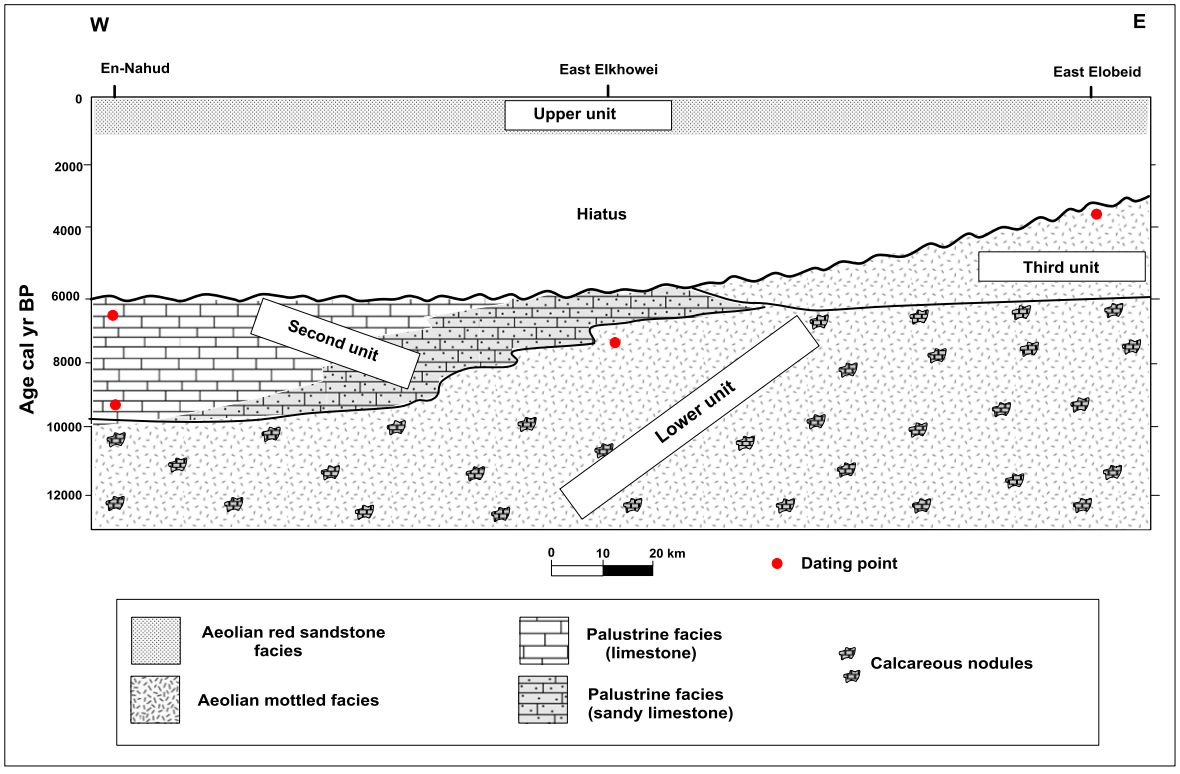


*Fig. 3.17: Time-correlation transect between En Nahud and El Obeid.*

This transect represents the central part of the study area, joining the En Nahud sections to the West and the El-Obeid sections to the East, through the El Khowei area, with a total distance

of 210 km. This transect exhibits the four stratigraphic units, the Second unit being apparently absent in the El Obeid area, and the Third unit being missing in the En Nahud-El Khowei areas.

The Lower unit is correlated with its equivalent of the southern transect, where a maximum age of ≈ 13 kyr BP has been measured. The youngest age of this unit is variable along the transect: it is older than ≈ 10 kyr BP in the En Nahud area, but it may extend up to ≈ 7.5 kyr BP in the El Khowei area. The Second unit encompasses the ≈ 10 to ≈ 6 kyr BP time-span, according to dates obtained in the En Nahud area. The top of the Third unit is dated at ≈ 3 kyr BP in the East El Obeid section. Based on the dates obtained in the South El Obeid and Dilling sections, the upper unit is assumed to be younger than ≈ 1 kyr BP.

The time gap between the Middle and Upper units encompasses the ≈ 6 - 1 kyr BP time interval to the West (En Nahud, El Khowei), and the ≈ 3 - 1 kyr BP time span to the East. It is interpreted as a hiatus due to erosion occurring before 1 kyr BP, or to non-deposition, or to both processes (Fig. 3.17).

### 3.3.3. El Ga'ah – Dilling transect

This transect correlates the southern and northern parts of the study area. The total length of this profile is 390 km, with a 90 km long W-E segment between El Ga'ah and North Bara3, and a 300 km long segment from North Bara3 to Dilling. This transect comprises partially four stratigraphic units. The Lower unit is missing to the south, and the Third unit seems to be missing to the North (Fig. 3.18).

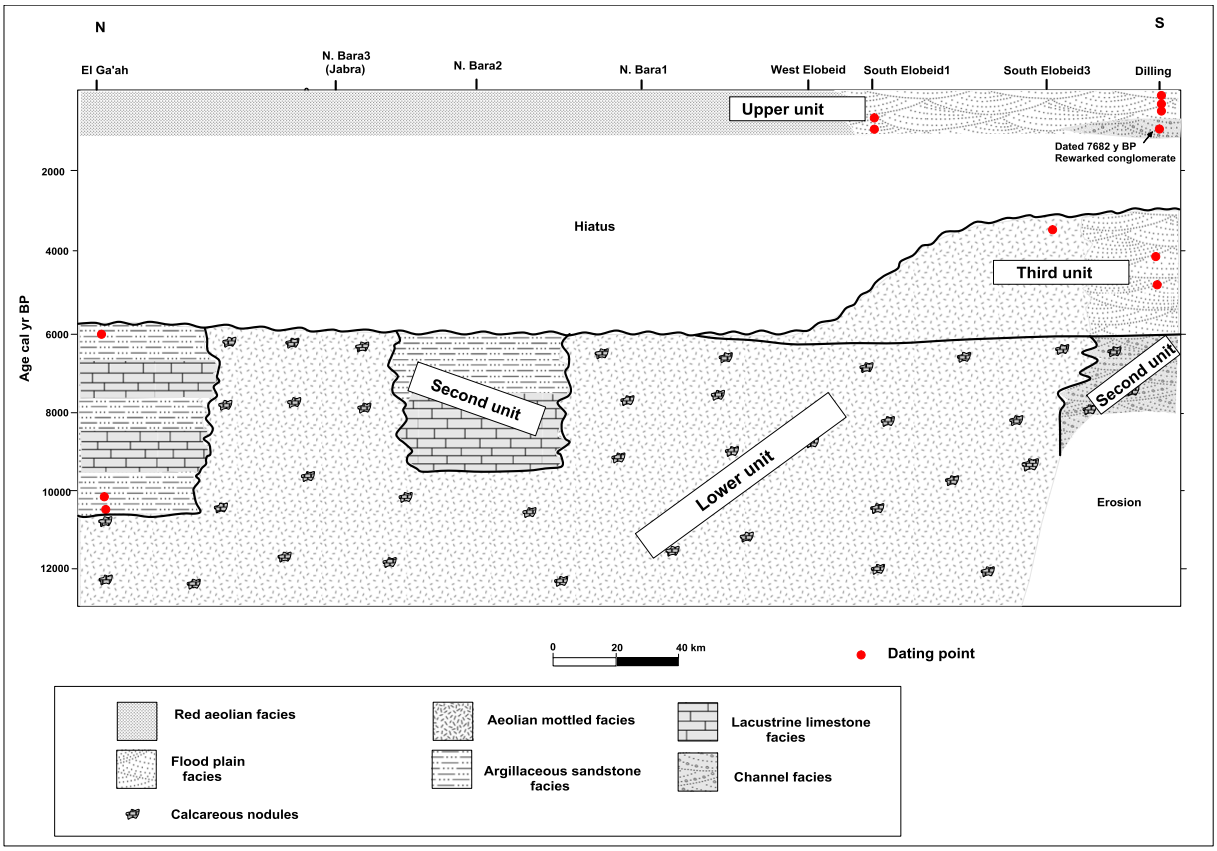


*Fig. 3.18: Time-correlation transect between El Ga'ah and Dilling.*

No age constraints have been found for the Lower unit in the northern area. It is, however, older than the Second unit, i.e. older than 10.5 kyr BP, as indicated by dates from the El Ga'ah section. In the latter section, the age of the Second unit is consistent with the correlated unit in the En Nahud area, i.e. ≈ 10 to 6 kyr BP. The Third unit is dated between ≈ 3 and 4.9 kyr BP in south El Obeid and Dilling, respectively. The data from South El Obeid and Dilling suggest that the Upper unit is younger than 1000 yr BP.

Therefore, as noted in the Central transect, a hiatus occurred between ≈ 3 and 1 kyr BP in the southeastern area (Dilling, El Obeid), and probably between ≈ 6 and 1 kyr BP in the northwestern areas (Bara, El Ga'ah, Sodari).

### 3.3.4. Synthesis of the stratigraphy of the Late Quaternary deposits of Kordofan

The stratigraphic succession of the study area exhibits four stratigraphic units, corresponding to four distinct depositional periods, to which one must add a fifth period interpreted as a hiatus. These units show some variation from north to south, since the Lower unit is missing in the South (Dilling area) and the Third unit seems absent in the North. The periods corresponding to these units are: older than 10 kyr BP for the Lower unit (locally older than 7.5 kyr BP), between ≈ 10 and 6 kyr BP for the Second unit, between ≈ 6 and 3 kyr BP for the Third unit, the hiatus period extends from ≈ 6 to 1 kyr BP and from ≈ 3 to 1 kyr BP in the northern and southern parts, respectively, and the fifth period is younger than 1000 year and corresponds to the Upper unit.

## 3.4. Sedimentology

All geologic studies aim at a better understanding of Earth's history. Sedimentary rocks yield many information recorded by various kinds of sedimentological features (Boggs, 2006). During field work, great attention has been paid to the sedimentary record.

In addition to facies and lithological variations, the studied sections exhibit many sedimentary figures such as cyclic sedimentation, fining upward succession, unconformity surfaces, bedding pattern, as well as chemical (calcareous nodules) and biological features (bioturbation, root traces), which will be analyzed successively.

### 3.4.1. Sedimentary Facies

The present sedimentological study is based on the detailed measurement of twenty-four stratigraphic sections (Fig. 3.1 and table 3.1). Height sedimentary facies were recognized in a series of sections studied during field work. These facies are : (1) mottled sand or silty sand, (2) lens shaped conglomerate, (3) alternating sand and silt, (4) sandy carbonate, (5) carbonate, (6) argillaceous sand, (7) red sand and (8) clinoform bearing, coarse clastic facies. Table 3.3 summarizes the main features of these facies.

#### 3.4.1.1. Mottled sand sediments facies

*Description*: The mottled sand facies is characterized by mottling, root traces and a noticeable organic matter content. However, there are some differences according to the sites, or even along a same section. For instance, the mottled facies may vary in color from green, to various

shades of color, or to pale yellow. In addition, it exhibits intensive development of calcareous nodules in different contents and forms of occurrence (Fig. 3.19). Some differences in grain size have been also observed, varying according to the sites from silty sand to coarse sand, or locally poorly sorted sand. Fine grained mottled facies is restricted to the southern part of the area, whereas coarser grained facies dominates in the northern area.

*Distribution*: The mottled sand facies is distributed throughout the study area, except around Dilling.

*Interpretation:* Mottling or marmorization (Freytet and Verrecchia, 2002) in soil is primarily associated with soil wetness (Ciolkosz and Dobos, 1990), microorganism population, organic carbon energy source, lack of oxygen, time and temperature (Dobos, 1990, *in* Ciolkosz and Dobos, 1990). Generally, mottling feature occurs when the iron content of sediments is > 2% and if water table fluctuations occur, then ferrous iron moves easily and fixes as ferric iron. The result is a sediment with mottled pink, purple, red, and yellow patches in the accumulation area of ferric iron, and grey or white in the area depleted in iron. Manganese and calcium can also migrate with iron, resulting in a complex fabric of mottled patches and ferruginous nodules. As a consequence, the dominating mottling feature in this facies and its wide occurrence all over the area, indicate that the area experienced wet conditions under low oxidation rates (Freytet and Verrecchia, 2002).

***Table 3.3: Summary of the sedimentary facies.***

| Facies | Distribution | Marked Features |
|---|---|---|
| **Mottled sand or conglomerate** | All area except Dilling | Mottling, mostly contain calcareous calcretes, root traces, rich in organic matter, pale grey, dark grey and green color. |
| **Lens shaped conglomerate** | Widespread in Dilling, El Fula, scattered in Abu Zabad, south El-Obeid, El Khowei | Poorly sorted, quartzite and iron oxide clasts, current features: locally planar and trough cross bedding. |
| **Alternating sand and silt** | Widely in Dilling, locally south El Obeid, east Abu Zabad, El Fula. | Mostly well sorted but locally poorly sorted; current features: planar cross bedding, trough cross bedding, planar laminae and current ripples, alternation of white sand and dark shale laminae (only in fine-grained beds), locally fining upward, and locally cyclic sedimentation. |
| **Sandy carbonate** | En Nahud - El Khowei area | Partially massive limestone, partially sandy limestone, white to pale grey, karsted, root traces, gastropod shells |
| **Carbonate** | North Bara, El Ga'a and Sodari | Grey, low density, deeply karsted, gastropod shells in most sites. Brecciated, exposed upper surface. |
| **Grey argillaceous sand** | North Bara, El Ga'a and Sodari | Grades of grey and yellow, friable, usually fine-grained |
| **Red sand** | All area except Dilling | Mostly fine grained, mostly red, rarely reddish brown, no or rare structures, coarse grain size only in northernmost parts |
| **Clinoform bearing coarse clastic** | El Ga'ah | Mostly coarse sand and gravels, gastropod shells, root molds |

The existence of organic matter in soils and sediments is a function of several factors, among which climate is the most important (e.g., Tóth et al., 2007; Forry et al., 2014; Priene and Lavee, 2015). Moreover, organic matter decays more rapidly at higher temperatures, so soils in warm climates tend to contain less organic matter than those in cool climates (Fact sheet No 3, 2009). Fine-textured soils tend to have more organic matter than coarse soils; they hold nutrients and water better, thus providing good conditions for plant growth. Coarse soils are better aerated, and the presence of oxygen results in a more rapid decay of organic matter. The wetter a soil is, the less oxygen is available for organic matter to decay, so that it accumulates. Roots are a great contributor to soil organic matter. Grassland produces deep roots that decay deep in the soil. Forest soils in contrast rely primarily on the decay of surface litter for organic matter input. Therefore, the existence of organic matter in mottled facies with variable amount indicates that the environment was wet or saturated especially those marked by dark colors (green and dark grey), while the mottled facies marked by their lighter colors (pale grey, yellow and reddish yellow) experienced less wet condition and became more oxidized than the dark ones. Additionally, the preservation of root molds, which are tubular voids that outline positions of former, now decayed roots (Freytet and Verrecchia, 2002), provides good indicator that the area was invaded by a significant vegetation cover.

The most important feature in this mottled facies is the development of calcretes or calcareous nodules. These calcretes present a variety of shape, size and form. Two forms of calcretes have been observed in the study area: nodular and tubular (Chen et al., 2002). The nodular form is the most abundant and widespread, whereas the tubular form is restricted to some sites.

In the study area, the shape of the nodules is irregular, though leaning to be equal in the three dimensions. It does not contain any biogenic features, but instead it contains locally some iron concretions and quartz grains. The lack of biogenic features indicates their groundwater origin (Alonso-Zarza and Wright, 2010; Alonso-Zarza et al., 201I), related to shallow aquifer systems (Netterberg, 1969; Mann and Horwitz, 1979, *in* Alonso-Zarza, 2003). The precipitation of carbonate occurs within a previous host rock and around the groundwater table (Alonso-Zarza, 2003). The degree of complexity of individual profiles is largely influenced by the geomorphological setting and hydrological history of the local groundwater systems (Arakel, 1996). The amount of carbonate in a calcrete profile tends to exceed the original pore space of the host. This produces an increase in volume and physical displacement of the original host components.

The development of calcretes occurs in different ways: direct calcium carbonate precipitation (Chen et al., 2002), replacement, and displacement (Chen et al., 2002; Alonso-Zarza, 2003). During replacement, some host components are dissolved and/or removed and are replaced by calcium carbonates, while displacement occurs when the amount of carbonate in a calcrete profile tends to exceed the original pore space of the host. This produces an increase in volume and physical displacement of the original host components (Chen et al., 2002).

Tubular calcretes (Chen et al., 2002) or rhizoliths (Klappa, 1980), root calcretes (Alonso-Zarza and Jones, 2007) and rhizogenic or root formed calcrete (Freytet et al., 1997) have been found

locally, mostly around El Khowei (specifically east El Khowei) and rarely in north Bara. Generally, it is marked by an elongated shape more and is concentrated in specific zones.

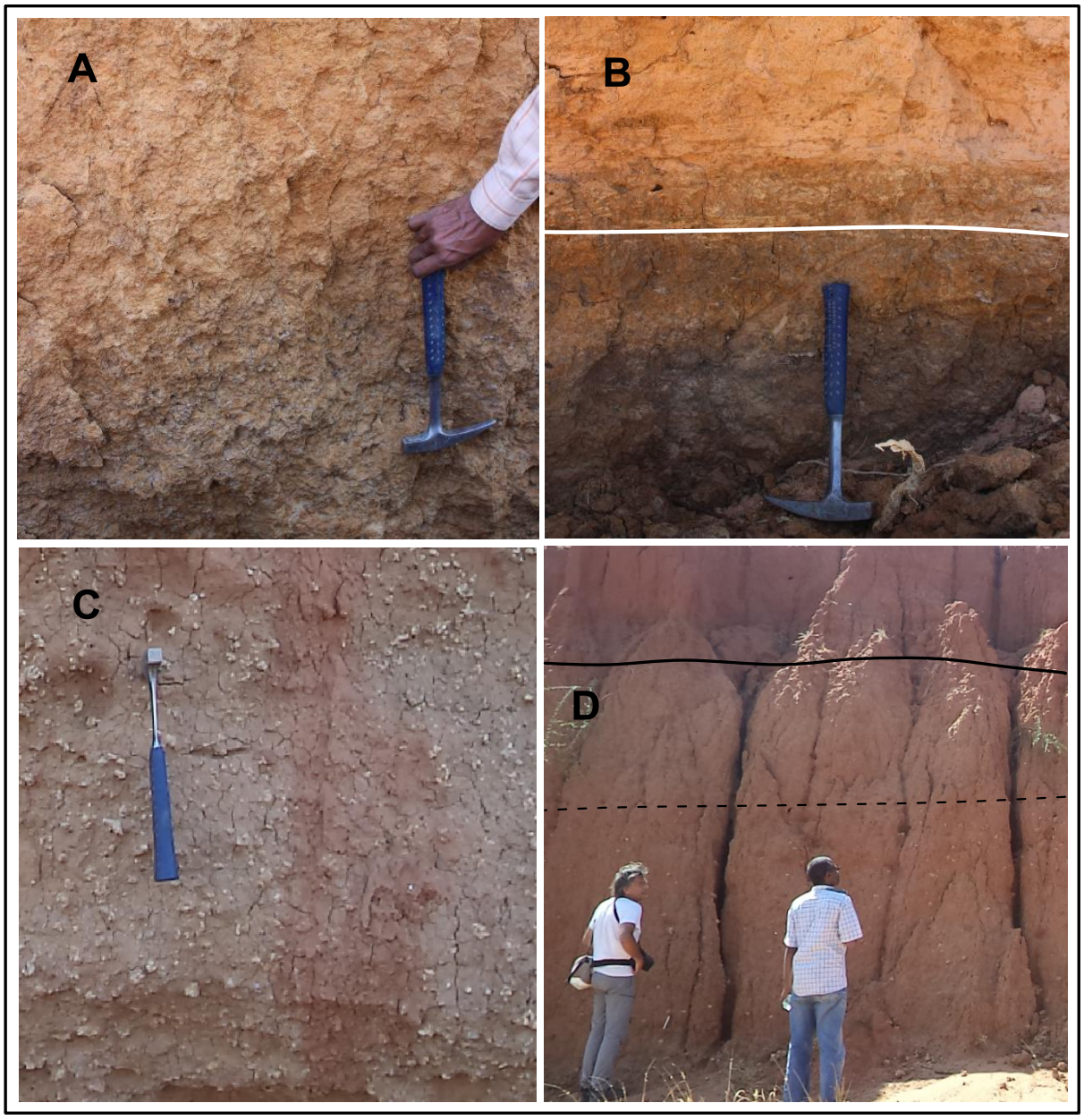


*Fig. 3.19: Mottled facies examples.* ***(A)*** *Mottled horizon from east El Obeid section: the lower part is greenish to grey, rich in organic matter, while in the reddish brown upper part, organic matter is scarcer or oxydized.* ***(B)*** *South El Obeid3 section (Khour Es-Sonjokaya): the mottled facies crops out below the white line, the dark lower part is richer in preserved organic matter than the upper part.* ***(C)*** *El-Fula area: pale grey mottled facies rich in calcareous nodules.* ***(D)*** *East Abu Zabad section: thick unit of mottled sand sediments (below the solid line). The dashed line separates a lower part containing calcareous nodules, from an upper part devoid of calcareous nodules.*

The typical morphology of tubular calcrete indicates that they formed by replacement of the root organic matter by calcium carbonate, the role of roots being important (Alonzo-Zarza et al., 2010). Moreover, the existence of some biogenic features in the tubular calcrete indicates that it formed in the vadose zone (Arakel, 1996), where precipitation of carbonate takes place mostly above the water table and within the sediment (Alonso-Zarza, 2003).

As shown in figure 3.22a, the tubular calcretes are more or less vertical with different inclination, and they are larger in size in the upper part than in the lower part. This may be due to the variation in the roots density and to the fact that root size is usually greater in the upper part than in the lower part, nodules being larger in the upper part. Difference in nodule size could also be due to additional re-precipitated carbonate, since re-precipitated carbonate tends to concentrate near the surface and within the voids, due to preferential cohesive bonds between carbonate crystals (Chen et al., 2002).

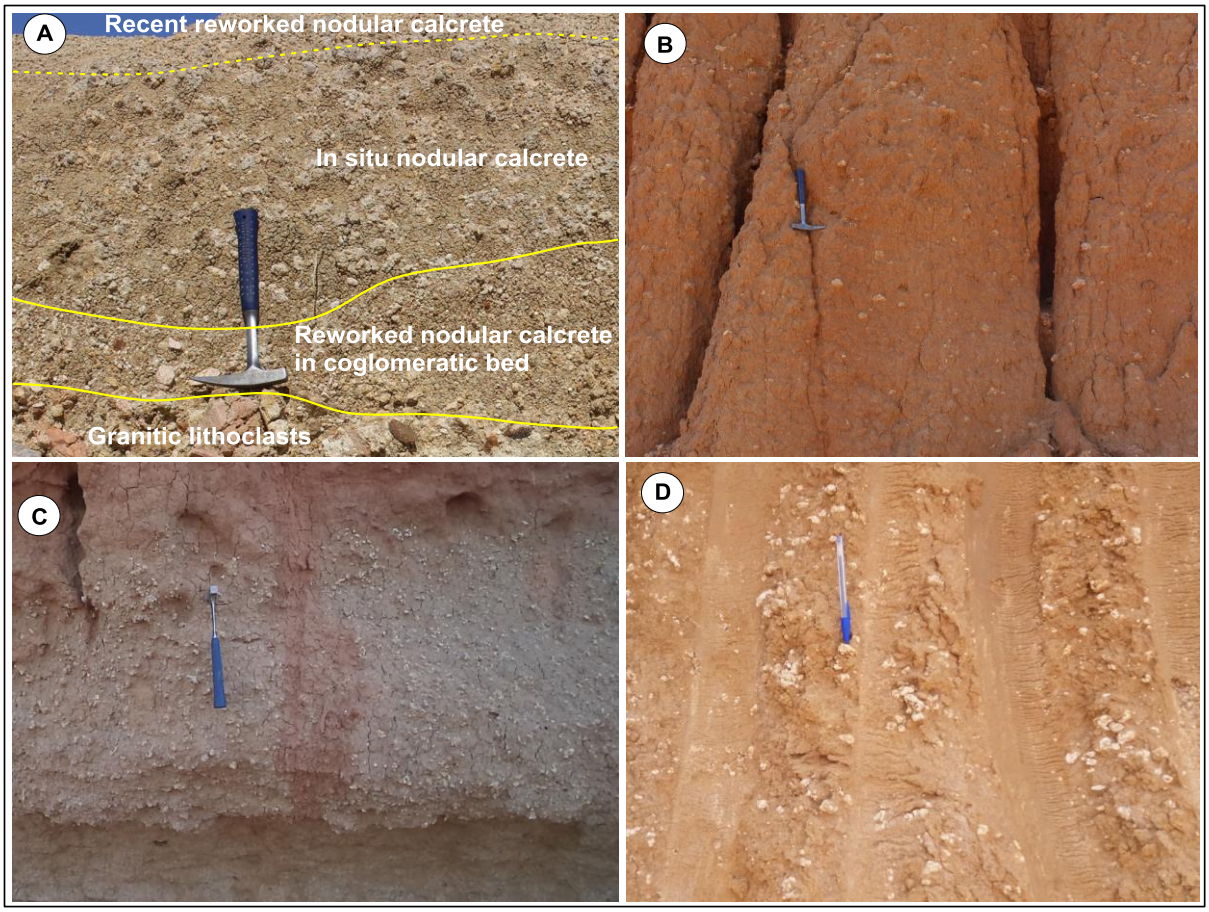


*Fig. 3.20: Nodular calcrete or calcareous nodules. (**A**) Numerous nodules formed in flood plain facies -Dilling area; (**B**) Rare nodules formed in mottled, fine sand sediments facies – East Abu Zabad; (**C**) Numerous calcareous nodules formed in mottled fine sand sediments – El Fula; (**D**) Moderately abundant nodules in mottled, medium to coarse sand sediments – North Bara.*

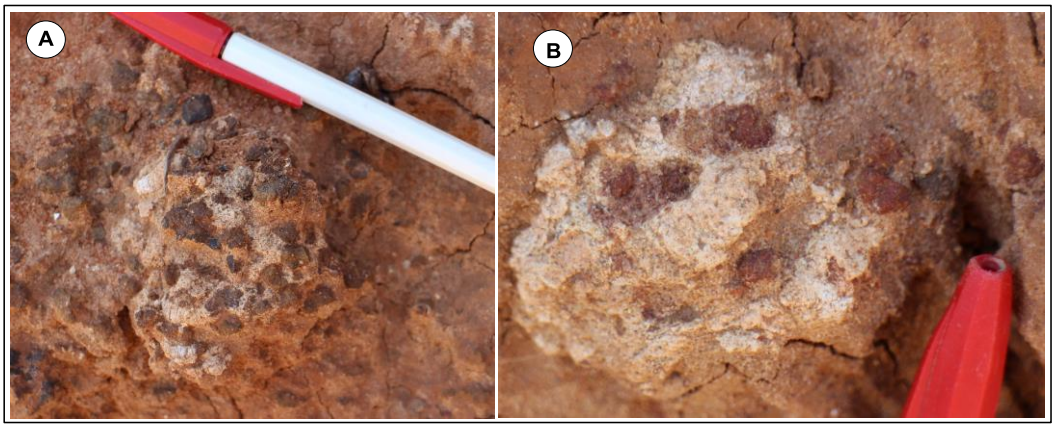


*Fig. 3.21: Nodular calcrete including iron concretions. A and B from east Abu Zabad.*

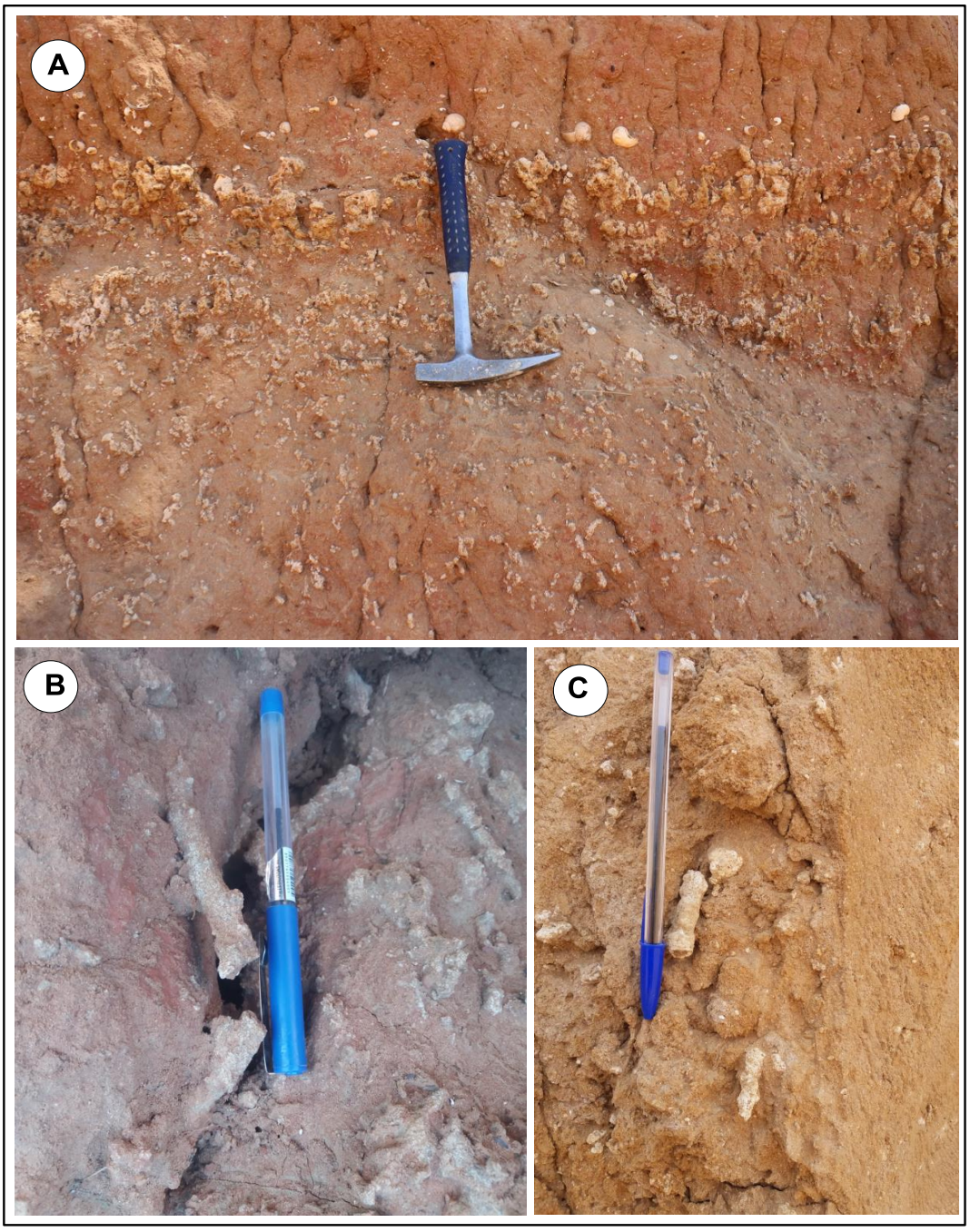


*Fig. 3.22: Tubular calcrete. **A** and **B** : East El Khowei; **C** : North Bara.*

### 3.4.1.2. Channel facies

#### 3.4.1.2.A. High regime channel facies (lens-shaped conglomerate beds)

The channel facies includes the lens-shaped conglomerates and the sediments of poorly sorted sand beds. The former indicates high energy sedimentation, while the latter indicates lower energy regime.

*Description*: In the Dilling area, the conglomerate is made of poorly sorted, dominantly quartz clasts, with other lithoclasts and some reworked calcareous nodules, while around Abu Zabad and El-Fula it comprises iron concretions and quartz clasts. In some horizons, the iron

concretions occur in lenses intercalated with other facies like the mottled facies. The thickest beds of conglomerates (325 cm) are found East of El-Fula. The base of the conglomerate beds is mostly an undulated surface, which separates the conglomerate from the underlying mottled facies or from the basement rocks.

The conglomerate facies is also observed in the El Khowei area, where it contains angular iron concretions of different sizes, ranging between 0.5 and 3.5 cm in size, as well as smaller well rounded quartz grains (Fig. 3.23). Locally, this facies is characterized by well observable current features (e.g., trough and planar cross beddings in Dilling area).

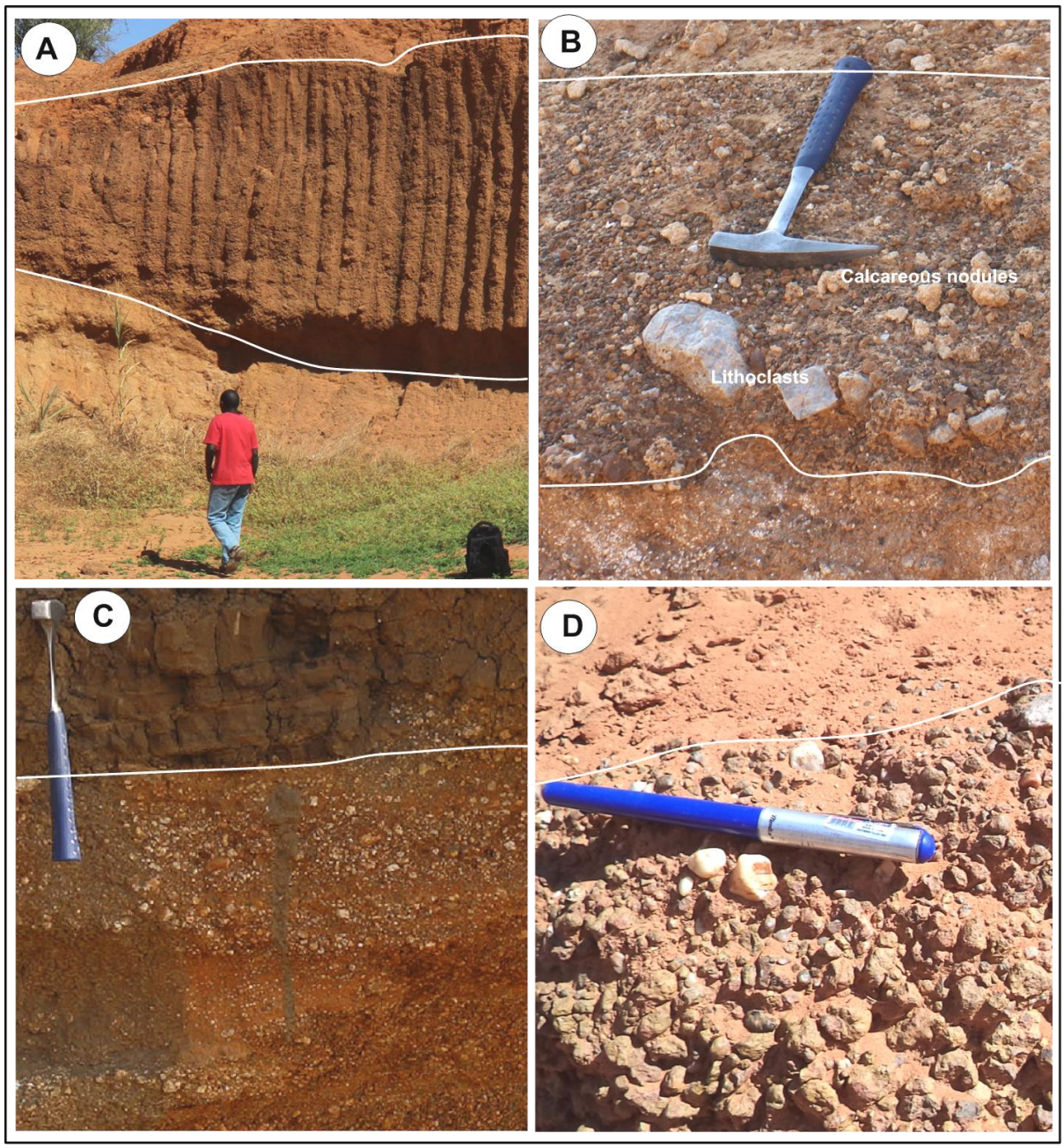


*Fig. 3.23: Examples of conglomerates.* ***(A)*** *Conglomerate exclusively made of iron concretion, East of El Fula.* ***(B)*** *Conglomerate made of iron concretion with subordinate reworked calcareous nodules and poorly sorted lithoclasts, East of Abu-Zabad.* ***(C)*** *Conglomerate with abundant quartz and calcareous nodules, Dilling area.* ***(D)*** *Conglomerate with iron concretions and minor quartz clasts, El Khowei.*

*Distribution*: This facies is restricted to the southern, and some central western parts of the studied area. It is observed around Dilling, El-Fula and very locally east of Abu Zabad and around El Khowei.

*Interpretation*: The angular shape of lithoclasts in the conglomerate near Dilling suggests that the elements of the conglomerate were transported for a short distance. As a matter of fact, several basement rock outcrops are found around Dilling, which may represent the main source to the quartz clasts and other crystalline lithoclasts. The local occurrence of conglomerate beds or lenses in the Dilling area, otherwise dominated by fine material, indicates a strong, localized alluvial activity. The existence of cross bedding features indicating high energy deposits, supports the interpretation of a fluviatile environment. The calcareous nodules in conglomerates of the Dilling area are interpreted as reworked from previously deposited units containing these nodules.

Channel conglomerates around El Fula, Abu Zabad and El Khowei are made almost exclusively of iron concretions. Rodis et al. (1968) classified this iron concretions as laterite deposits. These authors reported that the ironstone developed extensively in the Nubian Formation over much of the Kordofan province during early and middle Tertiary time, and corresponds to a prolonged period of deep, in-situ weathering of the host rock under tropical climatic conditions of alternating wet and dry seasons. Outcrops of Nubian sandstones bearing such iron concretions have been observed during field work between El Fula and En Nahud and southeast of En Nahud.

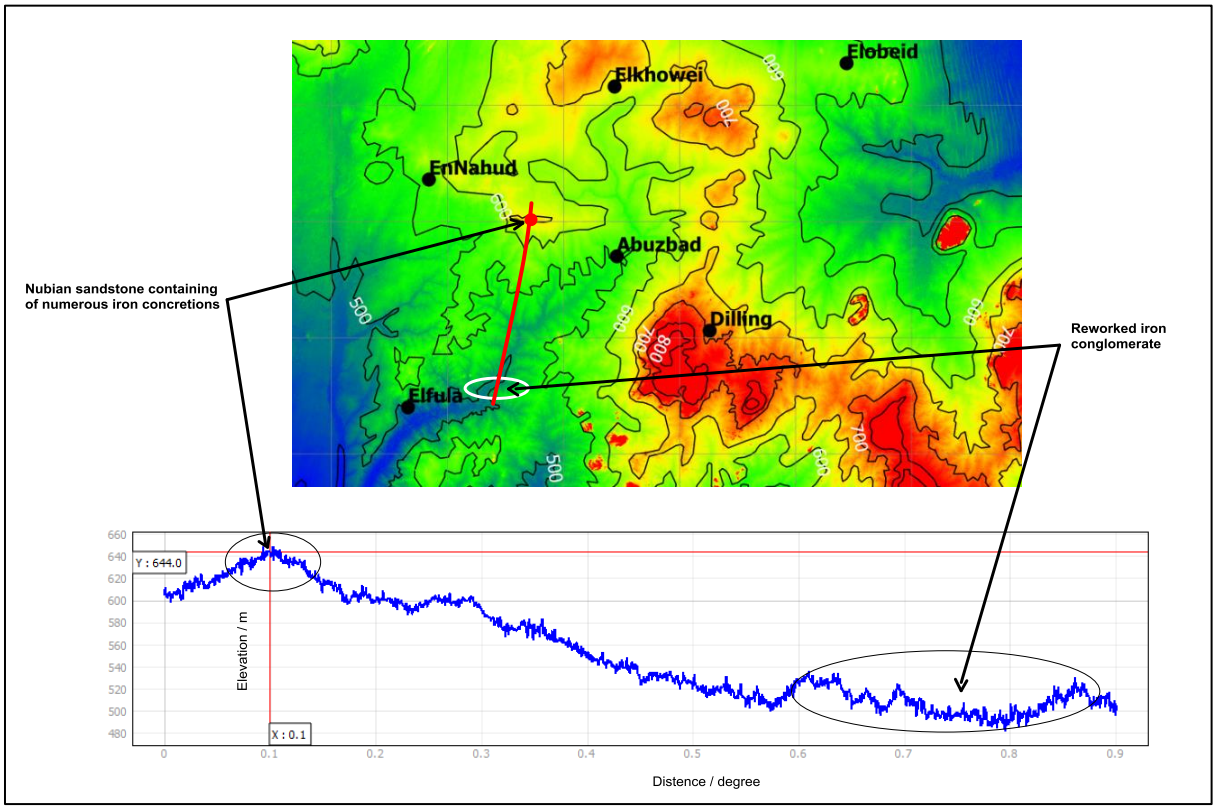


*Fig. 3.24: Topographic profile from southeast En Nahud to east El Fula. The topographic profile passes across an iron-rich outcrop of Nubian sandstone in the North to the iron-rich conglomerate of the El Fula section to the South.*

Therefore, the iron concretions of the conglomerates of the Abu Zabad, El Fula and El Kohwei are interpreted as reworked from the Nubian sandstone located to the West and North. The topography supports this interpretation, since El Fula and Abu Zabad are located on the southern slope of the Nubian sandstone plateau, while En Nahud and El Khowei are located upon the latter (Fig. 3.24).

#### 3.4.1.2.B. Low regime channel facies (poorly sorted sand sediment beds)

*Description*: This facies is formed of poorly sorted sand, which exhibits some small lithoclasts within the size-range of fine gravel. Its color varies from pale grey to reddish brown (Fig. 3.25). This facies is marked by current features, such as trough cross bedding and planar cross bedding. Local planar lamination and current ripples are observed in the medium to fine sand beds. Locally these poorly sorted sand beds are lens-shaped (Fig. 3.26). In this case, their basal contact is abrupt and conformable separating it from the underlying high regime channel facies (southern areas), while it is either an erosional unconformable contact when this facies overlies the mottled facies, or abrupt and conformable contact when overlying other alluvial sediments (northern areas).

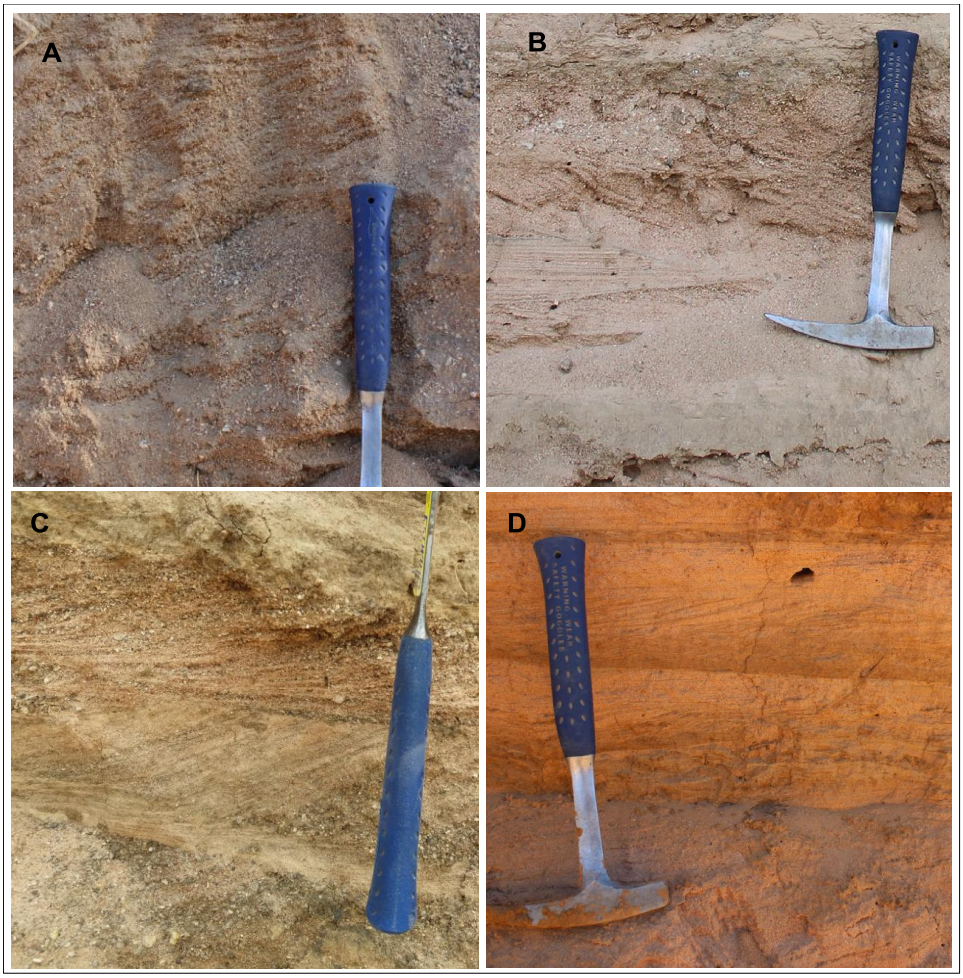


*Fig. 3.25: Moderate regime channel facies.* ***(A)*** *Planar cross bedded, poorly sorted sand with some lithoclasts mostly concentrated in the lower part, Dilling area.* ***(B)*** *Coarse, planar cross-bedded sand in the upper part, laminated medium sand in the middle part, medium sand in the lower part, and few lithoclasts in the upper part, Dilling area.* ***(C)*** *Alternating coarse- and medium-grained, trough cross-bedded sand beds, East Abu-Zabad. The coarse sand is poorly sorted and contains gravels (lithoclasts).*

***(D)*** *Fine to medium rippled sand, planar laminae and planar cross bedding in the upper part; medium to coarse sand sediments with some planar cross bedding in the lower part, South El-Obeid2.*

*Fig. 3.26: Lens-shaped bed, medium-grained sand sediments.*

*Distribution:* This facies is common in the southern part of the study area, around Dilling, east of Abu-Zabad and south of El-Obeid.

*Interpretation*: The occurrence of planar and trough cross-bedding, planar lamination and current ripples in the sand sediment beds supports a moderate-energy fluviatile depositional environment (Boggs, 2006; Hewaidy et al., 2018). The high flow energy resulted in development of the trough and planar cross bedding, while the moderately to low energy resulted in the development of planar lamination and current ripples. The poor sorting of sediment may indicate energy variability, sudden lowering down in the energy, or high amount of transported sediment loads. It may also indicate sand bar deposition under braided system conditions (Smith, 1970).

### 3.4.1.3. Alternating sand and silt sediments (flood plain facies)

*Description*: Lithologically this facies is formed of fine- to medium-grained sand, alternating with sandy shale and fine-grained sand sediments beds. Medium- to coarse-grained sand beds are observed in some sites (e.g. Dilling, south El-Obeid2). The color of sand beds is red to reddish brown, while that of silt or shale beds varies from dark grey to green in the Dilling area, and from reddish-brown to dark grey in northern parts (south El Obeid) (Fig. 3.27).

The alternating beds result in an apparently cyclic sedimentation (Fig. 3.28). Sand sediment beds are locally lens-shaped, as observed south of El Obeid (Fig. 3.26); they are marked by planar or trough cross-bedding, current ripples, planar lamination, and are locally poorly sorted or may present a fining-upward evolution (Fig. 3.29). The base of sand sediment beds in the Dilling area is an abrupt and conformable contact, while South of El Obeid, the sand sediments base is an erosional unconformable contact, eroding the underlying mottled facies. The contacts between the sand and silt sediments are all abrupt and conformable. The fine-grained beds are marked by current ripples and planar laminations. Laminae are mostly 2 to 5 mm thick, but may be 5 mm to 1 cm thick, and rarely reach 1 to 2 cm thick, as observed in the south El-Obeid1 section.

*Distribution*: This facies is common in the southern part of the study area, around Dilling, El-Fula, east of Abu-Zabad, and south of El-Obeid.

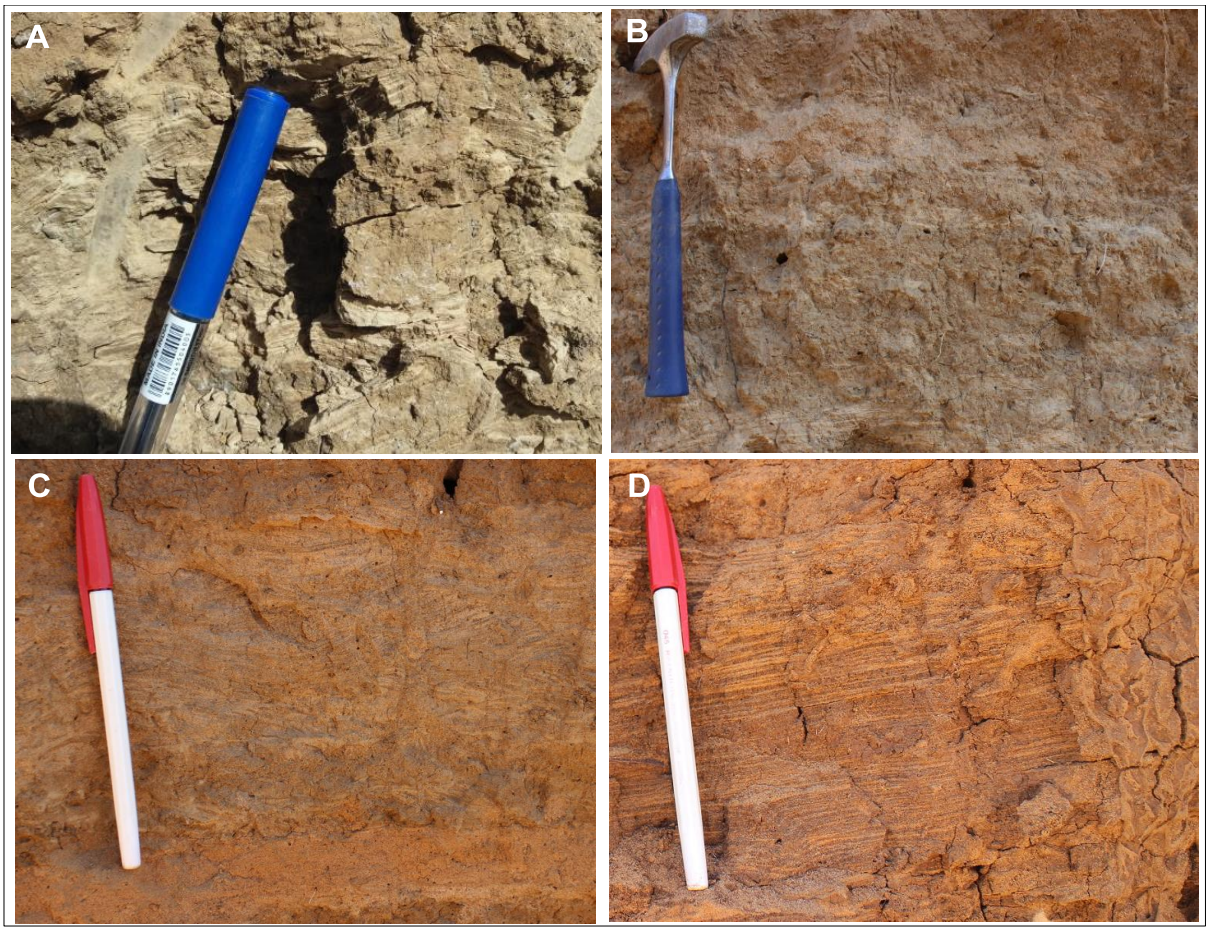


*Fig. 3.27: Flood plains Facies.* ***(A)*** *South El-Obeid3 (Es-Sonjokaya): alternating silt and rippled fine sand.* ***(B)*** *Dilling: sandy shale, rippled in the upper part and laminated in the lower part.* ***(C)*** *South El-Obeid2: laminated fine sand and shale.* ***(D)*** *South El-Obeid1 (Khour Kazgail): well sorted, medium rippled sand, planar laminae and planar cross bedding in the upper part; well sorted coarse sand sediments with low degree of planar cross bedding in the lower part.*

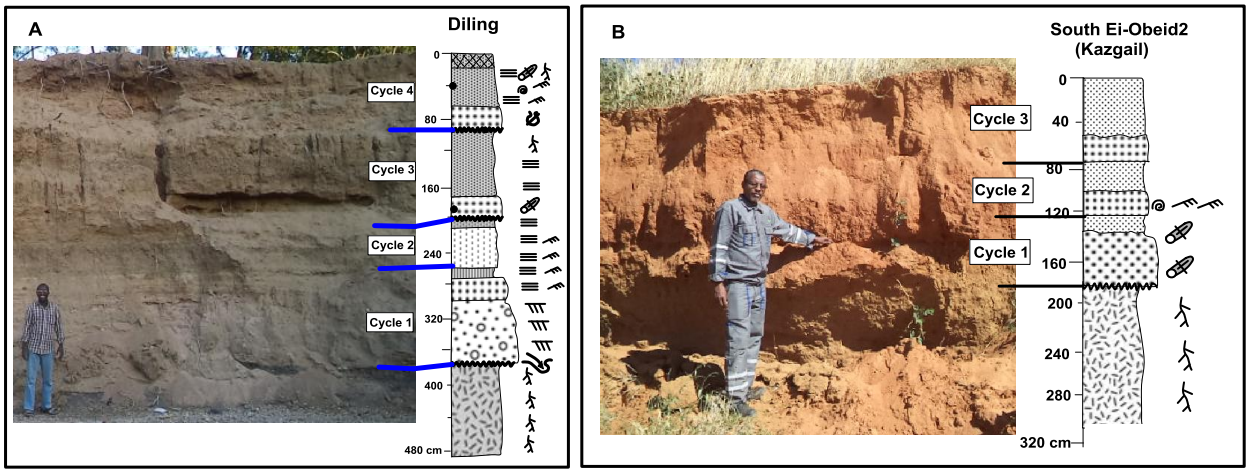


*Fig. 3.28: Cyclic sedimentation. (****A****) Section made of four cycles: the lower cycle is composed of conglomerate, medium sand, and sandy shale; the second cycle comprises fine sand and sandy shale sediments; the third cycle consists of medium sand and sandy shale; and the fourth one is also composed of medium sand and sandy shale sediments (****B****) Section composed of sand sediments beds of various*

*granulometry. The lower cycle is made of two beds: coarse sand and fine sand sediments; the second and third cycles consist of medium sand and fine sand sediments.*

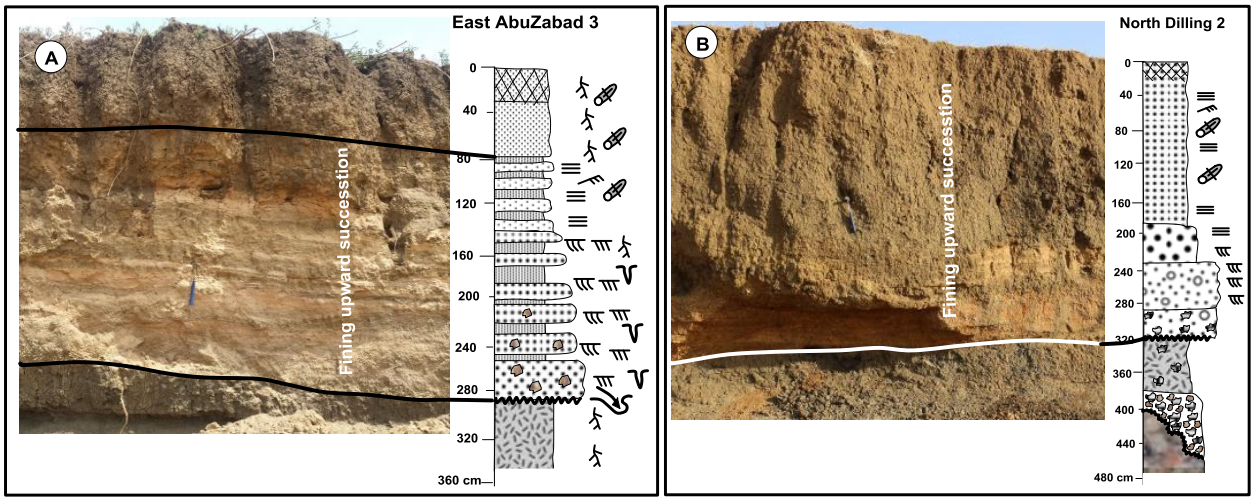


*Fig. 3.29: Fining upward successions. (**A**) The grain size evolves from coarse conglomeratic sand at the base to clayey sand to the top. (**B**) The mean grain size evolves upward from conglomerate to medium sand.*

*Interpretation*: The occurrence of planar and trough cross-bedding, planar lamination and current ripples in the sand sediment beds supports a high- to low-energy fluviatile depositional environment (Boggs, 2006; Hewaidy et al., 2018). As a matter of fact, fluviatile deposits commonly display abundant traction structures, such as planar and trough cross-bedding, upper-flow-regime planar bedding and ripple-marked surfaces (Boggs, 2006).

The alternating beds of sand and silt sediments are assumed to be formed in the flood plain of a river. When the river comes out of its channel, it first deposits the coarse-grained sediments in a high energy regime, and as the flood decreases in intensity, the fine particles are laid down (Boggs, 2006). The locally observed fining upward evolution that indicates a gradual decrease in current strength through time, supports the flood plain environment for this facies. This repeated mechanism leads to a cyclic sedimentation. The lens shape of the sand (e.g., south El Obeid1) may be formed due to subsequent erosion, to flood deposits, to the topography of the flood plain, or may represent crevasse splay deposits.

### 3.4.1.4. Red sand facies

*Description*: The granulometry of the sand is dominated by fine grains, but coarser sands are found in the northernmost part of the study area. Generally, this facies is very homogeneous and devoid of any current features. The sediment is usually harder than the flood plain deposits and looks compacted or cemented. The red color is common in all parts, but reddish brown colors are found locally (Fig. 3.30).

*Distribution*: It is the most widespread facies; it is common in all sites but the Dilling area.

*Interpretation*: The usual absence of sedimentary features and the prevailing fine grained sand, suggest that this facies has been deposited by aeolian processes. However, in the southern areas, some fine- to medium-grained intercalations of fluviatile sands suggest that the aeolian deposits were spradically reworked by alluvial processes. Note that these southern areas are presently

the wettest and steepest zones of the study area, which may explain stronger alluvial processes than in the northern regions. The hardness of the sediment and its reddish color is probably due to its cementation with iron oxide cement.

Edmond (1942) reported that these deposits in Kordofan, are typical wind deposited sand with well-rounded quartz grains and a color varying from pale buff to deep red. He also noted that the red color is due to iron staining on the surface of the quartz grains. Investigations on mid-Pleistocene red sediments in sub-tropical China, concluded that these deposits were subject to considerable mixing prior to deposition and strong subsequent chemical weathering (Hong et al., 2013).


*Fig. 3.30: Red clayey sand facies.* ***(A)*** *Red clayey fine sand facies (above the white line, South El-Obeid2 (Kazgail)).* ***(B)*** *Red clayey fine sand sediments facies, the upper half part is laminated (El Khowei).* ***(C)*** *Red clayey fine sand sediments facies (above the white line), eroded by the overlying laminated fine sand (El-Fula).* ***(D)*** *Medium to fine, red clayey sand sediments (above the white line, North Bara).*

Many soils within the tropical, subtropical, equatorial and Mediterranean climatic zones contain a significant amount of clay minerals - dominantly kaolinite - and are frequently characterized by a moderate to high amount of "free" iron oxides. These oxides, which include hydroxides and hydrous oxides, either occur in the form of amorphous gels, discrete particles as coatings on sand *grains*, or form part of the soil matrix as micro aggregates, cemented aggregates of a few centimeters in diameter, or cemented continuous soil layers. Many of these soils present red colors (Volkoff, 1998).

#### 3.4.1.5. Sandy carbonate facies

*Description:* This facies is partially formed of massive, poorly lithified limestone beds and partially of sandy to silty limestone beds. Generally, it is deeply karsted and presents root traces (casts / molds) and minor desiccation cracks. Well preserved gastropod shells are common, and are usually highly concentrated at the top of the bed. Locally however, gastropod shells are concentrated within the facies itself (Fig. 3.31). This facies also occurs locally as clasts reworked in subsequent channel deposits (Fig. 3.32).

*Distribution*: This facies is widespread in the western-central part of the study area, from the En-Nahud to the El-Khowei areas.

*Interpretation*: The lithology and sedimentary features of this facies indicate a shallow, subaqueous deposition, frequently exposed to desiccation. They are consequently interpreted as palustrine deposits (Freytet and Verrecchia, 2002; Alonso-Zarza, 2003; Alonso-Zarza et al., 2011). Pure or granular limestone is formed in the bottom of shallow water bodies (Alonso-Zarza, 2003), while silty and/or sandy limestone is formed in less shallower water. However, soils accumulated in the lake shores are sometimes very rich in carbonates and are true palustrine limestones (Freytet and Verrecchia, 2002). In palustrine carbonates, precipitation of lime mud occurs in a lacustrine water body, the palustrine carbonates necessarily form on previous lacustrine mud (Alonso-Zarza, 2003).

Roots induce movement of water and chemical elements (Clothier and Green, 1997, *in* Alonso-Zarza, 2003) and act in two different ways: (i) by penetrating the lacustrine mud when the level of the lake drops, and/or (ii) inducing the biochemical precipitation of carbonate around the rhizosphere. In either case, the carbonates formed in these conditions present evidences of active pedogenic processes or long-lasting exposure periods (Alonso-Zarza, 2003). Limestones with root cavities indicate the presence of a well-established vegetation cover and suggest that the root system had to penetrate the recently deposited sediments to reach the water table (Alonso-Zarza, 2003).

Desiccation cracks are common in the palustrine facies (Alonso-Zarza, 2003; Alonso-Zarza et al., 2011) and are usually due to subsequent sub-aerial exposure (Alonso-Zarza, 2003).

The intensity and duration of the desiccation and root penetration, as well as any later rise in the water table during more humid periods, can cause the reworking, concentration, and coating of the mud fragments (Alonso-Zarza, 2003). Karstification, desiccation and root penetration make easy the fragmentation of this facies and its reworking into subsequent sedimentary deposits (Alonso-Zarza et al., 2011).

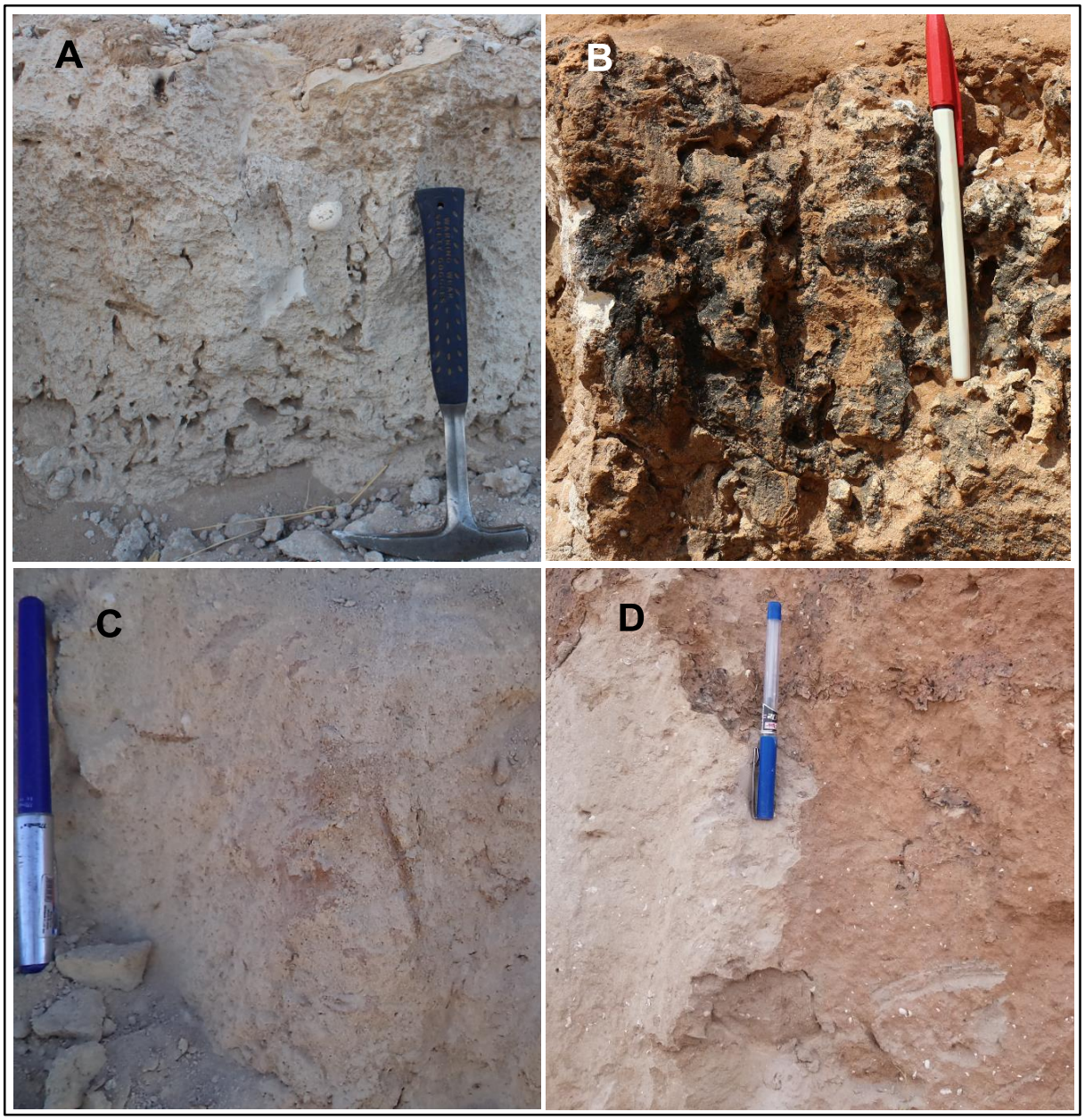


*Fig. 3.31: Palustrine facies. (**A**) Lithified whitish-grey limestone, containing gastropod shells within the unit and on its upper surface (En Nahud). (**B**) White limestone, deeply karsted, with gastropod shells on its top (the black color is due to surficial iron coating) (El Khowei). (**C**) Grey friable sandy limestone (El Khowei). (**D**) Pale grey sandy limestone containing calcareous nodules and gastropod shells (West El Khowei).*

### 3.4.1.6. Carbonate facies

*Description*: This facies consists of low density, 15 to 45 cm thick, marly or chalky limestone beds, deeply karsted, brecciated in its upper part, white to pale grey in color, and is marked by the occurrence of abundant gastropod shells and locally ostracods (Fig. 3.33). In the El-Ga'ah well, three horizons of this facies have been observed alternating with argillaceous sand sediments facies.

*Fig. 3.32: Palustrine facies reworked in channel deposits.*

*Distribution*: This facies is restricted to the northern part of the study area, around El-Ga'a and Sodari and locally in north Bara. It has been observed in outcrops only in topographic depressions (Sodari).

*Interpretation*: The formation of this facies requires the presence of water bodies, but probably different than those required to form the palustrine facies of the En Nahud – El Khowei area. The scarcity of sandy component and the low density ascribed to the presence of abundant diatoms shells suggest a deeper depositional depth. This facies is, therefore, interpreted as deposited in lacustrine environments. The deeply karsted and brecciated upper surfaces of the limestone beds indicate subaerial exposure and is common in lacustrine environment (Freytet and Verrecchia, 2002; Alonso-Zarza, 2003). An idealized sketch of the distribution of continental carbonate facies in Uruguay proposed by Alonso-Zarza et al. (2011) shows that the lacustrine facies are formed under a thicker water column than the palustrine facies.

Lakes are dynamic systems sensitive to subtle changes in climate, such as fluctuations in precipitation and run-off. Lacustrine environments, therefore, are unstable, and as a result, lacustrine facies patterns are vertically and laterally complex (Tucker and Wright, 1990). This variability leads to alternating sedimentation features in these lacustrine facies.

This alternating feature and the existence of karsted and brecciated features in the upper surface of each carbonate level, indicates that the lake has filled up and evaporated more than one time. After each filling up stage, argillaceous sand sediments are overlain by lacustrine deposits, and after each evaporative stage, desiccation and brecciated features took place on the upper surface

of the lacustrine limestone. Alonzo-Zarza et al. (2011) reported that lacustrine facies may alternate with palustrine facies. In continental series, lacustrine limestone is often associated with other deposits including shales or varved clays, sometimes rich in organic matter, and fine, medium or coarse sand (Freytet, 1973).

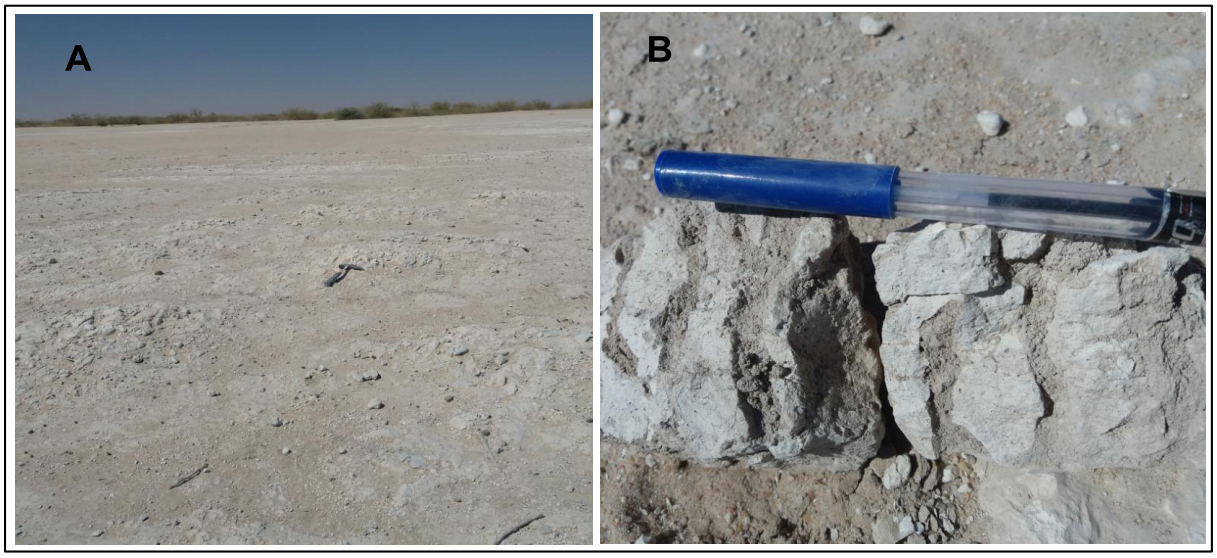


*Fig. 3.33: Carbonate facies.* ***(A)*** *Outcrop of diatomite limestone formed in a small lake (Sodari).* ***(B)*** *Detail of photograph A, showing deep karstifications infilled with argillaceous sand sediments.*

### 3.4.1.7. Argillaceous sandstone facies

*Description*: It consists of fine sand grains in a friable argillaceous matrix, locally containing irregular lacustrine limestone clasts. Its color is mainly grey, especially around El-Ga'ah and Sodari, and is yellowish in north Bara (Fig. 3.34). In the El-Ga'ah section it is intercalated with the lacustrine limestone facies.


*Fig. 3.34: Argillaceous sand sediments facies.* ***(A)*** *Yellow argillaceous sand (below the dashed line) (North Bara).* ***(B)*** *Grey argillaceous sand (below the dashed line), marked by well-preserved gastropod shells in the upper part (Sodari).*

*Distribution*: This facies is restricted to the northern parts of the area, around El-Ga'ah and Sodari, and locally in north Bara.

*Interpretation*: The alternation of this facies with the lacustrine facies suggests alternating lacustrine and alluvial depositional environments, resulting in the deposition of alternating lacustrine limestone and argillaceous sand sediments, respectively.

The existence of lacustrine limestone fragments in this argillaceous facies indicates that the underlying lacustrine limestones have been reworked and redeposited with the argillaceous sand sediments.

### 3.4.1.8. Clinoform bearing, coarse clastic facies

*Description*: This facies comprises coarse sand and gravel beds, the strata of which exhibit a marked inclination. The color varies between red and pale yellow; the red color dominates in the upper part, while the pale yellow is restricted to the lower beds. It overlies the lacustrine limestone facies of the El Ga'ah paleo-lake. The thickness of these sediments exceeds 5 meters in the excavated section and decreases toward the lake, as a result of the clinoform nature of the beds (Fig. 3.35). The beds are inclined toward the East or Southeast (toward the lake). Moreover, some fine-grained beds exhibit well preserved gastropod shells and thick root molds (Fig. 3.36).

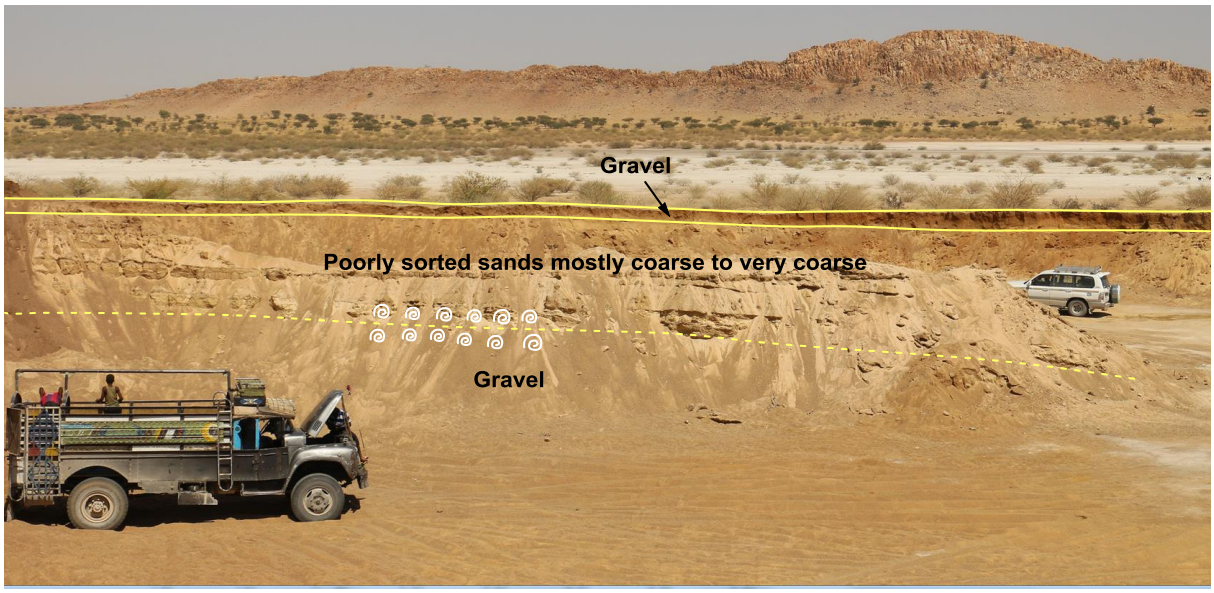


*Fig. 3.35: View of the clinoform bearing coarse clastic facies in El Ga'ah.*

*Distribution*: It is a very local facies, observed only in the El Ga'ah area.

*Interpretation*: The coarse material of this facies indicates the proximity of a stream that supplied the clastic material. The well-marked clinoforms and the fact that these coarse-grained clastic deposits overly lacustrine sediments led us to interpret them as delta sediments prograding into the El Ga'ah paleolake. This indicates that this area, and probably part of the northern study area, locally experienced a strong fluvial activity during the late phase of lake

forming. The presence of shells of gastropods mostly living at the shoreline, suggests an intermittent regime of the river feeding the delta. The thick root molds indicates vegetation growing close to the shoreline.


*Fig. 3.36: Details of the delta facies. (A) Gastropod shells. (B) Gastropod shells horizon between the two yellow lines, very coarse sand above the upper yellow line, and gravelly bed at the lower part of the image. (C) Root molds concentration zone.*

## 3.5. Grain size analysis

### 3.5.1. Introduction

The grain size of a total of 48 samples, collected from excavated sections in four sites, were analyzed. All sections are formed of two facies: the mottled facies in their lower part and the red sand facies in their upper part (Fig. 3.37). Field observation showed that these facies display variations in terms of grain size. Therefore, the grain size analysis have been carried out not only to understand how important these variations are, but also to specify the origin of the sands and the transport and deposition processes. The studied sections are North Bara3, North Bara1, West El-Obeid (Ayara) and East Abu-Zabad (Dabkar). They are aligned along a 280 km long, NNE-SSW trending transect (Fig. 3.38). The topographic profile shows a NNE-dipping slope with average gradient of 0.85 m/km, and a short, steep SSW-dipping slope to the South (Fig. 3.39).

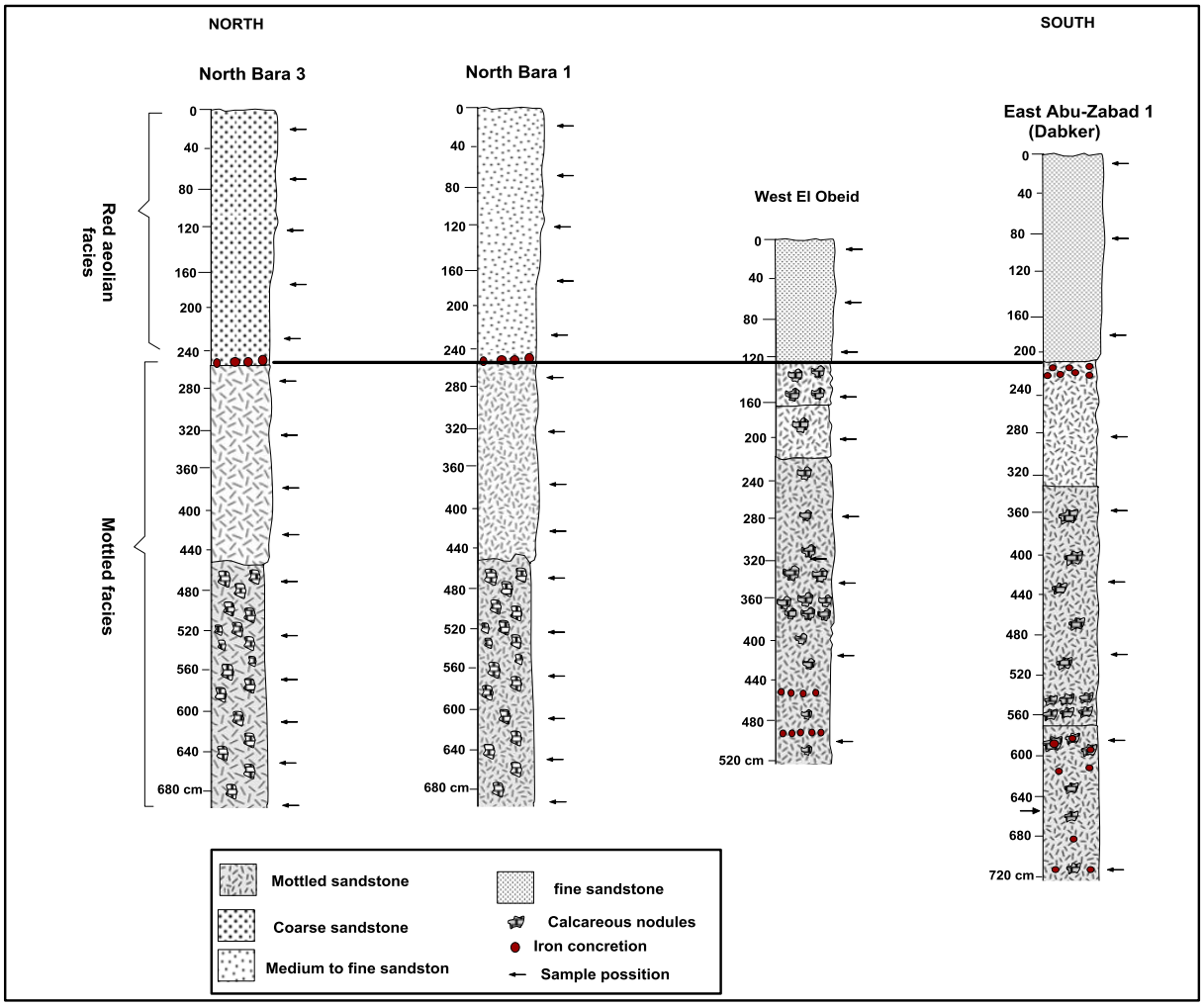


*Fig. 3.37: Lithology of the studied sections and location of the samples analyzed for grain size analysis.*

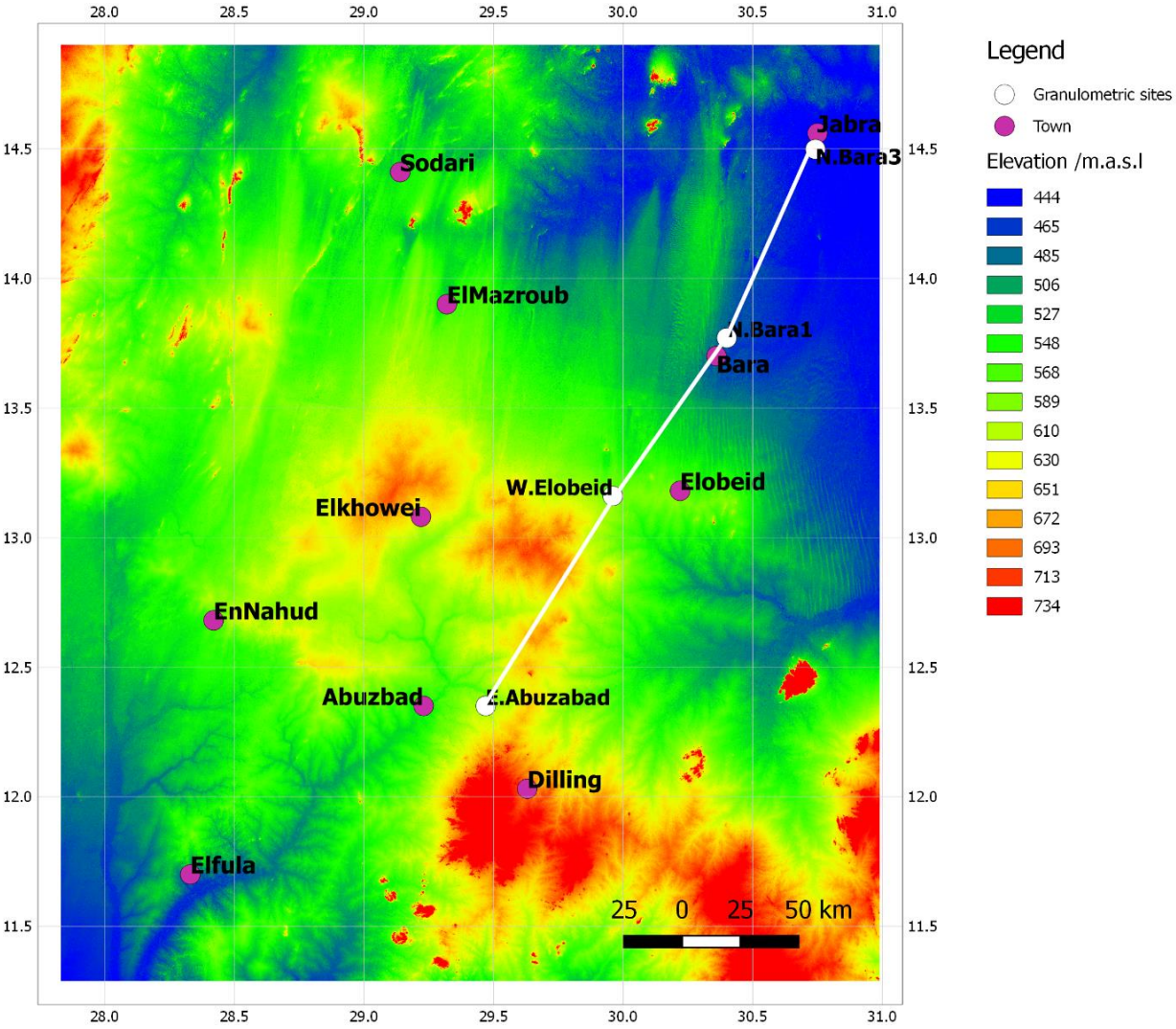


*Fig. 3.38: Location map of the sections studied for grain size analysis.*

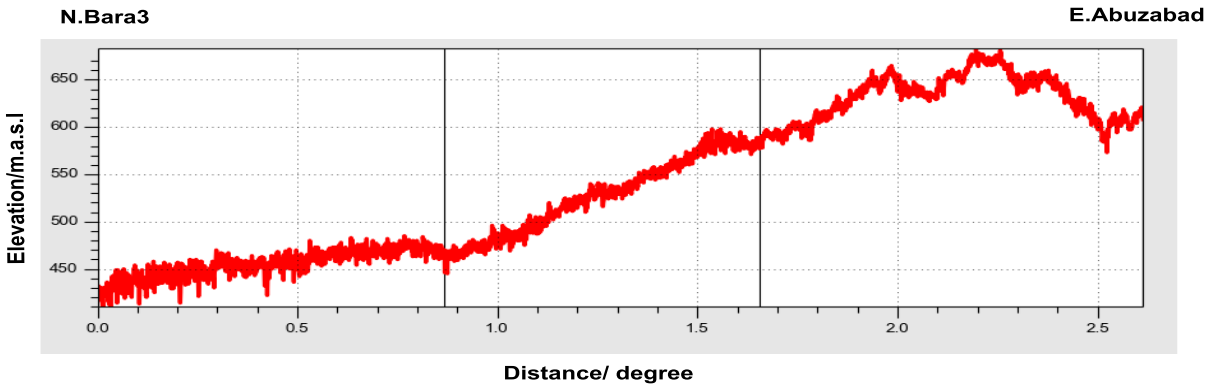


*Fig. 3.39: NE-SW topographic profile showing the gradient in the study area (NW is on the left).*

### 3.5.2. Results

#### 3.5.2.1. Cumulative curves

The 48 cumulative curves representing the 48 samples from four sections have been plotted in semi-log distribution graph, and compiled on one graph gathering data from each section (Fig.

3.40). The curves are distributed in size range between 2.6 and 0.012 mm. The maximum and minimum grain sizes are recorded in the North Bara3 and East Abu Zabad sections, respectively. On the other hand, the size range is different from one section to another. While in north Bara3, it ranges between 2.6 and 0.029 mm, it is comprised between 1.1 mm and 0.015 mm in North Bara1, between 1.0 to 0.015 mm in west El Obeid, and between 0.8 and 0.012 mm in East Abu Zabad.

The measures in phi units for Φ 5, Φ 16, Φ 25, Φ 50, Φ 75, Φ 84, and Φ 95 have been obtained from each curve, in order to calculate the graphical statistics of the mean, standard deviation (sorting), skewness and kurtosis (Table 3.4). Frequency curves have been built from the cumulative curves following Folk (1974). However, the frequency curves are not applicable to calculate graphical statistics (Folk, 1974); therefore, some representative frequency curves presented in fig. 3.41 only show the normal grain size distribution.

Abbreviations (table 3.5) have been used to characterize the graphical statistic descriptions presented in Table 3.6 and Figures 3.42 to 3.45.

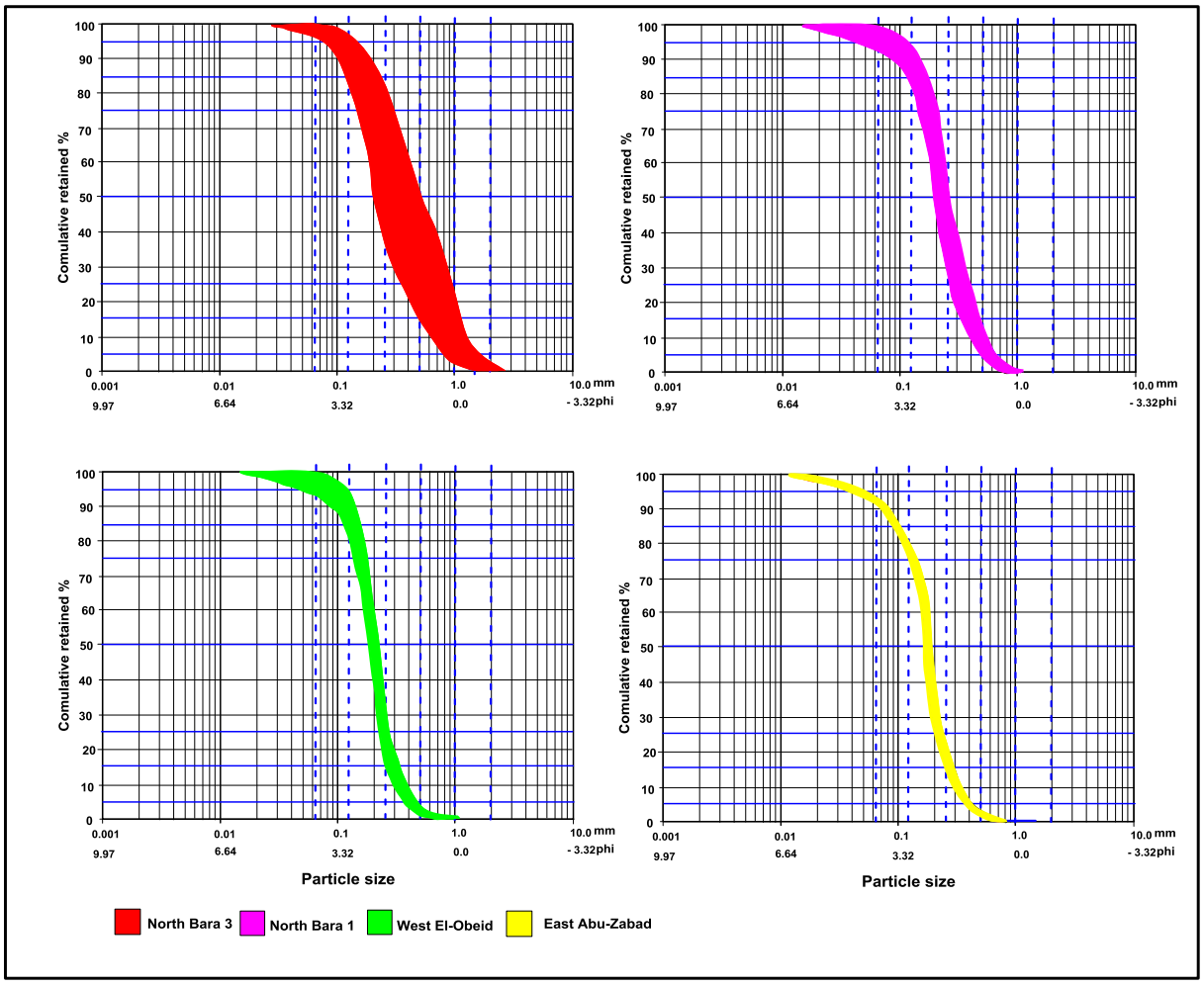


*Fig. 3.40: Cumulative grain size distribution zones of all sample's curves.*

***Table 3.4: Graphic measure of phi unit from curves of the analyzed samples.***

| Sample | Φ 5 | Φ 16 | Φ 25 | Φ 50 | Φ 75 | Φ 84 | Φ 95 |
|---|---|---|---|---|---|---|---|
| **N.Bara 3-6** | -0,58 | 0,03 | 0,42 | 1,43 | 2,47 | 2,74 | 3,32 |
| **N.Bara 3-7** | -0,38 | 0,12 | 0,42 | 1,45 | 2,47 | 2,74 | 3,25 |
| **N.Bara 3-8** | -0,38 | 0,07 | 0,36 | 1,00 | 1,79 | 2,00 | 2,93 |
| **N.Bara 3-9** | -0,49 | -0,14 | 0,12 | 1,00 | 2,12 | 2,64 | 3,18 |
| **N.Bara 3-10** | -0,38 | 0,01 | 0,25 | 1,29 | 2,40 | 2,72 | 3,18 |
| **N.Bara 3-11** | -0,38 | -0,14 | 0,23 | 1,56 | 2,51 | 2,74 | 3,32 |
| **N.Bara 3-12** | -0,32 | 0,06 | 0,47 | 1,84 | 2,74 | 3,00 | 3,18 |
| **N.Bara 3-13** | -0,32 | 0,06 | 0,45 | 1,67 | 2,51 | 2,84 | 3,64 |
| **N.Bara 3-14** | -0,26 | 0,34 | 0,89 | 2,00 | 2,74 | 2,95 | 3,64 |
| **N.Bara 3-16** | 0,29 | 0,97 | 1,43 | 2,22 | 2,71 | 2,89 | 3,44 |
| **N.Bara 3-17** | 0,25 | 0,84 | 1,36 | 2,18 | 2,64 | 2,90 | 3,40 |
| **N.Bara 3-18** | 0,20 | 0,79 | 1,25 | 1,89 | 2,66 | 2,86 | 3,46 |
| **N.Bara 3-19** | 0,15 | 0,59 | 0,97 | 1,84 | 2,64 | 2,84 | 3,56 |
| **N.Bara 3-20** | 0,10 | 0,56 | 0,94 | 1,89 | 2,64 | 2,89 | 3,57 |
| **N.Bara 3-21** | 0,07 | 0,49 | 0,89 | 1,72 | 2,69 | 2,94 | 3,61 |
| **N.Bara 1-2** | 0,74 | 1,15 | 1,38 | 2,05 | 2,47 | 2,74 | 3,40 |
| **N.Bara 1-3** | 0,68 | 1,15 | 1,45 | 2,01 | 2,32 | 2,65 | 3,32 |
| **N.Bara 1-4** | 0,81 | 1,36 | 1,69 | 2,25 | 2,66 | 2,82 | 3,35 |
| **N.Bara 1-5** | 0,94 | 1,60 | 1,84 | 2,36 | 2,72 | 2,88 | 3,56 |
| **N.Bara 1-6** | 0,64 | 1,36 | 1,74 | 2,27 | 2,64 | 2,76 | 3,18 |
| **N.Bara 1-7** | 0,64 | 1,36 | 1,74 | 2,28 | 2,60 | 2,74 | 3,18 |
| **N.Bara 1-8** | 0,67 | 1,40 | 1,76 | 2,28 | 2,64 | 2,78 | 3,18 |
| **N.Bara 1-9** | 0,62 | 1,34 | 1,69 | 2,25 | 2,64 | 2,93 | 3,40 |
| **N.Bara 1-10** | 0,97 | 1,43 | 1,74 | 2,25 | 2,69 | 2,84 | 3,44 |
| **N.Bara 1-11** | 0,89 | 1,40 | 1,64 | 2,32 | 2,70 | 2,94 | 3,80 |
| **N.Bara 1-13** | 0,86 | 1,32 | 1,60 | 2,22 | 2,74 | 3,01 | 4,51 |
| **N.Bara 1-14** | 0,84 | 1,43 | 1,69 | 2,25 | 2,78 | 2,89 | 3,99 |
| **N.Bara 1-15** | 1,00 | 1,47 | 1,81 | 2,32 | 2,77 | 3,01 | 3,90 |
| **N.Bara 1-16** | 0,97 | 1,47 | 1,84 | 2,25 | 2,80 | 3,02 | 3,94 |
| **N.Bara 1-17** | 0,69 | 1,15 | 1,43 | 2,01 | 2,56 | 2,92 | 3,74 |
| **Ay 1** | 1,27 | 1,74 | 2,00 | 2,47 | 2,84 | 3,06 | 4,32 |
| **Ay 2** | 1,15 | 1,69 | 1,94 | 2,32 | 2,76 | 2,99 | 4,21 |
| **Ay 3** | 1,15 | 1,64 | 1,84 | 2,22 | 2,58 | 2,77 | 3,06 |
| **Ay 4** | 1,22 | 1,74 | 2,00 | 2,32 | 2,75 | 2,94 | 3,84 |
| **Ay 5** | 1,40 | 1,89 | 2,06 | 2,40 | 2,78 | 2,98 | 3,84 |
| **Ay 6** | 1,36 | 1,89 | 2,08 | 2,47 | 2,84 | 3,00 | 4,06 |
| **Ay 7** | 1,29 | 1,74 | 2,00 | 2,32 | 2,73 | 2,87 | 3,64 |
| **Ay 8** | 1,15 | 1,71 | 1,89 | 2,29 | 2,65 | 2,81 | 3,32 |
| **Ay 9** | 1,22 | 1,74 | 2,02 | 2,40 | 2,75 | 2,92 | 3,59 |
| **Dab 1** | 1,32 | 1,84 | 2,18 | 2,51 | 2,94 | 3,40 | 4,47 |
| **Dab 2** | 1,36 | 1,84 | 2,12 | 2,60 | 2,88 | 3,37 | 4,41 |
| **Dab 3** | 1,43 | 1,89 | 2,25 | 2,56 | 2,89 | 3,32 | 4,35 |

| | | | | | | | |
|---|---|---|---|---|---|---|---|
| **Dab 4** | 1,32 | 1,79 | 2,18 | 2,47 | 2,90 | 3,35 | 4,51 |
| **Dab 5** | 1,40 | 1,84 | 2,12 | 2,56 | 2,87 | 3,37 | 4,44 |
| **Dab 6** | 1,36 | 1,94 | 2,25 | 2,60 | 2,97 | 3,40 | 4,64 |
| **Dab 7** | 1,42 | 1,89 | 2,18 | 2,56 | 2,94 | 3,35 | 4,54 |
| **Dab 8** | 1,29 | 1,79 | 2,06 | 2,47 | 2,89 | 3,32 | 4,47 |
| **Dab 9** | 1,32 | 1,84 | 2,16 | 2,56 | 2,95 | 3,35 | 4,44 |

***Table 3.5: Abbreviation of the graphical statistic descriptions.***

| **Standard deviation** | | **Skewness** | | **Kurtosis** | |
|---|---|---|---|---|---|
| Description | Abbreviation | Description | Abbreviation | Description | Abbreviation |
| Very well sorted | *VWs* | Very fine skewed | *Vfsk* | Very platykurtic | *Vpk* |
| Well sorted | *Ws* | Fine skewed | *Fsk* | Platykurtic | *Pk* |
| Moderately sorted | *Ms* | Symmetrical | *Sy* | Mesokurtic | *Mk* |
| Poorly sorted | *Ps* | Coarse skewed | *Csk* | Leptokurtic | *Lk* |
| Very poorly sorted | *VPs* | Very coarse skewed | *Vcsk* | Very leptokurtic | *Vlk* |
| Extremely poorly sorted | *ExPs* | | | Extremely leptokurtic | *Exlk* |

***Table 3.6: Calculated graphical statistics and their descriptions for all samples.***

| **Sample** | **Mean** | **Standard de deviation** | | **Skewness** | | **Kurtosis** | |
|---|---|---|---|---|---|---|---|
| | | **Value / phi** | **Description** | **Value / phi** | **Description** | **Value / phi** | **Description** |
| N.Bara 3-14 | 1,76 | 1,25 | Ps | -0,21 | Csk | 0,87 | Pk |
| N.Bara 3-13 | 1,52 | 1,30 | Ps | -0,08 | Sy | 0,79 | Pk |
| N.Bara 3-12 | 1,63 | 1,27 | Ps | -0,22 | Csk | 0,64 | Vpk |
| N.Bara 3-11 | 1,39 | 1,28 | Ps | -0,11 | Csk | 0,67 | Pk |
| N.Bara 3-10 | 1,34 | 1,22 | Ps | 0,06 | Sy | 0,68 | Pk |
| N.Bara 3-9 | 1,17 | 1,25 | Ps | 0,19 | Fsk | 0,75 | Pk |
| N.Bara 3-8 | 1,02 | 0,98 | Ms | 0,10 | Sy | 0,95 | Pk |
| N.Bara 3-7 | 1,44 | 1,20 | Ps | -0,01 | Sy | 0,72 | Pk |
| N.Bara 3-6 | 1,40 | 1,27 | Ps | -0,04 | Sy | 0,72 | Pk |
| N.Bara 3-21 | 1,72 | 1,15 | Ps | 0,04 | Sy | 0,80 | Pk |
| N.Bara 3-20 | 1,78 | 1,11 | Ps | -0,09 | Sy | 0,84 | Pk |
| N.Bara 3-19 | 1,75 | 1,08 | Ps | -0,05 | Sy | 0,83 | Pk |
| N.Bara 3-18 | 1,84 | 1,01 | Ps | -0,05 | Sy | 0,95 | Mk |
| N.Bara 3-17 | 1,97 | 0,99 | Ms | -0,27 | Csk | 1,00 | Mk |
| N.Bara 3-16 | 2,03 | 0,96 | Ms | -0,26 | Csk | 1,02 | Mk |
| N.Bara 1-11 | 2,22 | 0,83 | Ms | -0,057 | Sy | 0,99 | Lk |
| N.Bara 1-10 | 2,17 | 0,72 | Ms | -0,071 | Sy | 1,24 | Mk |
| N.Bara 1-9 | 2,17 | 0,82 | Ms | -0,180 | Csk | 1,07 | Lk |
| N.Bara 1-8 | 2,15 | 0,73 | Ms | -0,135 | Csk | 1,22 | Lk |
| N.Bara 1-7 | 2,12 | 0,73 | Ms | -0,287 | Vcsk | 1,15 | Lk |
| N.Bara 1-6 | 2,13 | 0,73 | Ms | -0,312 | Csk | 1,21 | Lk |
| N.Bara 1-5 | 2,28 | 0,72 | Ms | -0,281 | Csk | 1,17 | Lk |
| N.Bara 1-4 | 2,14 | 0,75 | Ms | -0,160 | Csk | 1,19 | Mk |

| | | | | | | | |
|---|---|---|---|---|---|---|---|
| N.Bara 1-3 | 1,94 | 0,78 | Ms | -0,101 | Sy | 1,06 | Lk |
| N.Bara 1-2 | 1,98 | 0,80 | Ms | -0,091 | Sy | 1,13 | Mk |
| N.Bara 1-13 | 2,18 | 0,97 | Ms | 0,098 | Sy | 1,31 | Lk |
| N.Bara 1-14 | 2,19 | 0,84 | Ms | -0,011 | Sy | 1,19 | Lk |
| N.Bara 1-15 | 2,27 | 0,82 | Ms | -0,007 | Sy | 1,24 | Lk |
| N.Bara 1-16 | 2,25 | 0,84 | Ms | 0,067 | Sy | 1,27 | Mk |
| N.Bara 1-17 | 2,03 | 0,90 | Ms | 0,086 | Sy | 1,11 | Mk |
| Ay 1 | 2,42 | 0,79 | Ms | 0,05 | Sy | 1,496 | Lk |
| Ay 2 | 2,33 | 0,79 | Ms | 0,13 | Fsk | 1,542 | Vlk |
| Ay 3 | 2,21 | 0,57 | MWs | -0,07 | Sy | 1,048 | Mk |
| Ay 4 | 2,33 | 0,70 | MWs | 0,09 | Sy | 1,438 | Lk |
| Ay 5 | 2,42 | 0,64 | MWs | 0,12 | Fsk | 1,395 | Lk |
| Ay 6 | 2,45 | 0,69 | MWs | 0,06 | Sy | 1,457 | Lk |
| Ay 7 | 2,31 | 0,64 | MWs | 0,04 | Sy | 1,328 | Lk |
| Ay 8 | 2,27 | 0,60 | MWs | -0,06 | Sy | 1,164 | Lk |
| Ay 9 | 2,35 | 0,66 | MWs | -0,05 | Sy | 1,345 | Lk |
| Dab 1 | 2,58 | 0,87 | Ms | 0,19 | Fsk | 1,70 | Vlk |
| Dab 2 | 2,60 | 0,84 | Ms | 0,09 | Sy | 1,65 | Vlk |
| Dab 3 | 2,59 | 0,80 | Ms | 0,15 | Fsk | 1,88 | Vlk |
| Dab 4 | 2,54 | 0,87 | Ms | 0,20 | Fsk | 1,82 | Vlk |
| Dab 5 | 2,59 | 0,84 | Ms | 0,15 | Fsk | 1,67 | Vlk |
| Dab 6 | 2,65 | 0,86 | Ms | 0,17 | Fsk | 1,89 | Vlk |
| Dab 7 | 2,60 | 0,84 | Ms | 0,18 | Fsk | 1,69 | Vlk |
| Dab 8 | 2,53 | 0,87 | Ms | 0,18 | Fsk | 1,57 | Vlk |
| Dab 9 | 2,58 | 0,85 | Ms | 0,13 | Fsk | 1,62 | Vlk |

#### 3.5.2.1.1. North Bara3 section

Samples of section North Bara3 show mean grain size values range between 0.29 and 0.57 mm (2.03 – 1.02 Φ) (average value : 0.43 mm (1.58 Φ)). 33% of the analyzed grains fall within the coarse sand range, while 67% fall within the medium sand zone. The standard deviation values range from 0.96 to 1.3 Φ (average of 1.15 Φ). 20% of the samples are moderately sorted and 80% are poorly sorted. The skewness values ranged between -0.27 and +0.19 Φ (average of -0.07 Φ). 60% of the samples can be described as symmetrical, 33% coarse are skewed, and only 7% (one sample) is fine skewed. The kurtosis values range between 0.64 and 1.02 Φ (average = 0.82 Φ). 73% of the kurtosis values fall within the platykurtic zone, 20% are mesokurtic and 7% (one sample) is very platykurtic (Fig. 3.42).

#### 3.5.2.1.2. North Bara1 section

For this section, the mean grain size of samples ranges between 0.22 and 0.29 mm (2.28 – 1.94 Φ) (average = 0.25 mm (2.15 Φ)). 53% of the samples fall within the medium sand range, while 47% are within the fine sand. The standard deviation values range between 0.72 and 0.97 Φ (average = 0.8 Φ). All standard deviation values described samples as moderately sorted. The skewness values range between -0.312 and +0.086 Φ (-0.098 Φ in average). 60% are considered symmetrical, 33% are coarse skewed and only 7% (one sample) is very coarse skewed. The

kurtosis values vary from 0.99 to 1.31 Φ (average = 1.17 Φ). 77% of the samples are leptokurtic and 33% are mesokurtic (Fig. 3.43).

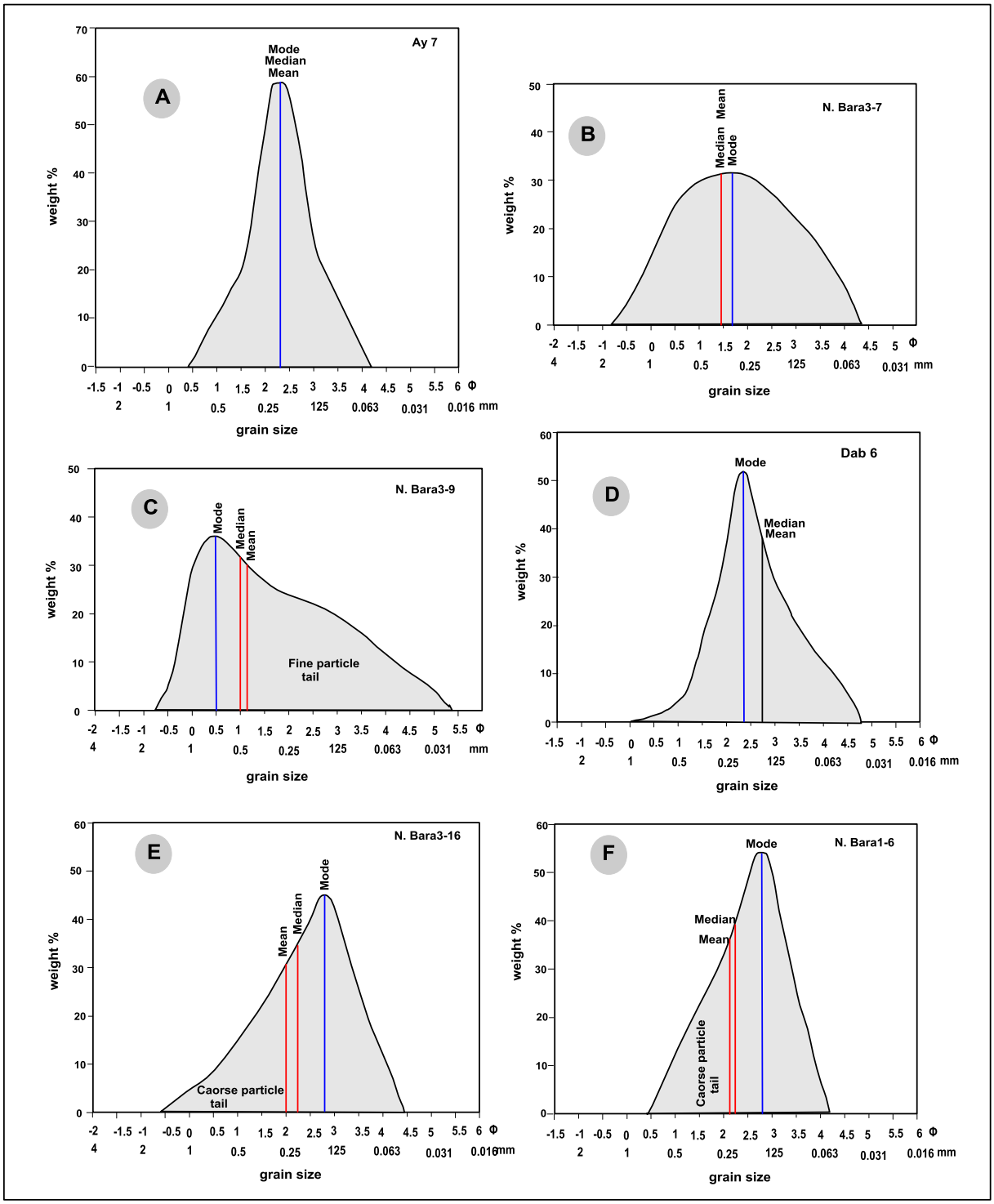


*Fig. 3.41: Representative frequency curves of the studied sections. A, B: Symmetrical curves, curve B can be classified as near-symmetrical. C, D: Fine skewed curves. E, F: Coarse skewed curves.*

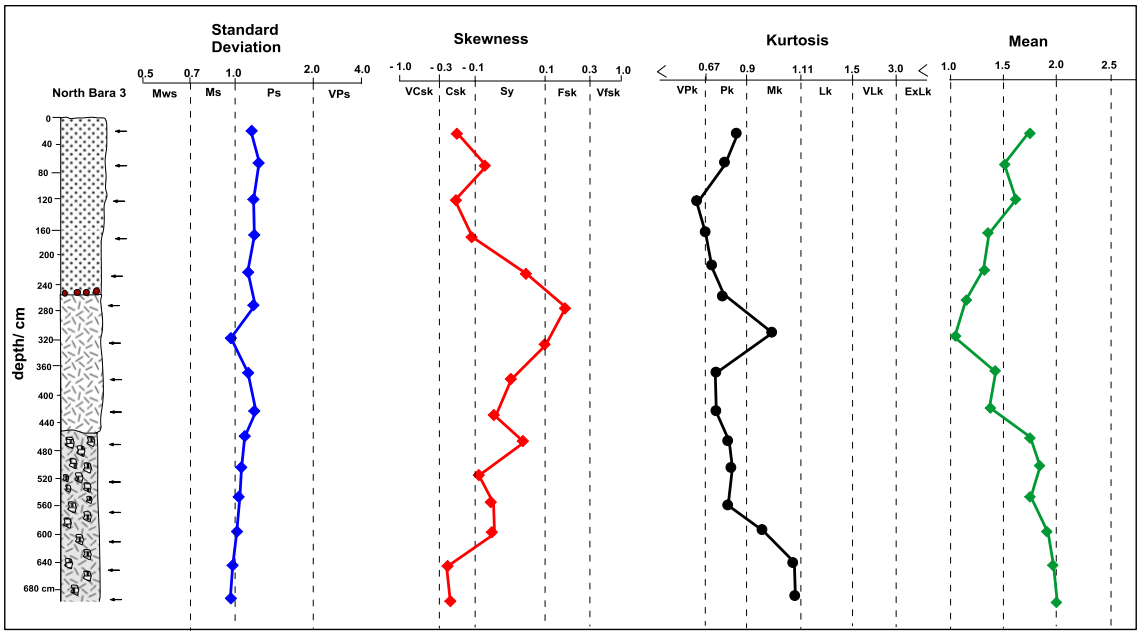


*Fig. 3.42: Graphical statistic plots against depths for the north Bara3 section.*

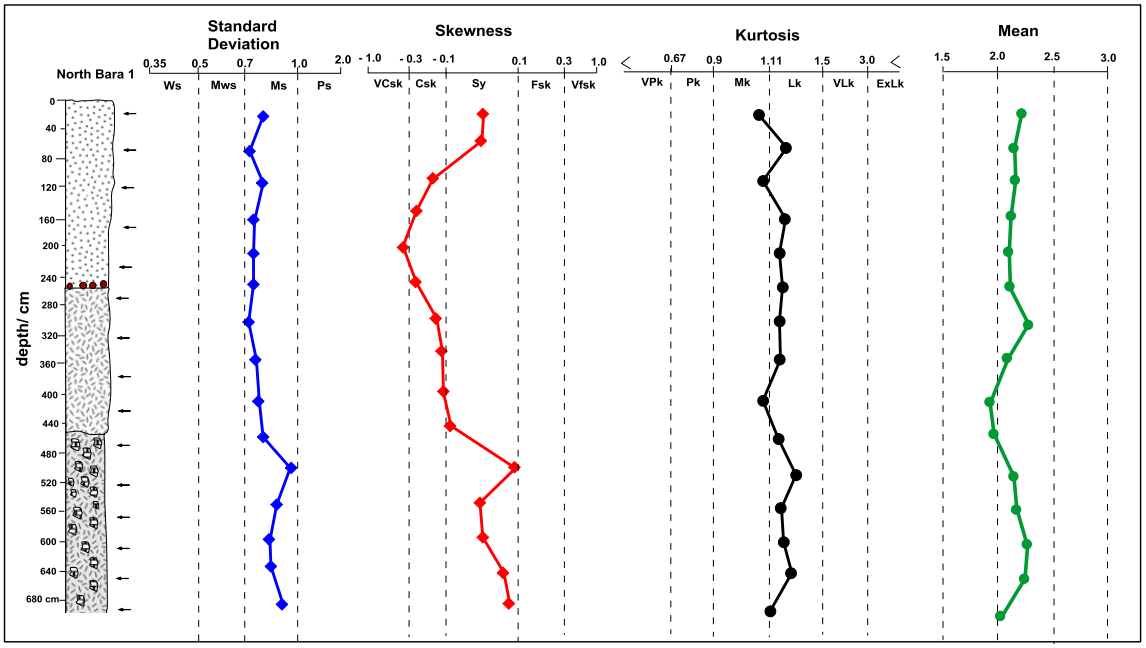


*Fig. 3.43: Graphical statistic plots against depths for the north Bara1 section.*

### 3.5.2.1.3. West El Obeid section

In this section, mean grain size values range between 0.19 and 0.23 mm (2.45 – 2.21 Φ) (average = 0.21 mm (2.35 Φ)). 89% of the samples are very fine sand, while only one sample (11%) fall within the fine sand zone. The standard deviation values range between 0.57 and 0.79 Φ (average = 0.68 Φ). 22% of the samples are moderately sorted and 78% are moderately well sorted. The skewness varies between -0.07 and +0.13 Φ (average = 0.04 Φ). Among these, 78% are symmetrical and 22% are fine skewed. The kurtosis values range from 1.05 to 1.54 Φ (average = 1.36 Φ). 78% of the kurtosis values fall within the leptokurtic zone, 6% (one sample) are very leptokurtic, and 6% (one sample) are mesokurtic (Fig. 3.44).

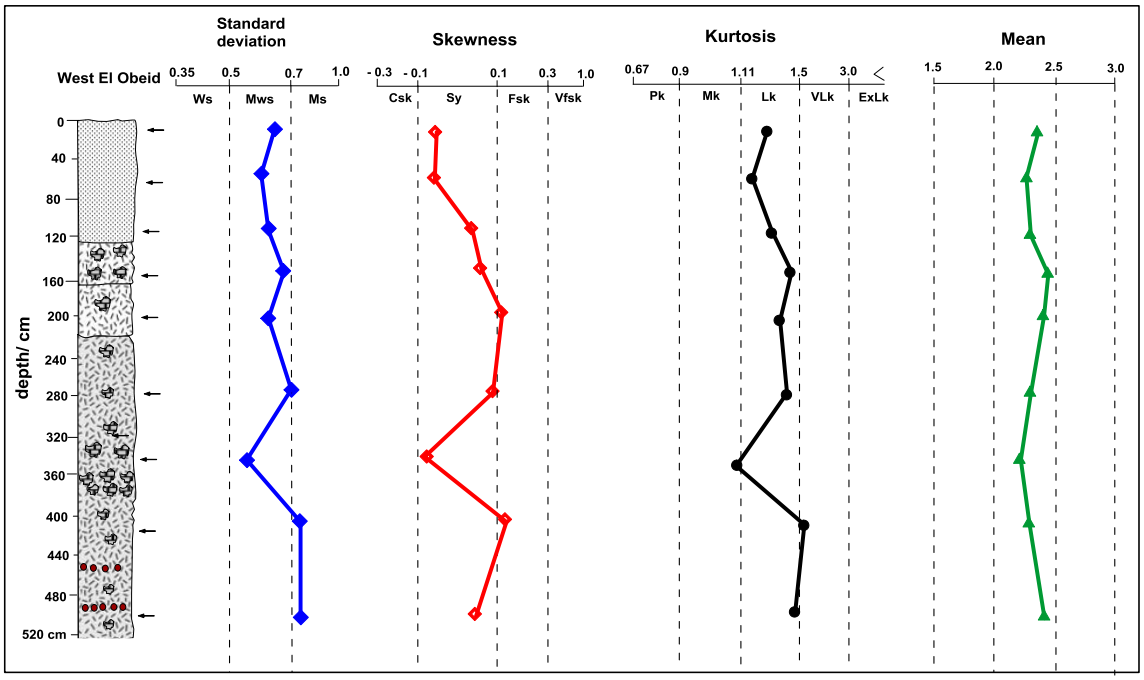


*Fig. 3.44: Graphical statistic plots against depths for the west El Obeid section.*

### 3.5. 2.1.4. East Abu Zabad section

Samples from this section show mean grain size values ranging from 0.17 to 0.19 mm (2.65 – 2.54 Φ), with average value of 0.18 mm (2.58 Φ). All samples are characterized by very fine sand mean value. The standard deviation ranges between 0.80 and 0.87 Φ (average = 0.85 Φ), and all samples are moderately well sorted. The skewness values range from 0.09 and 0.2 Φ (average = 0.16 Φ) and all samples are classified as fine skewed. The kurtosis values range from 1.57 to 1.89 Φ (average = 1.72 Φ) and all samples fall within the very leptokurtic zone (Fig. 3.45).

### 3.5.2.2. Log - Probability curves

The log-probability curve is believed to be meaningful with regard to depositional processes and to the modes of transport, which include: surface creep or traction, saltation and suspension. Each transportation mode represents an individual sub-population separated by truncation points (Visher, 1969). Bagnold (1956, *in* Visher, 1969) found that these populations of sediment transport may be mixed in the same sample. However, the log-probability curve normally exhibits two or three straight line segments, and in some cases, four segments could be found (Visher, 1969).

Forty-eight log-probability curves have been plotted in probability scale graphs. The plots were then categorized, on one hand to analyze the lower part of the mottled facies, the upper part of the same facies mottled and the red sand facies, and on the other hand, to show the horizontal variation and/or similarities (Fig. 3.46). In addition, log-probability curves of each section have been illustrated in one common graph to show the vertical variation and/or similarity of the curves with time (Fig. 3.47). Most of the curves show three straight line segments, considered as three populations of grains transported by distinct processes (traction, saltation, suspension). Only five curves from North Bara3 and two curves from East Abu Zabad show four straight

line segments; four populations are thus recognized, representing traction, suspension and two kinds of saltation transport processes (Fig. 3.47). The curves show remarkable variations when comparing the same facies or horizon from different sites. When comparing the curves of a same site, the North Bara3 section shows remarkable variations in the population, while the other sites show clear similarities in the shape of the curves and their positions in the plot. The most similar curves was that obtained from the West El Obeid section (Fig. 3.47).

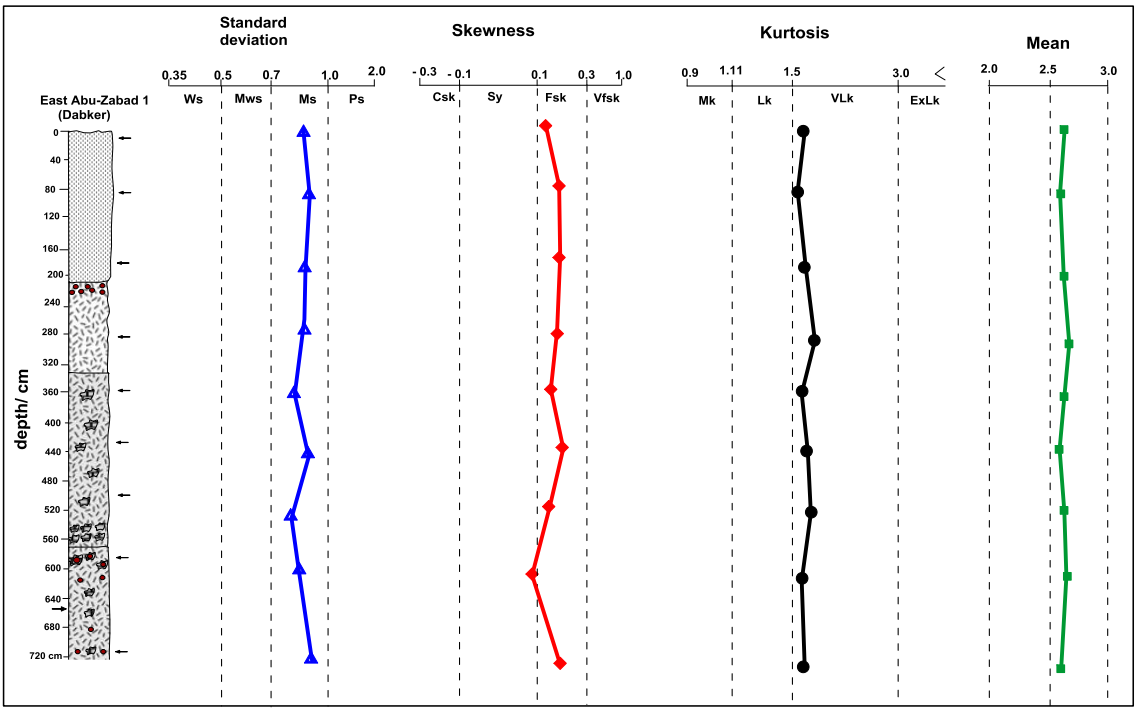


*Fig. 3.45: Graphical statistic plots with depth for the east Abu Zabad section.*

The truncation points of all curves have been determined and summarized in table 3.7 to present only the maximum (max) and minimum (min) values for : the coarse traction (the coarsest end in the curve), traction-saltation, and saltation – suspension truncation points (TP). However, the north Bara3 section shows the greatest values for the coarse traction (max and min) and also for the maximum traction-saltation truncation points, while it shows lower values for the minimum traction-saltation and saltation-suspension (max and min) truncation points. For the other three sites, the truncation points for each population are close to each other with some variations. Generally, according to these illustrated curves, it appears that the dominant population in terms of percentage is the saltation population.

***Table 3.7: Brief summary of truncation points.***

| Site | Truncation points in mm | | | | | |
|---|---|---|---|---|---|---|
| | Coarse traction TP | | Traction-saltation TP | | Saltation-suspension TP | |
| | max | min | max | min | max | min |
| North Bara3 | 2.378 | 1.149 | 1.366 | 0.406 | 0.117 | 0.058 |
| North Bara1 | 1.516 | 0.707 | 0.574 | 0.42 | 0.131 | 0.095 |
| West El Obeid | 0.93 | 0.841 | 0.536 | 0.354 | 0.125 | 0.108 |
| East Abu Zabad | 1.072 | 0.707 | 0.582 | 0.435 | 0.121 | 0.096 |

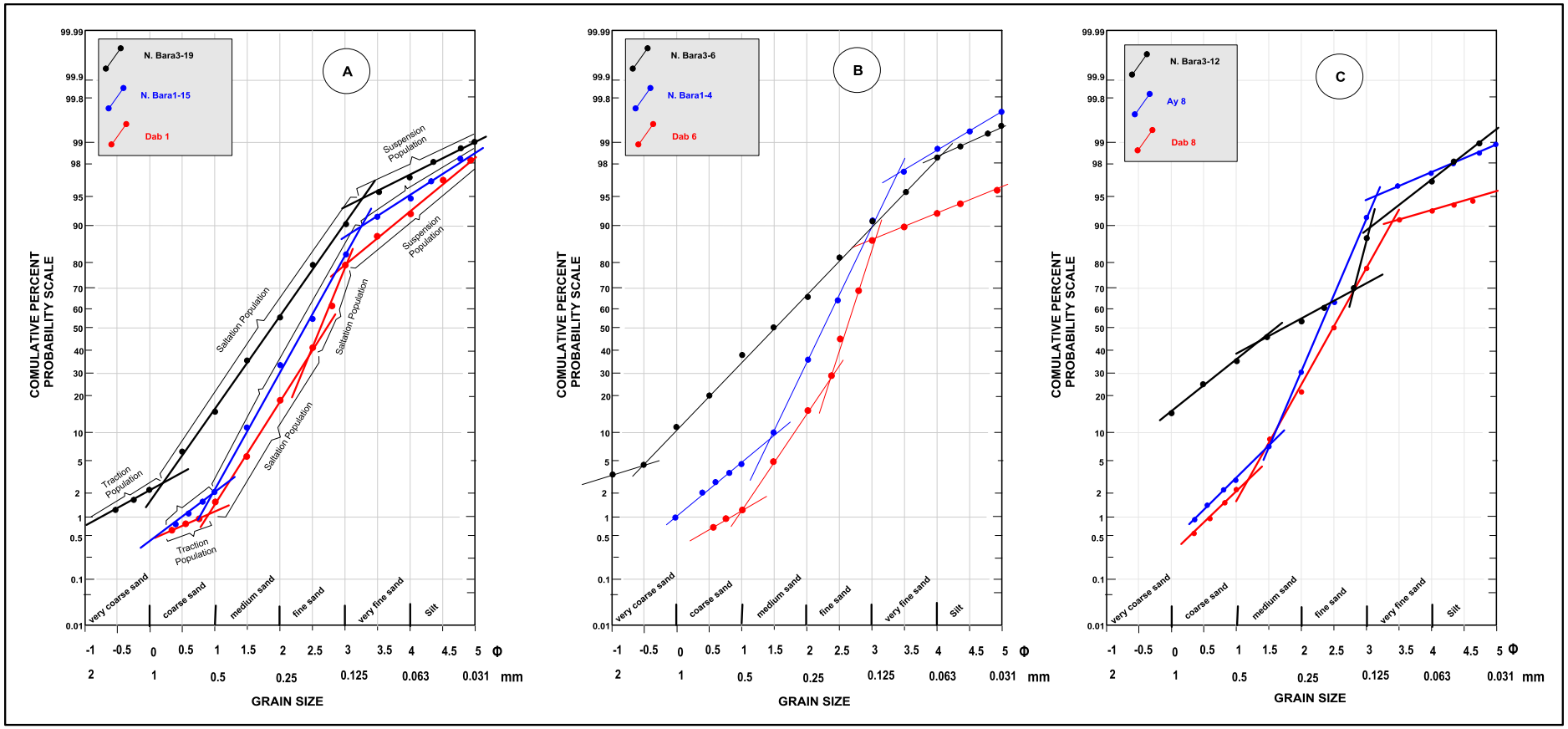


***Fig. 3.46: Representative Cumulative Probability Curves for the whole area***. *(A) Curves for the lower part of the mottled facies; (B) Curves for the upper part of the mottled facies; (C) Curves for the red sand sediments facies.*

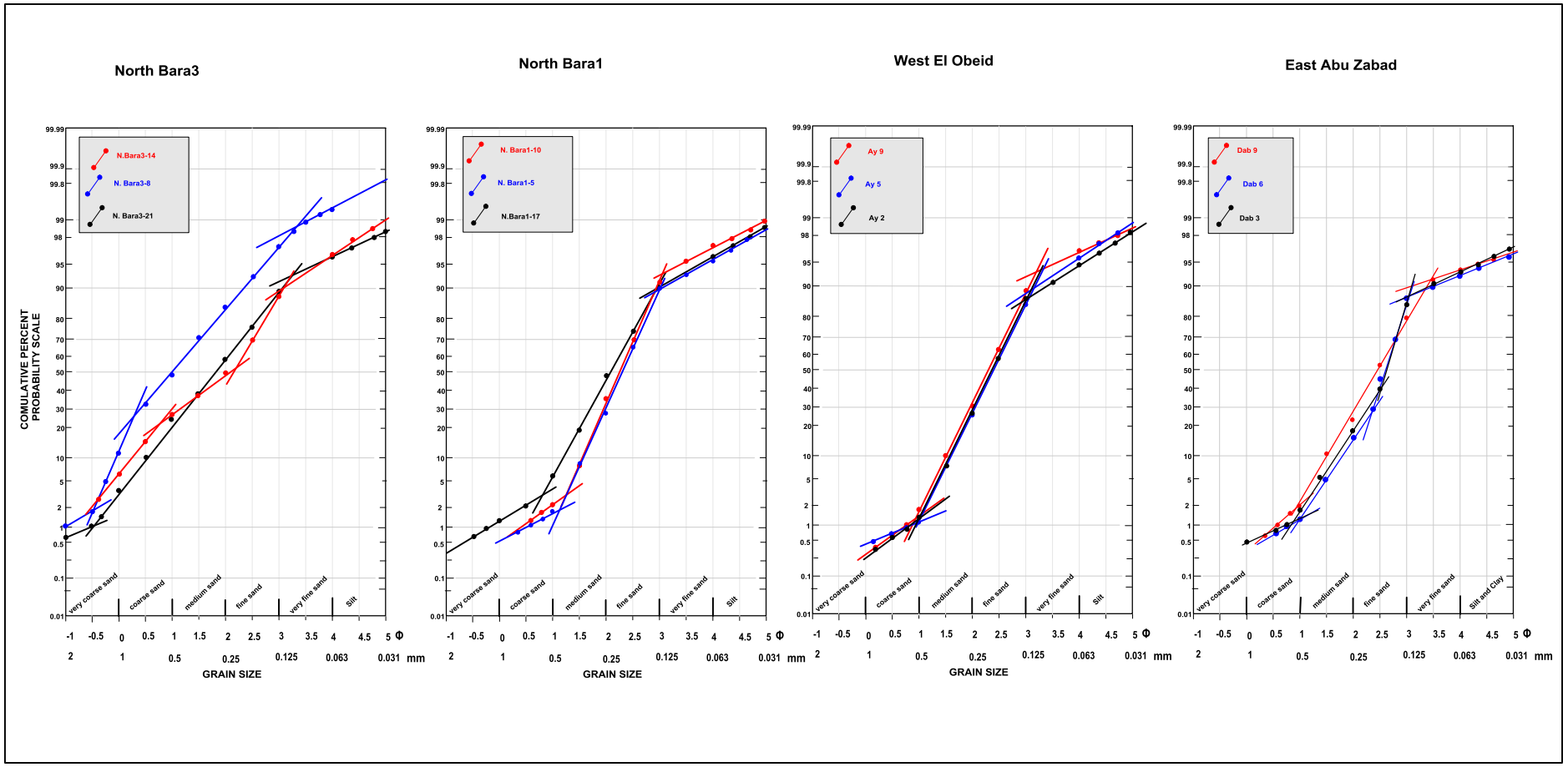


*Fig. 3.47: Representative Cumulative probability curves for the different sites.*

### 3.5.3. Interpretations

#### 3.5.3.1. Cumulative curves

According to the cumulative curves of grain size distribution and the grain size ranges (Fig. 3.40), the North Bara3 section is marked by the coarsest grain size, followed in decreasing grain size order, by the North Bara1, West El Obeid and East Abu Zabad section, thus expressing a southward fining trend. This strongly suggests a southward decreasing transportation energy. Figure 3.48 illustrates the grain size distribution for all sections. Moreover, the width of the grain size distribution areas of each section shows a remarkable variability. Curves from North Bara3 show a wide grain size distribution reflecting a strong variability in transport energy through time. In North Bara1, distribution curves are moderately wide, reflecting also energy variability along section. Curves from the other sites are narrow, indicating low variability of transport energy through time for West El Obeid, and energy stability for East Abu-Zabad.

#### 3.5.3.2. Grain size distribution

Grain size cumulative plots have been constructed for each sections (Fig. 3.49) and were correlated between the studied sections (Fig. 3.38), in order to obtain a stratigraphic and geographical image of the transportation processes and energy.

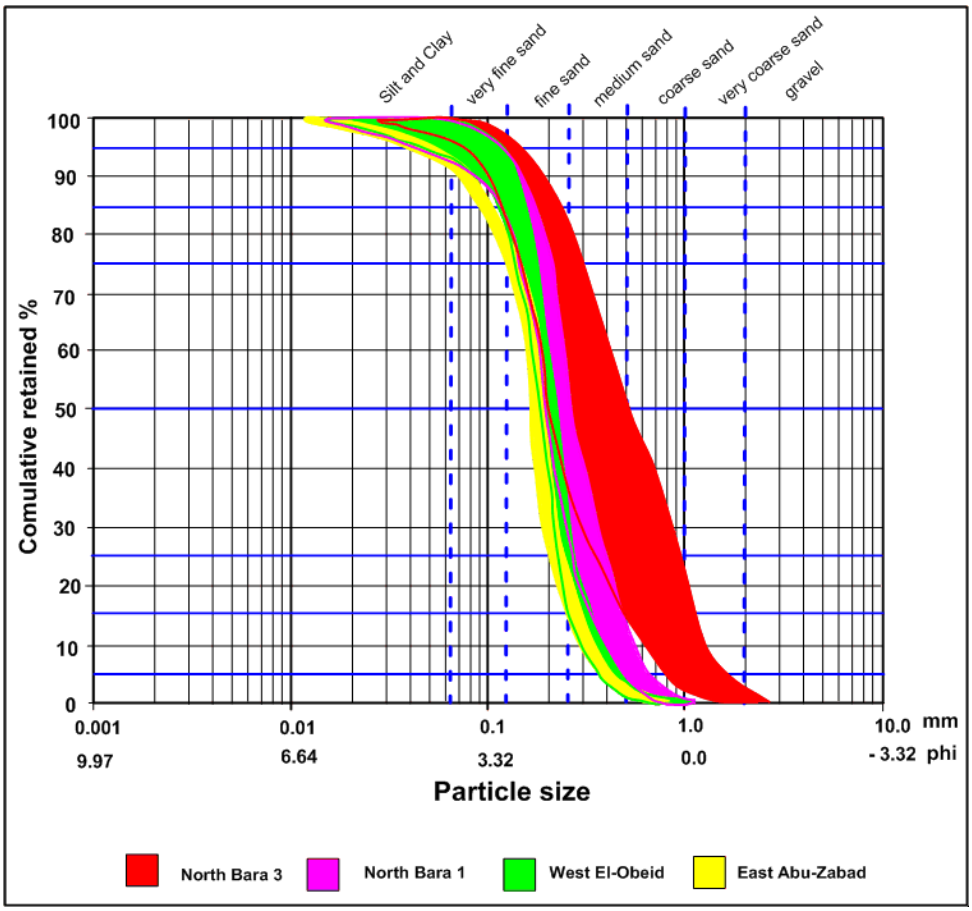


*Fig. 3.48: Grain-size distribution diagram for all samples from all sections.*

### 3.5.3.2.A. Vertical grain size distribution

Table 3.8 summarizes the grain size percentages along each section. The distribution indicates domination of the coarser sizes in the northern sections (north Bara 3 and north Bara 1), while the southern sections are dominated by fine grain sizes. This distribution indicates a general southward fining trend, which in turn reflects the southward decreasing energy.

***Table 3.8. Summary of the grain-size percentage for all sections.***

| Grain size | Location or section | | | |
|---|---|---|---|---|
| | North Bara3 | North Bara1 | West El Obeid | East Abu Zabad |
| Fine gravel% | 1 – 2 | - | - | - |
| very coarse sand % | 4 – 20 | 1 – 3 | - | - |
| Coarse sand % | 11 – 37 | 2.5 – 7 | 1.5 – 3 | 2 – 4 |
| Medium sand% | 20 – 30 | 31 – 50 | 17 – 27 | 14 – 23 |
| Fine sand % | 15 – 45 | 26 – 56 | 56 – 60 | 51 – 65 |
| Very fine sand % | 3 – 17 | 8 – 17 | 12 – 16 | 17 – 20 |
| Silt % | 0.5 – 4 | 1 – 6 | 1.5 – 5 | 5 – 7 |

The distribution in the north Bara3 section shows mixed grain size percentages close to each other in the most of the size, except the fine gravel and the silt portions that show very low percentages, which indicate a poor sorting degree. The relatively high percentages of the very coarse and coarse sand indicate high energy along the north Bara3 section with some variation in this high energy (Fig. 3.49 A). Moreover, the uniform grain size distribution with time suggests uniform transportation energy and therefore, uniform of aeolian energy.

In the north Bara1 section, sediment distribution shows the domination of medium and fine sand, a considerable amount of very fine sand, rare silt and very coarse sand, very rare or absence of very coarse sand, and the lack of fine gravel. Therefore, this indicates generally moderate energy through time, although with some variation (Fig. 3.49 B). Moreover, the uniform grain size distribution through time suggests uniform transportation energy and therefore, uniform aeolian processes.

The sediment distribution in the west El Obeid section shows the predominance of fine sand, a considerable amount of medium and very fine sand, rare silt and very coarse sand, and the lack of very coarse sand and fine gravel. This distribution evidences a low energy through time, with very sporadic variations (Fig. 3.49 C). The uniform grain size distribution suggests uniform transportation energy and rather constant aeolian processes.

In the east Abu Zabad section, grain size distribution shows the domination of fine sand, a considerable amount of medium and very fine sand, a remarkable amount of silt, rare coarse sand, and the lack of very coarse sand and fine gravel. The predominance of fine sand and abundance of very fine sand and silt indicates very low energy through time with no variation (Fig. 3.49 D). This uniform grain size distribution suggests constant transportation energy and uniform aeolian processes.

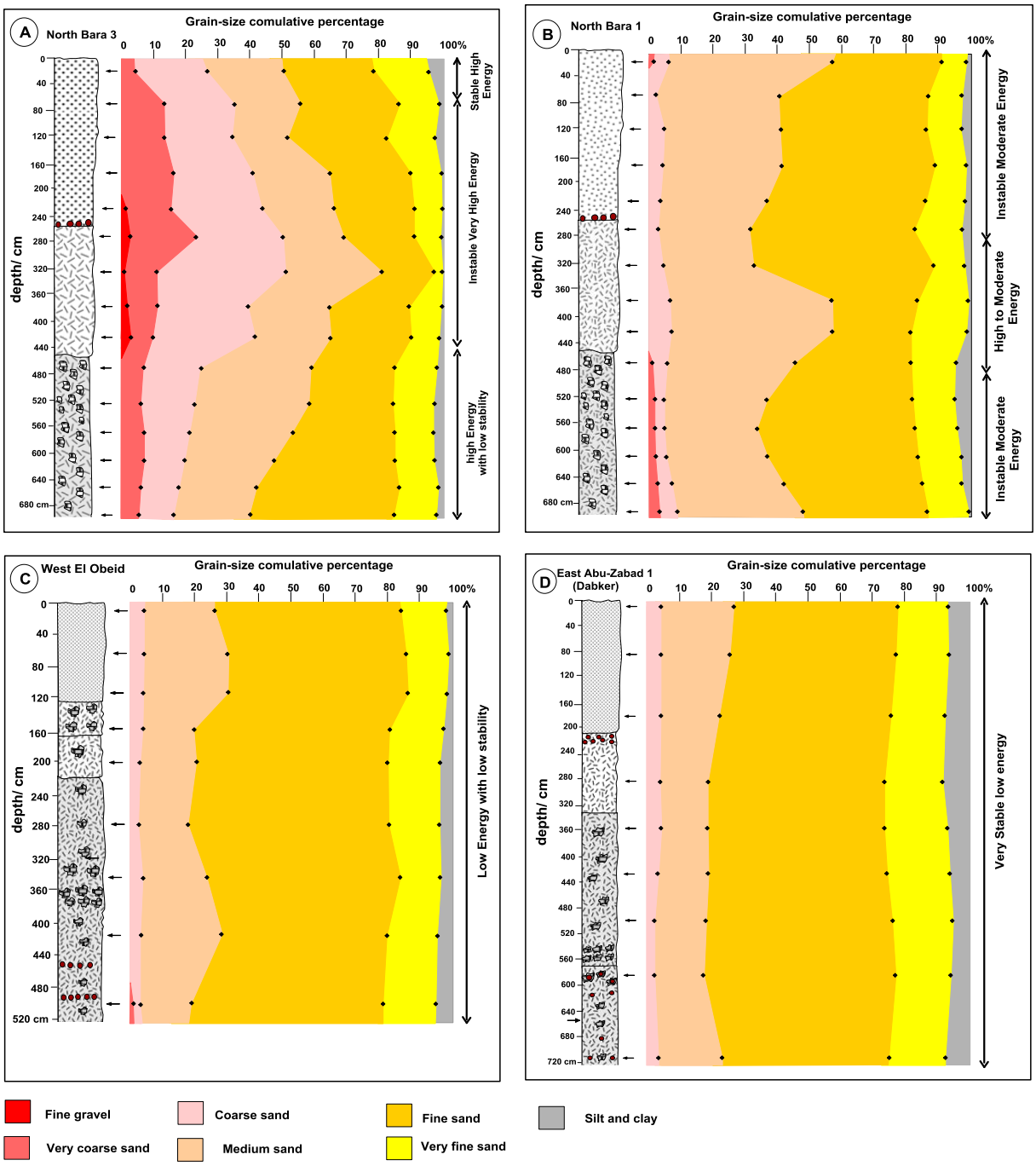


*Fig. 3.49: Vertical evolution of grain size percentages and their interpretation. (A) North Bara3 section; (B) North Bara1 section; (C) West El Obeid section; (D) East Abu Zabad section.*

### 3.5.3.2.B. Geographical grain size distribution

Based on the above mentioned data, I constructed horizontal profiles of grain size distribution for the three lithological units: upper red aeolian unit, upper part of the mottled unit, and lower part of the mottled unit (Fig. 3.50).

The grain size percentages for the red sand sediments are presented in Table 3.9. These percentages show (1) the lack of fine gravel and of very coarse sand, except in North Bara3, (2) the southward decrease of medium to coarse sand and overall southward increase of fine grained

sand, and (3) a relative stability of very fine sand and silt all along the profile. This pattern indicates a decreasing transport energy from north to south (Fig. 3.50 A), and thus, strongly suggests that the wind was blowing from North or NNE to South or SSW, and that its intensity was decreasing southward.

***Table 3.9: Grain size percentage for the red sand sediments facies.***

| Grain size | Location or section | | | |
|---|---|---|---|---|
| | North Bara3 | North Bara1 | West El Obeid | East Abu Zabad |
| Fine gravel % | - | - | - | - |
| very coarse sand % | 14 | - | - | - |
| Coarse sand % | 20 | 6 | 4 | 3 |
| Medium sand % | 18 | 35 | 26 | 26 |
| Fine sand % | 28 | 46 | 56 | 50 |
| Very fine sand % | 17 | 11 | 12.5 | 15 |
| Silt % | 3 | 6 | 1.5 | 6 |

The grain size percentages for the upper part of the mottled facies are presented in table 3.10. The fine gravel and very coarse sand are only present in North Bara3. The amount of coarse and medium sand decreases southward (except in North Bara), while the percentage of fine sand, very fine sand and silt increases southward. This distribution indicates that high energy transport dominated in the northern parts, and was decreasing southward (Fig. 3.50 B). As for the sand sediments facies, we conclude that the wind was blowing from North to South, and its energy was decreasing in the same direction.

***Table 3.10: Horizontal grain size distributional percentage for the upper part of the mottled facies.***

| Grain size | Location or section | | | |
|---|---|---|---|---|
| | North Bara3 | North Bara1 | West El Obeid | East Abu Zabad |
| Fine gravel % | 1.5 | - | - | - |
| very coarse sand % | 9.5 | - | - | - |
| Coarse sand % | 40 | 6 | 4 | 3 |
| Medium sand % | 19 | 35 | 16 | 17 |
| Fine sand % | 20 | 42 | 60 | 59 |
| Very fine sand % | 9 | 14 | 16.5 | 16 |
| Silt % | 1 | 3 | 3.5 | 5 |

The grain size percentages for the lower part of mottled facies are presented in Table 3.11. There is a total absence of fine gravel along the profile. The amount of very coarse, coarse and medium sand decreases southward, while that of fine sand and silt increases in the same direction. The percentage of very fine sand remains constant all along the profile. This distribution indicates that during deposition of this part of the mottled unit, the wind was blowing from North to South and its transportation energy was decreasing southward (Fig. 3.50C).

***Table 3.11: Horizontal grain size distributional percentage for the lower part of the mottled facies.***

| Grain size | Location or section | | | |
|---|---|---|---|---|
| | North Bara3 | North Bara1 | West El Obeid | East Abu Zabad |
| Fine gravel% | - | - | - | - |
| Very coarse sand % | 7 | 3 | 1 | - |
| Coarse sand % | 13 | 4 | 3 | 2 |
| Medium sand% | 30 | 34 | 21 | 18 |
| Fine sand % | 35 | 42 | 55 | 59 |
| Very fine sand % | 13 | 12.5 | 14.5 | 14 |
| Silt % | 2 | 4.5 | 5.5 | 7 |

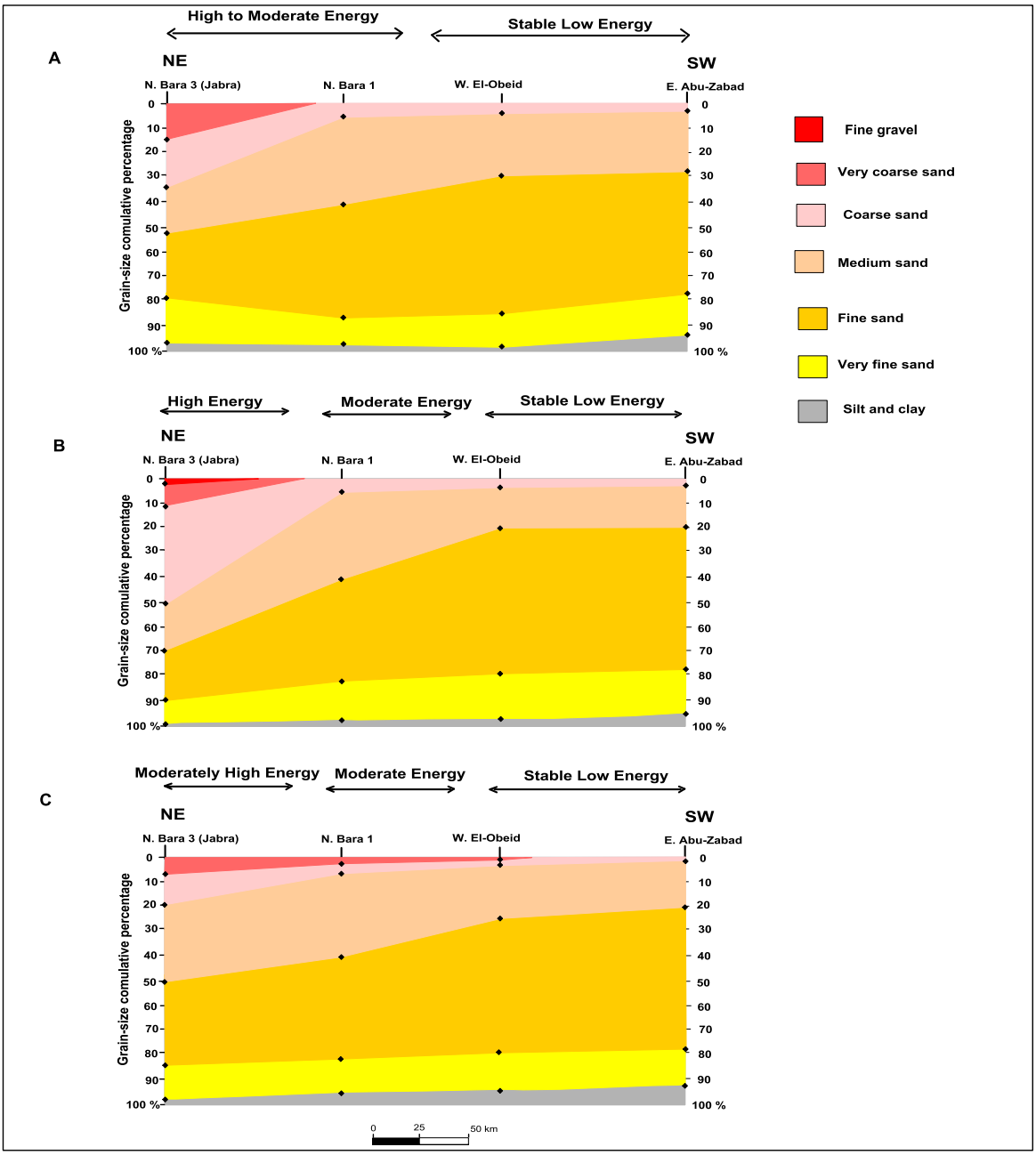


*Fig. 3.50: NNE-SSW distribution of the grain size percentages and interpretations. (A) Red sand sediments facies; (B) upper part of the mottled facies; (C) lower part of the mottled facies.*

### 3.5.3.3. Graphical statistic parameters

It is difficult to recognize the lateral evolution of the graphical statistic parameters through their individual plots (see the result section, Figs. 3.42 to 3.45). Therefore, a single plot of graphical statistic parameters of all studied sections through time have been built (Fig. 3.51). Other diagrams have been drawn according to the graphical statistic relations. This graphical relations include mean grain size-sorting (Fig. 3.52), mean grain size-skewness (Fig. 3.53) and skewness-sorting, relations (Fig. 3.54).

#### 3.5.3.3.A. Mean grain size

The diagram showing the mean grain size for each site shows a very organized distribution (Fig. 3.51) that strongly supports the gradual decrease in wind energy from North to South. The very similar mean size along the East Abu Zabad, similar mean size along the West El Obeid, and semi similar mean size along the North Bara1 section indicates very stable, stable, and semi stable energy in the East Abu Zabad, West El Obeid, and North Bara1 respectively. On the other hand, this vertical similarity in the mean size for each section indicates uniformity of the sediment origin, uniformity of sedimentation processes, and energy stability through time for both the red aeolian and mottled facies. Dispersion of mean grain size value in North Bara3 indicates variable energy through time.

#### 3.5.3.3.B. Kurtosis

As the sections have a North-South arrangement, the kurtosis shows a systematic lateral variations : the curves evolve from North to South, from platykurtic to leptokurtic and very leptokurtic. This indicates a wide range of grain size and energy variability in the North, and a narrow range of grain size and the stability of transportation energy in the South.

#### 3.5.3.3.C. Skewness

The skewness shows strong variability in all sections, except in East Abu Zabad, which shows almost constant values.

The skewness is only a function of the available size and it is difficult thus to use it as direct indicator for the energy strength, but it can be used as indicator for the energy fluctuation through time. According to the skewness values shown in fig. 3.51, these are variable in the northern sections (North Bara 3 and 1), semi-homogenous in the west El Obeid section, and very homogeneous for the East Abu Zabad section (southern end of the studied sections). This indicates a more variable energy in North Bara3, less variations in North Bara1, stable to semi-stable energy in West El Obeid, and a very stable energy in the East Abu Zabad section.

#### 3.5.3.3.D. Standard deviation (sorting)

The sorting plot shows very little vertical variation in each individual section, but geographical variations of the sorting degree are well visible.

Except in East Abu Zabad, the sorting is poor in the North and better in the southern areas. The moderate sorting in East Abu Zabad is discussed below (cf. intercorrelations section).

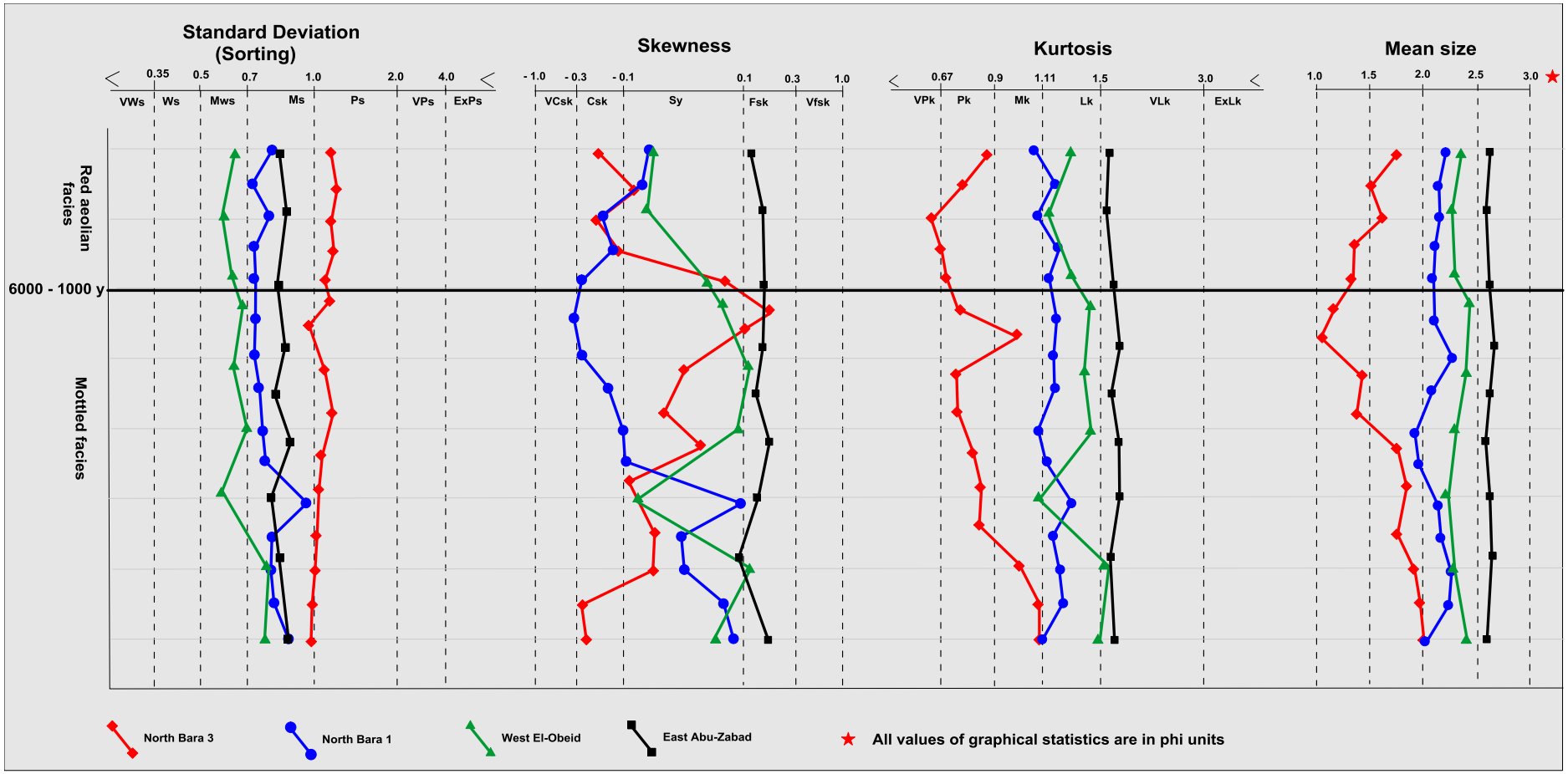


*Fig. 3.51: Curves of pre- and post-hiatus graphical statistic plots for all sections. The curves for both parts have been homogenized according to the thickest sections (North Bara 1 for the post-discontinuity, East Abu Zabad for the pre-discontinuity). For more details of each section refer to Figures 3.42 to 3.45.*

### 3.5.3.4. Intercorrelations

#### 3.5.3.4.A. Mean grain size *vs* sorting

The mean grain size – sorting plot (Fig. 3.52) shows very good linear relation between the different sites, and a clear trend from North to South. This relation indicates a gradual decreases in the energy from the North Bara3 to the West El Obeid section. The southern end of the studied profile (East Abu Zabad section) is marked by the finest mean grain size, but a less good sorting than the West El Obeid site (Fig. 3.52). This peculiarity can be ascribed to a sudden lowering down of the wind energy, due to the geographical location of East Abu Zbad on the lee side of a topographic crest, which shelters this place from high energy dominant winds (see topographic profile, Fig. 3.39). This lowering down of energy would lead to the rapid deposition of the transported load with less efficient sorting. This interpretation is supported by some morphological features: (1) what is called the Kordofan sand zone extends about 40 km south of East Abu Zabad, and (2) the higher vegetation cover in the more humid southern areas may contribute to the decrease of wind energy.

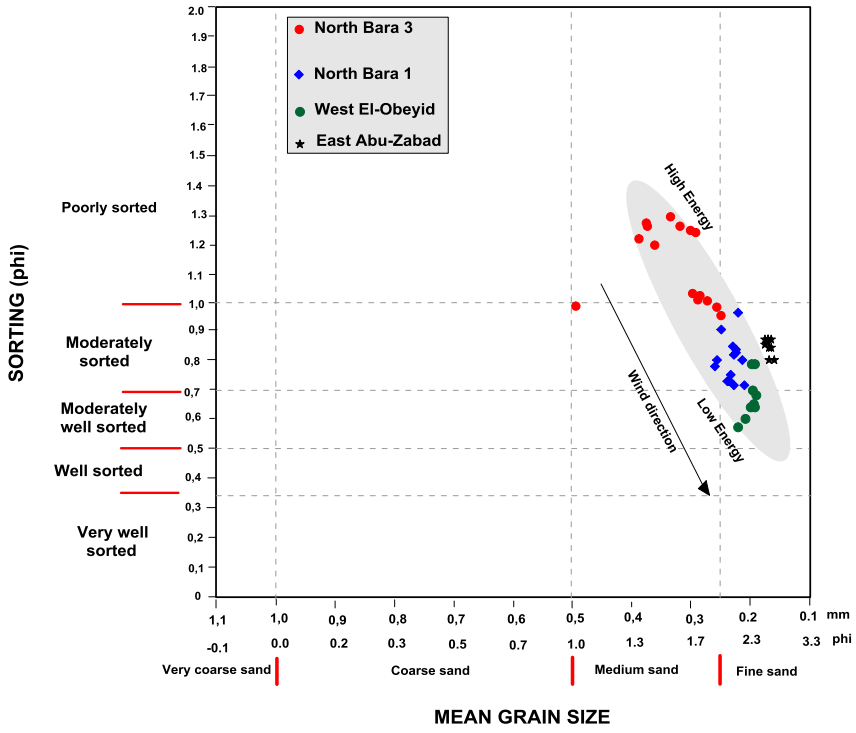


*Fig. 3.52: Plot of mean grain size* vs *sorting of the studied samples indicating the wind energy.*

#### 3.5.3.4.B. Mean grain size *vs* skewness

The mean grain size *vs* skewness relation does not show a linear relationship, but rather a "V" shape (Fig. 3.53). Energy is a positive function of the mean grain size (the greater the size, the greater the energy), while the same skewness value can be found in both high and low energy. The turning point of the "V" indicates in general the medium energy (whatever the strength is), while the arms of the "V" indicate high energy and low energy trends : the arm toward the coarser mean size indicates high energy, and the other arm indicates low energy.

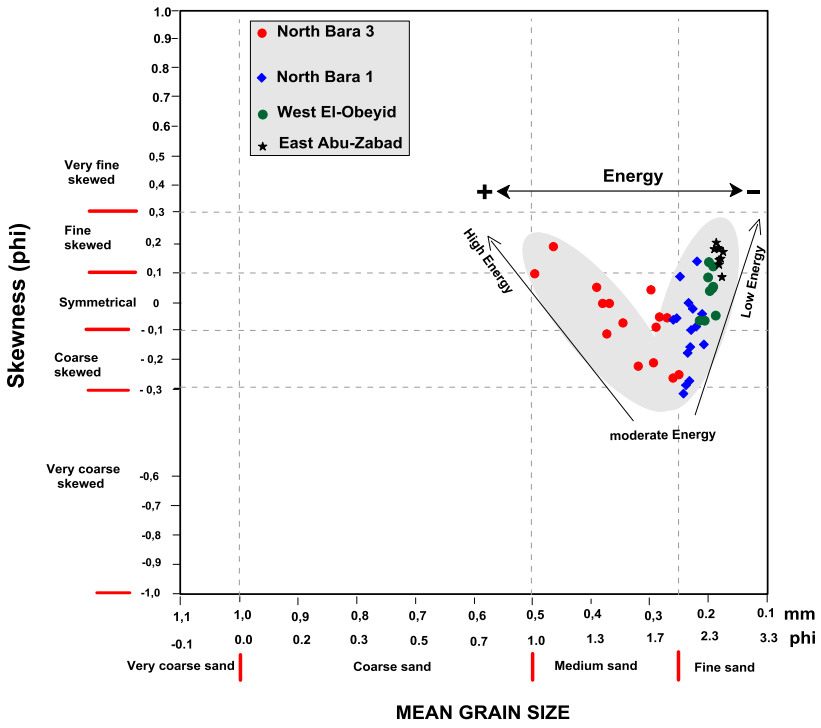


*Fig. 3.53: Plot of mean grain size* vs *skewness of the studied samples indicating the transportation energy.*

### 3.5.3.4.C. Sorting *vs* skewness

The sorting (standard deviation) *vs* skewness relationship provides linear relation from North Bara3 to West El Obeid. However, the East Abu Zabad samples do not fall in a logical position according to the wind direction, since East Abu Zabad sands are less sorted than the West El Obeid samples and part of those of North Bara1. However, this diagram supports a decreasing transport energy from North to South (Fig. 3.54).

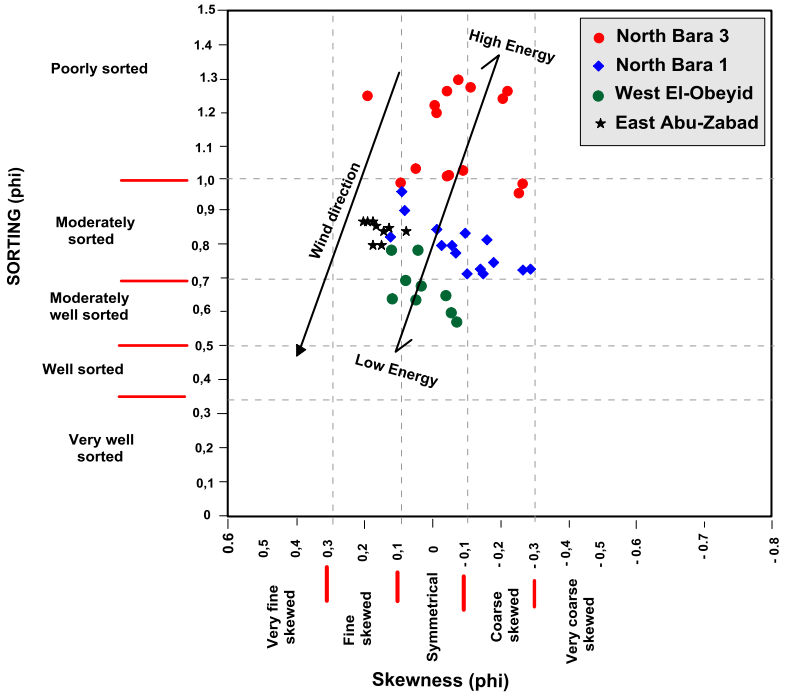


*Fig. 3.54: Plot of Skewness* vs *Sorting of the studied samples indicating the transportation energy.*

### 3.5.3.5. Log-probability curves

#### 3.5.3.5.1. Vertical interpretation

The log-probability curves have been interpreted as vertical population percentages and vertical populations, expressed in grain size variations for each individual section, in order to recognize the vertical variations of these populations. The variation in wind energy through time have been estimated too (Fig. 3.55 – 3.58). Moreover, three horizontal population percentages and horizontal populations expressed in size variation diagrams, were plotted along the profile of the studied sections. This helps in the understanding of the lateral variations of transportation processes and therefore, of wind energy along the wind blowing direction (Fig. 3.59 – 3.61).

The saltation population shows variable percentages in the red sand sediments facies (Upper unit) with average value of ≈ 56 %, while it prevails in the mottled facies with an average of ≈ 94%. In terms of grain size, the saltation population is coarser and less sorted in the mottled facies than in the sand sediments facies. The suspension population represents ≈ 9 % in the red sand sediments facies, while it represents an average percentage of ≈ 4 % in the mottled facies.

The domination of the traction and saltation populations in the red sand sediments facies, highly contributes in the development of sand dunes in this area. The very high percentage of the saltation population in the mottled sand sediments facies, indicates the dominance of aeolian processes for this facies, and it may also have contributed in the dune forming in the northern part of the region. Moreover, the relatively coarse grain of the traction population indicates high energy of wind transport.

##### 3.5.3.5.1.A. North Bara3 section

The traction population along the north Bara3 section shows strong variations, since it reaches up to 50 % in the red sand sediments facies (average value : 35 %), while in the mottled facies it only represents ≈ 2 % in average (Fig. 3.55A). When translated into grain size, this traction population of the mottled facies is coarser than that in the red sand sediments facies.

##### 3.5.3.5.1.B. North Bara1 section

In North Bara1, the traction population shows a small percentage (average ≈ 3 %) (Fig. 3.56A). When expressed in grain size, it shows a slight fining upward trend. The saltation population is fairly dominant all along the section with an average percentage of ≈ 90 %. Its grain size is almost constant, although a slight fining upward trend can be seen (Fig. 3.56B). The suspension population represents an average ≈ 7 % of the grains, and its maximum grain size is about 0.125 mm.

In general terms, this indicates that (1) transport and depositional processes did not change significantly through time, (2) the predominant saltation population resulted in the formation of numerous sand dunes during deposition of both the mottled sand and red sand sediments facies (former sand dunes are expressed by presently undulated topographic surface around North Bara1 and further south, as discussed in the next section), and (3) the wind energy did not evolve significantly through time, during deposition of the studied units.

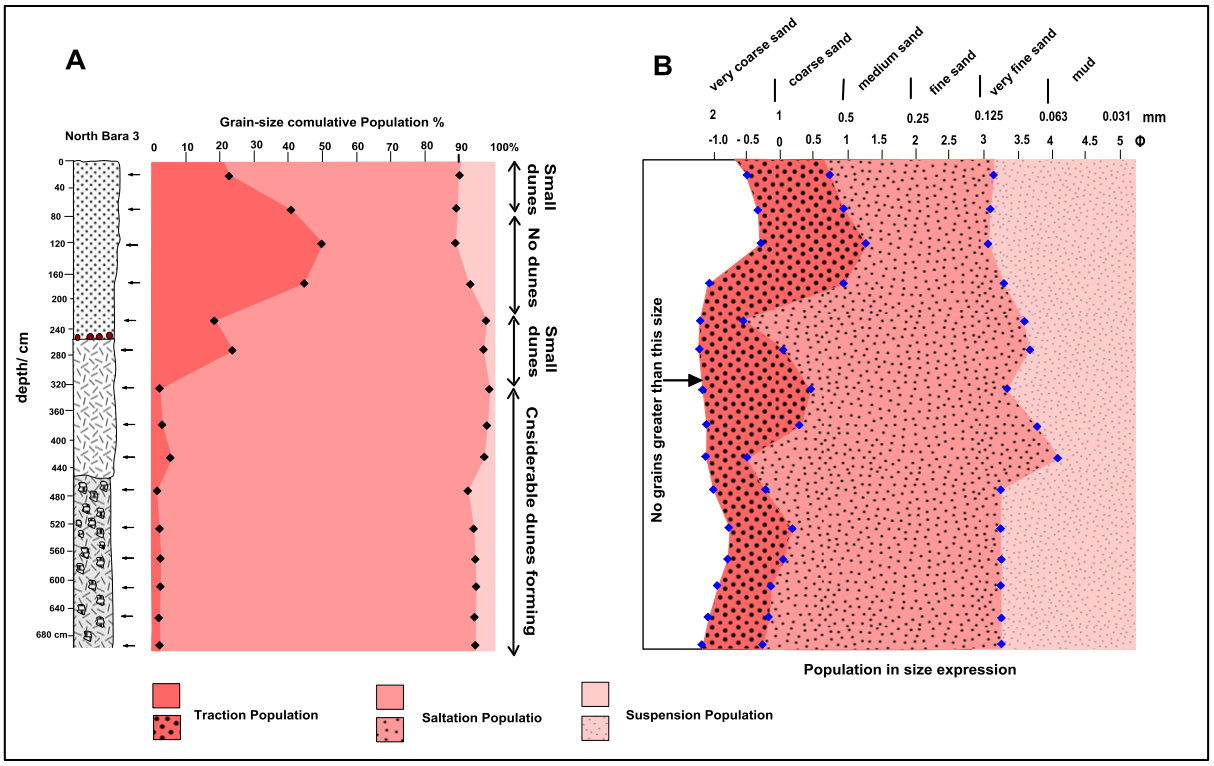


***Fig. 3.55:*** *Evolution of transport processes in the North Bara3 section. (A) expressed in percentages; (B) expressed in grain size.*

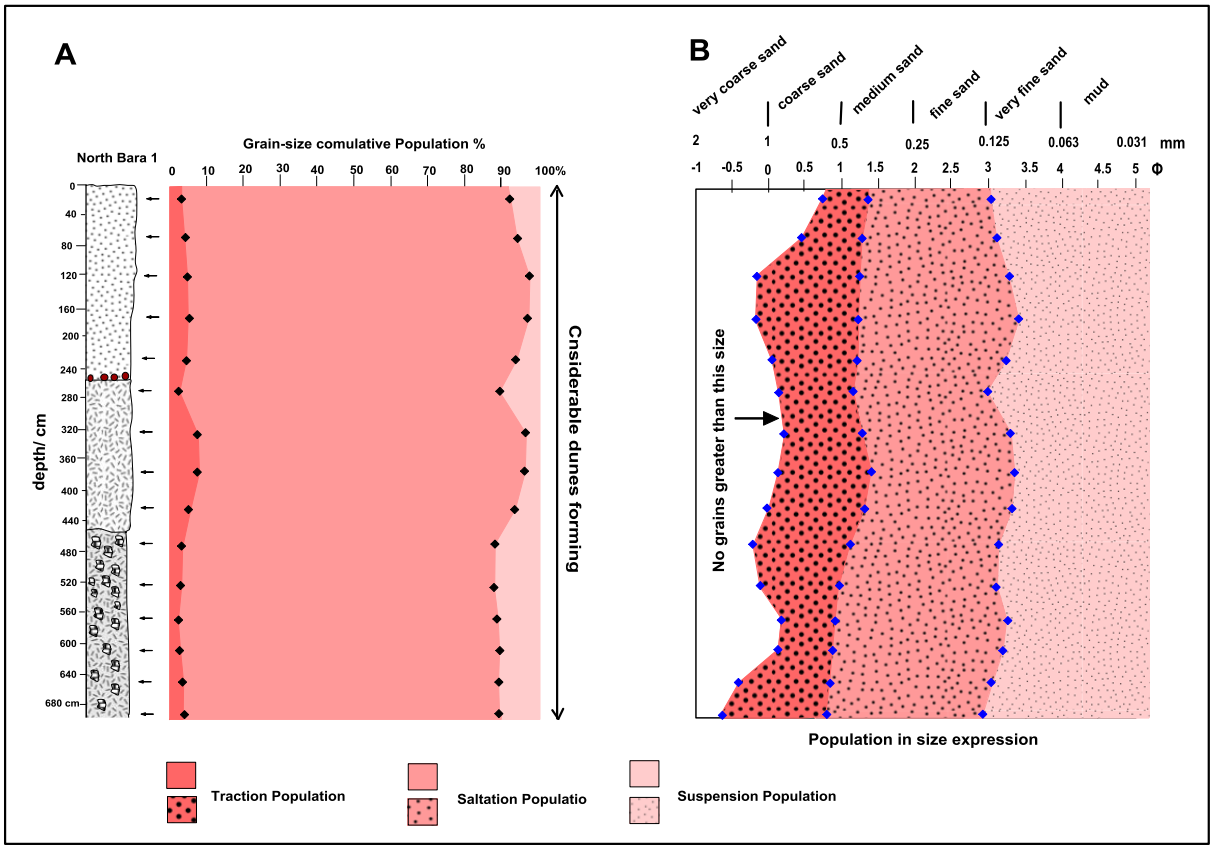


***Fig. 3.56:*** *Evolution of transport processes in the north Bara1 section. (A) expressed in percentages; (A) expressed in grain size.*

### 3.5.3.5.1.C. West El Obeid section

Grains transported by traction in West El Obeid represent a low percentage, with average value of ≈ 2 % in the mottled facies, and ≈ 4 % in the red sand sediments facies (Fig. 3.57A). The grain size range of this population is generally narrow and stable through time, ranging from ≈ 1 to ≈ 0.5 mm in the mottled facies, and 1 to 0.35 mm in the red sand sediments facies. The saltation population is quite predominant all along the section with an average percentage of ≈ 87 % in the mottled facies, and ≈ 92 % for the red sand sediments facies. When expressed in grain size, the saltation population is very constant through time with minimum size ≈ 0.109 mm. The suspension population represents ≈ 11 % in the mottled facies and ≈ 4 % in the red sand sediments facies, and its grain size is generally less than 0.109 mm.

This analysis shows that (1) the depositional processes did not change through time, (2) the high amount of saltation population in both facies suggests active dune formation, and (3) wind energy remained stable through time, at least during deposition of the studied units.

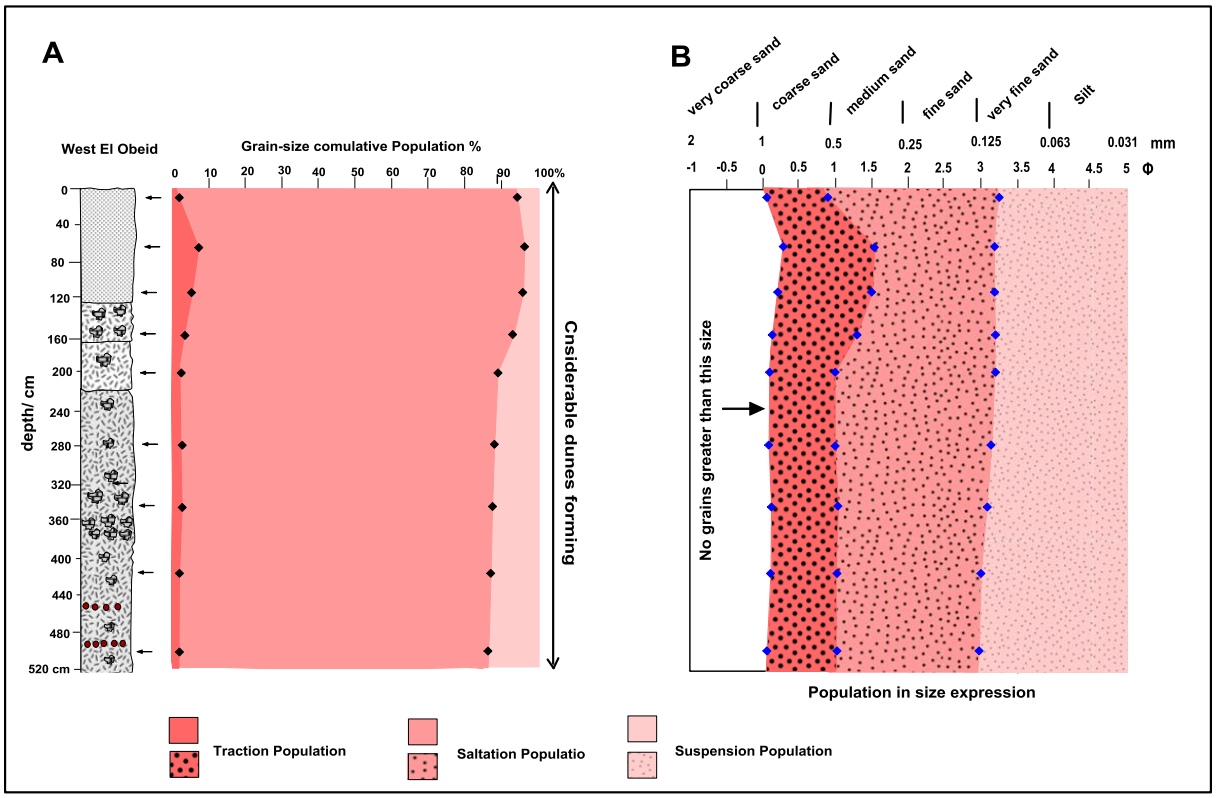


*Fig. 3.57: Evolution of transport processes of the West El Obeid section. Expressed (A) in percentages; (B) in terms of grain size.*

### 3.5.3.5.1.D. East Abu Zabad section

In East Abu Zabad, the traction population shows very low percentage (average ≈ 2 %) (Fig. 3.58 A). Its grain size range is narrow and constant, varying between ≈ 0.812 and ≈ 0.5 mm. The saltation population is highly dominant all along the section, with an average of ≈ 82 % in the mottled facies and ≈ 89 % in the red sand sediments facies. Expressed in grain size, the saltation population is finer and less well sorted in the red sand sediments facies than in the mottled facies. The minimum grain size of this population is ≈ 0.117 mm in the mottled facies

and ≈ 0.102 mm in the red aeolian deposits. The suspension population have an average value of ≈ 16 % in the mottled facies and ≈ 9 % in the red sand facies. Grain size of this population is usually less than 0.109 mm.

These data indicate that (1) the aeolian depositional processes did not change between the mottled and red sand sediments facies, (2) sand dune likely formed as suggested by the high percentage of the saltation population in both facies, (3) wind energy remained stable through time, and (4) the relatively small maximum size of the traction population indicates the domination of a low aeolian energy regime.

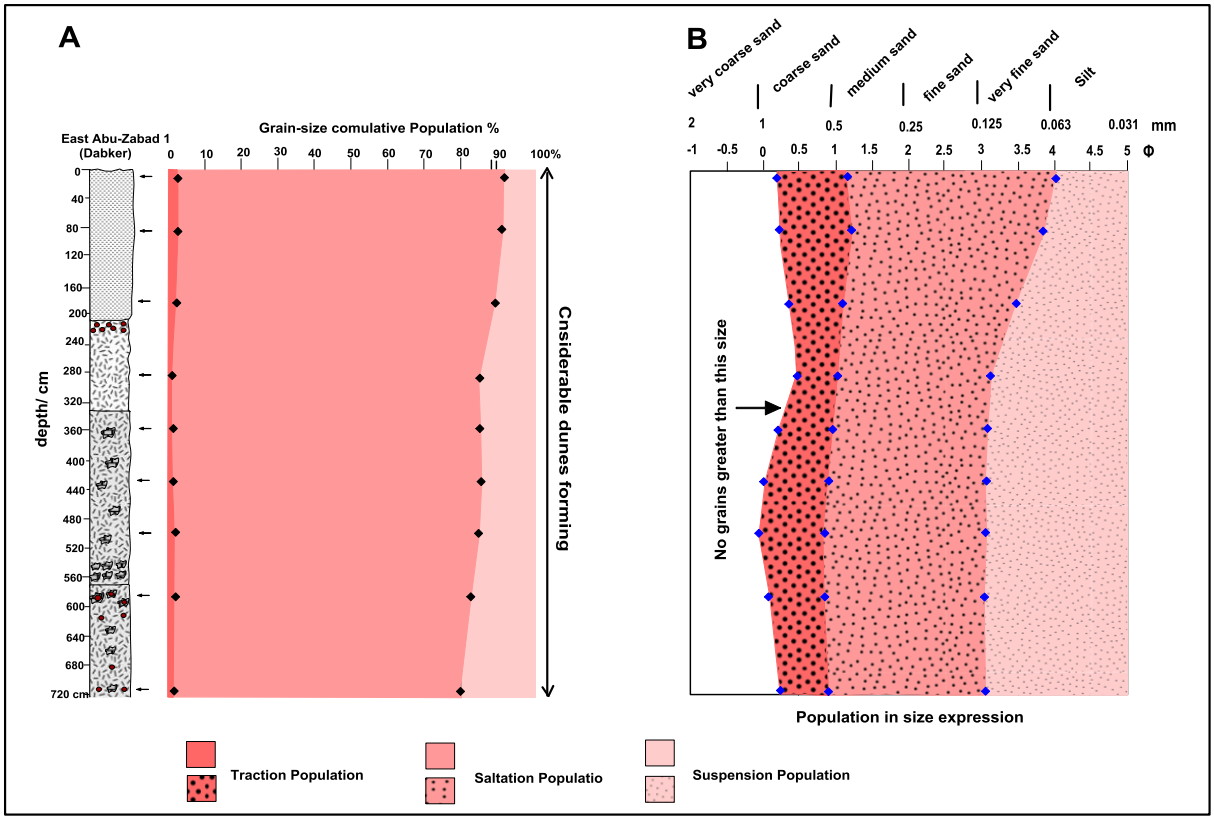


***Fig. 3.58:*** *Evolution of transport processes in the East Abu Zabad section. Expressed (A) in percentages; (B) in terms of grain size.*

### 3.5.3.5.2. Geographical interpretation

Three horizontal plots of the mode of transport population illustrate its variation across the studied area. These populations are shown in percentage and grain size, for the lower part and upper part of the mottled facies, and for the red sand sediments facies (Figs. 3.59 and 3.60).

#### 3.5.3.5.2.A. Variation in the mottled facies

Both parts of the mottled facies show an absolute domination of the saltation population through time, which favors sand dune building during deposition of this facies. The suspension population in the mottled facies remarkably increases southward, while the grain size of the traction population decreases southward in a comparable amount, thus indicating a southward decrease of the energy regime (Fig. 3.59).

### 3.5.3.5.2.B. Variation in the red sand sediments facies

The saltation population highly dominates during deposition of the red sand sediments facies, except in North Bara3, where the traction population is significant. Therefore, sand dune building should be rare to the North, and increased to the south. The suspension population shows low and stable percentages in the area. Grain size of the traction population is relatively fine and slightly decreases southward. This suggests a relatively low and stable energy regime, both in time and space (Fig. 3.60).

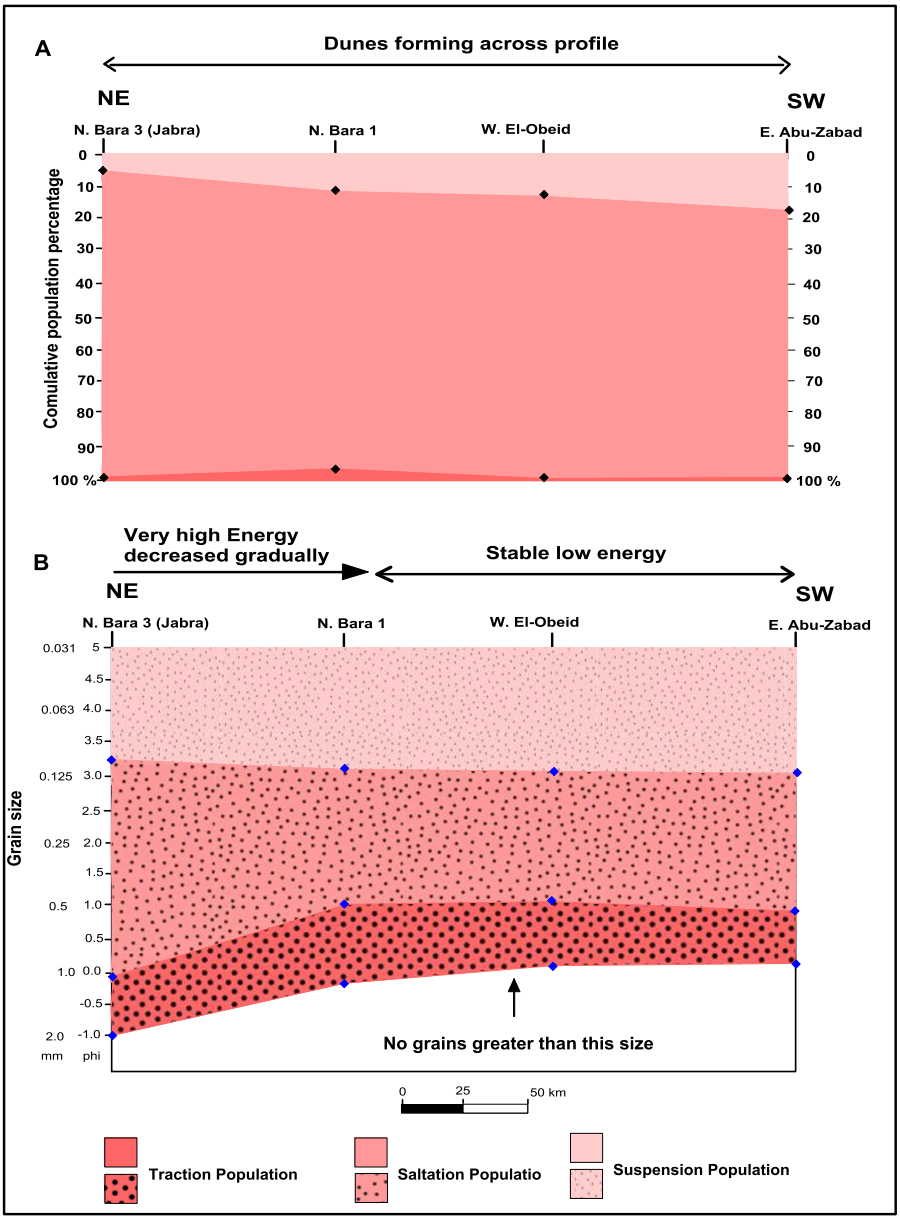


***Fig. 3.59:*** *North-South evolution of the transport processes for the mottled facies. Expressed (A) in percentages; (B) in terms of grain size.*

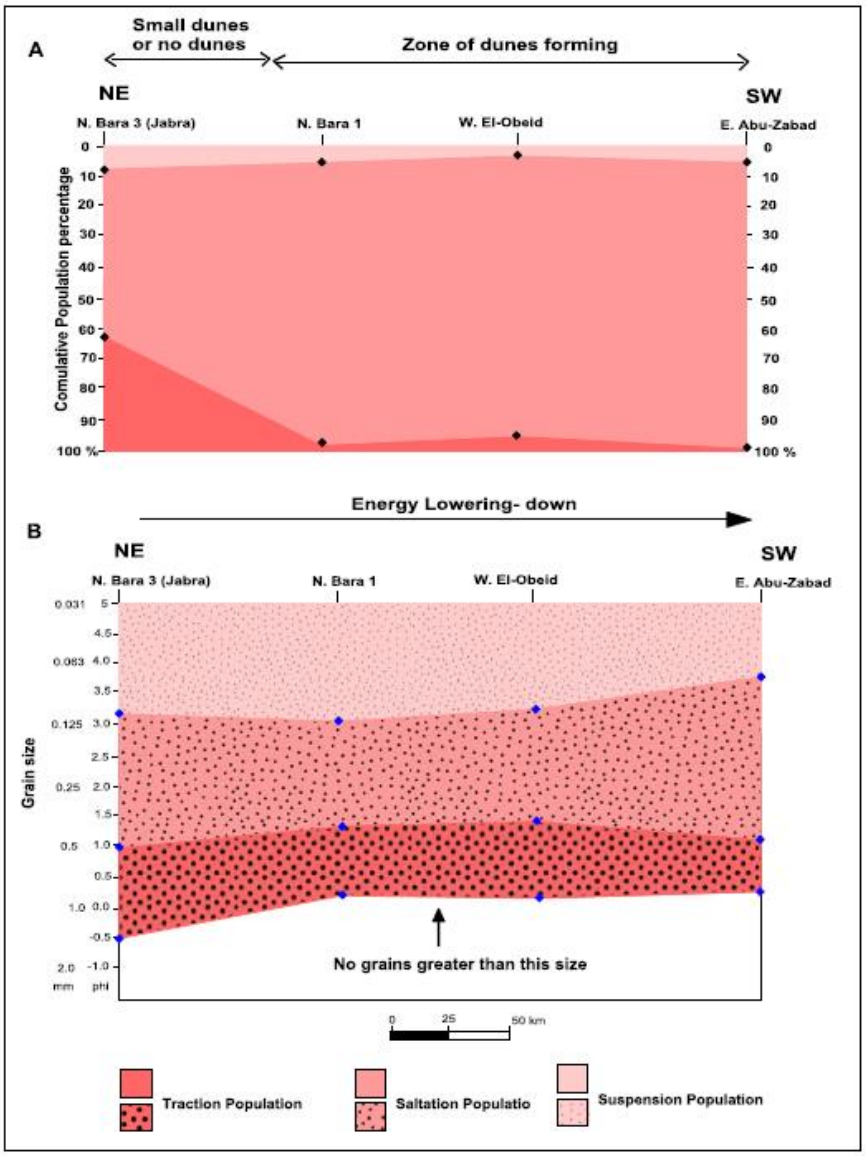


***Fig. 3.60:*** *North-South evolution of the transport processes red sand sediments facies. Expressed (A) in percentages; (B) in terms of grain size.*

### 3.5.4. Conclusion on the grain size analysis

- The result and interpretations show a southward fining trend through the domination of the very fine sand sediments in the southern sections. This suggests a southward decreasing energy (Fig. 3.61).
- The samples from the northern part show a wide grain size distribution that indicates variations of transportation energy through time. Conversely, the samples from the southern areas show a narrow grain size distribution, indicating constant or low variability of transportation energy during the deposition of both the red sand and mottled sand sediments facies.
- The domination of the saltation transportation mode in all area indicates a common aeolian depositional mechanism during the deposition of both the red sand sediments and the mottled facies.

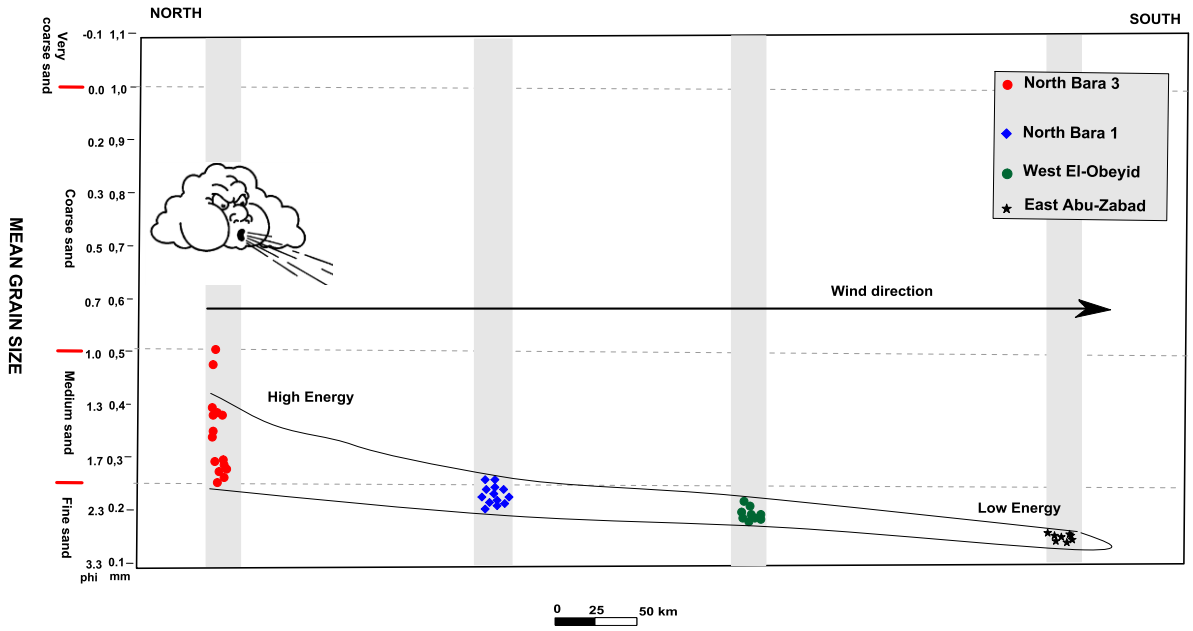


*Fig. 3.61: Mean grain-size distance relation, illustrating the variation in transport energy.*

## 3.6. Sedimentary and paleogeographic evolution

According to the local variations in sediments from one site to another, the study area has been divided into five areas : the Dilling, Abu Zabad-El Fula, El Obeid-South El Obeid, En Nahud-El Khowei and North Bara-Sodari areas. The sedimentary evolution has been described for each area, and based on these areas, a summary of the paleogeograhic evolution for the study area is presented. To understand the paleogeographic and environmental evolution through time, six paleogeographic maps have been constructed for the following periods : 13000 – 10000, 10000 – 8000, 8000 – 6000, 6000 – 3000, 3000 – 1000, and 1000 cal. yr. BP to present.

### 3.6.1. Sedimentary evolution

#### 3.6.1.1. Sedimentary evolution of the Dilling area

The Dilling area is dominated by fluviatile channel deposition at the base of the succession. These deposits are overlain by distal flood plain deposits, in which pedogenetic activity is evidenced by abundant root molds and development of calcareous nodules. This kind of pedogenesis indicates the development of a significant vegetation cover, the existence of a relatively shallow water table and therefore, a humid climate. Fluviatile channel deposits overly the flood plain deposits. These coarse fluviatile deposits are made of conglomerate containing numerous reworked calcareous nodules. As evidenced by the current features (trough and planar bedding), these conglomerates were deposited by powerful streams, which supports a humid climate.

The upper and thickest deposits around Dilling are dominated by either proximal fluviatile, or distal flood plain sediments, as well as by local aeolian deposition. However, these local aeolian

deposits are highly pedogenetized as shown by the intensive development of calcareous nodules and root traces, indicating a highly vegetated landscape and a humid climate (Fig. 3.63).

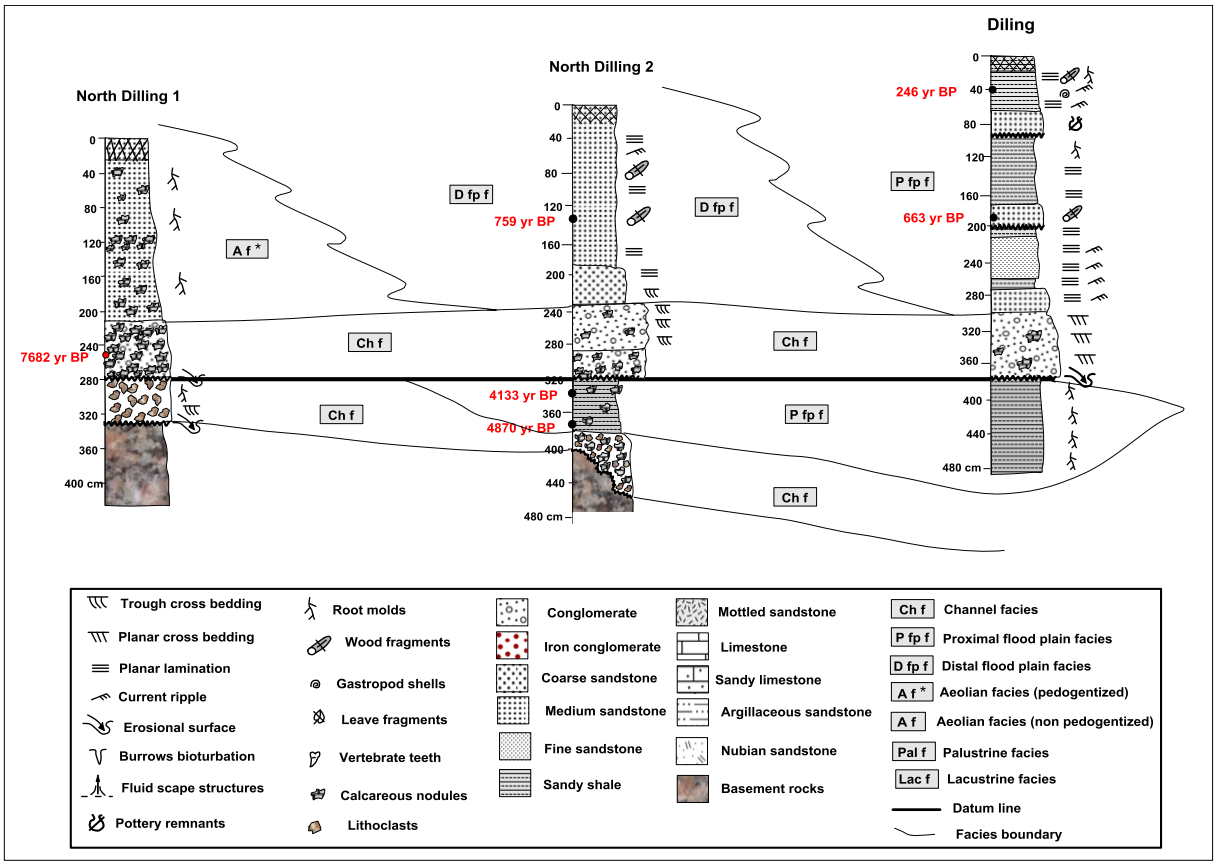


*Fig. 3.63: Sedimentary evolution of the Dilling area.*

### 3.6.1.2. Sedimentary evolution of the Abu Zabad – El Fula area

Aeolian deposition is the dominant depositional mechanism in this area in addition to local channel deposition (Fig. 3.64). According to the existence or absence of the pedogenetic processes, these aeolian deposits are thought to have been submitted to two different environments.

The subsequently pedogenetized aeolian deposits, which dominate most of the succession (First and possibly Second stratigraphic unit), are assumed to have experienced wet vegetated environment. Moreover, this wet environment was coeval with strong fluviatile activity leading to the deposition of thick reworked conglomerate between Abu Zabad and El Fula, and of some lenses of conglomerate East of Abu Zabad.

Non pedogenetized fine aeolian sand mark top of the sedimentological succession (Fourth unit). Because of the lack of subsequent pedogenesis, these upper aeolian deposits suggest deposition under arid climate.

### 3.6.1.3. Sedimentary evolution of the El Obeid – South El Obeid area

In the El Obeid-South El Obeid area, the lower part of the succession is dominated by mottled, fine sand of aeolian origin. These aeolian deposits recorded a rather dense vegetation, evidenced by abundant calcareous nodules and root molds and traces (Fig. 3.65).

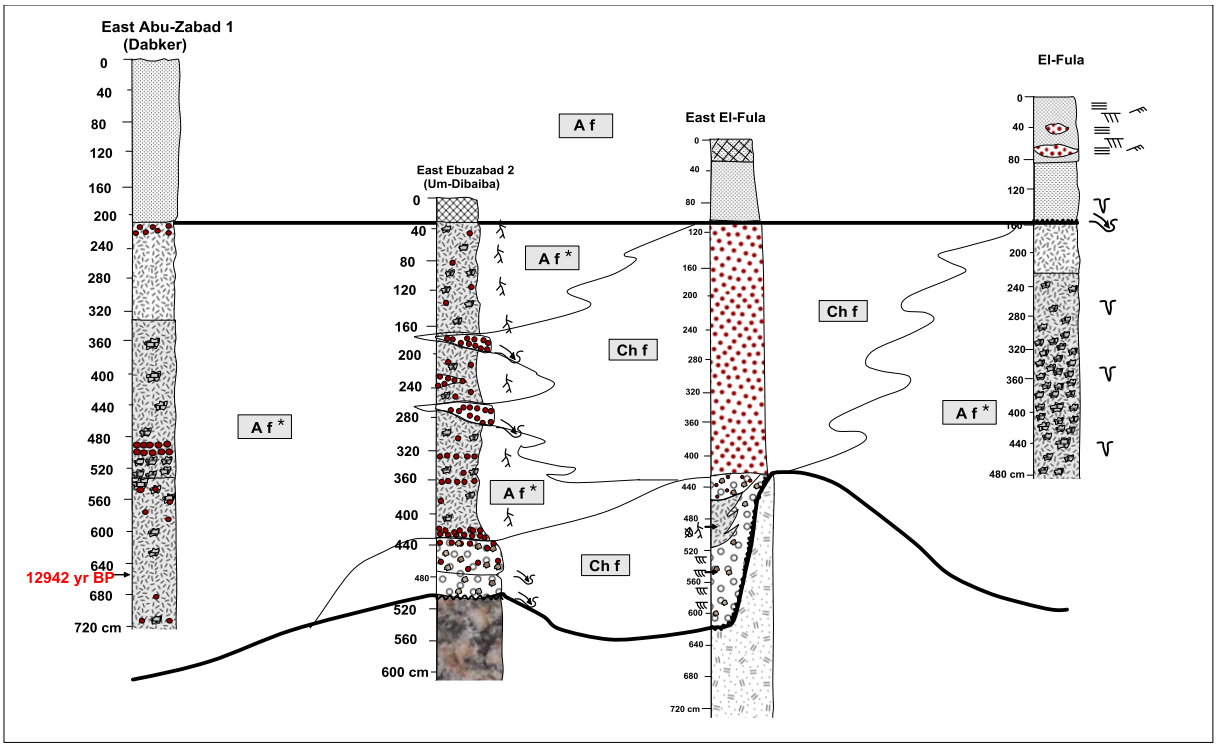


***Fig. 3.64**: Sedimentary evolution of the Abu Zabad – El Fula area. Same caption as Fig. 3.63.*

The upper part of the succession (Fourth stratigraphic unit) is dominated, either by aeolian, non pedogenetized, red fine sand sediments, or by fluviatile alternation of fine to medium sand, as indicated by current ripples and cross beddings. This upper part of the succession is interpreted as deposited by aeolian activity suggesting a dry climate, and was locally reworked by rivers indicating the occurrence of significant, although possibly rare, rainfalls, and thus suggesting a semi-arid climate.

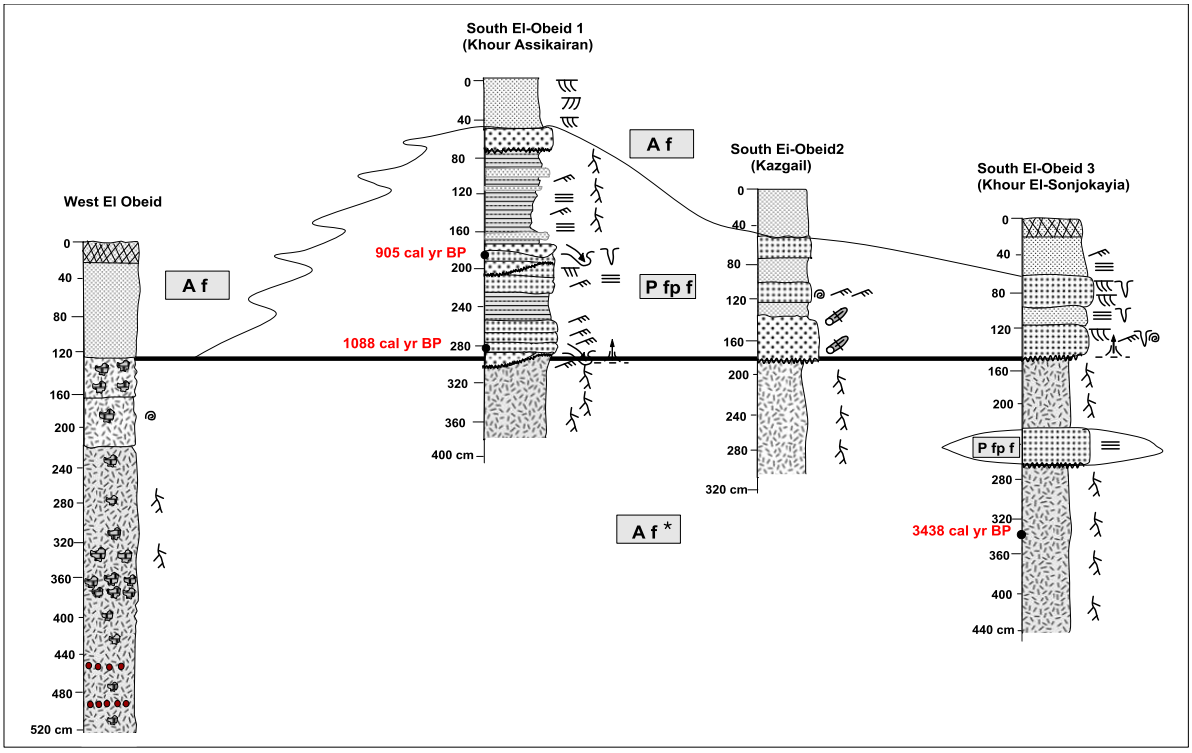


***Fig. 3.65**: Sedimentary evolution of the El Obeid – South El Obeid area. Same caption as Fig. 3.63.*

### 3.6.1.4. Sedimentary evolution of the En Nahud – El Khowei area

The succession in this area is divided into three unis. The lower or First unit is dominated by fine sands deposited by aeolian processes. However, the present-day mottled facies indicates subsequent pedogenesis processes (calcareous nodules and root molds), indicative of a rather dense vegetated cover, as mentioned for the previous areas.

The middle part of the succession (Second unit) is dominated by limestone and sandy limestone beds, marked by gastropod shells, root molds and karstification. These features indicate a palustrine environment (Fig. 3.66).

The upper part of the succession (Fourth unit) is dominated by non pedogenetized, red fine sands, deposited through aeolian mechanism, and marked by the occurrence of well-preserved gastropod shells. The gastropod shells provide good arguments for a seasonally dry and wet or semi-wet climate, depending on the nature of the gastropods, which require some seasonal water to build their shells. The lack or scarcity of root marks suggests a semi-arid to arid environment.

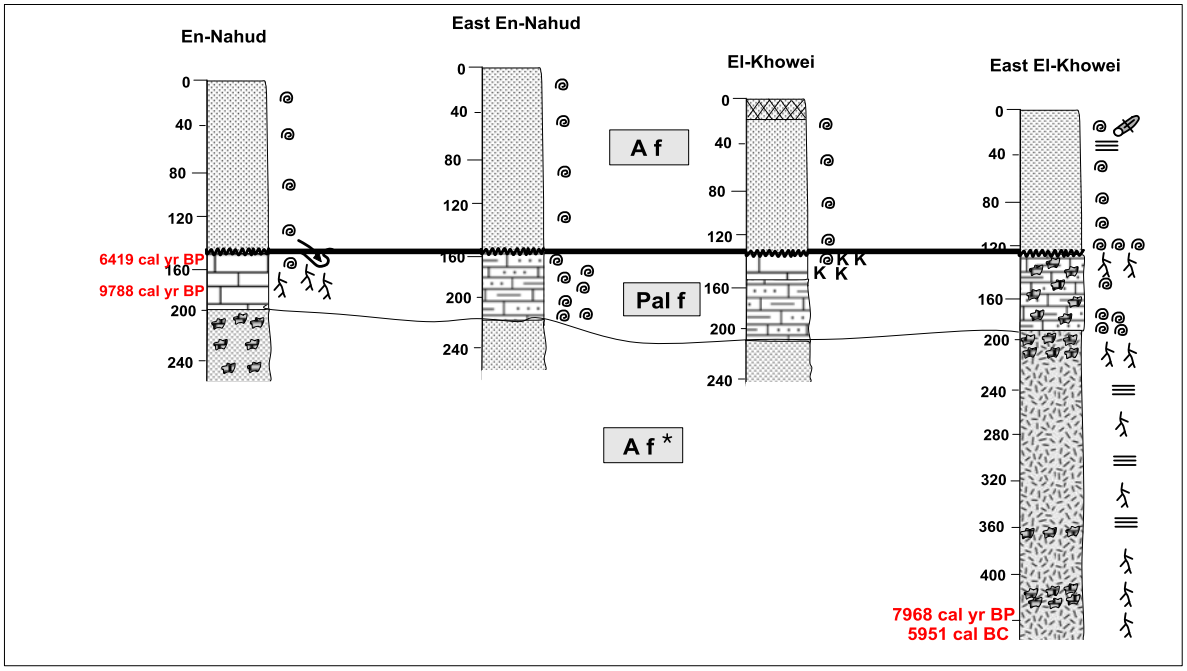


***Fig. 3.66****: Sedimentary evolution of the En Nahud – El Khowei area. Same caption as Fig. 3.63.*

### 3.6.1.5. Sedimentary evolution of the Sodari – North Bara area

In this area, the succession comprises three parts. The lower part of the succession is formed by pedogenetized, medium to coarse sand ascribed to the First unit. As indicating by the grain size analysis, they were deposited by aeolian processes, while pedogenesis indicates a further evolution under humid climate, and a vegetated environment.

The middle part of the succession is formed of an alternation of argillaceous sand and limestone beds, marked by karstification, gastropod shells, ostracods, root molds, wood and leave remnants (Second unit). The limestone and its mentioned features indicate a lacustrine environment, while the interbedded argillaceous sand sediments indicate periods of low lake levels, or the activity of stream flowing into the lake (Fig. 3.67).

The upper part of the succession (Fourth unit) is dominated by non pedogenetized, medium to coarse, red sand, deposited through aeolian processes, mostly during a dry climate period.

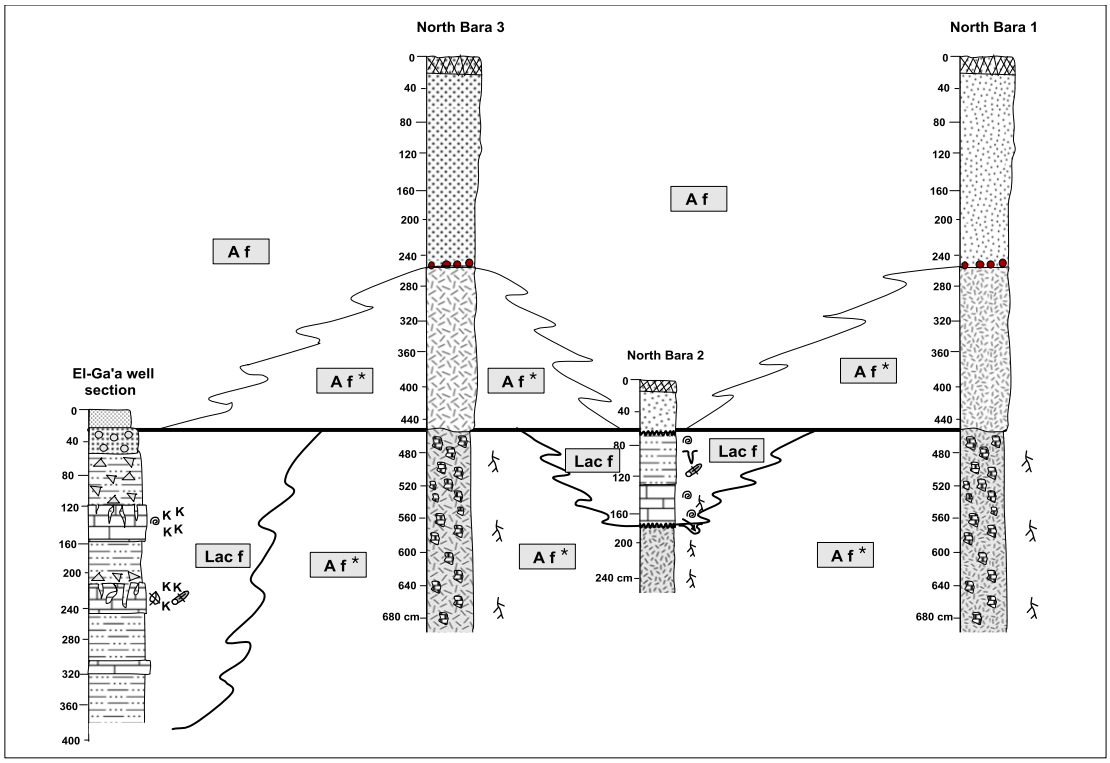


*Fig. 3.67: Sedimentary evolution of the Sodari – North Bara area. Same caption as Fig. 3.63.*

### 3.6.2. Sedimentation and paleogeography for the ≈ 13 000 – 10 000 yr BP period

This period is marked by mottled facies in most of the study area and by erosion around, and south of, the Dilling area, since no sedimentation is recorded for this period in the latter areas (Fig. 3.68). According to the grain size analysis (section 3.2.2), the mottled facies is an aeolian deposit brought by Southward blowing winds, since the grain size of these sediments decreases southward. Once deposited, pedogenesis occurred (calcareous nodules and root molds), indicating that the area was covered by vegetation and experienced a relatively humid climate, probably after deposition.

Around Dilling, the humid climate combined with a rough topography favored erosion and sediment transport by rivers, thus explaining the observed sedimentary hiatus. This contrast between the northern and southern part of the studied area illustrates a marked climatic gradient between the northern areas submitted to deposition of aeolian sands proceeding from the Sahara located farther North, rapidly colonized by vegetation responsible for mottling, and the southern area submitted to heavier rainfalls responsible for erosion and removing of sediments by rivers.

### 3.6.3. Sedimentation and paleogeography for the ≈ 10 000 - 6000 yr BP period

During the first 2000 yr of this period, the Dilling area may have experienced erosion or non-deposition, hence maximum recorded age for sediments overlying the Basement rocks is about

7600 yr BP in fluviatile conglomerates of reworking basement rocks and calcareous nodules. This channel facies is also locally present in East Abu Zabad, between Abu Zabad and El Fula.

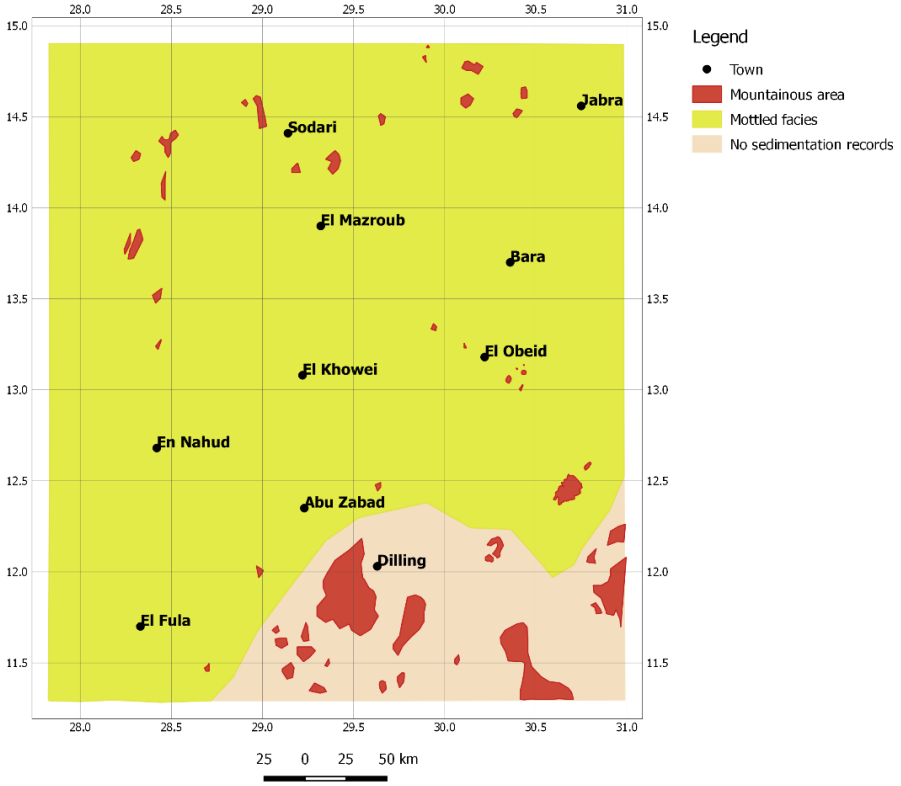


***Fig. 3.68**: Paleogeographic map for the period 13000 – 10000 yr BP.*

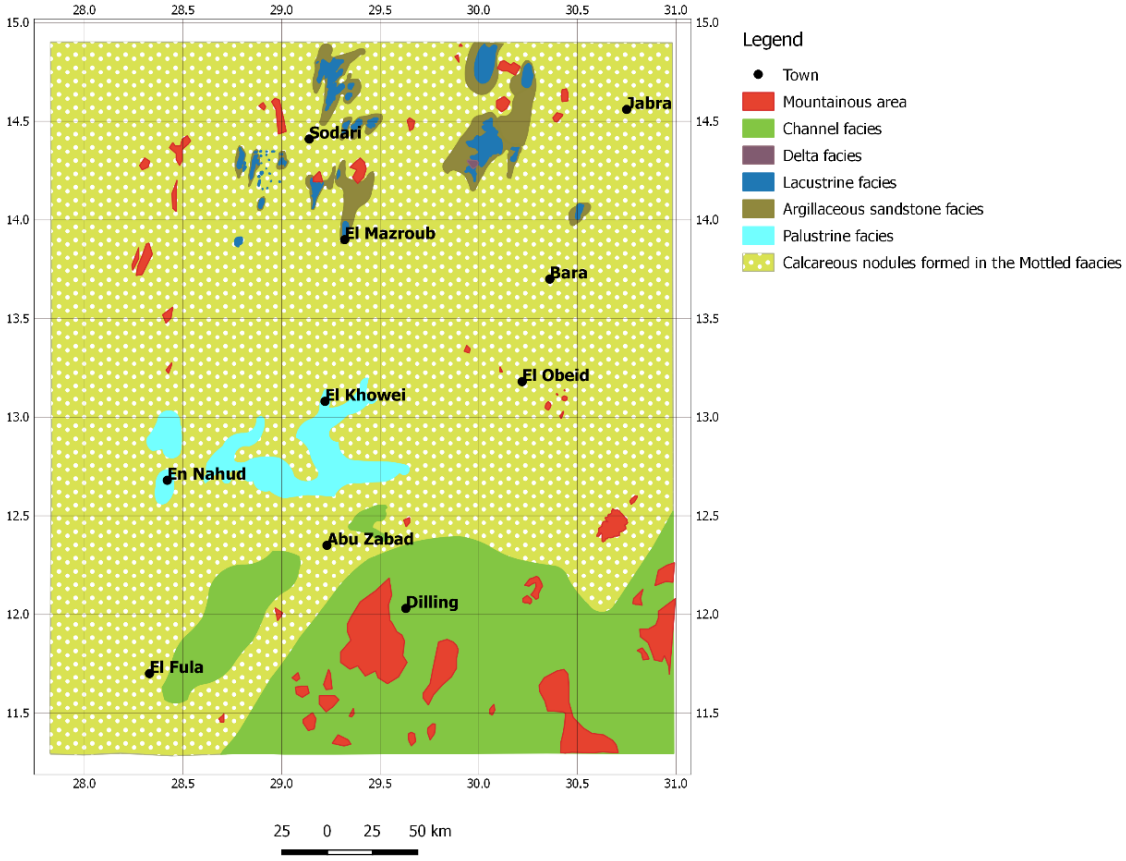


***Fig. 3.69**: Paleogeographic map for the 10000 – 6000 yr BP period*

In the northern parts of the region, beside the local deposition of lacustrine, palustrine and argillaceous sand sediments facies, the mottled facies experienced pedogenetic processes represented by mottling and the development of calcareous nodules (Fig. 3.69).

The topography and geology of the northern areas played an important role in the distribution of facies. Limestone and sandy limestone deposited in the En Nahud-El Khowei area, are known only on Nubian sandstone outcrops, which form a slightly undulating plateau, 600 to 700 m above sea level (asl) (Fig. 1.6). Interbedded limestone and argillaceous sand sediments are only known in the North, where they are restricted to small depressions located along dry rivers dammed downstream by large rectilinear dunes (El Ga'ah, Sodari). They are located at 450 to 550 m asl.

The depositional environment during this period was generally wet and vegetated as indicated by the deposition of limestone and sandy limestone in the En Nahud-El Khowei area that indicate palustrine environment in this area. Development of calcareous nodules and root molds in the mottled facies is assumed to occur during this humid period. In the northern part, the limestone level is thicker suggesting deposition under thicker water column, and suggests a lacustrine environment with local strong fluvial activities in the northern parts as evidenced by the progradation of the El Ga'a delta sediments, which indicates strong freshwater runoff and sediment influx (Fig. 3.70). This lacustrine environment was interrupted by periods of low lake level or of fluviatile activity, resulting in the deposition of interbedded argillaceous sand sediments.

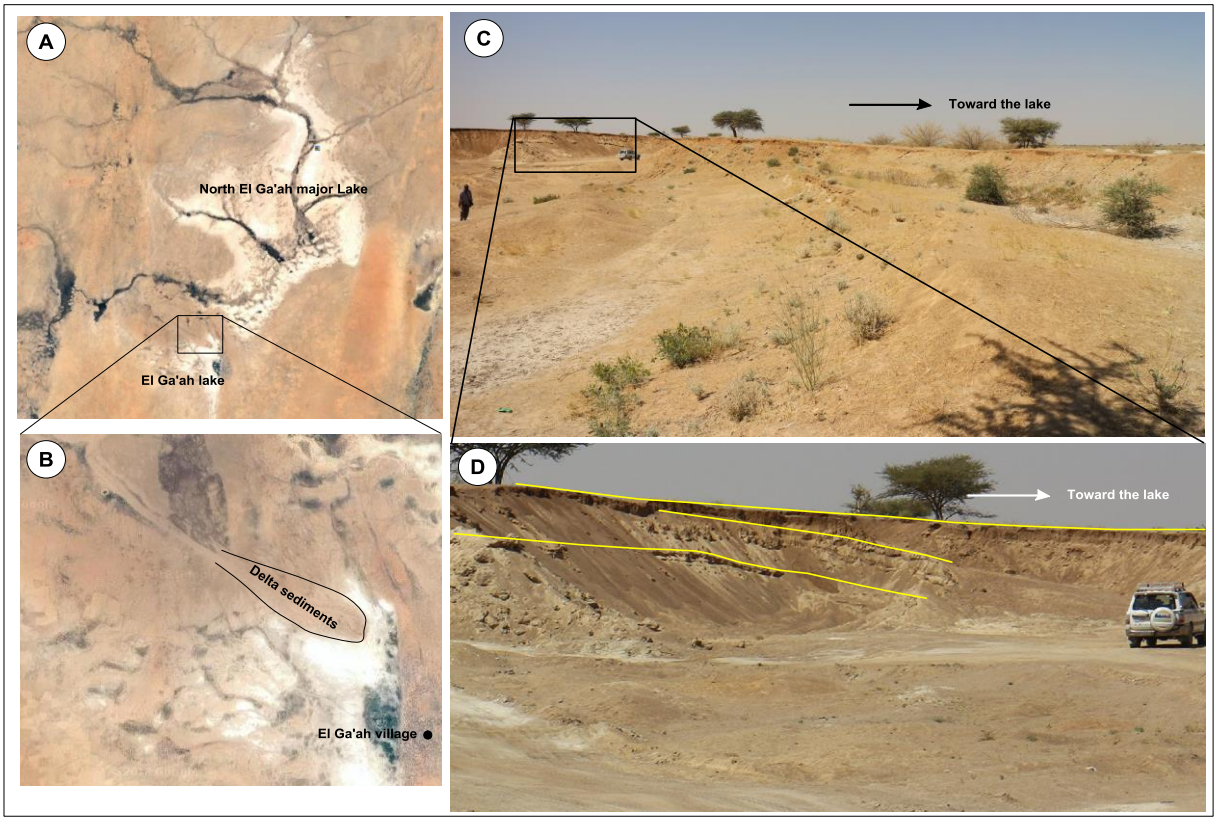


***Fig. 3.70**: Progradation of deltaic sediments in the El Ga'a lake. (A and B) Location of the lakes and delta sediments. (C) Distal photograph showing the clinoforms of the delta sediments toward the lake. (D) Detail of the delta progradation (yellow lines). This delta overlies lake sediments (white color).*

### 3.6.4. Sedimentation and paleogeography for the ≈ 6000 - 3000 BP period

At this time the northern parts of the study area and the northern part of the Kordofan region in general did not record deposits, while in the central and southern parts (El Obeid, Abu Zabad, El Fula areas), aeolian deposition took place, with local flood plain deposition in the southern parts around the Dilling area and further south (Fig. 3.71). These flood plain deposits are marked by root molds and the development of calcareous nodules in the Dilling area, and by mottling of previously deposited aeolian sands in the south El Obeid area. These mottled deposits are rich in organic matter.

Although the En Nahud-El Khowei area (which extends to the south close to Abu Zabad) is located at the central part of the study area, it did not receive any sediments during the period 6 – 3 ky BP. This may be due to its high topographic elevation which may have provoked a stronger exposition to wind activity. As matter of fact, aeolian erosion is evidenced by deflation surfaces in the northern part of the studied region, locally marked by iron gravel horizon observed north of Bara and representing deflation lags (Glennie, 1987) (Fig. 3.72). Such deflation surfaces indicate that the northern part of the studied area experienced aeolian erosion probably after 6 kyr BP. In addition, deep erosion is clearly evidenced in the En Nahud-El Khowei area by the undulated erosional surface on top of the palustrine carbonates (Fig. 3.73). Therefore, the apparent 6 – 1 ky BP hiatus observed there, may be due to the aeolian erosion of sediments deposited after 6 ky BP.

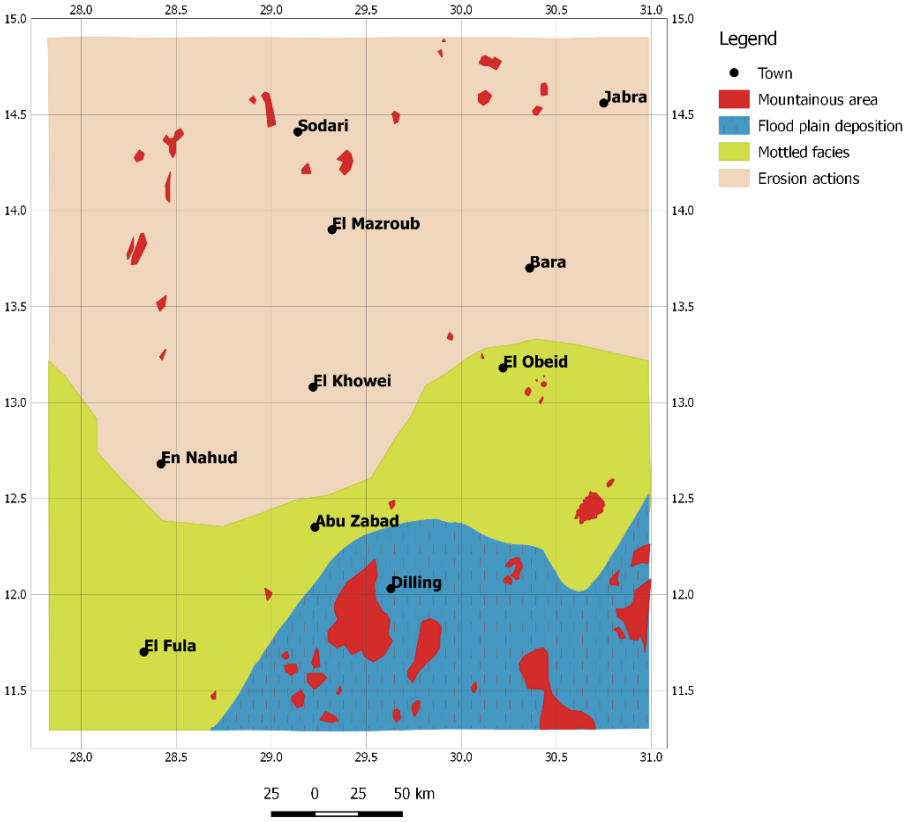


***Fig. 3.71**: Paleogeographic map for the 6000 – 3000 yr. BP period*


***Fig. 3.72:*** *Deflation surface – north Bara.*

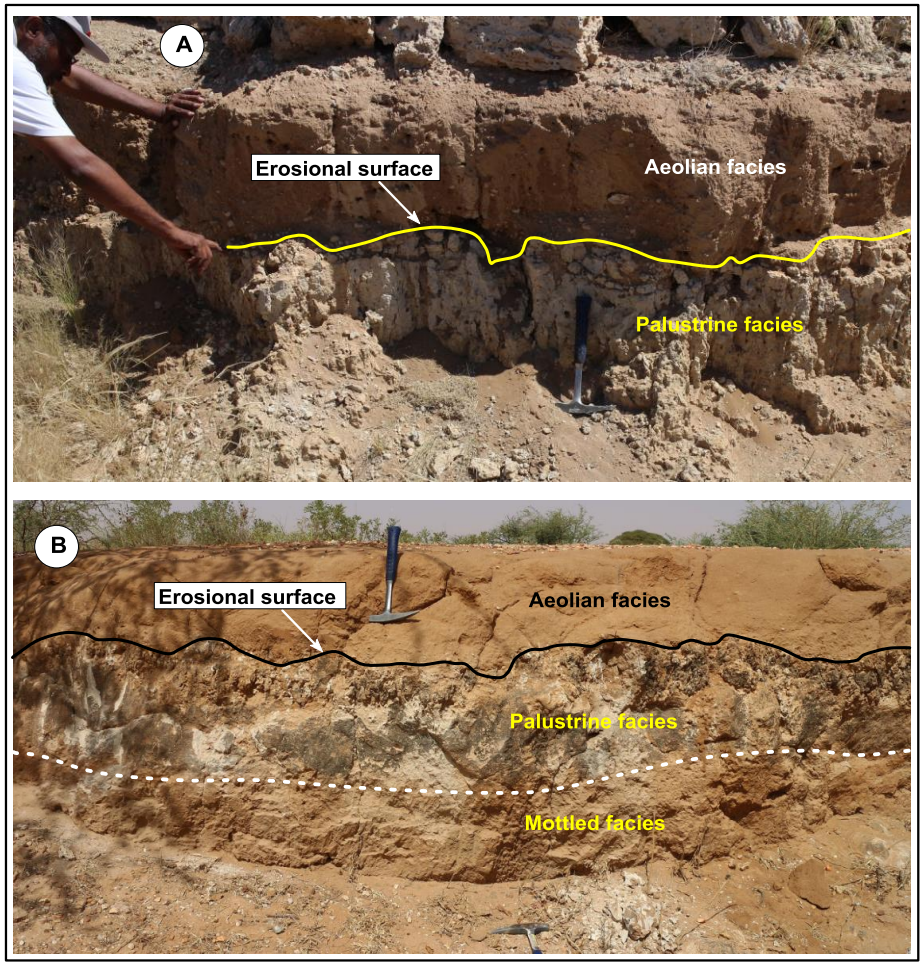


***Fig. 3.73:*** *Erosional surface separating the palustrine facies (Second unit) from the upper aeolian facies (Fourth unit) in En-Nahud (**A**) and El Khowei (**B**).*

### 3.6.5. Sedimentation and paleogeography for the ≈ 3000 - 1000 yr BP period

This period is marked by an erosional hiatus evidenced by the eroded surface capping the mottled facies in southeast El Obeid, and the flood plain facies in the Dilling area (Fig. 3.74). This period was thus marked by aeolian erosion and/or non-deposition in most of the study area, although fluviatile activity cannot be ruled out in the southern part of the Kordofan region, where dates are scarce.

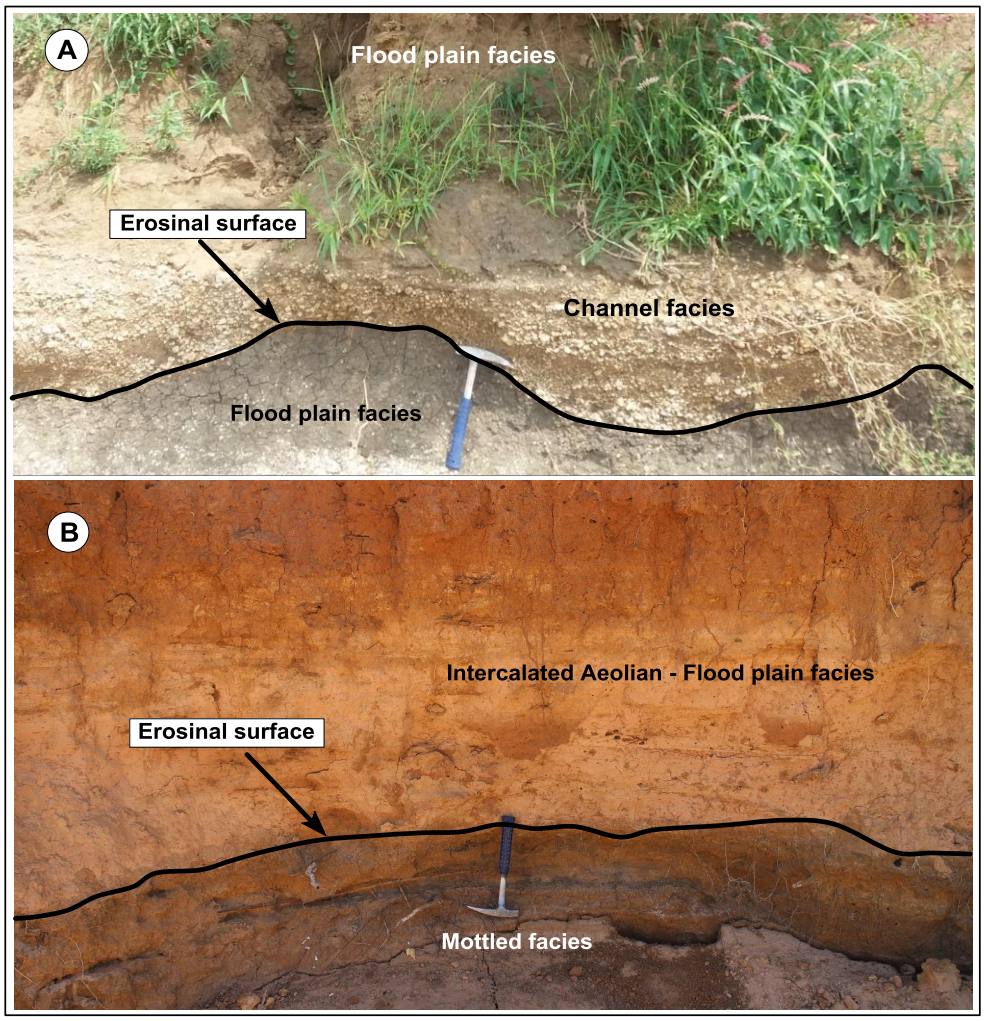


***Fig. 3.74:*** *Erosional surfaces. (**A**) Dilling area. (**B**) South El Obeid area (Khour Es Sonjokaya).*

### 3.6.6. Sedimentation and paleogeography between ≈ 1000 yr BP and Present

After a prolonged period of erosion which continued from ≈ 3 to ≈ 1 kyr BP in the Kordofan region, deposition resumed ≈ 1000 year ago in the whole region with aeolian deposits (Fig. 3.76). The southward decreasing grain size of the iron-rich aeolian sand sediments indicate that the sand proceed from the northern Saharan areas. The absence of the pedogenetic processes of the aeolian deposits in the northern part of the Kordofan region, indicates that depositional environment was mainly dry and windy. The aeolian deposits are locally interbedded with flood plain deposits south of El Obeid and in the Abu Zabad-El Fula area. Around Dilling, deposition resumed with channel deposits, and went on with flood plains deposits. Therefore, the southern part of the region recorded a more humid climate than the northern part during this last 1000

year, as evidenced by the current features, the root molds, some plant remnants (leave and wood fragments), and the local development of calcareous nodules, observed in the upper deposits.

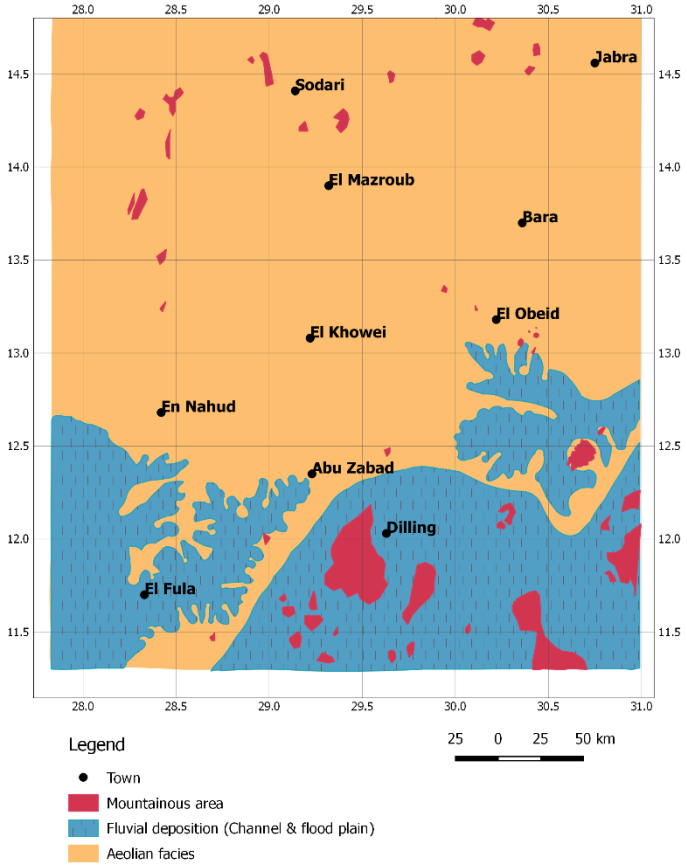


***Fig. 3.76**: Paleogeographic map for the period 1000 yr BP to Present*


***Fig. 3.77**: Present-day fluvial system in the southern part of the study area (Google earth image).*

# IV. PALEOCLIMATIC EVOLUTION

## 4.1. Introduction

Several proxies have been used in this investigation in order to reconstruct the climate evolution of the Kordofan region during the latest Pleistocene-Holocene period. Beside the initially presented sedimentological proxy in the previous chapter, this chapter includes the results and interpretation of a variety of studies : paleontology and paleobiology of the gastropod sub-fossil shells in five sections, palynology in three sites, oxygen and carbon stable isotopes of gastropod shells and calcareous nodules in five sections, major elements geochemistry in two sections, clay mineralogy in one section, and paleohydrology of the area.

## 4.2. Paleontology and paleobiology

Paleontological investigation includes the study of the gastropod sub-fossil shells and of the palynological assemblages.

### 4.2.1. Gastropod paleontology and paleobiology

Gastropods shells are observed in abundance in the central and northern parts of the study area (Fig. 4.1). Twelve species of gastropod shells have been identified with the help of Dr Dirk Vandamme (Ghent University, Belgium). The identified species include: *Biomphalaria sudanica*, *Biomphalaria pfeifferi*, *Gabbiella senaariensis*, *Bulinus truncatus*, *Melanoides tuberculata*, *Radix natalensis*, *Pila wernei*, *Lanistes carinatus*, *Caracolus* sp., *Limicolaria flammea*, *Limicolaria caillaudi* and *Zootecus insularis* (plate 4.1).

#### 4.2.1.1. Geographic range and habitat of the identified gastropods

Nowadays, it is rare to find living snails in the study area. To use these shells as clues to understand the ecological and climatic conditions during their life, it is important to obtain information about the habitat of these species from literature. The identified species included aquatic, semi-aquatic and land snail species. Seven of them are aquatic freshwater snails : *Biomphalaria sudanica*, *Biomphalaria pfeifferi*, *Gabbiella senaariensis*, *Bulinus truncatus*, *Melanoides tuberculata* and *Radix natalensis*. The semi-aquatic species are : *Pila wernei* and *Lanistes carinatus.* The land snail species are : *Limicolaria flammea*, *Limicolaria caillaudi* and *Caracolus* sp.

Table 4.1 shows the relative abundances of these gastropod shells in studied sites. Among the twelve species, only five were found in En Nahud, the most abundant being *Pila wernei*. Eight species were found in the East En Nahud section, among which *Radix natalensis* was the most abundant, and *Limicolaria caillaudi* the less abundant. In the east El Khowei site, eleven species were recognized (the only missing species is *Zootecus insularis*), *Radix natalensis* was the most abundant, and *Caracolus* sp. was the less abundant species and has been only observed in this site. Eight species were found in the El Ga'ah area, *Melanoides tuberculata* is the most abundant, and *Limicolaria flammea* is the less abundant. In the Sodari area, seven species were recognized, *Melanoides tuberculata* was the most abundant, *Gabbiella senaariensis* was the less abundant, and *Zootecus insularis* has been only observed in the Sodari area. Six species

were identified in the north Bara site, among which *Biomphalaria sudanica* and *B. pfeifferi* dominate, while *Limicolaria caillaudi* is the scarcest.

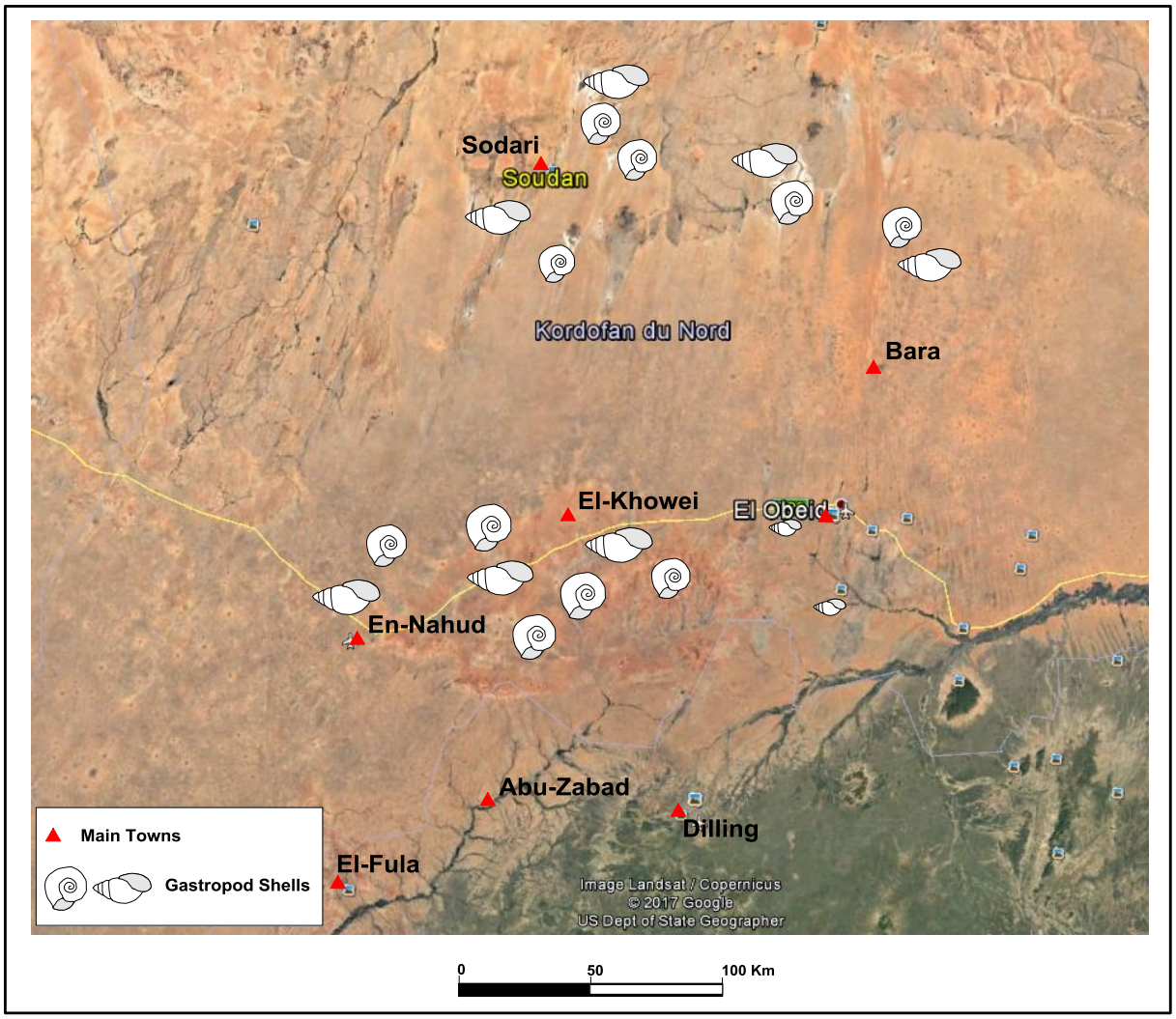


*Fig. 4.1: Geographic distribution of the studied gastropod shells*

The distribution and abundance of gastropods differ considerably according to the species (Table 4.1). Four species are consistently abundant and widespread : *Biomphalaria sudanica*, *B. pfeifferi*, *Melanoides tuberculata* and *Radix natalensis*; four species are common (*Pila wernei*, *Lanistes carinatus*, *Limicolaria flammea*, *Gabbiella senaariensis*), and three species are uncommon (*Limicolaria caillaudi*, *Bulinus truncatus*, *Zootecus insularis*). The only rare genus was *Caracolus* sp., since only two shells were observed in the East El Khowei section.

#### 4.2.1.1.A. Aquatic snails

***Biomphalaria pfeifferi*** *(*Krauss 1948)

*Geographic range:* most of Africa from the Sudan southwards; isolated populations living in the Sahara are recorded (Brown, et al 1984). In Sudan it is distributed in a variety of areas of the Darfur province and southwards from the Nile/Atbara confluence, with scattered localities in the Sudd (Southern Sudan); it is common in the eastern Gezira region (Williams and Hunter, 1968, *in* Brown et al., 1984).

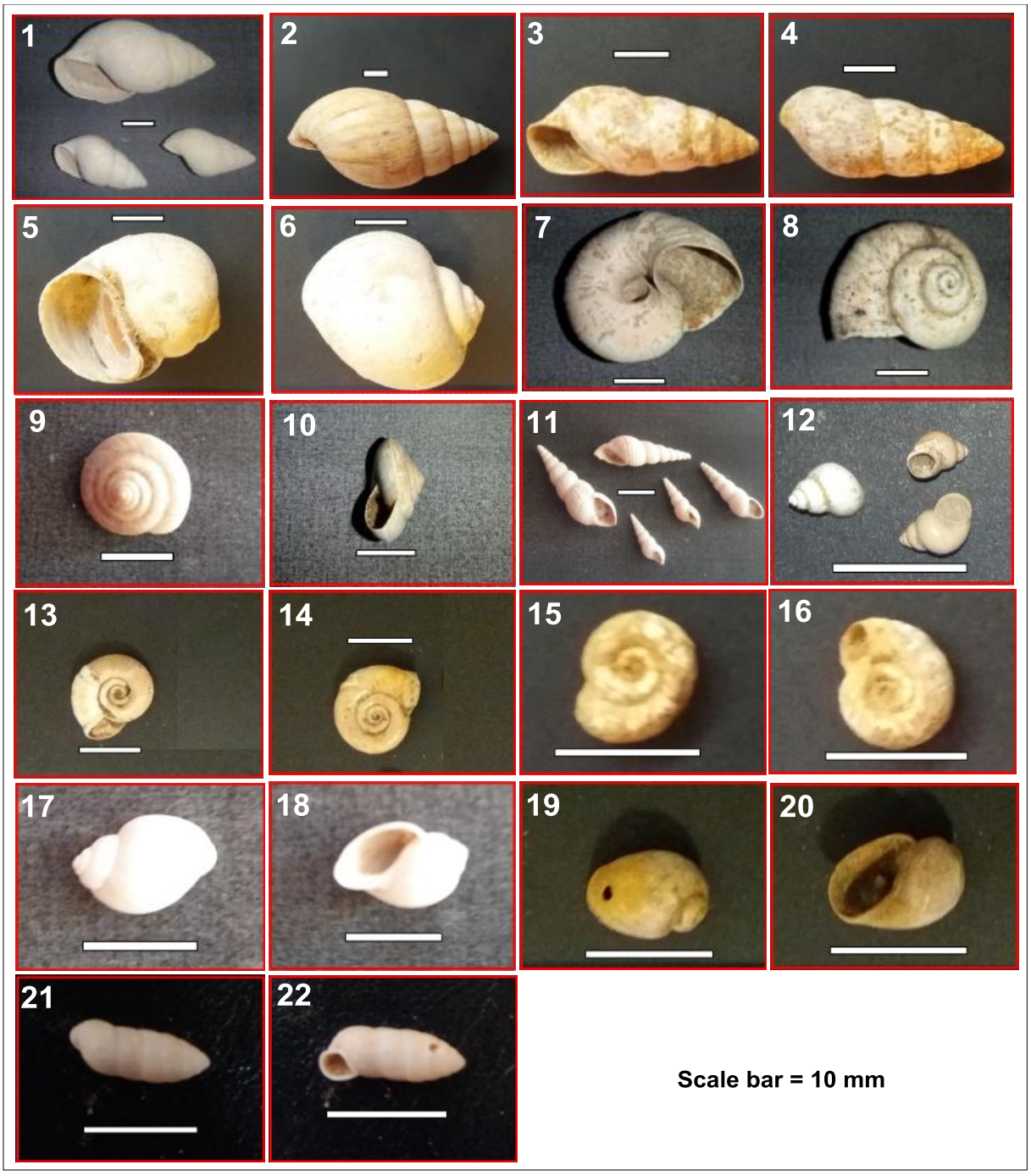


***Plate. 4.1: Identified gastropod shells***. ***1, 2****: Limicolaria flammea* (Müller, 1774). ***3, 4****: Limicolaria caillaudi* (Pfeiffer, 1852). ***5, 6****: Pila wernei* (Philippi, 1851). ***7, 8****: Lanistes carinatus* (Olivier, 1804). ***9, 10****: Caracolus* sp. ***11****: Melanoides tuberculate* (Müller, 1774). ***12****: Gabbiella senaariensis* (Kuster, 1852). ***13, 14:*** *Biomphalaria pfeifferi* (Krauss 1948). ***15, 16:*** *Biomphalaria sudanica* (Martens, 1870). ***17, 18:*** *Radix natalensis* (Krauss, 1848). ***19, 20:*** *Bulinus truncates* (Audouin, 1827). ***21, 22:*** *Zootecus insularis* (Ehrenberg 1831).

*Habitat: Biomphalaria pfeifferi* occurs in habitats of widely varying stability; in the stable African Great Lakes (Dupouy et al., 1993) and in streams (Magendants, 1972), yet isolated populations living in the Sahara are also recorded (Brown et al., 1984). However, *B. pfeifferi* prefers permanent water bodies and seems to prefer minimal (0-25 %) shade in their habitats

(marginal, floating and emergent vegetation; Ndifon and Ukoli, 1989). It has been recorded in comparatively permanent sites in rivers, khors and lagoons, where some plant species as *Echinochloa, Eichhornia, Vossia* and *Typha* are present in some localities. Williams and Hunter (1968) noted that *B. pfeifferi* was more common where the vegetation was dominated by grass (Brown et al., 1984). In Congo, *B. pfeifferi* has been collected from irrigation channels with mainly clayey substratum (Schultheiß et al., 2011).

*Table 4.1: Relative abundances of gastropod sub-fossil shells in the study area.*

| Gastrpod sp. / Area | Land snails | | | | Semi-aquatic | | Aquatic | | | | |
|---|---|---|---|---|---|---|---|---|---|---|---|
| | *Limicolaria flammea* | *Limicolaria caillaudi* | *Caracolus sp.* | *Zootecus insularis* | *Pila wernei* | *Lanistes carinatus* | *Biomphalaria sudanensis and B. pfeifferi* | *Melanoides turberculata* | *Bulinus trucatus* | *Gabbiella sennariensis* | *Radix natalensis* |
| En-Nahud | ● | | | | ● | | ● | | | | ● |
| Er-Rawyiana (Khowei-Nahud road) | ● | ● | | | ● | ● | ● | ● | | | ● |
| East El-Khowei | ● | ● | · | | · | ● | ● | ● | ● | ● | · |
| El-Ga'ah | ● | | | | ● | ● | ● | ● | | · | ● |
| Sodari | ● | | | · | ● | ● | | ● | | · | ● |
| North Bara | | ● | | | | | ● | ● | | ● | ● |

The most abundant ● ● ● ● ● ● ● ● · · The less abundant

Recent studies on alive *B. pfeifferi* distribution and habitat carried out in South Africa, shows that this species was present in a wide variety of water bodies: dams, rivers and streams, although it prefers the perennial, standing, clear and fresh water bodies. The majority of samples came from sites where mean annual temperature ranges from 15 to 25°C. *B. pfeifferi* is sensitive to low temperatures. In addition, the highest percentages of samples were recovered from sites that fell within the two intervals of mean annual rainfall ranging from 300 to 600 mm and 600 to 900 mm (Kock et al., 2003).

***Biomphalaria sudanica*** (Martens, 1870)

*Geographic range:* The distribution of *Biomphalaria sudanica* is Sudan, Southern Ethiopia to Lake Chad to the West; and southwards through Uganda and the basins of the lakes Victoria and Tanganyika. Brown et al. (1984) reported that it was common in the White Nile and in various parts of the Sudd region.

*Habitat: B. sudanica* is found in a variety of habitats such as flooded area near the main Nile river, rainwater lakes and swamps, in the White Nile where papyrus islands were grounded

(Malek, 1958, *in* Brown et al., 1984) and in numerous habitats above the lake level, near the shores of the Lake Victoria, particularly in grassy seepages and irrigation furrows (Magendants, 1972). The latter author reported that Webbe (1962) found specimens of *B. sudanica* (infected by *S. mansoni*) in backwaters behind the lakeshore, and regarded them as an important source of *S. mansoni* transmission.

According to Brown et al. (1984), Williams and Hunter (1968) noted that this snail was commonest where *Eichhornia* (water hyacinth) is dominant. *Biomphalaria* found in Sudan prefers rather stable conditions with fairly dense vegetation (Brown et al., 1984). This is supported by our field observations that *Biomphalaria* is often associated with abundant root traces.

***Melanoides tuberculata*** (Müller, 1774)

*Geographic range:* The genus *Melanoides* is restricted to the Old World tropics (Pilsbry and Bequaert, 1927, *in* Kock and Wolmarans, 2009). About 30 species of *Melanoides* occur in Africa, of which only *M. tuberculata* is widespread. It is also indigenous to India and the Southeast Asian mainland to northern Australia, and was widespread in the present-day Sahara during the late Pleistocene-Holocene (Kock and Wolmarans, 2009).

*Habitat:* The preferred habitat of *M. tuberculata* is permanent water bodies (standing or running) including rivers, shallow seepages, man-made habitats (Kock and Wolmarans 2009), lakes, lagoons, canal, khors (Brown et al., 1984), streams and pools (Ndifon and Ukoli, 1989). According to Brown (1994) *M. tuberculata* is not found in temporary waters. Generally, it prefers moderately shaded habitats (marginal, floating and emergent vegetation) but is also often found in low (25-50%) shade (Ndifon and Ukoli, 1989). In Jonglei (Southern Sudan), its habitat was characterized in some sites by the presence of *Eichhornia* and *Vossia* (Brown et al., 1984). In our study area, the association of *M. tuberculata* with numerous root traces supports the above points.

Concerning its preferred temperature, a study from South Africa reported that the majority of samples were recovered from loci that fell within the mean annual temperature interval from 21˚C to 25°C (Kock and Wolmarans, 2009).

In the course of worldwide monitoring, *M. tuberculata* has been reported to invade brackish and even marine water bodies of up to 33 ‰ salinity, and under experimental condition, survive extreme high condition of salinity up to 45 ‰ (Bolaji et al., 2011).

***Gabbiella senaariensis*** (Kuster, 1852)

*Geographic range:* Few studies related to *Gabbiella senaariensis* are available. Generally, its distribution comprises Egypt, Sudan, Uganda, Central African Republic and northern Nigeria (Brown et al., 1984).

*Habitat: G. senaariensis* is widespread in a variety of relatively permanent waters. In Sudan and South Sudan, it has been found in lakes, in the Nile and Atem Rivers, irrigation canals, ditches and pools. *Eichhornia, Vossia* and water lilies were present in some sites (Brown et al., 1984). In Egypt it has been found in the Nile Valley, Nile delta, Lake Nasser and Fayoum (Lotfy and Lotfy, 2015).

***Bulinus truncatus*** (Audouin, 1827)

*Geographic range:* This species is widely distributed in Africa, but the main areas of distribution are Lower Egypt, Sudan and westwards into Mauritania. It has been found in all oases in northern Africa and is widespread in western and eastern Africa (IUCN, 2012). However, its general distribution is Southwest Asia, Arabia, Mediterranean regions and Portugal, Northwest Africa and from the Nile delta southwards to Angola and Malawi (Brown and Rollinson, 1982; Brown et al., 1984).

*Habitat:* It can be found in various water bodies, flowing and standing, some of which becoming seasonally dry. It is often found in standing waters, irrigation channels and other man-made structures (IUCN, 2012). In Sudan it has been found in clear or muddy waters, including the Nile and Atem rivers, lakes, lagoons, pools and canals. A preferred niche was amongst the deeply floating roots of *Eichhornia* (Brown et al., 1984).

***Radix natalensis*** (Krauss, 1848) or ***Lymnaea natalensis*** (Krauss, 1848)

*Geographic range:* Radix natalensis is widespread in tropical Africa, but it is rare in the northeastern coastal area. It is known throughout the Congo in Central Africa, widespread in West, East and Southern Africa (except for the ephemeral aquatic systems in Namibia and Botswana), and from the Western Cape Province (South Africa). In North Africa, it is very common in the Nile River and Nile Delta but has only been reported in northwestern Africa from three localities in Algeria, although it was previously known from many prehistoric localities (8-10,000 years ago; IUCN, 2017) as subfossil shells found in the Sahara (Brown et al., 1984). Outside the mainland of Africa, this species is possibly present in Yemen (Al-Safadi, 1990), Oman (Smythe and Gallagher, 1977; Brown and Wright, 1980; Brown and Gallagher, 1985) and Saudi Arabia (Neubert, 1998), but molecular research needs to confirm the taxonomic status of these subpopulations (IUCN, 2017). In Sudan, it is found in Darfur, White Nile, Gezira area and southern Bahr el Jebel. It was first found in the southern region of Sudan (Southern Sudan country) by Longstaff (1914) who obtained no more than 5 specimens; the sites now reported show *L. natalensis* to be widespread in the Sudd region (Brown et al., 1984).

*Habitat:* It is found in permanent standing and running waters of different sizes (IUCN, 2017) including lakes, rivers, khors, flooded areas and irrigation canals; a wide variety of macrophytes grew at these sites (Brown et al., 1984).

**4.2.1.1.B. Semi-aquatic snails**

***Pila wernei*** (Philippi, 1851)

*P. wernei* belongs to the wide family of Ampullariidae (IUCN, 2010; Köhler and Glaubrecht, 2006). It is also known under the name of *Ampullaria wernei* (IUCN, 2010; Pallary, 1902; Longstaff, 1914 *in* Brown et al., 1984; Philippi, 1851 *in* Köhler and Glaubrecht, 2006)

*Geographic range: Pila wernei* is generally known from scattered localities over a wide area in Africa, from Mali to Somalia, but it represents a native species in Cameroon, Central African Republic, Chad, Egypt, Ethiopia, Mali, Nigeria, Somalia, South Sudan and Sudan (IUCN, 2010). In Sudan it is found in the White Nile, Bahr el Ghazal (Southern Sudan), Darfur and Bahr el Jebel (Brown et al., 1984).

*Habitat: P. wernei* prefers highly shaded habitat (Ndifon and Ukoli, 1989) in various standing waterbodies, both permanent and seasonal freshwater systems (IUCN, 2010) like seasonal pools (Brown et al., 1984), lakes such as Lake Chad, and rivers, especially the White Nile (Gardner, 1932; Van Damme, 1984; Pachur and Kröpelin, 1987; Peters, 1991; Brown, 1994 *in* Fuller and Smith, 1998). However, it requires at least semi-permanent water (Fuller and Smith, 1998). In Jonglei (Southern Sudan), its habitat is characterized by the full presence of some plant like *Echinochloa*, *Ipomoea* and water lilies (Brown et al., 1984).

***Lanistes carinatus*** (Olivier, 1804)

*Geographic range:* The Nile and canals of Egypt; Sudan, southeast Ethiopia, Somalia, Kenya and Uganda. Its distribution in Sudan was formerly widespread, according to the occurrence of subfossil shells (Brown et al., 1984).

*Habitat:* Ditches and pools flooded by rain and the Nile, where *Echinochloa* and *Eichhornia* were present (Brown, et al 1984).

**4.2.1.1.C.** ***Land snails***

***Limicolaria flammea*** (Müller, 1774)

*Geographic range: Limicolaria flammea* has been known in western Africa for a long time, but it has been found recently in tropical Asia, in particular Singapore (Tan and Clements, 2011).

*Habitat:* Few information is gathered about the habitat of these species. It is very common during the wet season (Amusan et al., 2002; Idohou et al., 2013). However, *Limicolaria* species are known to occur in abundance in forest edges and modified habitats such as plantations and farms (Raut and Barker, 2002, *in* Tan and Low, 2011). It has been observed more active in long grass at forest edges (Tan and Clements, 2011).

***Limicolaria caillaudi*** (Pfeiffer, 1852)

*Geographic range:* Its present-day distribution extends from eastern Sudan to Ethiopia, and southward to Tanzaniya (Crowley and Pain, 1970, *in* Peters, 1991).

*Habitat:* The exact requirements of this species are not well known but it seems that *L. caillaudi* has a considerable tolerance with respect to mean annual precipitation (Peters, 1991). Williams and Adamson (1980) describe it as typical of the acacia tall grass plains, bounded by the 500-800 mm isohyets. According to Tothill (1948b), *L. fiammata* (= *L. caillaudi*, cf. Crowley and Pain, 1970) occurs in well-drained areas with tall grass, and in clay-pans, characterized by a mean annual precipitation between 400 and 800 mm (Peters, 1991).

***Zootecus insularis*** (Ehrenberg 1831)

*Geographic range:* The *Zootecus* genus in general is widely spread all over the world including Pakistan, India, Afghanistan, Africa and Arabian countries (Qamar et al., 2017). *Zootecus insularis* nowadays occurs in the semi-arid regions of India, Arabia, Eritrea, Egypt, Sudan, Senegal and the Cape Verde Islands. In Africa, the distribution in prehistoric times of this species includes, for the moment, Nubia (Martin 1968), the Western Desert (Gautier 1980), the Acacus Massif (Gautier and Van Neer 1982) and central Sudan (Peters, 1991).

*Habitat*: Living species of *Zootecus insularis* in Pakistan indicate that it occurs in the grass land habitat.

***Caracolus* sp.**

The genus *Caracolus* in general is a land snail (Bishop, 1979). Van der Schalie (1948) found *Caracolus* most commonly on trees of wet tropical forest at El Yunque, while along the dry, haystack knolls of the northern coast, it was usually buried or moving (in wet weather) among the decayed leaves and stones on the slopes. Also in Puerto Rico, Baker (1961) noted that the species is a very good climber on tree trunks, often seen 5-7 m above ground (Bishop, 1979).

### 4.2.1.2. Quantitative analysis of the stratigraphic distribution of gastropods

The analysis of the stratigraphic distribution of gastropod shells was carried out in the sections of En Nahud and East El Khowei. In both sections, the gastropod shells are concentrated in the sandy carbonate facies and the upper red sand facies (Second and Fourth units). Only the *in situ*, well-preserved gastropod shells were counted. 175 shells of four different species were counted in the En-Nahud section (Fig. 4.2), and 739 shells of eleven species were counted in the east El Khowei section (Fig. 4.3).

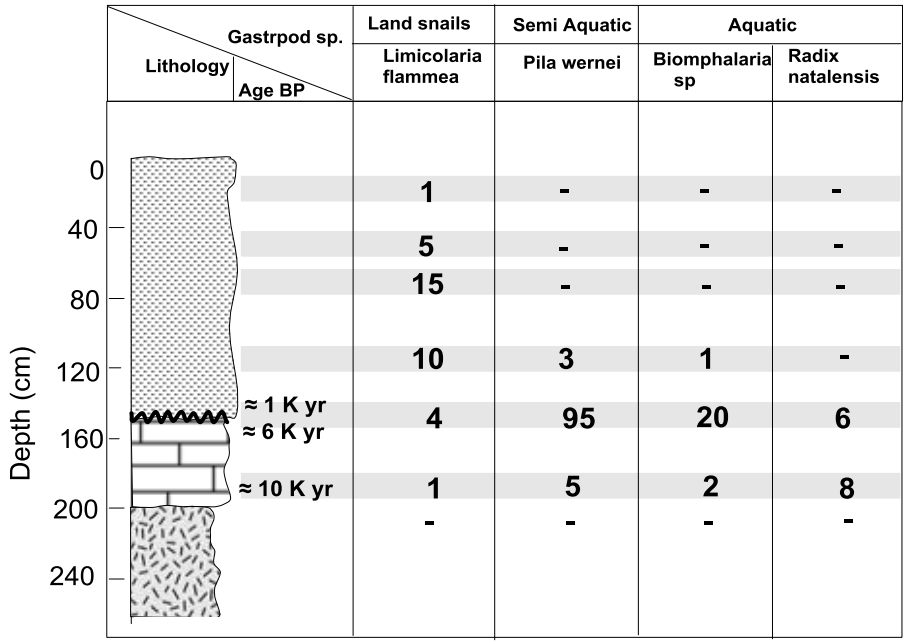


*Fig. 4.2: Quantitative analysis of the gastropod shells in the En Nahud section.*

In En Nahud, the fauna of the sandy limestone is dominated by the aquatic species *Radix natalensis* and the semi-aquatic species *Pila wernei*. The contact between the sandy limestone and the overlying red sand sediments is dominated by the semi-aquatic species *Pila wernei*, while the land snail species *Limicolaria flammea* dominates in the upper part of red sand sediments faciest.

In the east El Khowei section, the sandy carbonate is dominated by the aquatic species *Gabbiella sennariensis, Biomphalaria* sp., *Melanoides turberculata, Bulinus truncatus* and *Radix natalensis*; the contact between the sandy carbonate and the upper red sands are dominated by the aquatic species *Gabbiella sennariensis* and in a lesser extent, by the semi-aquatic species *Lanistes carinatus*, while the land snail species *Limicolaria flammea* dominates in the red sand facies.

### 4.2.1.3. Interpretation

As mentioned previously, the identified gastropod species belong to aquatic, semi-aquatic and terrestrial environments. Their stratigraphic distribution in the En Nahud and East El Khowei sections, have been plotted in term of cumulative percentages for each group (Figs. 4.4 and 4.5). These diagrams clearly indicate an absolute domination of the aquatic and semi-aquatic species in the sandy carbonate facies, reflecting humid climatic conditions between ≈ 10 and ≈ 6 ky BP.

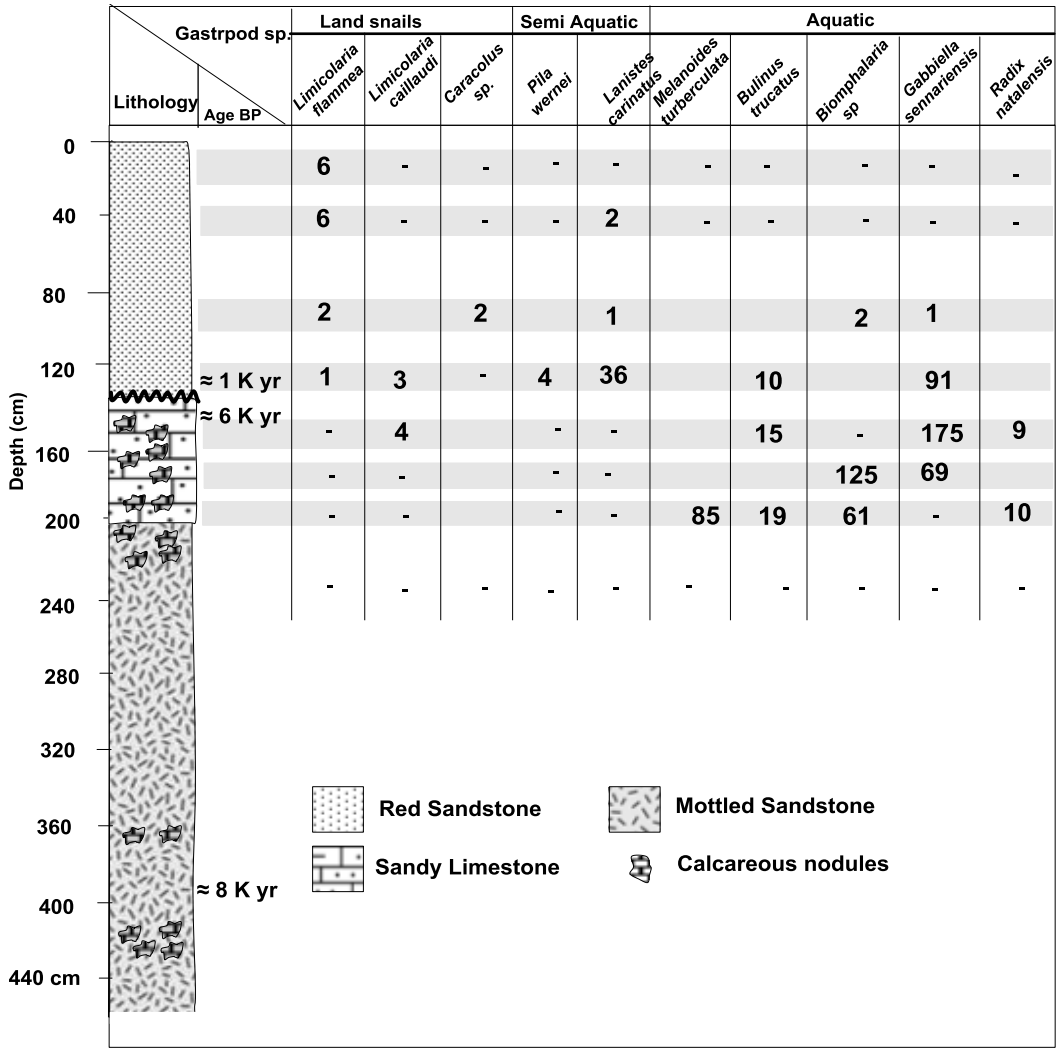


*Fig. 4.3: Quantitative analysis of the gastropod shells in the East El Khowei section*

The lower part of the red sand facies is mostly dominated by the land snails, and "locally" by semi-aquatic and aquatic groups. This distribution in the lower part of the red sand unit indicates wet to dry conditions environment (*i.e.* the area had experienced sub-humid to semi-arid climate) between ≈ 1000 and ≈ 700 yr BP. However, aeolian erosion took place between ≈ 6 and 1 ky BP, or at least ≈ 3 and 1 ky BP, and the local abundance of the semi-aquatic and aquatic groups at the base of the red sand may indicate that, either these shells were reworked from the lower palustrine limestone, or the early 300 years from this 1000 years period were wetter than the rest of the time-span, or climate was seasonally wet.

In both sections, the upper part of the red sand unit is totally dominated by land snail species, which indicates that the area experienced arid climatic conditions during the last ≈ 1000 yr.

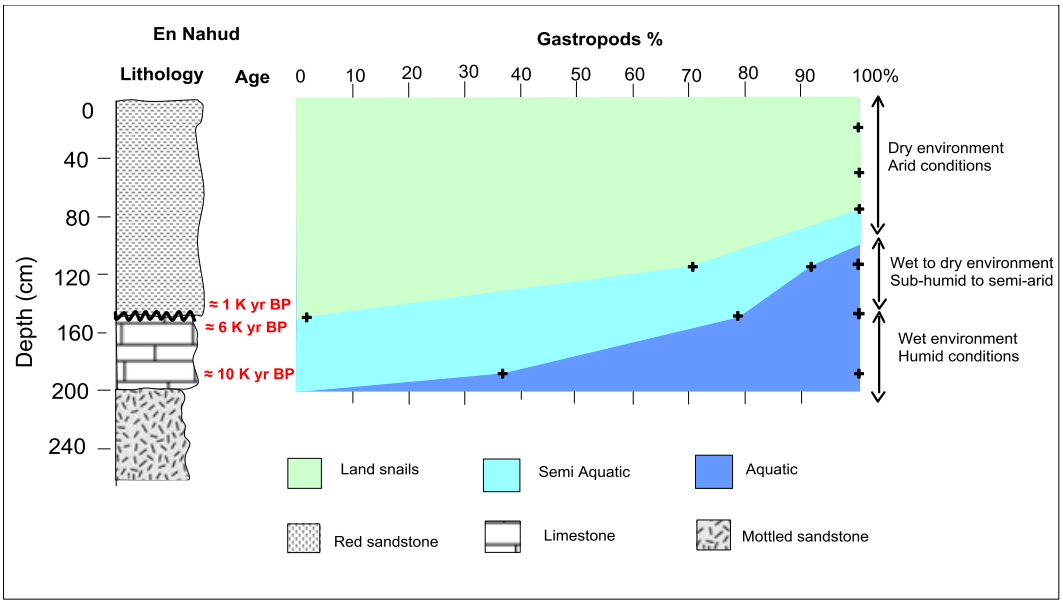


*Fig. 4.4: Evolution of the gastropod assemblages in the En Nahud section.*

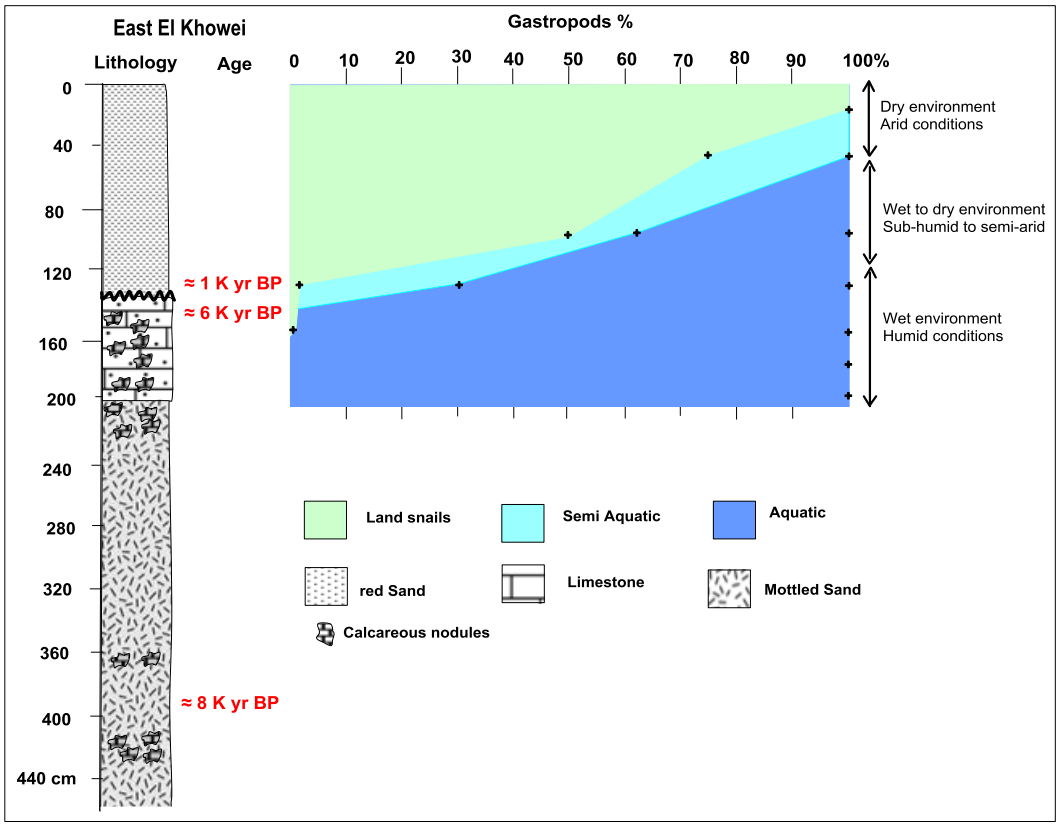


*Fig. 4.5: Evolution of the gastropod assemblages in the East El Khowei section.*

This vertical evolution, changing from typical aquatic to terrestrial land snail species, occurred as a normal adaptation of the gastropod communities to the gradual climatic change from mostly humid to mostly arid conditions, of course passing through sub-humid and semi-arid conditions. On the other hand, the presence of the aquatic species *Gabbiella senaariensis*, *Bulinus truncatus*, *Melanoides tuberculata* and the semi-aquatic species *Lanistes carinatus* around El-Khowei and their absence around En-Nahud, reflect paleoenvironmental differentiation

between the two sites. This suggests that the El-Khowei area was more vegetated between ≈ 10 and 6 ky BP than the En-Nahud area, the former being characterized by swampy environments, while the latter was marked by isolated ponds or pools, in spite of being submitted to the same climate.

### 4.2.2. Palynology

Twenty-nine samples from six sites were analyzed for palynological studies. The investigated sites are: North Dilling, South El Obeid 3 (Khour Es Sonjokaya), South El Obeid 1 (Khour Es Sikairan), East El Obeid (Khour Taggat), West El Obeid (Ayara), En Nahud, and El Ga'ah (Fig. 4.6). The last three sites were barren of pollens, and have been excluded from the results.

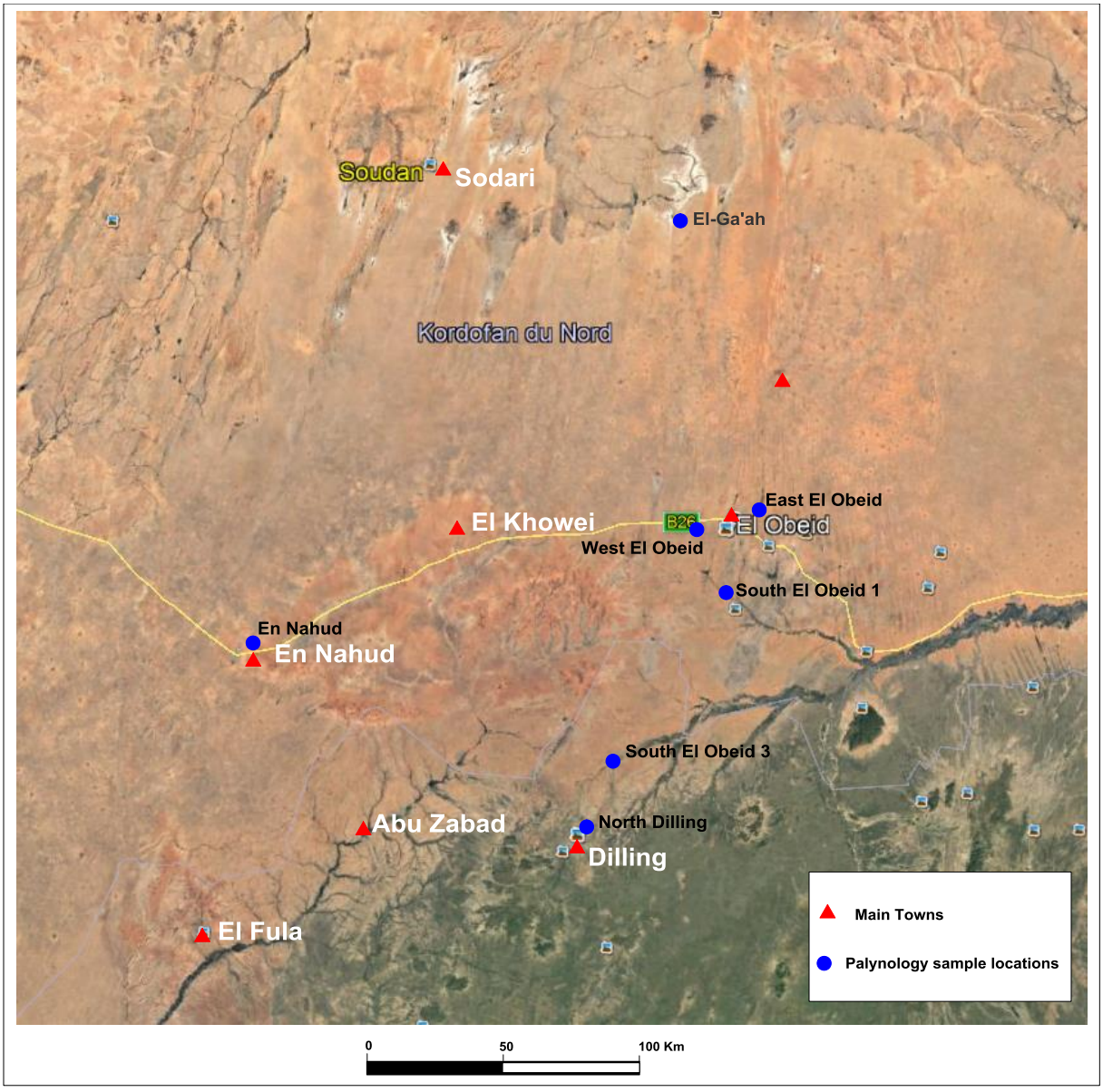


*Fig. 4.6: Location map of the sites investigated for palynology.*

The twenty-two analyzed samples from the first three sites yielded a total of 1408 pollen and spores. The South El Obeid 3 site yielded 831 palynomorphs, 399 were counted in samples from North Dilling, and only 178 palynomorphs were counted in samples from South El Obeid 1.

All palynomorphs have been identified, they produced 90 different types table 4.2. 1213 palynomorphs out of the total counted specimens have been classified into four main groups in order to help in the paleoclimate interpretation. The identified groups are : aquatic, tropical, savanna, and arid indicators. This classification is based on the understanding of the related habitat and ecological information, which have been gathered from various studies.

The **aquatic group** includes freshwater algae and other aquatic flora. This group includes *Chomotriletes* (Latrubesse et al., 2010; Akyuz et al., 2016), *Ovoidites* (Scafati et al., 2009; Worobiec and Gedl, 2010), *Schizosporis* (Scafati et al., 2009; Latrubesse et al., 2010; Akyuz et al., 2016), *Lecaniella forma* (Worobiec, 2014), *Spirogyra (zygospore)* (Chambers et al., 2014), *Chlorosarcina superba* (Lukavský, 2009), *Sigmopollis laevigatoides* (Worobiec and Gedl, 2010), *Alternanthera nodiflora* (El Ghazali, 1993), *Alternanthera sessilis* (El-Amier, 2015), *Lemna gibba* (El-Amier, 2015; Perveen, 1999), *Inaperturopolenites*, *Potamogeton pectinatus* (El-Amier, 2015), *Limnophyton obtusifolium* (El Ghazali, 1993) and *Echinochloa crusgalli* (El-Amier, 2015). Plates 4.2 and 4.3 show some representative pollens of this group.

The **tropical climate indicators** group includes *Proxapertites* (Monga et al., 2015), *Retipollenites, Longapertites, Laevigatosporites* (Paul et al., 2015), *Araucariaceae* (Lu et al., 2012; Stukins et al., 2013), *Aneilema johnstonii* (Gosling et al., 2013), *Tiliacora funifera* (Gosling et al., 2013), *Palmidites plicatus* (Monga et al., 2015), *Lygodiumsporites* (Monga et al., 2015), *Borassus aethiopum* (Gosling et al., 2013) and *Plantago major* (Clapham et al., 1989). Plate 4.4 shows some of the representative pollens of this group.

The **savanna group** indicators include *Baissea multiflora*, *Graminidites* (Worobiec and Gedl, 2010), *Silene burchellii* (El Ghazali, 1993), *Cymbopogon schoenanthus* (El Ghazali, 1993) and *Monolites alveolatus.* Plate 4.5 shows some representative specimens of this group.

The **arid indicator group** includes *Hyphaene thebaica* (El Ghazali, 1993), *Hyparrhenia hirta* (El Ghazali, 1993), *Classopollis* spp. (Volkheimer et al., 2008; Riding et al., 2013; Stukins et al., 2013), *Evolvulus alsinoides* (El Ghazali, 1993), *Desmodium dichotonum* (El Ghazali, 1993), *Bracharia ramosa* (El Ghazali, 1993), *Gynandropsis gynandra* (El Ghazali, 1993), *Farsetia stenoptera* (El Ghazali, 1993), *Farsetia hamihonni* (El Ghazali, 1993). *Gelasinospora* cf. (Chambers et al., 2014), *Leoisphaeridia* sp. (Onoduku and Okosun, 2014), *Leiotriletes adriennis* (Uzodimma, 2013), and *Erica arbora* (Lézine et al., 2011). Plate 4.6 illsutrates some representative pollens of this group.

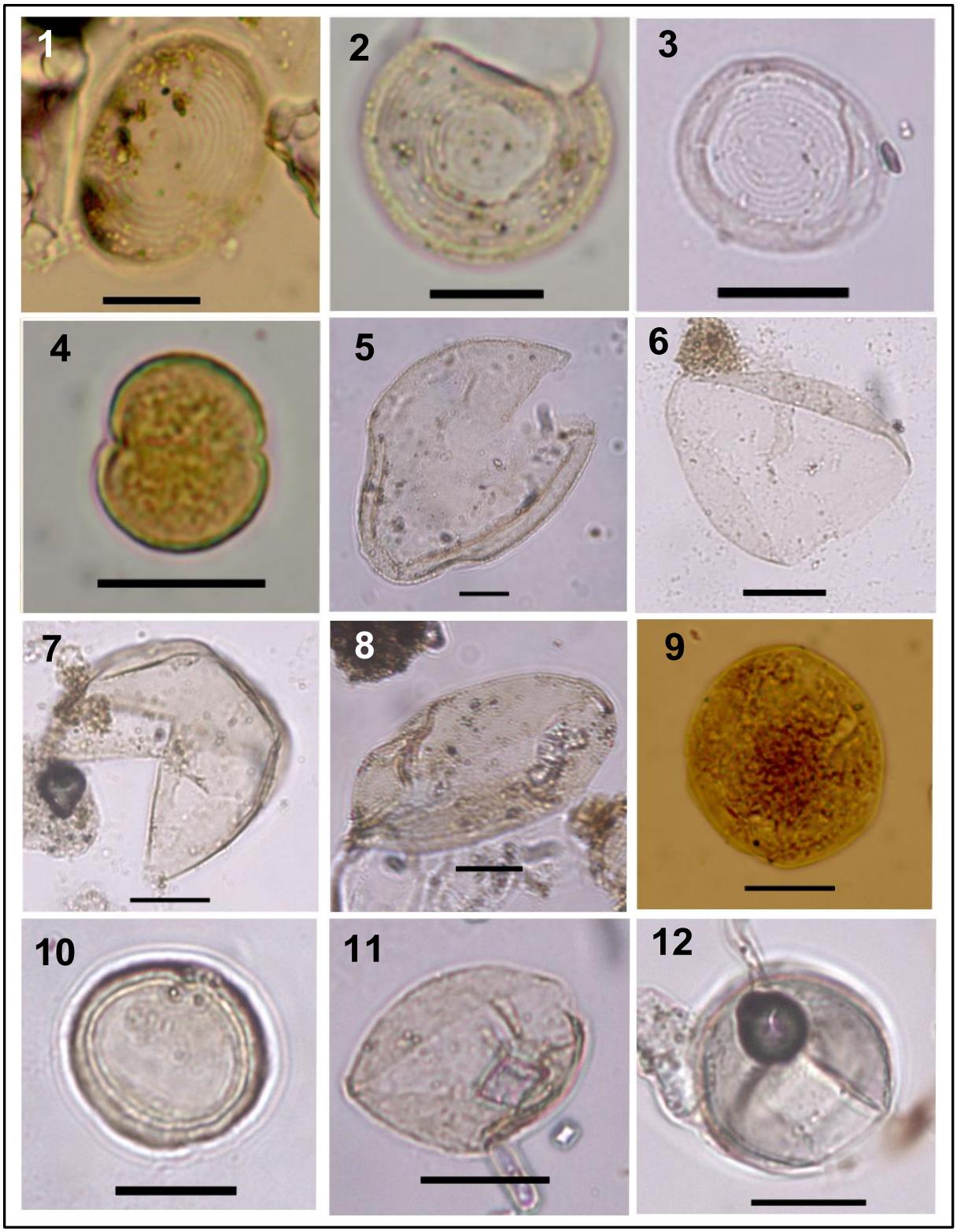


*Plate 4.2: Representative pollens of freshwater algae,* ***Aquatic Group indicator****. Scale bar = 20 µm.*

***1:*** *Chomotriletes rubinus,* ***2:*** *Chomotriletes circulus,* ***3:*** *Chomotriletes minor,* ***4:*** *Chlorosarcina superba,* ***5, 6*** *and* ***7:*** *Ovoidites* sp., ***8:*** *Ovoidites vangeelii,* ***9:*** *Schizosporis reticulatus,* ***10:*** *Lecaniella forma,* ***11:*** *Spirogyra (zygospore)****, 12:*** *Sigmopollis laevigatoides.*

*Table 4.2: Counting of the identified palynomorphs.*

| | North Dilling | | | | | | | | South El-Obeid | | | | | Sonjokaya (El-Obeid Dilling road) | | | | | | | | |
|---|---|---|---|---|---|---|---|---|---|---|---|---|---|---|---|---|---|---|---|---|---|---|
| | **D 11** | **D 9** | **D 8** | **D 7** | **D 5** | **D 3** | **D 2** | **D 1** | **Kh 1** | **Kh 2** | **Kh 4** | **Kh 5** | **Kh 6** | **Sonj 14** | **Sonj 12** | **Sonj 10** | **Sonj 8** | **Sonj 6** | **Sonj 5** | **Sonj 4** | **Sonj 2** | **Sonj 1** |
| ***Aquatic*** | | | | | | | | | | | | | | | | | | | | | | |
| *Chomotriletes minor* | 4 | 6 | | 1 | | | 2 | | 4 | 8 | 2 | 3 | 1 | 15 | 2 | | | | 4 | 4 | | 1 |
| *Chomotriletes circulus* | 7 | 10 | 1 | 2 | 1 | | 2 | 1 | 7 | 7 | 1 | 4 | | 19 | 4 | | 1 | | 7 | 5 | | |
| *Chomotriletes rubinus* | 3 | 4 | 1 | | 1 | | | | 5 | 3 | 1 | 2 | | 10 | 1 | | | | 2 | 3 | | |
| *Ovoidites* sp. | 5 | | 4 | 3 | | | | | 3 | 2 | 4 | 2 | | 12 | 5 | 2 | 2 | | 7 | | | 6 |
| *Ovoidites vangeelii* | | | | | | | | | | | | | | | | | | 1 | | | | |
| *Schizosporis reticulatus* | | | | | | | | | | | | | | 9 | 1 | 1 | 2 | 3 | | | | |
| *Lecaniella forma* | | | | | | | | | | | | | | 40 | 9 | 6 | 4 | | 4 | | 5 | 3 |
| *Spirogyra (zygospore)* | | | 2 | | | | | | 3 | | | | | | | | | | 10 | | 5 | 1 |
| *Sigmopollis laevigatoides* | | 5 | 1 | 5 | 3 | 1 | | | | | | | | | | | | | | | | |
| *Chlorosarcina superba* | | | | | | | | | 2 | | | | | | | | | | | | | |
| *Alternanthera nodiflora* | | | | | | | | | 3 | 2 | 1 | 1 | | | | | | | 2 | | | |
| *Alternanthera sessilis* | | | | | | | | | 3 | | | | | | | | | | 2 | | | |
| *Lemna gibba* | | | | | | | | | | 3 | | | | | | | | | | | | |
| *Inaperturopolenites* sp. | | | | | 5 | | 12 | | | | | | | | | | | | | | | |
| *Inaperturopolenites dubius* | | | | | | | | | 7 | | | | | | | | | | | 31 | | |
| *Potamogeton pectinatus* | | | | | | | | | | | | | | 4 | | 1 | | | 1 | | | |
| *Inaperturopollenites hiatus* | | 5 | | | | | | | | | | | | 3 | | | 1 | | | | | |
| *Limnophyton obtusifolium* | | | | | | | 6 | | | | | | | | | | | | | | | |
| *Echinochloa crus-galli* | | | | | | | | | | | | | | 7 | | | | | | | | |
| **Tropical climate indicators** | | | | | | | | | | | | | | | | | | | | | | |
| *Proxapertites assamicus* | | 5 | | | | | | | | | | | | | | | | | | | | |
| *Proxapertites cursus* | | 3 | | | | | | | | 1 | | | | | | | | | | | | |
| *Proxapertites operculatus* | | 4 | | 3 | | | | 1 | | 2 | | | | | | | | | | | | |
| *Retipollenites enigmata* | | | | | | | | | | | | 1 | | | | | | | | | | |
| *Longapertites marginatus* | | | | | | | | | 1 | | | | | | | | | | | | | |
| *Laevigatosporites haardtii* | | | | | | | | | 3 | | | | | | | | | | | | | |

*Continue (Table 4.2):*

| | North Dilling | | | | | | | | South El-Obeid | | | | | Sonjokaya (El-Obeid Dilling road) | | | | | | | | |
|---|---|---|---|---|---|---|---|---|---|---|---|---|---|---|---|---|---|---|---|---|---|---|
| | **D 11** | **D 9** | **D 8** | **D 7** | **D 5** | **D 3** | **D 2** | **D 1** | **Kh 1** | **Kh 2** | **Kh 4** | **Kh 5** | **Kh 6** | **Sonj 14** | **Sonj 12** | **Sonj 10** | **Sonj 8** | **Sonj 6** | **Sonj 5** | **Sonj 4** | **Sonj 2** | **Sonj 1** |
| *Laevigatosporites ovatus* | | | | | | | | | 1 | | | | | | | | | | | | | |
| *Araucariacites* sp. | | 2 | 2 | 20 | 2 | | 2 | | 5 | 2 | | | | | 3 | | | 2 | | 22 | | |
| *Araucariacites australis* | | | | | | | | | | | | | | | | | | | | | 11 | |
| *Aneilema johnstonii* | | | | | | | | | | | | | | 8 | 2 | 16 | | | | | | |
| *Tiliacora funifera* | | | | | | | | | | | | | | | | | | | | | 14 | 3 |
| *Borassus aethiopum* | | 6 | | | | | | | | | | | | | | | | | | | | |
| *Palmidites plicatus* | | | | | 6 | | | | | | | | | | | | | | | | | |
| *Lygodiumsporites* | | | | | | | | | | | | | | | | | | | | 4 | 11 | 1 |
| *Plantago major* | 6 | | | 5 | 4 | | | | | | | | | 5 | 3 | | | | | | | |
| ***Savanna group*** | | | | | | | | | | | | | | | | | | | | | | |
| *Baissea multiflora* | 6 | 7 | | | | | | | | | | | | 19 | 6 | 13 | 1 | 6 | | 10 | | |
| *Graminidites boivinii* | | | | | | | | | | 1 | | | | | | | | | | | | |
| *Graminidites* sp. | | | | | | | | | | | | | | | | | | | | | | 7 |
| *Silene burchellii* | | | | | | | 16 | | | | | | | 16 | 5 | 3 | 5 | 3 | | | 8 | 3 |
| *Cymbopogon schoenanthus* | | | | | 9 | | | | | | | 19 | 3 | | | | | | | | | |
| *Monolites alveolatus* | | | | | | | | | 1 | | | 1 | | 2 | 1 | | | | | 6 | 12 | 4 |
| ***Arid group*** | | | | | | | | | | | | | | | | | | | | | | |
| *Hyphaene thebaica* | | | | | | | | 3 | | | | 2 | | | | | | | | | 7 | 3 |
| *Hyparrhenia hirta* | | | | 4 | 9 | 2 | 7 | | | | | 14 | 1 | | | | | | | | 28 | 8 |
| *Classopollis* sp. | | | | | | 2 | 6 | | | | 1 | | | | | | | | 26 | 3 | | |
| *Classopollis meyerianus* | | | | | | | | | | | | | | | | | | | 13 | | | |
| *Evolvulus alsinoides* | | | | | | | | 17 | | | | | | | | | | | | | | |
| *Desmodium dichotonum* | | | | | | | | 10 | | | | | | | | | | | | | | |
| *Bracharia ramosa* | | | | | | | | 5 | | | | | | | | | | | | | 15 | 13 |
| *Gynandropsis gynandra* | | | | | | | 8 | 22 | | | | | | | | | | | | 1 | | |
| *Farsetia stenoptera* | | | | | | | | | | | | | | | | | | | | | 7 | 35 |

*Continue (Table 4.2):*

| | North Dilling | | | | | | | | South El-Obeid | | | | | Sonjokaya (El-Obeid Dilling road) | | | | | | | | |
|---|---|---|---|---|---|---|---|---|---|---|---|---|---|---|---|---|---|---|---|---|---|---|
| | **D 11** | **D 9** | **D 8** | **D 7** | **D 5** | **D 3** | **D 2** | **D 1** | **Kh 1** | **Kh 2** | **Kh 4** | **Kh 5** | **Kh 6** | **Sonj 14** | **Sonj 12** | **Sonj 10** | **Sonj 8** | **Sonj 6** | **Sonj 5** | **Sonj 4** | **Sonj 2** | **Sonj 1** |
| *Farsetia hamihonni* | | | | | | | 5 | | | | | | | | | | | | | | 5 | 37 |
| *Gelasinospora* cf. | | | | | | | 2 | 3 | | | | 11 | | | | | | | | | | |
| *Leoisphaeridia sp.* | | | | | | | | | | | | | | | | | | | | | 9 | |
| *Leiotriletes adriennis* | | | | | | | | | | | | | | | | | | | 9 | | | |
| *Erica arbora* | | | | | | | | | 1 | 2 | | | | | | | | | | 2 | | |
| ***Not classified*** | | | | | | | | | | | | | | | | | | | | | | |
| *Cola hispida* | | | | 3 | | | | | | | | | 2 | | | | | | | | | |
| *Lasiosphon kraussianus* | | | | | 6 | | | | | | | | | | | | | | | | | |
| *Pycnanthus dinklagei* | | | | | | | 4 | | | | | | | | | | | | | | | |
| *Pinuspollenites* | | | | | | | 4 | 1 | | | | | | | | | | | | | | |
| *Polygalaceae* cf | | | | | | | 6 | | | | | | | | | | | | | | | |
| *Maerua oblongifolia* | | | | | | | | 3 | | | | | | | | | | | | | | |
| *Polygala abyssinica* | | | | | | | | | | | | | | | | | | | 1 | | | |
| *Leoisphaeridia sp.* | | | | | | | | | | | | | | | | | | | | | 9 | |
| *Kapurdipollenites gemmatus* | | | | | | | | | | | | | | | | | | | 2 | | | |
| *Limnobiophyllum* sp. | | | | | | | | | | | | | | | | | | | | | 3 | 12 |
| *Pycnanthus dinklagei* | | | | | | | | | | | | | | | | | | | 2 | | | |
| *Piptostigma mayumbense* | | | | | | | | | | | | | | | | | | | | 5 | | |
| *Rhynchelytrum repens* | | | | | | | | | | | | | | | | | | | | 11 | | |
| *Iodes ovalis* | | 3 | | | | | 2 | | | | | | | | | | | | | | | |
| *Aeschynomene indica* | | | | 7 | | | | | | | | | | | | | | | | 1 | | |
| *Dandotiaspora plicata* | | | 3 | | | | | | | | | | | | | | | | | | | |
| *Baculatisporites* sp. | | | | | | | | | | | 1 | | | | | | | | | | | |
| *Nevesisporites vallatus* | | | | | | | | 4 | | | | | | | | | | | | 2 | 7 | 2 |
| *Chlorosarcina superba* | | | | | | | | 1 | | | | | | | | | | | | | | |
| *Hibiscus* sp. | | | | | | | | | | 2 | | | | | | | | | | | | |

*Continue (Table 4.2):*

| | North Dilling | | | | | | | | South El-Obeid | | | | | Sonjokaya (El-Obeid Dilling road) | | | | | | | | |
|---|---|---|---|---|---|---|---|---|---|---|---|---|---|---|---|---|---|---|---|---|---|---|
| | **D 11** | **D 9** | **D 8** | **D 7** | **D 5** | **D 3** | **D 2** | **D 1** | **Kh 1** | **Kh 2** | **Kh 4** | **Kh 5** | **Kh 6** | **Sonj 14** | **Sonj 12** | **Sonj 10** | **Sonj 8** | **Sonj 6** | **Sonj 5** | **Sonj 4** | **Sonj 2** | **Sonj 1** |
| *Mimosa oudica* | | | | | | | | | | 1 | | | | | | | | | | | | |
| *Xylia avansii* | | | | | | | | | | 3 | | | | | | | | | | | | |
| *Spinomonosulcites achinatus* | | | | | | | | | | | | 3 | | | | | | | | | | |
| *Cephalomappa* | | | | | | | | | | | | 1 | | | | | | | | | | |
| *Acacia* sp. | | | | | | | | | | | | | 3 | | | | | | | | | |
| *Cicatricosisporites dorogensis* | | | | | | | | | | | | | | 5 | | | | | | | | |
| *Abutilon ramosum* | | | | | | | | 3 | | | | | | | | | | | | | | |
| *Pinuspollenites* | | | | | | | | | | | | 1 | | | | | | | | | 5 | |
| *Mauritidites crassibaculatus* | | | | | | | | | | | | | | 3 | | | | | | | | |
| *Commelina africana* | | | | | | | | | | | | | | 5 | 1 | | | | | | | |
| *Chlorophytum floribundum* | | | | | | | | | | | | | | | | | | 1 | | | | |
| *Typha domingensis* | | | | | | | | | | | | | | | | | | 1 | | | | |
| *Suaeda sp* | | 4 | 2 | | | | | | | | | | | | | | | | | | | |
| *Borreria densiflora* | 3 | | | | | | | | | | | | | | | | | | | | | |
| *Chenopodiaceae* | 3 | 5 | 2 | | | | | | | | | | | | | | | | | | | |
| | | | | | | | | | | | | | | | | | | | | | | |

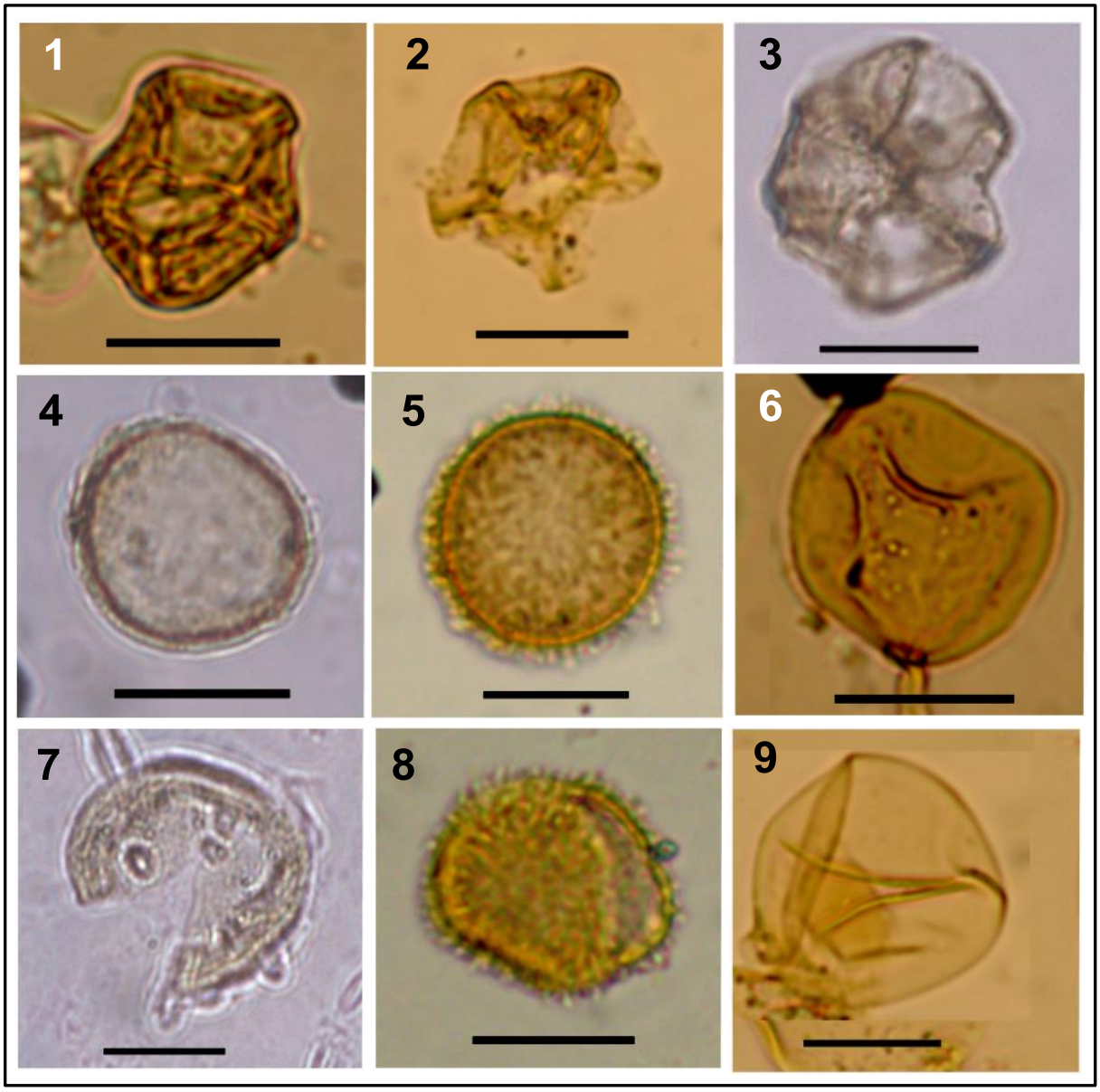


*Plate 4.3: Representative pollens of the aquatic flora -* ***Aquatic Group indicator.*** *Scale bar = 20 µm.*

***1&2:*** *Alternanthera nodiflora* ***3:*** *Alternanthera sessilis* ***4:*** *Potamogeton pectinatus* ***5:*** *Lemna gibba* ***6:*** *Inaperturopolenites dubius* ***7:*** *Inaperturopollenites hiatus* ***8:*** *Limnophyton obtusifolium* ***9:*** *Echinochloa crus-galli.*

#### 4.2.2.1. North Dilling site

Eight samples were analyzed from this site, with a total thickness of 380 cm. Among the aquatic flora, the *Chomotriletes* freshwater algae are the most abundant, with secondary abundance of *Sigmopollis laevigatoides* and *Inaperturopolenites*. The *Araucariaceae* sp. recorded the highest occurrence among the tropical group, followed by *Proxapertites*. The savanna group is dominated by *Silene burchellii, Graminidites bombusoidis* and *Baissea multiflora.* The arid

group is dominated by *Gynandropsis gynandra*, *Hyparrhenia hirta* and *Evolvulus alsinoides*, with secondary abundance of *Desmodium dichotonum* and *Classopollis* spp. (table 4.2).

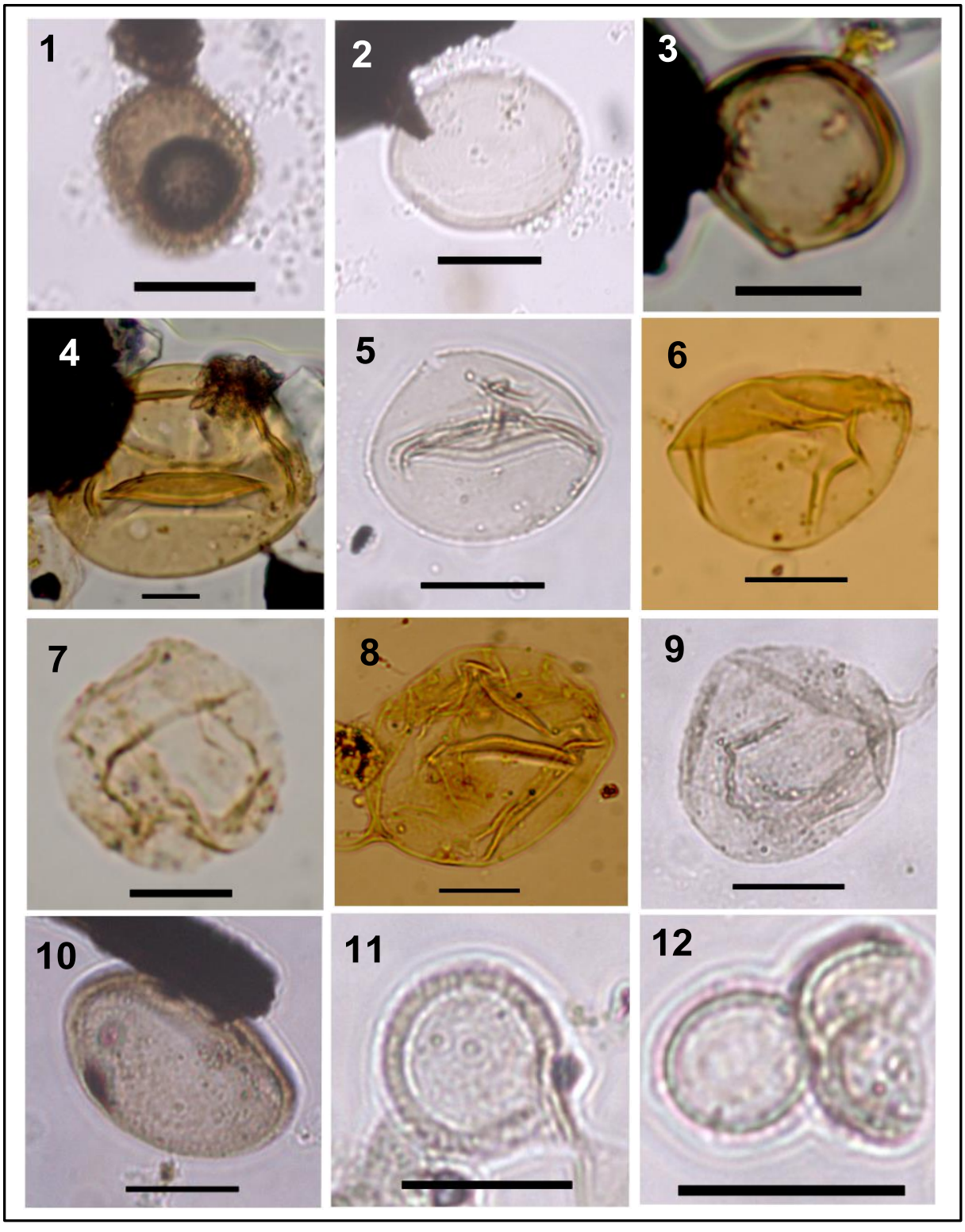


*Plate 4.4: Representative pollens of the* ***Tropical Group indicator.*** *Scale bar = 20 µm.*

***1:*** *Proxapertites cursus,* ***2:*** *Proxapertites operculatus,* ***3:*** *Laevigatosporites haardtii,* ***4:*** *Laevigatosporites ovatus,* ***5:*** *Lygodiumsporites,* ***6:*** *Longapertites marginatus,* ***7:*** *Araucariacites australis,* ***8*** *and* ***9:*** *Araucariacites* sp.*,* ***10:*** *Aneilema johnstonii,* ***11:*** *Plantago major,* ***12:*** *Tiliacora funifera.*

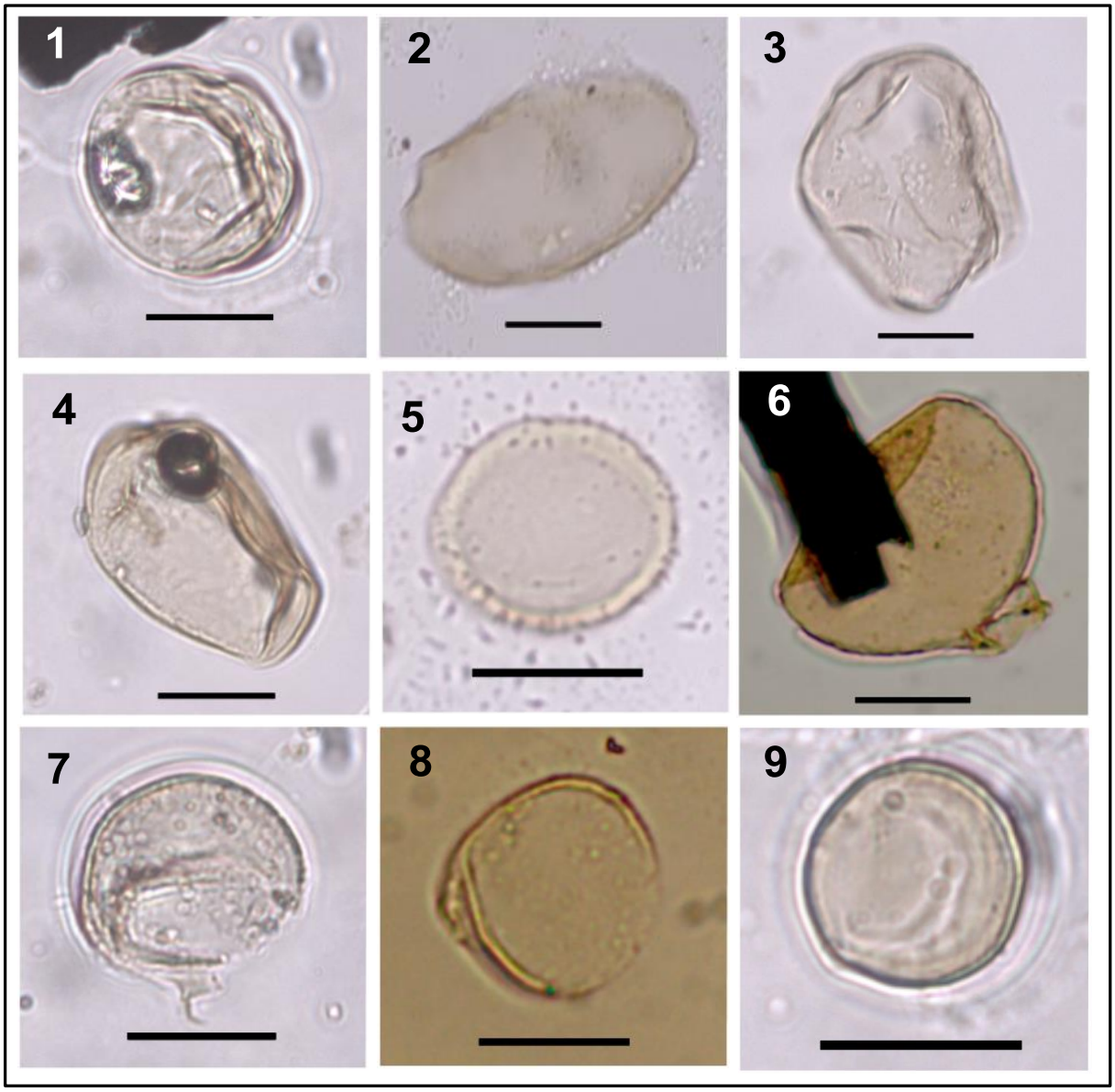


*Plate 4.5: representative pollens of the* ***Savana Group indicator.*** *Scale bar = 20 µm.*

***1:*** *Graminidites annulatus,* ***2:*** *Graminidites boivinii,* ***3*** *and* ***4:*** *Graminidites bambusoides,* ***5:*** *Cymbopogon schoenanthus,* ***6:*** *Monolites alveolatus,* ***7*** *and* ***8:*** *Silene burchellii,* ***9:*** *Baissea multiflora.*

The vertical distribution chart of these groups (Fig. 4.7) shows that the lower part of the section is dominated by the aquatic group with percentages up to 65%, followed by the tropical indicators (20%), and the savanna group (15%), species form the arid group being absent. The upper part of the section is dominated by the arid indicator group with an average percentage of about 75 % that increases upward, the aquatic group representing about 20%, whereas the tropical and savanna groups are very rare. The middle part contains balanced percentages of these groups, although one sample presents a high percentage of pollens of the savanna group.

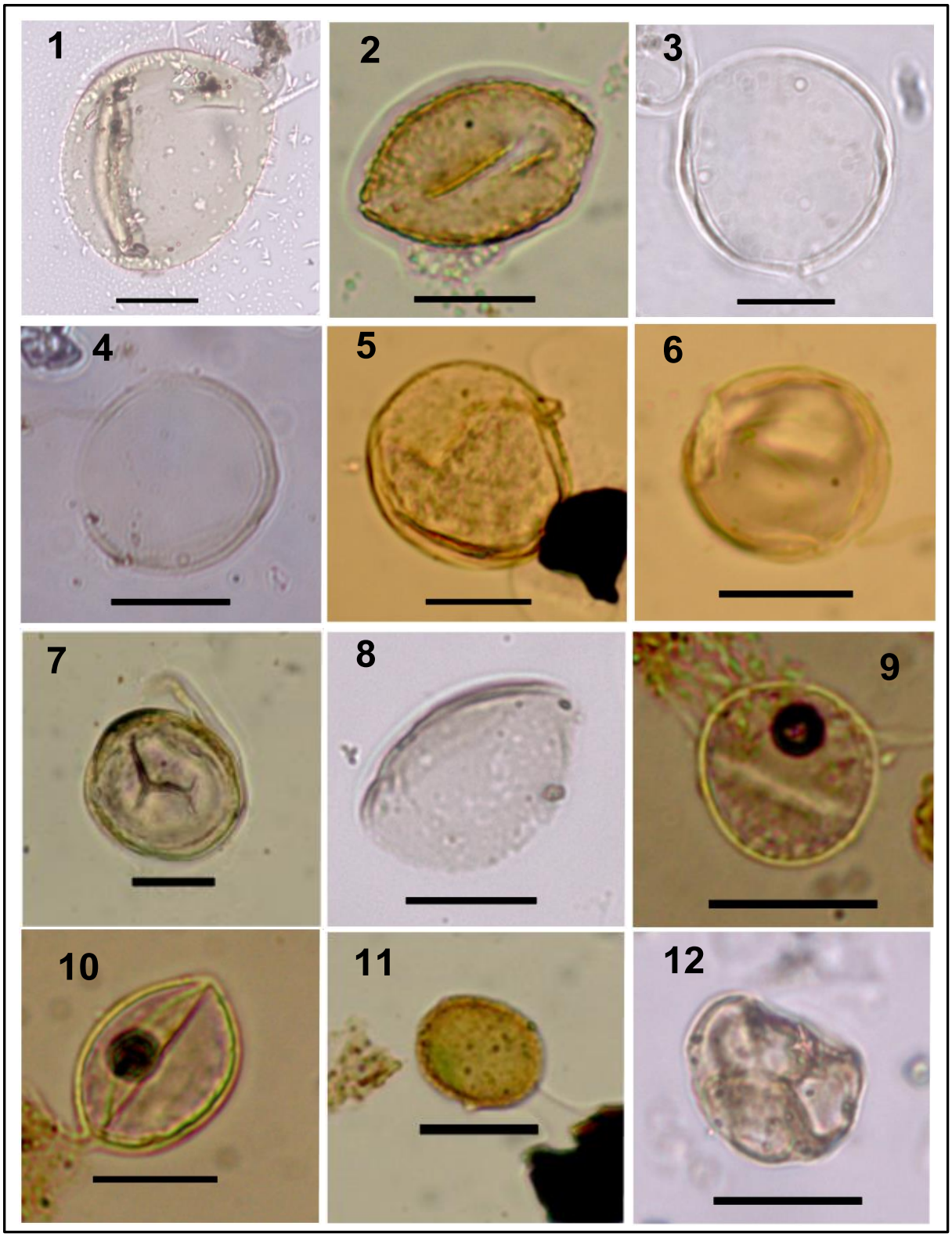


*Plate 4.6: representative pollens for the* ***Arid Group indicator.*** *Scale bar = 20 µm.*

***1:*** *Hyparrhenia hirta,* ***2:*** *Hyphaene thebaica,* ***3:*** *Bracharia ramose,* ***4:*** *Gynandropsis gynandra,* ***5:*** *Classopollis meyerianus,* ***6:*** *Classopollis* sp., ***7:*** *Evolvulus alsinoides,* ***8:*** *Desmodium dichotonum,* ***9:*** *Farsetia hamihonni,* ***10:*** *Farsetia hamihonni,* ***11:*** *Gelasinospora* cf., ***12:*** *Erica arbora.*

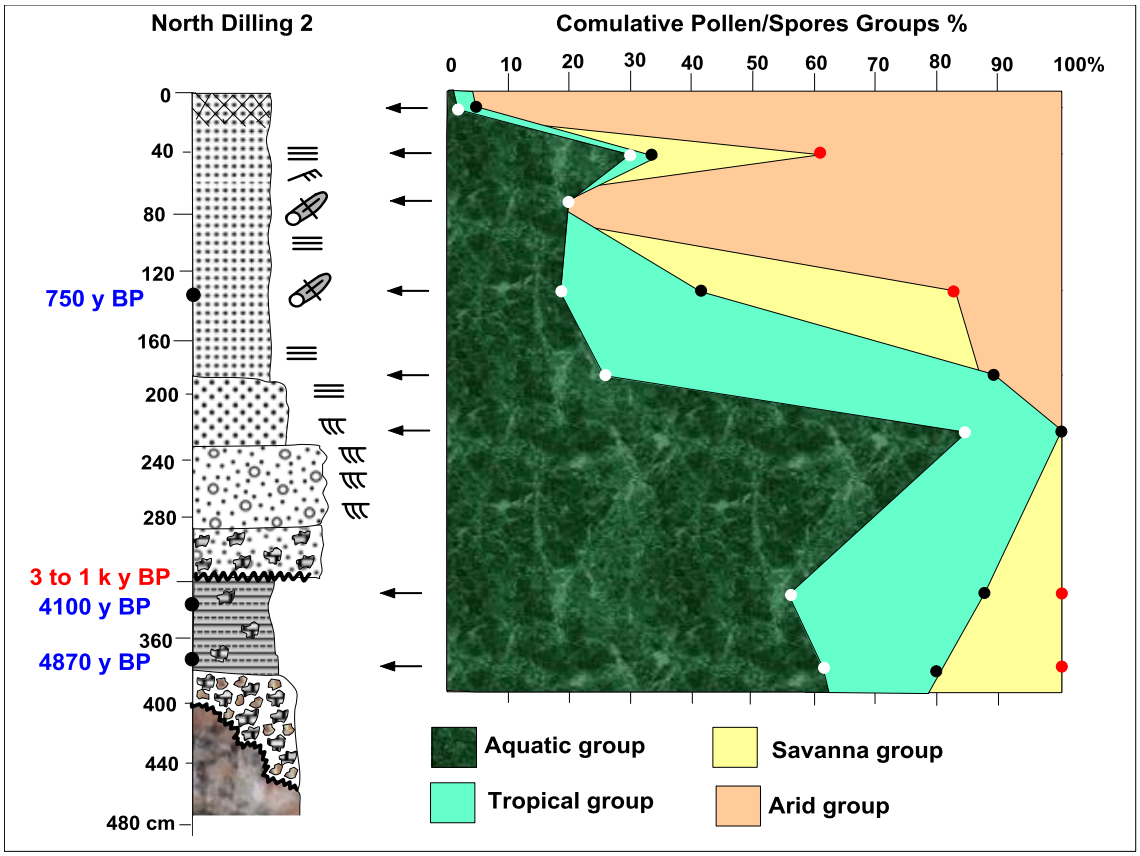


*Fig. 4.7: Proportions of the pollen groups in the North Dilling section.*

### 4.2.2.2. South El Obeid 3 site

Nine samples were analyzed samples from this site along a 440 cm thick section. The freshwater algae *Chomotriletes* and *Lecaniella forma* dominate the aquatic flora, with secondary abundance of the freshwater algae *Schizosporis*. The tropical group is dominated by *Araucariaceae* sp., *Aneilema johnstonii* and *Tiliacora funifera*. The savanna group is dominated by *Baissea multiflora, Silene burchelli* and *Graminidites*, while *Farsetia stenoptera, Farsetia hamihonni, Classopollis* spp., *Hyparrhenia hirta* and *Bracharia ramosa* dominate the arid group (table 4.2).

In the lower part of the section (Fig. 4.8), the aquatic and savanna groups are dominant with percentages up to 47 % each, the tropical indicator group is very rare (≈ 6%) and species of the arid group are recorded. The upper part of the section is dominated by arid indicators with an average percentage of about 70 % (increasing upward), while the tropical group records ≈ 17 % and the aquatic group ≈ 11 % in average; specimens of the savanna group are very rare in this part of the section (≈ 2 %). The middle part is more balanced, with ≈ 45 % of aquatic, ≈ 15 % of tropical, ≈ 20 % of savanna and ≈ 20 % of arid indicator group.

### 4.2.2.3. South El Obeid 1 site

We analyzed five samples from this 380 cm thick section. The freshwater algae *Chomotriletes* and *Ovoidites* dominate the aquatic flora. The tropical group is generally rare and its most abundant representant is *Araucariaceae* sp. (7 pollens). The savanna group is also rare, except

*Cymbopogon schoenanthus* with 22 counted pollens, while 9 pollens are classified in four different savanna species. The arid group is dominated by *Hyparrhenia hirta* and *Gelasinospora* cf. (table 4.2).

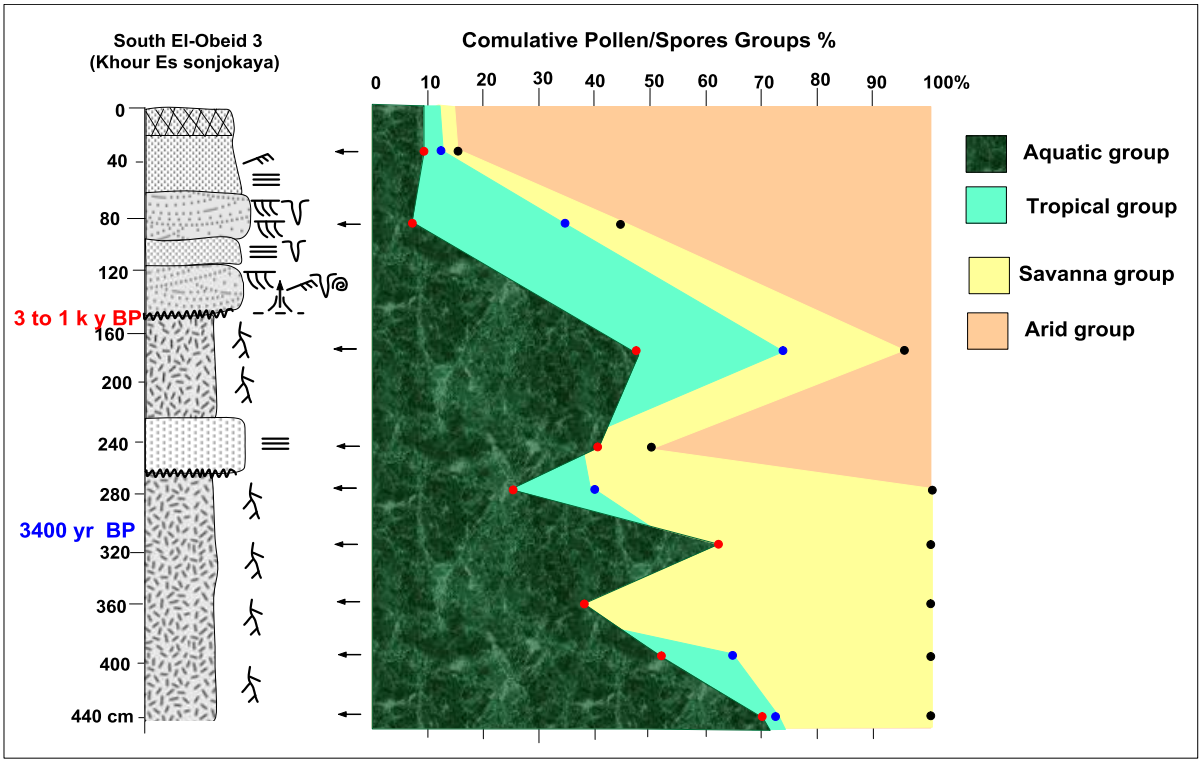


*Fig. 4.8: Proportion of pollen groups in the South El Obeid 3 section.*

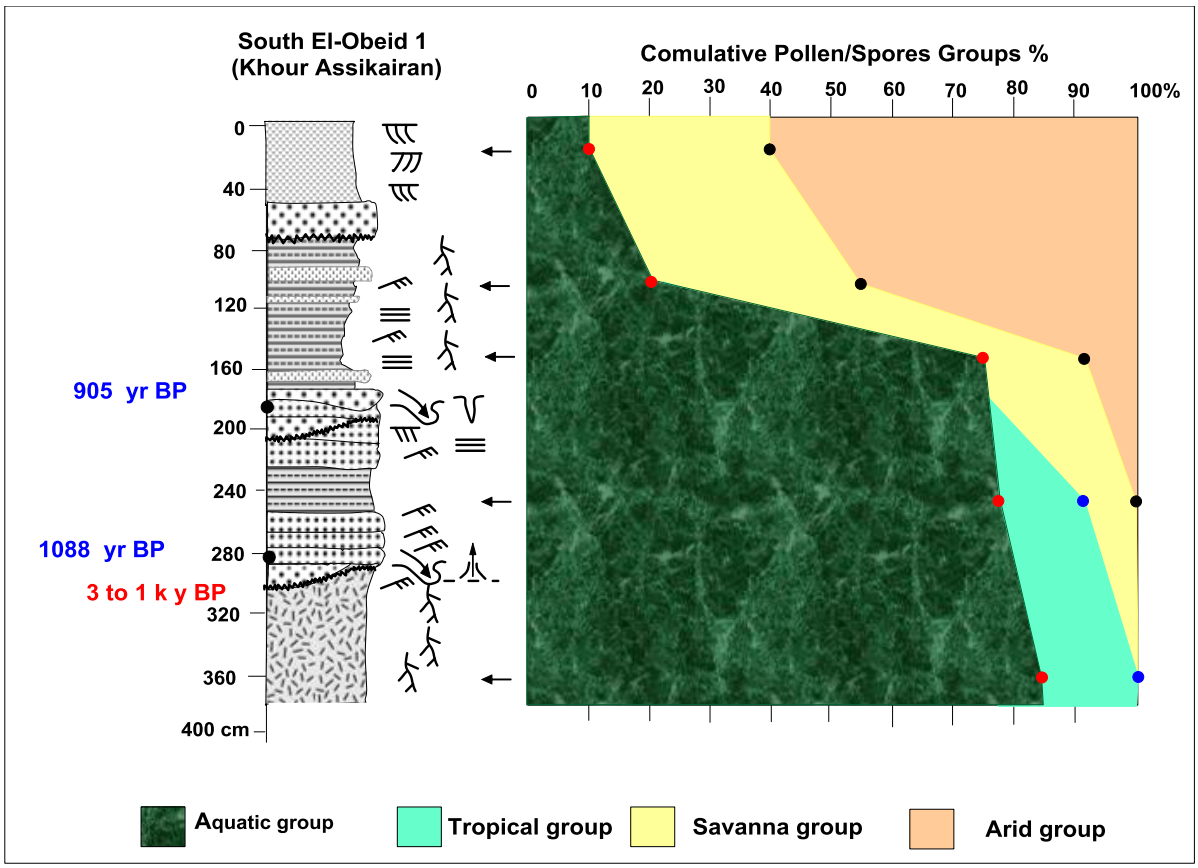


*Fig. 4.9: Proportion of pollen groups in the South El Obeid 1 section.*

According to the stratigraphic distribution (Fig. 4.9), no pollens of the arid group have been found in the lower part of the section, which is dominated by the aquatic group (up to 82 %), followed by tropical indicators (≈ 14 %), the savanna group being very rare (≈ 3 % in average). The middle part (depth 125 – 240 cm) contains ≈ 76 % of aquatic pollens, ≈ 8 % in average of tropical, ≈ 12 % of savanna, and ≈ 4 % of arid, indicators. The upper part of the section is dominated by the arid indicator group (average of 55 %), with subordinate species of the savanna (≈ 30 %) and aquatic (≈ 15 %) groups, and is devoid of palynomorphs of the tropical group.

The interpretation includes both the stratigraphic and geographical distribution. The stratigraphic interpretations are presented in figs 4.10 to 4.12. The geographical interpretation have been carried out through the correlations between the three studied sites and includes correlation for three different periods: ≈ 3500, ≈ 1000, and ≈ 500 y BP (Figs. 4.13 to 15).

### 4.2.2.4. Interpretation of the palynological results

#### 4.2.2.4.1. Stratigraphic interpretation

In the lower parts for the North Dilling and South El Obeid 1 sections (≈ 4.8 to ≈ 3 ka BP), the domination of the aquatic and tropical groups, indicates that the region experienced a wet climate, probably sub-humid to semi-arid. Moreover, the marked predominance of freshwater algae in the aquatic group indicates that many swamps were present in the area. This climate, however, experienced some local fluctuations as shown in the South El Obeid 3 site, the lower part of which is dominated by the aquatic and savanna groups. These conditions suggest that the region was probably located within the tropical rainy belt of the African continent.

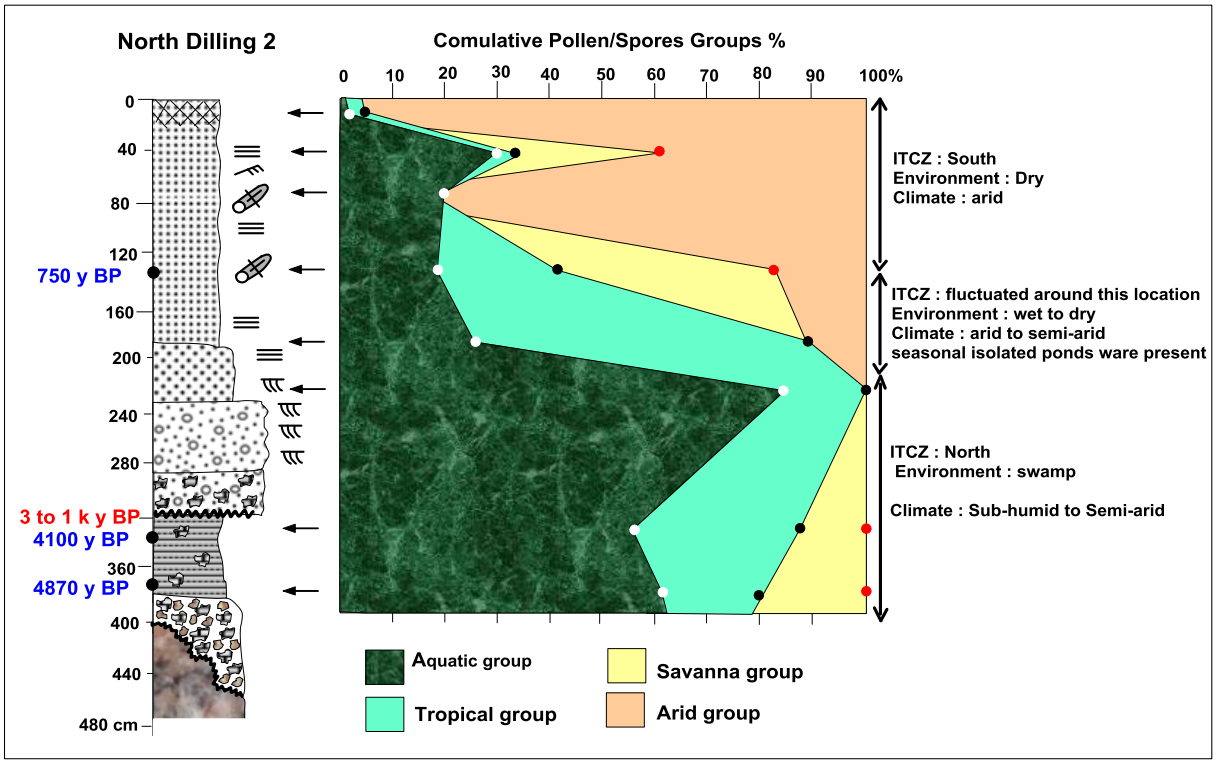


*Fig. 4.10: Interpretation of the pollen groups for the North Dilling site.*

The appearance of the arid group in the middle parts of the three sites (≈ 1000 to ≈ 800 yr BP) indicates environmental and climatic shifts toward less swampy environment and less wet climate than in the lower part.

The arid group increases then rapidly upward (younger than 1000 yr BP) and the upper parts of the sections show relatively few percentages of the other groups. This rapid increase in the arid group percentages reflects an abrupt environmental and climatic change to dry environment and arid climate. Therefore, this indicate that the studied region was probably located north of the rainy tropical belt of the African continent.

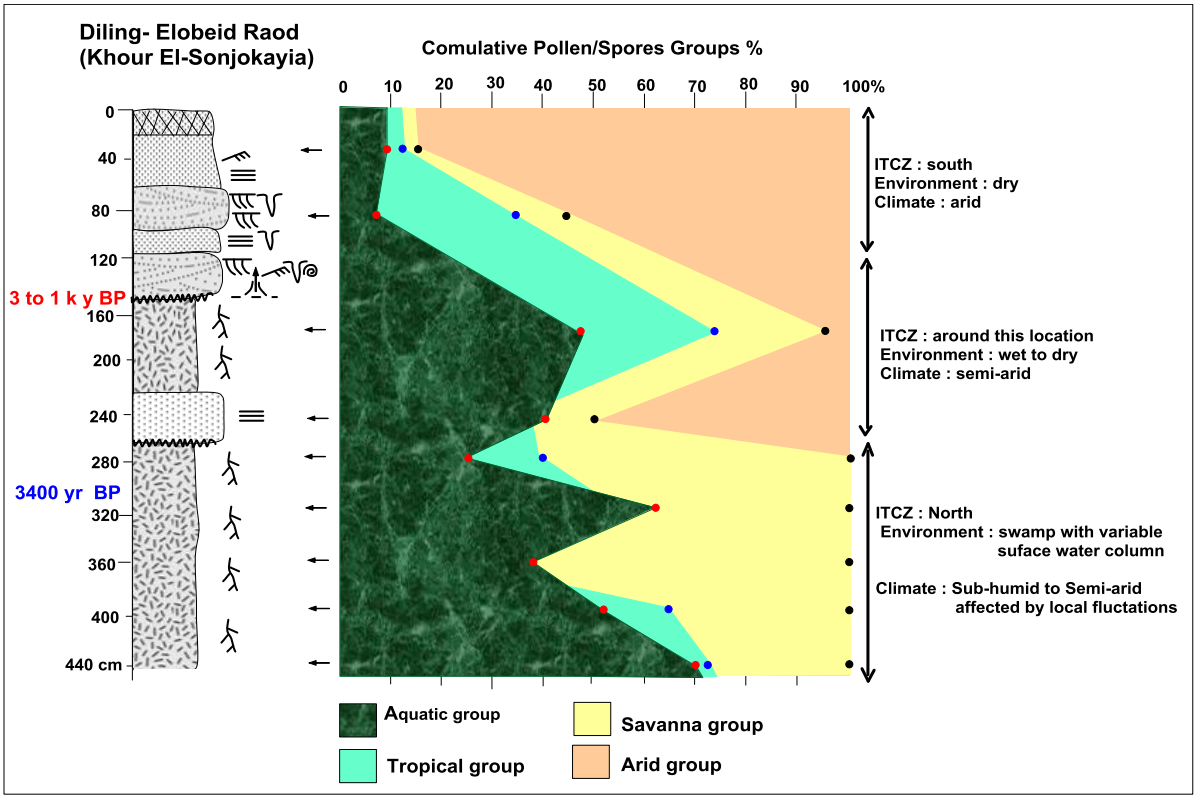


*Fig. 4.11: Interpretation of the pollen groups for South El Obeid 3 site.*

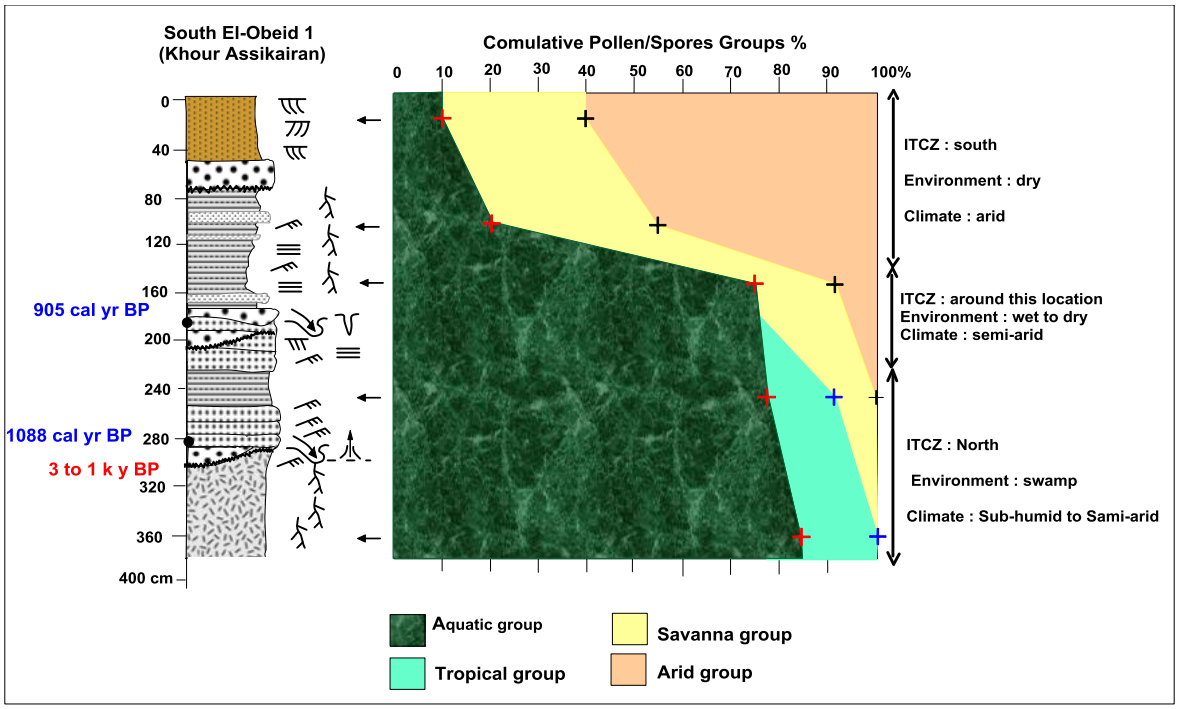


*Fig. 4.12: Interpretation of the pollen groups for the South El Obeid 1 site.*

### 4.2.2.4.2. Geographical interpretation

Around 3500 yr BP the southern part of the studied area was dominated by the aquatic group, although in south El Obeid 3, both the savanna and aquatic groups prevailed (Fig. 4.13). This indicates that this region experienced wet conditions, which reflect sub-humid climate and swampy environment. Thus, between ≈ 5 and 3 ka BP, this area was located within the rainy belt of the tropical Africa.

Around 1000 yr BP, the Kordofan region recorded the appearance of an arid vegetation cover, although the aquatic flora and freshwater algae were still the prevailing groups (Fig. 4.14). The tropical climate indicators are still abundant and the savanna group is locally abundant. These data indicate that, by ≈ 1000 yr BP, the environment and climate was drier than at 3 ka BP. This climatic shift may have already started during the hiatus, ≈ 3000 yr ago. Around 1000 yr BP, the climate between El Obeid and Dilling was semi-arid, the environment was swampy along the rivers and dry elsewhere, and the investigated sites were probably located at the northern end of the tropical rainy belt.

From ≈ 500 yr BP up to the present, the investigated sites are dominated by the arid group, with locally high percentages of the savanna group, while the aquatic and tropical groups do not exceed together 30 % (Fig. 4.15). The domination of the arid group indicates that the studied area experiences mostly dry conditions, with only seasonal swamps. This arid climate suggests that the region was located north of the African tropical rainy belt.

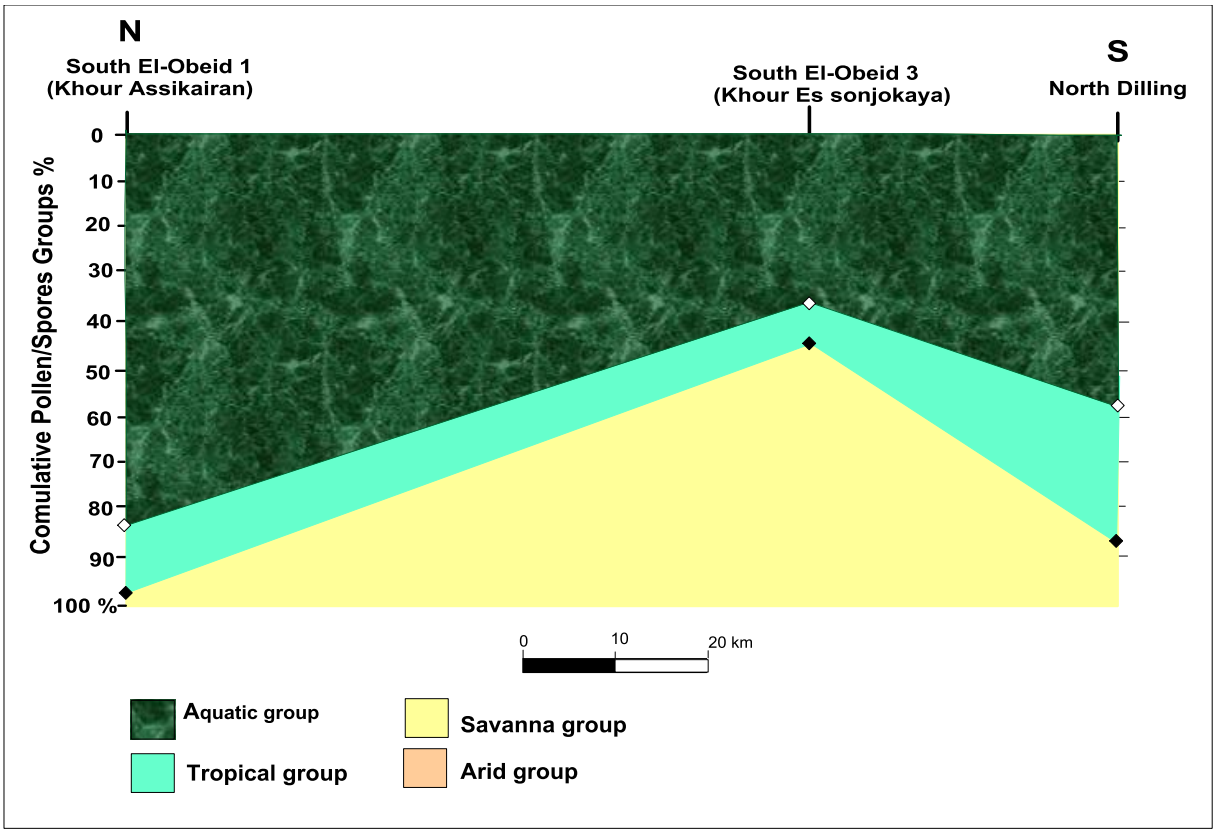


*Fig. 4.13: Percentages of the pollen groups at ≈ 3500 y BP.*

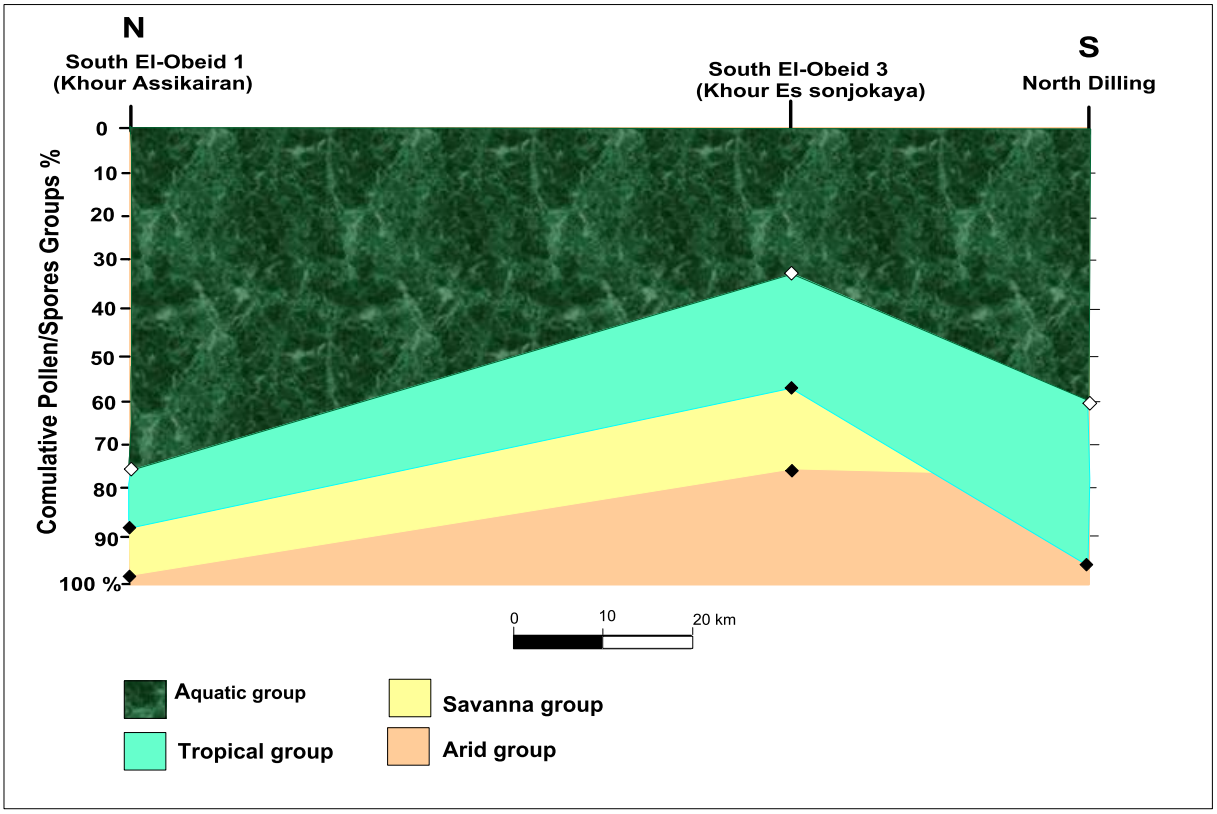


*Fig. 4.14: Percentages of the pollen groups at ≈ 1000 y BP.*

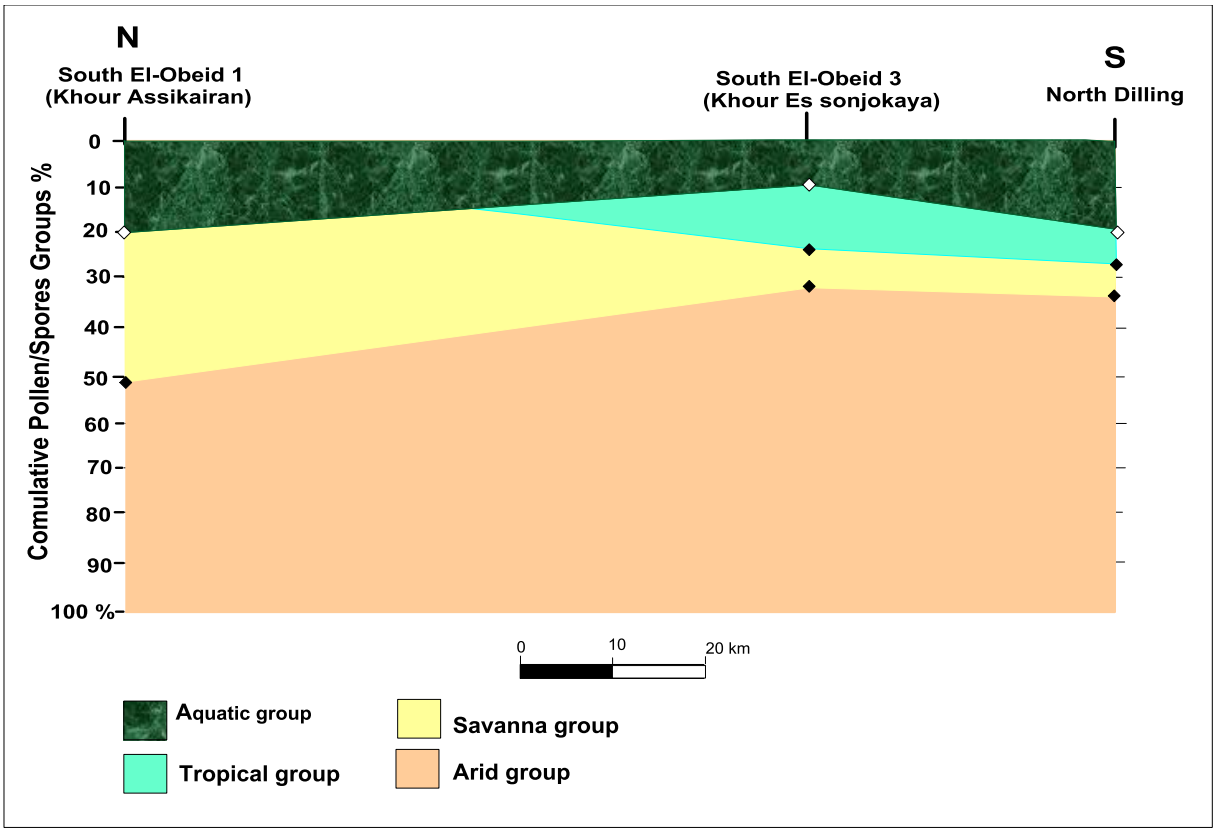


*Fig. 4.15: Percentages of the pollen groups at ≈ 500 y BP.*

## 4.3. Oxygen and carbone isotopes

### 4.3.1. En-Nahud 1 and En Nahud 2 section

#### 4.3.1.1. Results

All analyzed samples of the En-Nahud 1 and En-Nahud 2 sites were gastropod shells from the red sand sediments (Upper unit), which included the semi-aquatic species *Pila wernei* and terrestrial land-snails *Limicolaria flammea*. The results show $\delta^{18}O$ values from – 11.5 ‰ to – 0.012 ‰ and $\delta^{13}C$ from – 8.62 ‰ to – 1.33 ‰ (Figs. 4.16 and 4.17).

The evolution of the C and O isotopes in both En-Nahud sections (Figs. 4.16 and 4.17) shows that the samples of the lowermost part of red sand facies are depleted in the heavier $^{18}O$ ($-12 < \delta^{18}O < -11$) compared to samples from the upper part of the same unit ($-2.5 < \delta^{18}O < 0$), which shows gastropod shells enriched in $^{18}O$ and depleted in $^{16}O$. The evolution of the C isotopes is less clear, but shows a decrease of the $^{13}C$ through time.

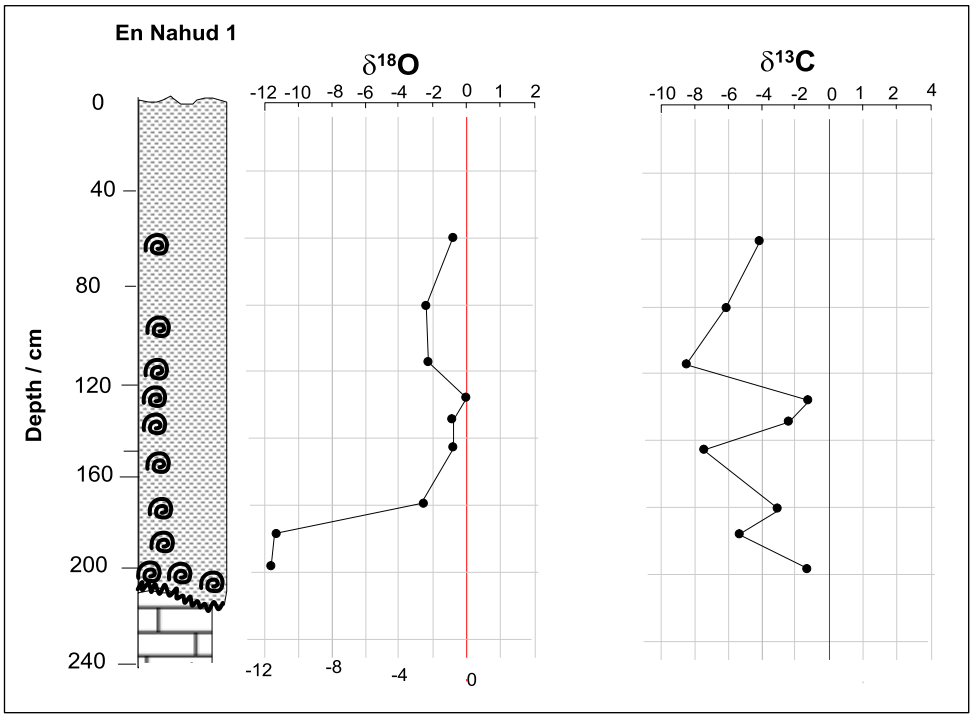


*Fig. 4.16: Evolution of the oxygen and carbon isotopes in the En Nahud 1 section.*

### 4.3.1.2. Interpretation

The wide range of $\delta^{18}O$ values reflects climatic variation through time. The highly negative values of $\delta^{18}O$ in the lower part of the red sand sediments facies can be interpreted as due either to a high flux of regional water vapors enriched in $^{16}O$ and depleted in $^{18}O$, or to little evaporation, and therefore moderate temperature. This suggests that the area has experienced a wet climate at that time (Figs. 4.18 and 4.19). The depleted $\delta^{18}O$ values in gastropds in the Nile Valley is considered an evidence of high rainfall episodes (Abell and Williams, 1989) derived from a distant oceanic source (Ayliffe et al., 1996). The latitude effect may have played an important role, since the more distant from the coast, the lower the $\delta^{18}O$ values (Rozanski et al., 1993). The study area is relatively far from the Atlantic Ocean (more than 3000 km) therefore, the isotopic composition of the rainwater in this area may be normally depleted. However, since the variation is recorded at the same site, it means climatic change through time, rather than a latitudinal effect.

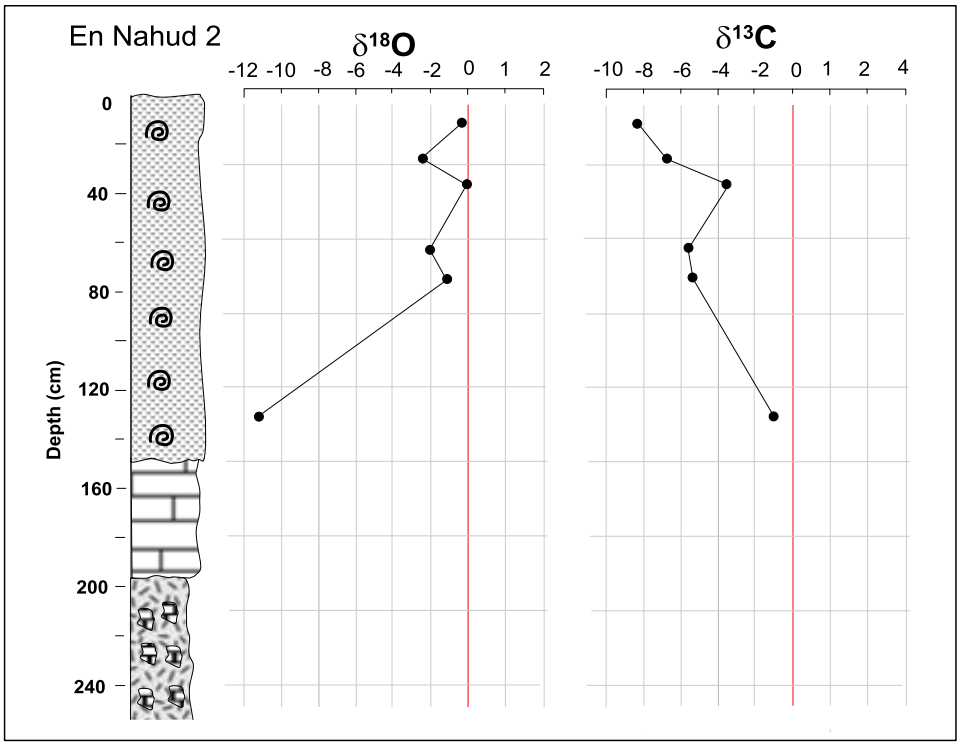


*Fig. 4.17: Evolution of the oxygen and carbon isotopes in the En Nahud 2 section.*

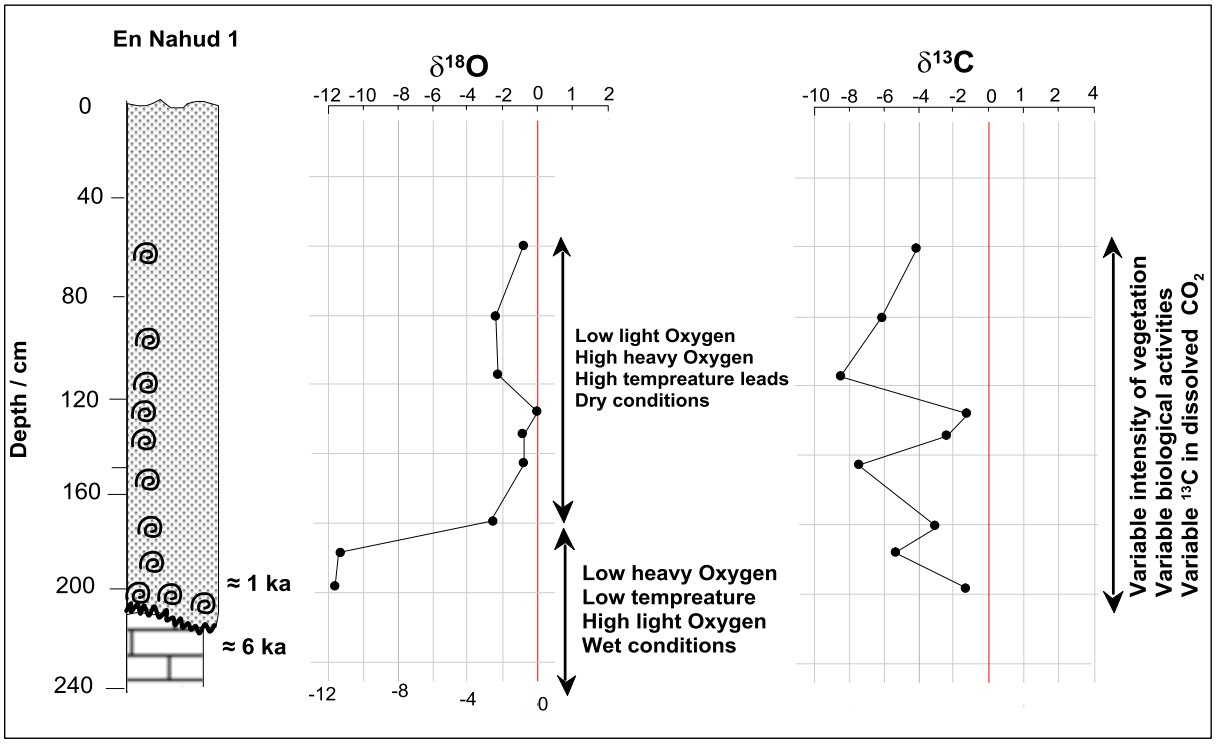


*Fig. 4.18: Interpretation of the oxygen and carbon isotopes - section En Nahud1.*

The sedimentological analysis of the red sand Unit showed that the latter is of aeolian origin, which is inconsistent with the interpretation of the isotopic data. However, gastropods from the lower part of the red sand facies are *Pila wernei*, a semi-aquatic species, and their shell was filled and covered with the carbonate mud of the underlying palustrine limestone. This strongly

suggests that these snails were actually leaving during deposition of the palustrine carbonate, and were reworked during the aeolian erosional period (≈ 3 to 1 kyr BP). Thus, the negative $\delta^{18}O$ values may correspond to the time the underlying limestone were deposited (≈ 10 to 6 ky BP), which corresponds to the African Humid Period (AHP), as supported by the aquatic and semi-aquatic way of life of the gastropods.

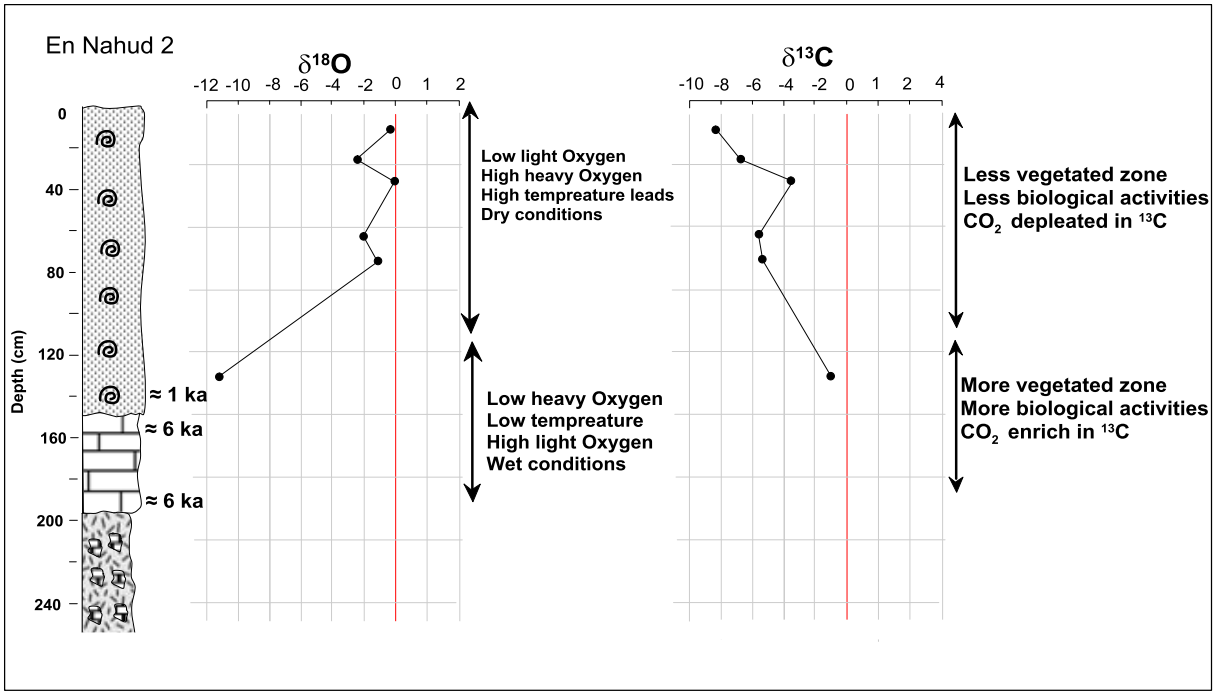


*Fig. 4.19: Interpretation of the oxygen and carbon isotopes in the En Nahud 2 section.*

In contrast, in the upper part of the En-Nahud 1 and 2 sections, the shells of terrestrial land snails are enriched in $^{18}O$ and depleted in $^{16}O$. Since evaporation has a major influence on the isotope composition of standing water bodies (Leng and Marshall, 2004) and $^{16}O$ is easier to evaporate than $^{18}O$, the isotopic enrichment in $^{18}O$ is interpreted as indicating an arid climate (Abell and Williams, 1989). Moreover, the water body may have played an important role in the variation of $\delta^{18}O$ between the lower aquatic shells and the upper land snail shells. As a matter of fact, if the water body remains for a long time, more evaporation is expected to occur, and the light oxygen ($^{16}O$) must be reduced through this evaporation, which makes the water body less depleted in $^{18}O$ than the isotopic composition of the initial rainfall. Goodfriend et al. (1989) reported that the isotopic composition of snail in a water body is related to atmospheric water vapor and the isotopic composition of the water body, while the land snail shell carbonate $^{18}O$ should provide a reliable indication of rainfall $^{18}O$. This assumption or interpretation indicates that the oxygen incorporated in the aquatic shells is isotopically less depleted than the real depletion of meteoric water at time of precipitation. Hence the enriched composition of the land snails of the upper part reflects a real $^{18}O$ enrichment of the meteoric water.

### 4.3.2. East El-Khowei site

#### 4.3.2.1. Results

All analyzed samples of the East El-Khowei site were gastropod shells. The lower three samples, from the palustrine sandy limestone unit, are the semi-aquatic *Pila wernei*, and the aquatic *Biomphalaria pfeifferi* and *Melanoides tuberculate* gastropods. The upper five samples are the terrestrial land snails *Limicolaria flammea.*

Their $\delta^{18}O$ values varies from – 9.6 ‰ to 0.1 ‰, while the $\delta^{13}C$ values range between – 10.0 ‰ and - 3.7 ‰. The samples from the sandy limestone (Second unit) and from the base of the red sand sediments facies (Upper unit), show highly negative $\delta^{18}O$ values. Samples from the red sand sediments have less negative $\delta^{18}O$ values, except for one of them. The $\delta^{13}C$ values are generally negative (depleted in $^{13}C$). Samples from the red sand show more negative $\delta^{13}C$ values than those from the sandy limestone unit (Fig. 4.20).

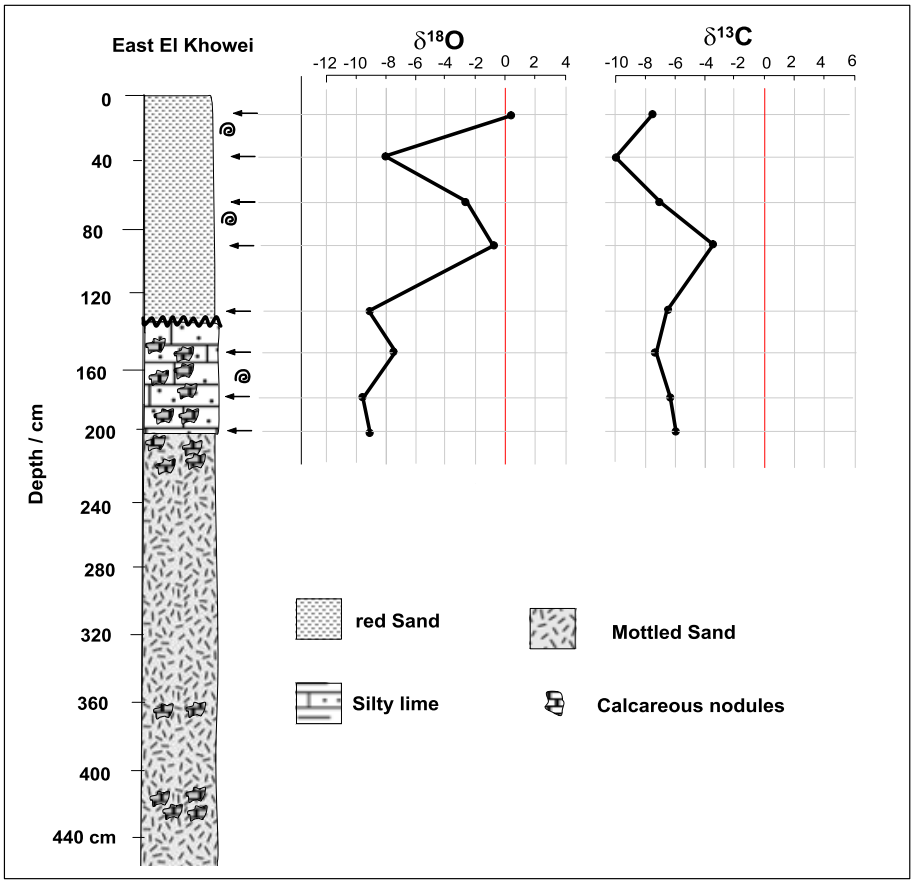


*Fig. 4.20: Evolution of the oxygen and carbon isotopes in the East El Khowei section.*

### 4.3.2.2. Interpretation

The highly negative values of $\delta^{18}O$ for samples from the sandy limestone unit (≈ 10 to 6 ky BP) are consistent with low evaporation rates and therefore, humid condition for the palustrine sandy limestone (Fig. 4.21).

The upper part of the east El Khowei section shows shells of terrestrial snail enriched in $^{18}O$ and depleted in $^{16}O$. This change in the isotopic compositions between the lower and upper parts indicates that the climate shifted to dry conditions between deposition of the palustrine carbonates and deposition of the red sand sediments, *i.e.* between ≈ 6 and 1 ky BP. Among the

samples from the Upper red sand Unit, one shows oxygen isotope values highly depleted in $^{18}O$ ($\delta^{18}O$ = - 8.0). An acceptable explanation is that the shell may has been reworked from the palustrine limestone, eroded in the surrounding area.

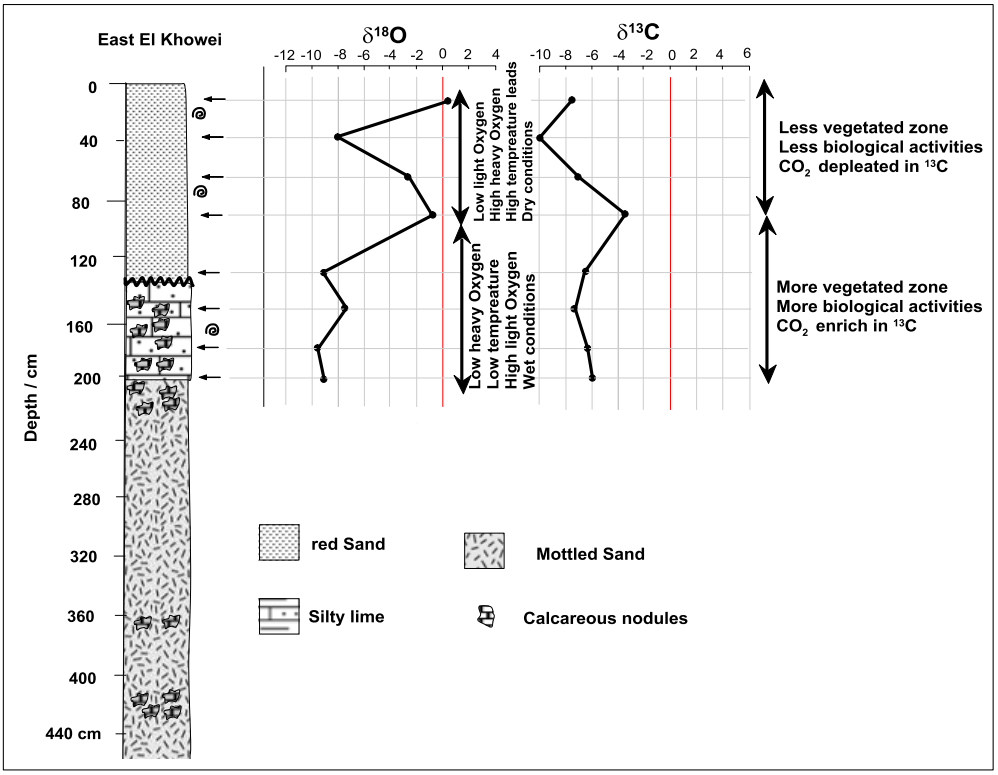


*Fig. 4.21: Evolution of the oxygen and carbon isotopes in the East El Khowei section.*

### 4.3.3. West El-Obeid site

#### 4.3.3.1. Results

All analyzed samples of the West El-Obeid site are calcareous nodules formed within a horizon of mottled fine sand sediments facies (Lower Unit). The isotopic results for these nodules show variations of the $\delta^{18}O$ and $\delta^{13}C$ values from – 9.6 ‰ to – 4.6 ‰, and from – 7.8 ‰ to 0.6 ‰, respectively (Fig. 4.22).

The vertical distribution of $\delta^{18}O$ values shows two distinct parts in the Lower Unit. These two parts correspond to the grey mottled, and pale-yellow mottled horizons, respectively. The grey mottled horizon (520 – 230 cm) shows $\delta^{18}O$ values mostly ranging between -7 and -6.3 ‰ (except one sample > -6.3 ‰), while the pale-yellow mottled horizon (230 – 120 cm) shows $\delta^{18}O$ values comprised between -8.3 and -9.8 ‰. On the other hand, the $\delta^{13}C$ values decrease upward in the mottled facies; the lower part of the succession shows little negative $\delta^{13}C$ values, compared to the upper part that is depleted in $^{13}C$.

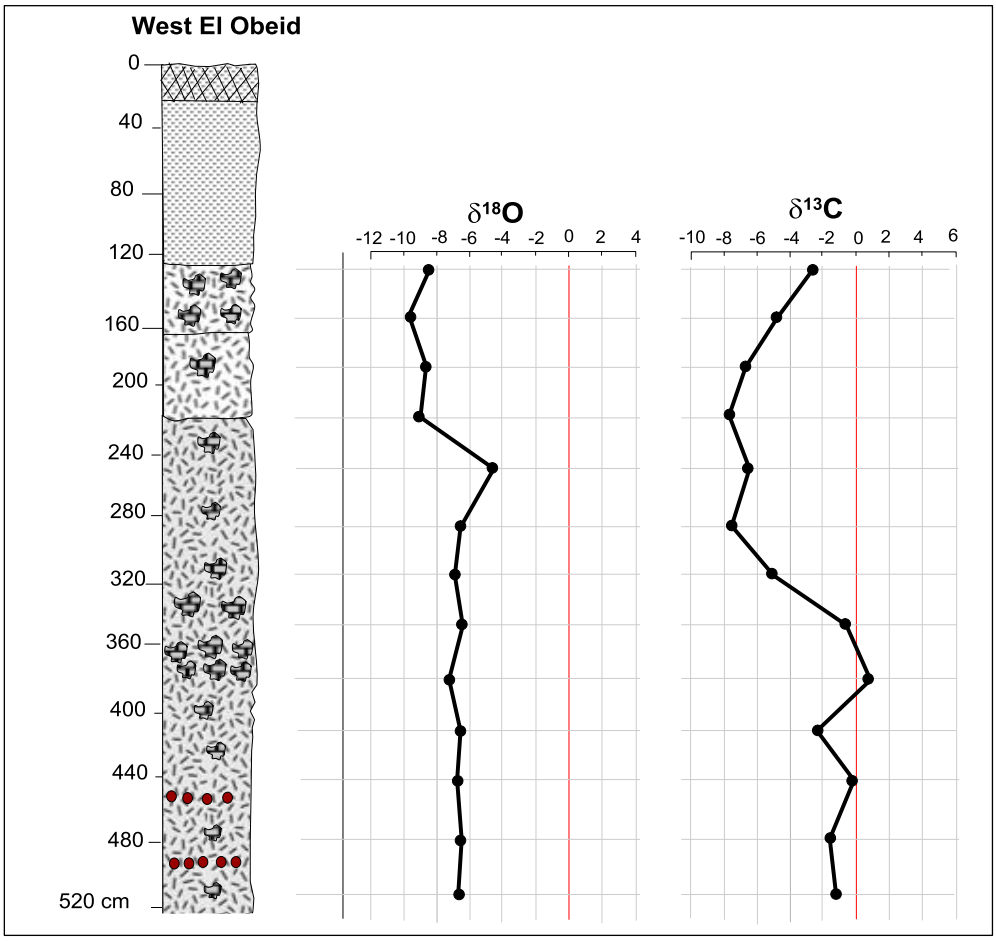


*Fig. 4.23: Evolution of the oxygen and carbon isotopes in the West El Obeid section.*

### 4.3.3.2. Interpretation

The West El-Obeid site shows generally negative $\delta^{18}O$ values, with narrow range indicating that wet conditions prevailed during the formation of the calcareous nodules. As a matter of fact, the development of calcareous nodules, occurred after deposition of the enclosing matrix. Moreover, the upper part of the curve (above depth 240 cm) shows more negative $\delta^{18}O$ values, than those of the lower part (below depth 240 cm). This may indicate that the calcareous nodules of the upper part developed under wetter conditions that those developed in the lower part (Fig. 4.23). The variation in $\delta^{18}O$ below and above depth 220 cm, maybe due to groundwater effects, which may reduce the lighter oxygen ($^{16}O$) through the previous continued evapotranspiration from the lower part, while calcareous nodules above the depth 220 cm, represent more recent water of the AHP and therefore, more depleted than the lower part.

Regarding the interpretation of carbon isotopes, the variation from less negative $\delta^{13}C$ values in the lower part, to more negative $\delta^{13}C$ values in the upper part, may reflect a difference in vegetation type and/or density, differentiation in the biological activities, or variation in the $^{13}C/^{12}C$ ratio in the dissolved $CO_2$.

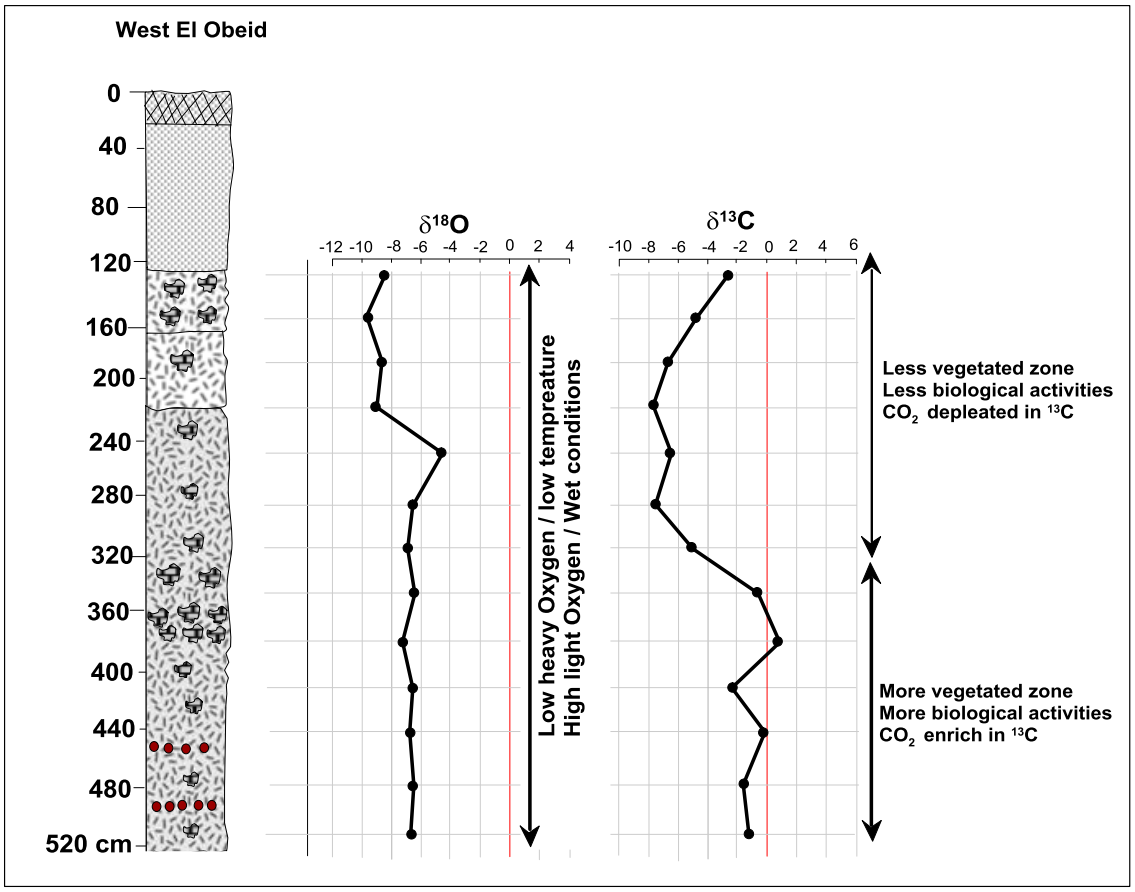


*Fig. 4.23: Interpretation of the oxygen and carbon isotopes - West El Obeid section.*

### 4.3.4. North Dilling site

#### 4.3.4.1. Results

All analyzed samples from North Dilling site are calcareous nodules formed within silty sand or reworked in conglomerate beds. For these nodules, $\delta^{18}O$ varies from – 8.2 ‰ to – 5.9 ‰ (with narrow range of only up to 2.3 ‰ difference) and $\delta^{13}C$ from – 4.7 ‰ to 0.4 ‰ (with relatively narrow range of up to 5.1 ‰ difference). Generally, samples from the lower part of the section show less negative $\delta^{18}O$ values than samples from the upper part (Fig. 4.24).

#### 4.3.4.2. Interpretation

The negative values of $\delta^{18}O$ and their narrow range indicate that the nodules developed under relatively wet conditions, with little or no climatic variation, although a mild shift toward less depleted values upward is visible. The relatively more positive $\delta^{13}C$ values with their relatively narrow range indicate little environmental variability with some stability in vegetation type and/or density, little variation in the biological activity, and low variability of $^{13}C$ ratios in the dissolved $CO_2$ (Fig. 4.25).

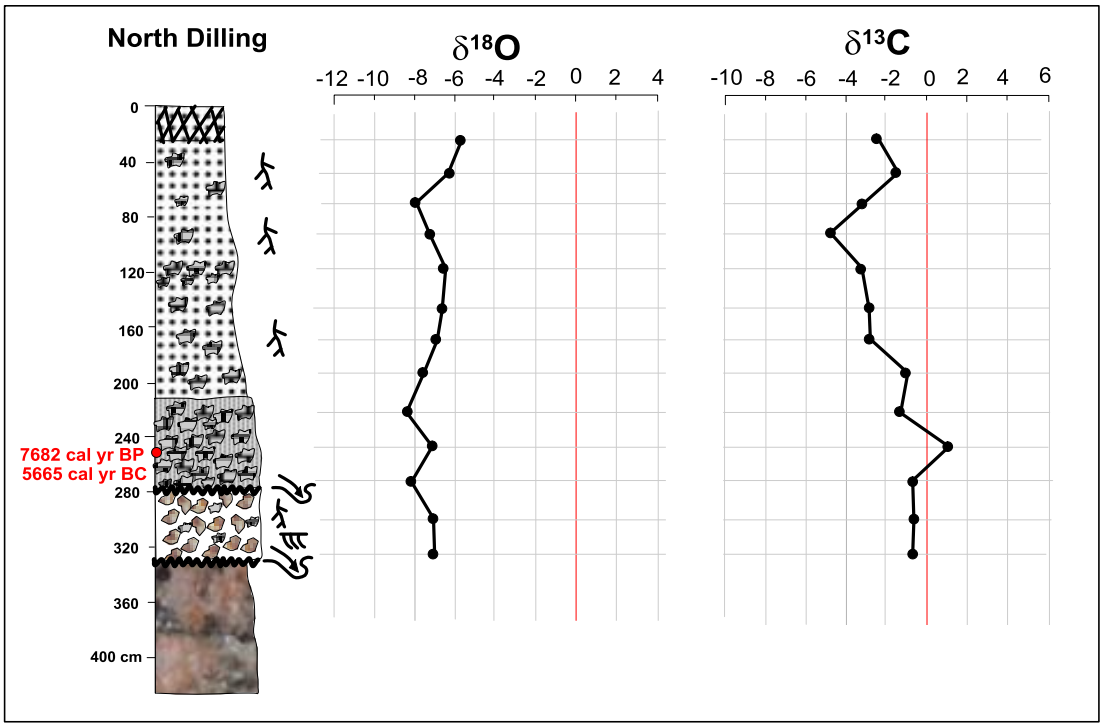


*Fig. 4.24: Evolution of the oxygen and carbon isotopes in the North Dilling section.*

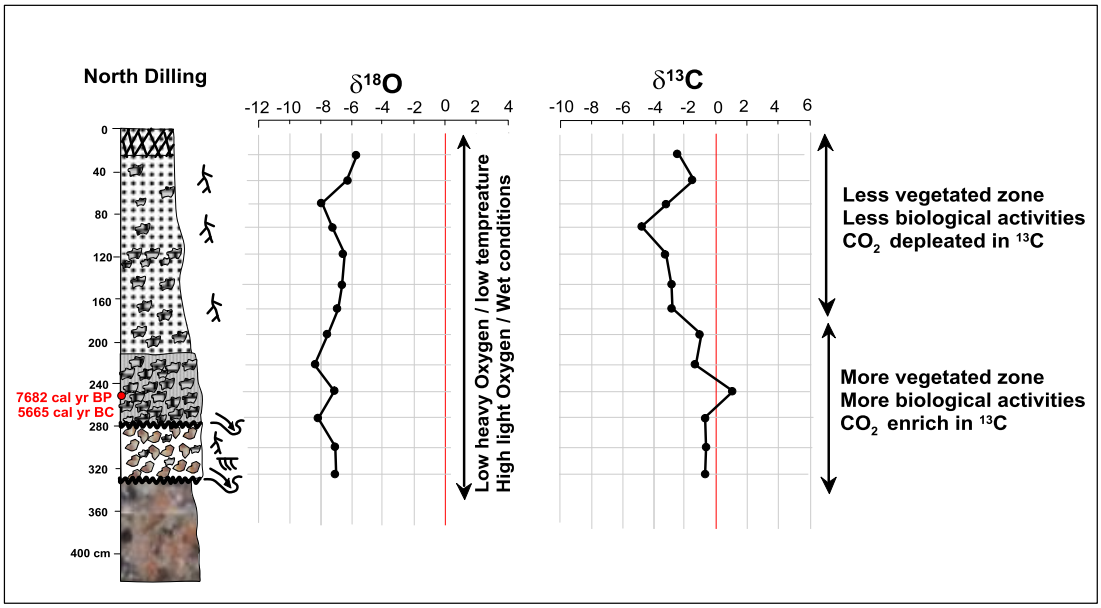


*Fig. 4.25: Interpretation of the oxygen and carbon isotopes – North Dilling section.*

## 4.4. Geochemistry of major elements

XRF analyses of major elements were carried out for twenty-two samples collected from two sites : North Bara 3 (Jabrat Esh Sheikh) and West El-Obeid (Ayara). The results are presented in table 4.3 and figures 4.17 and 4.18.

### 4.4.1. Results

$SiO_2$ is the most dominant element in both sites, with concentrations between 74.42 and 54.31 % in North Bara 3 and between 57.03 and 58.4 % in west El Obeid. $Al_2O_3$ is the second

most abundant element with values of 15.39 to 12.75 % in North Bara 3, and 15.22 to 13.93 % in west El Obeid. The third element in abundance is $Fe_2O_3$ with values of 7.95 to 5.32 % in North Bara 3, and 7.52 to 5.1 % in west El Obeid. CaO follows with concentration of 0.95 to 4.75 % in North Bara and 0.54 to 10.67 % in west El Obeid. $TiO_2$ records the fifth range with values of 2.91 to 4.79 % in North Bara 3, and 1.84 to 2.16 % in west El Obeid.

The calculated values for the chemical index of alteration (CIA) show high values ranging from 82.9 to 91.4 (average 89.4) in the North Bara 3 section, and from 87.5 to 90.3 (average 88.8) in the West El Obeid section. The CIA values are very homogeneous in both sections with very little variations (Figs. 4.26 and 4.27). In the North Bara 3 section, the mottled unit is marked by slightly higher values than the Upper unit of red sand sediments (Fig. 4.27), while the relation is reversed in the West El Obeid section.

The ratio of $SiO_2$ to $Al_2O_3$ is moderately high in both sections with little variability (Table. 4.3). It ranges between 6.4 and 5.0 in the West El Obeid section with a slight increasing upward trend toward the red sand of the Upper unit (Fig. 4.27). In the North Bara3 section the silica-aluminium ratio ranges between 6.0 and 3.8 with some variability along the section, in both the mottled sand facies of the Lower unit, and the red sand facies of the Upper unit (Fig. 4.27).

The ratio of CaO to $SiO_2$ is generally low in both sections (Table. 4.3). It ranges between 0.01 and 0.25 in the West El Obeid section with a remarkable upward decrease, so that the calcium-silica ratio of the mottled sands (Lower unit) is higher than the red sands of the Upper unit (Fig. 4.26). In the North Bara3 section, the CaO to $SiO_2$ ratio ranges between 0.01 and 0.36 with remarkably low ratios in the Upper unit and the upper part of the Lower unit (Fig. 4.27).

### 4.4.2. Interpretation of XRF analyses

The high content in $SiO_2$ is due to the sandy nature of the analyzed samples. $Al_2O_3$ generally accumulates in form of clay minerals (Sheldon and Tabor, 2009). The relatively high concentration in $Al_2O_3$ indicates significant amounts of clay minerals formed in the source area as a product of chemical weathering. The moderate concentration in iron oxide $Fe_2O_3$ may indicate an oxidation that mostly occurred in the source area, below the same conditions that led to the formation of the clay minerals. These concentrations in aluminum and iron oxide indicate that the source area probably experienced alternating seasonal wet and dry conditions, as aluminum tends to develop mostly in wet condition. If the climate is wet all over the year, the chance of oxidation will be reduced, and therefore, the iron oxides indicate an alternation of wet and dry environment.

CIA is a measurement of the hydration and weathering of feldspar minerals to form clay minerals. As clay content increases, Al should also increase, whereas Ca, K and Na contents should decrease, leading to higher CIA values (Sheldon and Tabor, 2009). High CIA values (76 to 100) in the sedimentary rocks suggest intense chemical weathering in the source region (Fadipe *et al*., 2011; Srivastava *et al*., 2013; Madhavaraju et al., 2016).

*Table 4.3: XRF analysis results.*

| Sample No | $Na_2O$ | MgO | $Al_2O_3$ | $SiO_2$ | $P_2O5$ | $SO_3$ | Cl | $K_2O$ | CaO | $TiO_2$ | $Cr_2O_3$ | MnO | $Fe_2O_3$ | CIA | $SiO_2/Al_2O_3$ | $CaO/ SiO_2$ |
|---|---|---|---|---|---|---|---|---|---|---|---|---|---|---|---|---|
| **N.B3-14** | 0.27 | 0.93 | 14.44 | 70.54 | 0.26 | 0.07 | 0.05 | 1.39 | 0.95 | 3.69 | 0.05 | 0.10 | 6.20 | 85.7 | 4.9 | 0.01 |
| **N.B3-13** | 0.16 | 0.77 | 14.95 | 69.92 | 0.23 | 0.08 | 0.05 | 1.26 | 0.68 | 4.27 | 0.06 | 0.07 | 6.31 | 88.8 | 4.7 | 0.01 |
| **N.B3-12** | 0.10 | 0.69 | 14.30 | 70.67 | 0.21 | 0.06 | 0.04 | 1.18 | 0.49 | 4.79 | 0.05 | 0.06 | 5.85 | 89.8 | 4.9 | 0.01 |
| **N.B3-11** | 0.31 | 1.08 | 12.34 | 74.42 | 0.26 | 0.11 | 0.06 | 1.41 | 1.33 | 2.70 | 0.03 | 0.09 | 5.32 | 82.9 | 6.0 | 0.02 |
| **N.B3-10** | 0.09 | 0.67 | 14.14 | 71.47 | 0.17 | 0.06 | 0.05 | 1.18 | 0.42 | 4.34 | 0.05 | 0.07 | 6.00 | 90.0 | 5.1 | 0.01 |
| **N.B3-9** | 0.10 | 0.76 | 14.57 | 70.82 | 0.14 | 0.07 | 0.06 | 1.20 | 0.41 | 4.34 | 0.05 | 0.08 | 6.02 | 90.0 | 4.9 | 0.01 |
| **N.B3-8** | 0.11 | 1.07 | 15.39 | 68.74 | 0.11 | 0.06 | 0.09 | 1.15 | 1.06 | 3.59 | 0.05 | 0.10 | 7.61 | 90.6 | 4.5 | 0.02 |
| **N.B3-7** | 0.14 | 1.20 | 14.69 | 69.74 | 0.09 | 0.04 | 0.05 | 1.12 | 1.16 | 4.08 | 0.04 | 0.10 | 6.52 | 89.9 | 4.7 | 0.02 |
| **N.B3-6** | 0.15 | 1.50 | 15.24 | 68.43 | 0.10 | 0.11 | 0.10 | 1.05 | 1.42 | 3.59 | 0.05 | 0.13 | 7.22 | 90.4 | 4.5 | 0.02 |
| **N.B3-20** | 0.11 | 1.55 | 12.74 | 54.31 | 0.08 | 0.09 | 0.04 | 0.73 | 1.54 | 3.54 | 0.04 | 0.11 | 6.21 | 91.8 | 4.3 | 0.36 |
| **N.B3-19** | 0.14 | 1.85 | 14.94 | 56.89 | 0.07 | 0.11 | 0.05 | 0.93 | 11.19 | 3.10 | 0.04 | 0.06 | 7.95 | 91.0 | 3.8 | 0.20 |
| **N.B3-18** | 0.13 | 1.86 | 15.28 | 58.95 | 0.07 | 0.11 | 0.02 | 0.93 | 11.02 | 2.91 | 0.04 | 0.07 | 7.93 | 91.4 | 3.9 | 0.19 |
| **N.B3-16** | 0.11 | 1.54 | 13.27 | 67.22 | 0.09 | 0.33 | 0.04 | 0.98 | 4.75 | 3.60 | 0.04 | 0.08 | 7.09 | 90.4 | 5.1 | 0.07 |
| **Ay9** | 0.15 | 0.89 | 14.06 | 75.03 | 0.15 | 0.42 | 0.05 | 1.08 | 0.54 | 2.08 | 0.04 | 0.07 | 5.50 | 89.5 | 6.4 | 0.01 |
| **Ay8** | 0.14 | 0.95 | 14.19 | 74.73 | 0.12 | 0.56 | 0.04 | 1.09 | 0.59 | 2.04 | 0.03 | 0.04 | 5.63 | 89.6 | 6.3 | 0.01 |
| **Ay7** | 0.15 | 1.23 | 15.22 | 72.53 | 0.07 | 0.11 | 0.05 | 1.07 | 0.92 | 2.16 | 0.02 | 0.09 | 6.05 | 90.3 | 5.7 | 0.01 |
| **Ay6** | 0.17 | 1.70 | 14.81 | 70.66 | 0.07 | 0.04 | 0.03 | 1.09 | 2.03 | 2.14 | 0.03 | 0.13 | 6.70 | 89.5 | 5.7 | 0.03 |
| **Ay5** | 0.25 | 1.65 | 13.89 | 72.51 | 0.08 | 0.05 | 0.05 | 1.21 | 2.41 | 2.31 | 0.03 | 0.09 | 5.10 | 86.6 | 6.2 | 0.03 |
| **Ay4** | 0.25 | 2.18 | 14.72 | 63.42 | 0.09 | 0.09 | 0.03 | 1.01 | 8.68 | 2.03 | 0.02 | 0.09 | 7.02 | 88.5 | 5.1 | 0.14 |
| **Ay3** | 0.32 | 2.40 | 14.89 | 63.82 | 0.09 | 0.10 | 0.07 | 1.00 | 7.25 | 2.08 | 0.03 | 0.08 | 7.52 | 87.5 | 5.1 | 0.11 |
| **Ay2** | 0.21 | 2.12 | 13.93 | 58.40 | 0.10 | 0.10 | 0.04 | 0.88 | 14.46 | 1.84 | 0.02 | 0.10 | 7.44 | 89.4 | 5.0 | 0.25 |
| **Ay1** | 0.29 | 2.28 | 14.35 | 61.35 | 0.12 | 0.17 | 0.07 | 0.90 | 10.67 | 2.06 | 0.02 | 0.07 | 6.85 | 88.2 | 5.1 | 0.17 |

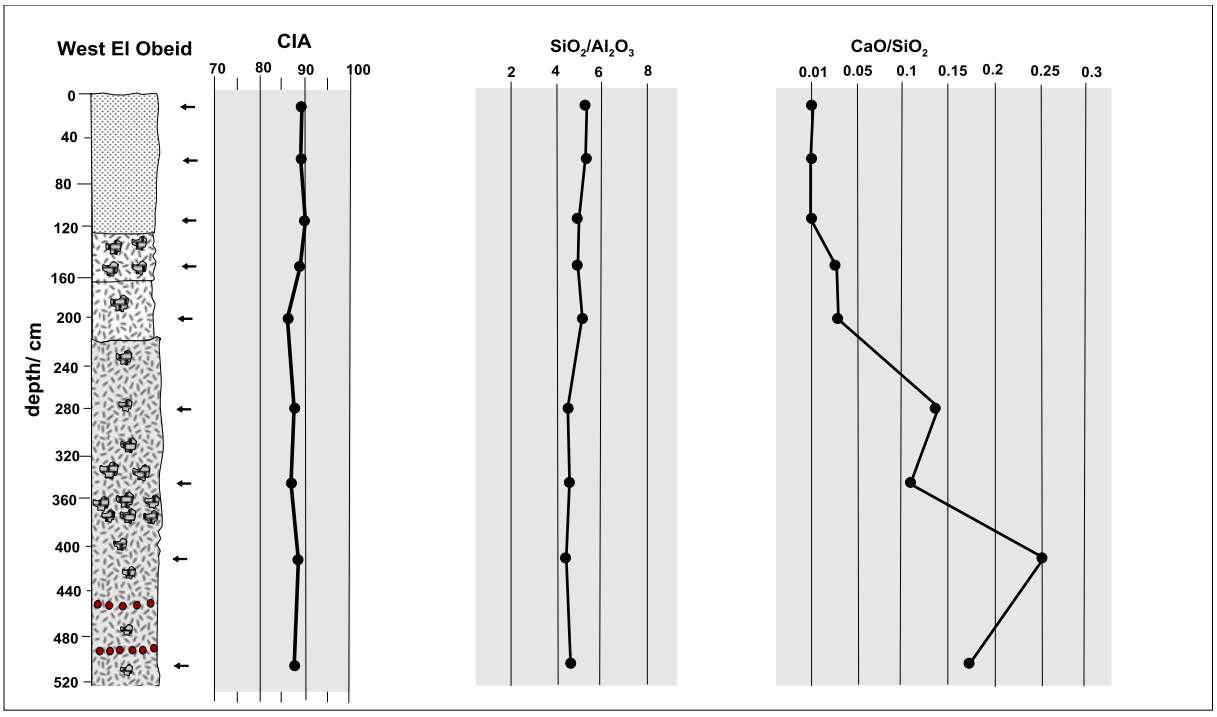


*Fig. 4.26: Plot of the climofunctions in the West El Obeid section.*

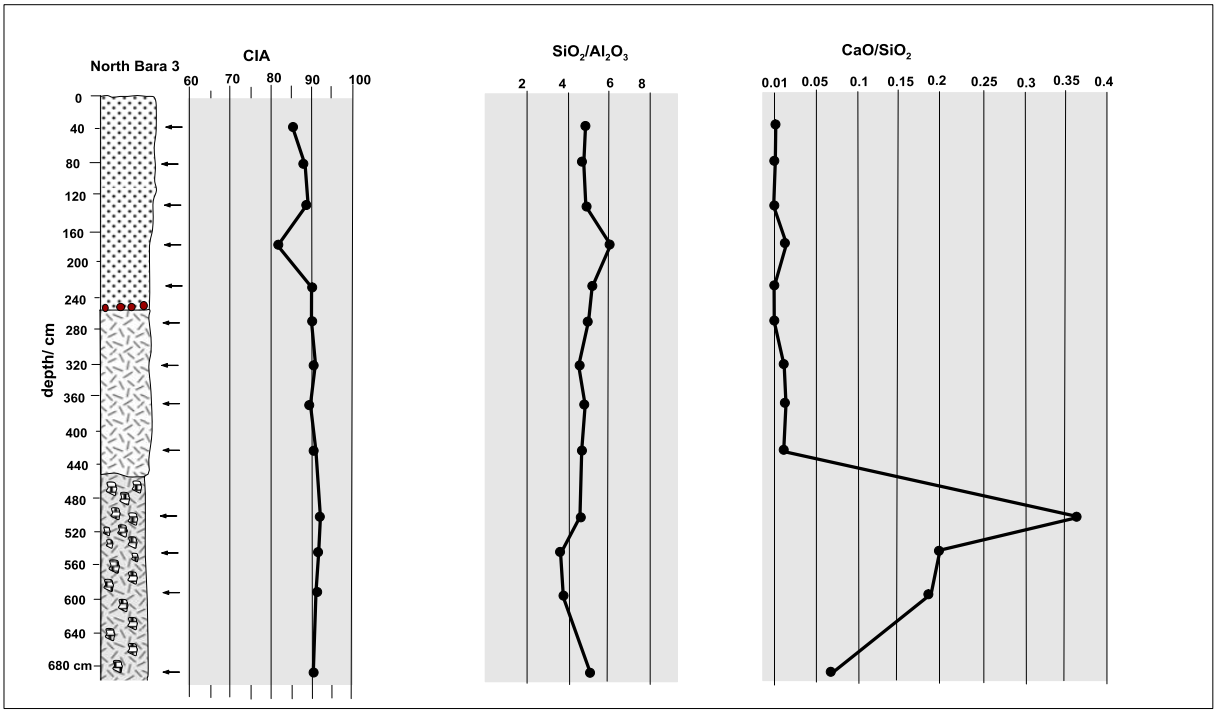


*Fig. 4.27: Plot of the climofunctions in the North Bara3 section.*

CIA values ranging from 95 to 100 indicate intensive chemical weathering, whereas CIA values lower than 50 indicate the near absence of chemical weathering and suggest cool and arid conditions (Fedo et al., 1995). Depending on the parent material chemistry, CIA changes during weathering may be quite large or relatively small. Parent materials that have already been cycled as sediments, or which are clay-rich in the first place, may start out with CIA values of 60–70, with weathering leading to even higher values (Sheldon and Tabor, 2009). Therefore,

our very high CIA values, almost constant through time in both sections, indicate that the source area experienced wet condition resulting in high chemical weathering (Figs. 4.29 4.30).

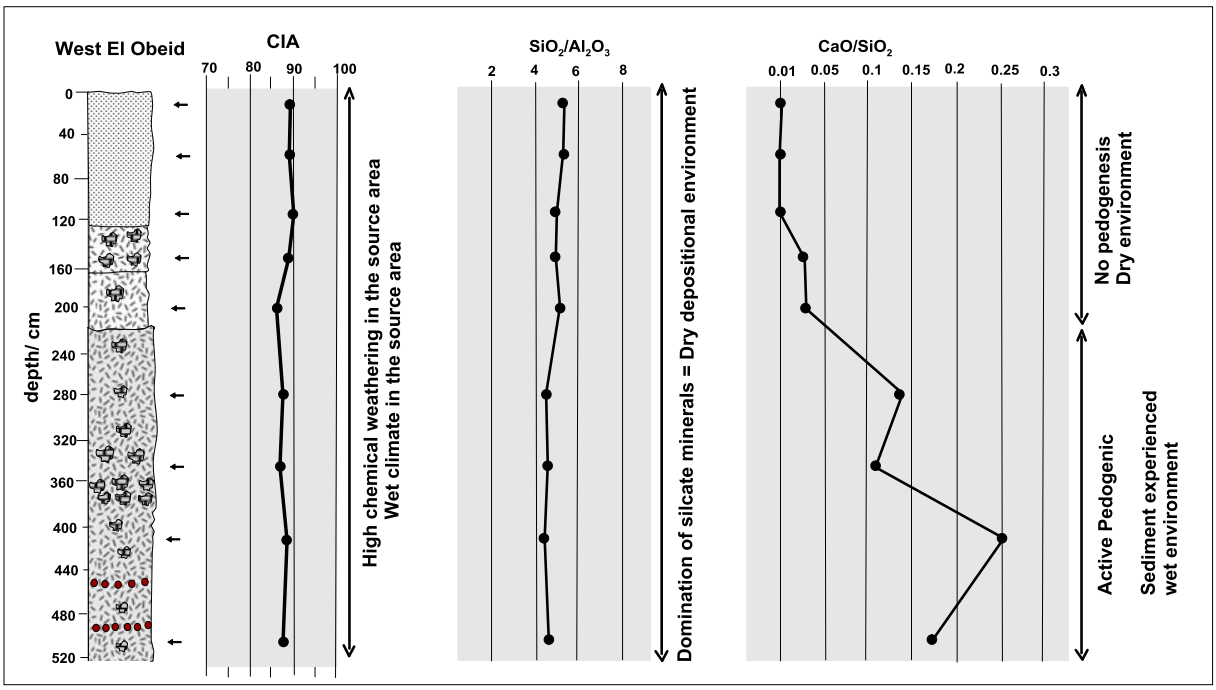


*Fig. 4.29: Interpretation of the climofunctions in the West El Obeid section.*

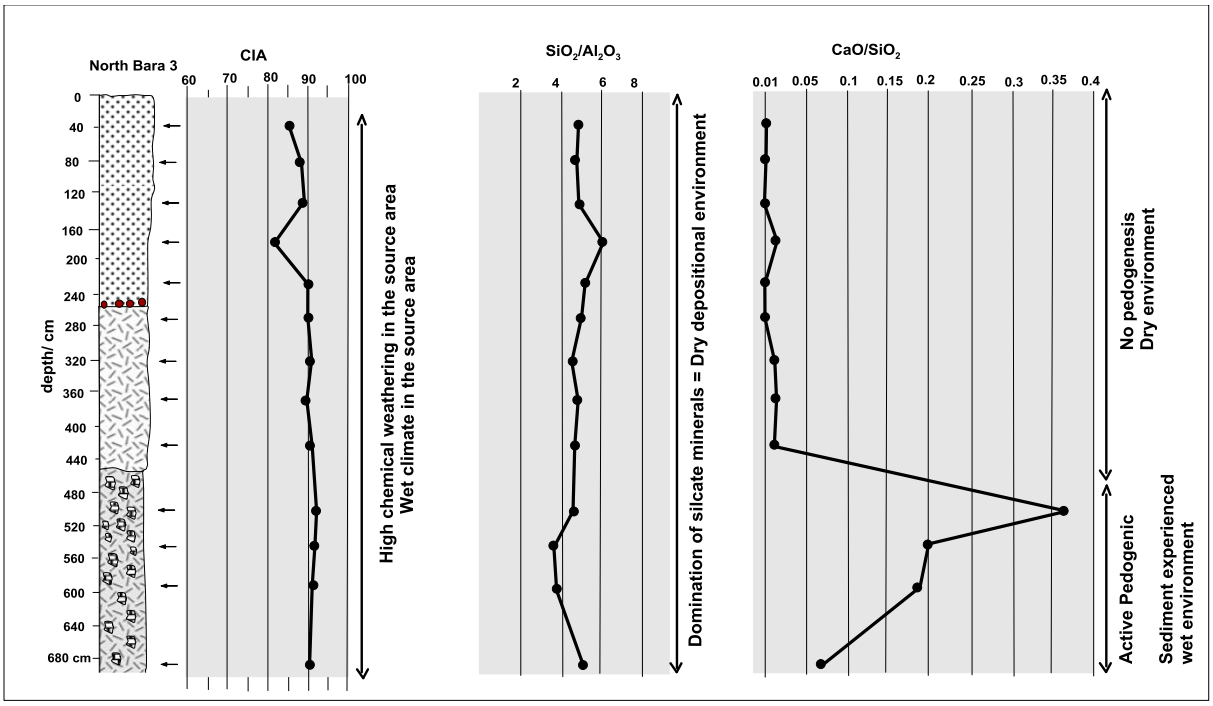


*Fig. 4.30: Interpretation of the climofunctions in the North Bara3 section.*

The $SiO_2$ content and $SiO_2/Al_2O_3$ ratio are the most commonly used geochemical criteria to determine the abundance of quartz, feldspar and clay, and for differentiating mature and immature sediments (Potter, 1978; *in* Madukwe and Obasi, 2016). High ratios indicate mineralogically mature (quartzose, rounded) sediments, while low values of $SiO_2/Al_2O_3$ ratio

indicate high degree of clayness (Madukwe and Obasi, 2016). In our case study, the relatively high $SiO_2/Al_2O_3$ ratio indicates predominating silicate minerals and low degree of clayness. Since the formation of most of the clay minerals requires humid condition, the low degree of clayness in the studied sections may indicate that the Lower and Upper unit were deposited under dry environmental conditions (Figs. 4.29 and 4.30).

Low CaO oxide suggests a chemical destruction under oxidizing conditions during weathering (Oni and Olatuji, 2017). Therefore, the very low $CaO/SiO_2$ ratio for the Upper unit of the red sand deposits in both sections may indicate that oxidation rate was greater than the pedogenetic processes, resulting in the predominance of the silicate minerals (mainly $SiO_2$) which may deposited under dry conditions (Figs. 4.29 and 4.30). On the other hand the $CaO/SiO_2$ ratio in both sections increases in the mottled sand of the Lower unit, which may indicate that the Lower unit experienced remarkable pedogenetic processes. Moreover, since these pedogenetic processes decrease upward in the Lower unit and the $CaO/SiO_2$ ratio may provide an indicator of pedogenesis degree. If so, the fact that the upper part of the Lower unit shows $CaO/SiO_2$ ratios geater in the northern West El Obeid section than in the southern North Bara3 section, suggests that pedogenesis processes were more intense in the South than in the North, and therefore, that the southern part of the study area was wetter than the northern part dat that time.

## 4.5. Clay mineralogy

Clay mineralogy analyses has been carried out in eight samples from the Lower, Third, and Fourth Units of the East El Obeid section.

### 4.5.1. Results

The major clay mineral assemblages in the analyzed samples include smectite, kaolinite, illite in addition to interstratified layers illite-smectite, chlorite-smectite and kaolinite-smectite (Table 4.4). The smectite and illite represent the greater percentages among the interstratified minerals, and consequently these stratified layers are considered either smectite or illite according to the dominant species. The vertical distribution shows a remarkable predominance of smectite and kaolinite along the section, while illite is less present. The relation between kaolinite and smectite is reversed along the section, since smectite decreases upward, while kaolinite increases upward and becomes dominant in the upper unit (Fig. 4.31).

*Table 4.4. Results of clay mineralogy analysis.*

| Sample | Clay minerals | | |
|---|---|---|---|
| | Smectite % | Illite % | Kaolinite % |
| Tag 3 | 40.2 | 21.8 | 38 |
| Tag 7 | 35.7 | 25.1 | 39.2 |
| Tag 10 | 32.1 | 28.2 | 39.7 |
| Tag 12 | 42.4 | 20.5 | 37.1 |
| Tag 15 | 50 | 19.4 | 30.4 |
| Tag 17 | 47.3 | 23.8 | 29 |
| Tag 20 | 39.7 | 31.1 | 29.3 |
| Tag 25 | 61.1 | 12.3 | 26.6 |

### 4.5.2. Interpretation

Kaolinite and smectite form during chemical weathering in warm and wet climate, while illite and chlorite form during physical weathering (Madhavaraju et al., 2002). Smectite with mixed layered clays is indicative of seasonally warm climatic conditions (Madhavaraju et al., 2002). Prevailing smectite and kaolinite in the section indicate that the source area of the investigated units experienced chemical weathering rather than physical weathering before transport of the sediment. Moreover, the slight upward increase of kaolinite suggests a slight increase of chemical weathering in the source area of the Upper unit.

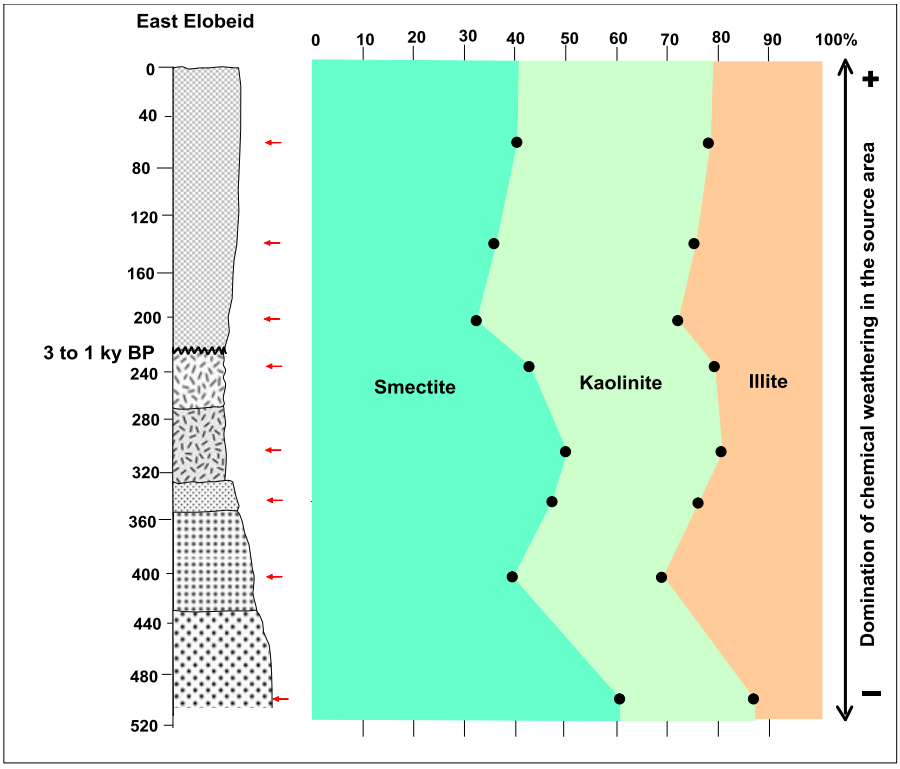


*Fig. 4.31: Clay mineralogy in the East El Obeid section: results and interpretation.*

## 4.6. Paleohydrogy

Past hydrological records are important to understand the variability of paleoclimate, since they provide information about the geometry of the water table.

### 4.6.1. Results

Paleohydrological information is given by some paleolakes and ponds or pools, which had never been mentioned before. These paleolakes are scattered in the northern part of the study area around El Ga'ah and Sodari, and in the central part, around El Khowei and En Nahud. In the northern part, the most important paleolakes are the El Ga'a Lake and the El Firja depression lake, north of Sodari (Fig. 4.32), beside many other small paleolakes or pools. In the northern part, the distribution of the paleolakes is controlled by former sand dunes, which form North-South trending dams or barriers across valleys or depressions.

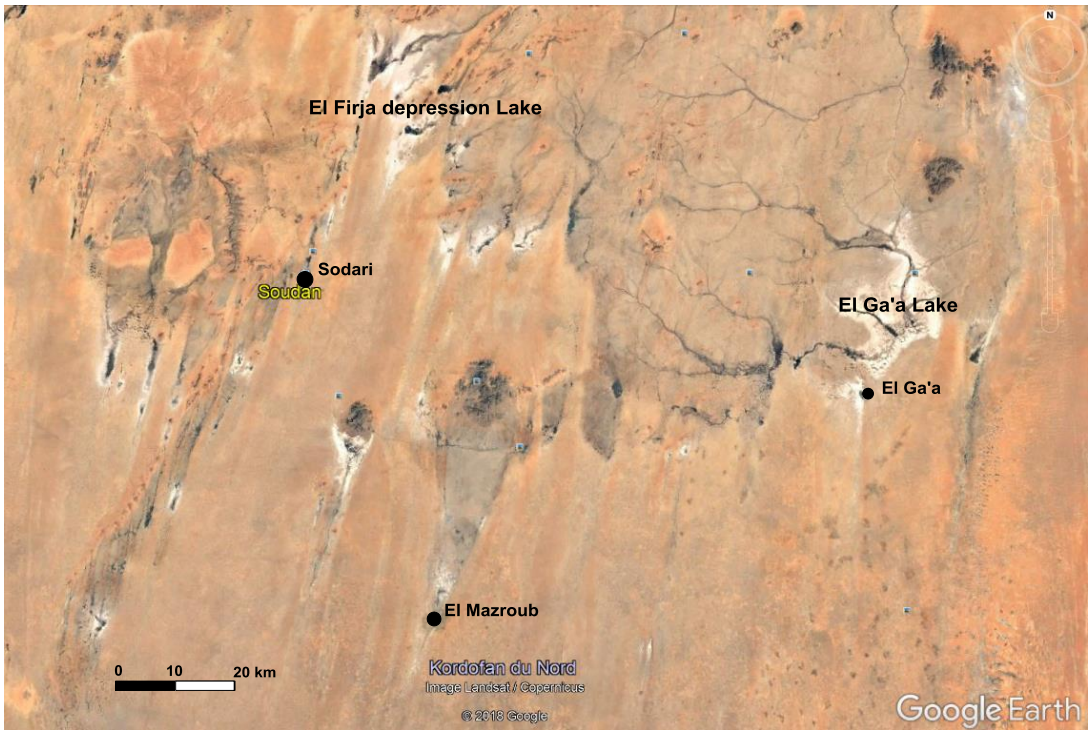


*Fig. 4.32: Location of the paleolakes in the northern area (white in this Google image). Note the N-S trending dunes, which dam the course of rivers or delineate small depressions.*

The El Ga'ah paleoake covers an approximately 490 km$^2$ wide area, is orientated north-south, with a maximum length of 38 km and a maximum width of 22 km, and the elevation of its deepest part is ≈ 450 m asl. The elevation of four shoreline points was measured: three at the eastern side of the lake and another point on its western side, which was identified by the concentration of gastropod shells, archeological and bone remnants. A topographic profile has been drawn from a digital elevation model (DEM) joining the western shoreline point to one of the eastern points (Fig. 4.33). This profile shows that the maximum lake level was ≈ 472 m asl (maximum depth of 22 m) and the average thickness of the water column was about 17 m. Therefore, the water volume of the El Ga'a Lake was ≈ 8.33 km$^3$ (8,330,000 m$^3$). According to similar potteries from dated sites in northern and central Sudan, the fragments of dotted wavy line potteries collected on the western shoreline of the paleolake indicate that the maximum lake level was achieved between ≈ 7000 and 6000 yr BP and gave way to human settlements.

The El Firja depression Lake (north of Sodari) covers an area of about 290 km$^2$ and ranges between 500 and 540 m asl. It has a very irregular shape due to sand dune tongues, and is orientated north-south with a maximum length of 32 km, and a maximum width of 17 km. Its shoreline is marked by concentrations gastropod shells and by archeological and bone remnants.

In the central part of the study area, the El Khowei and En Nahud swamps/pools are important hydrological features (Fig. 4.34). The El Khowei swamp seems to have been formed along what is today a semi-fossil river. These swamps are located between 590 and 620 m asl and are very irregular in shape, probably controlled by the drainage system. A topographic profile (Fig. 4.35) shows that the swamp level was around ≈ 605 m asl (i.e. maximum depth of 15 m).

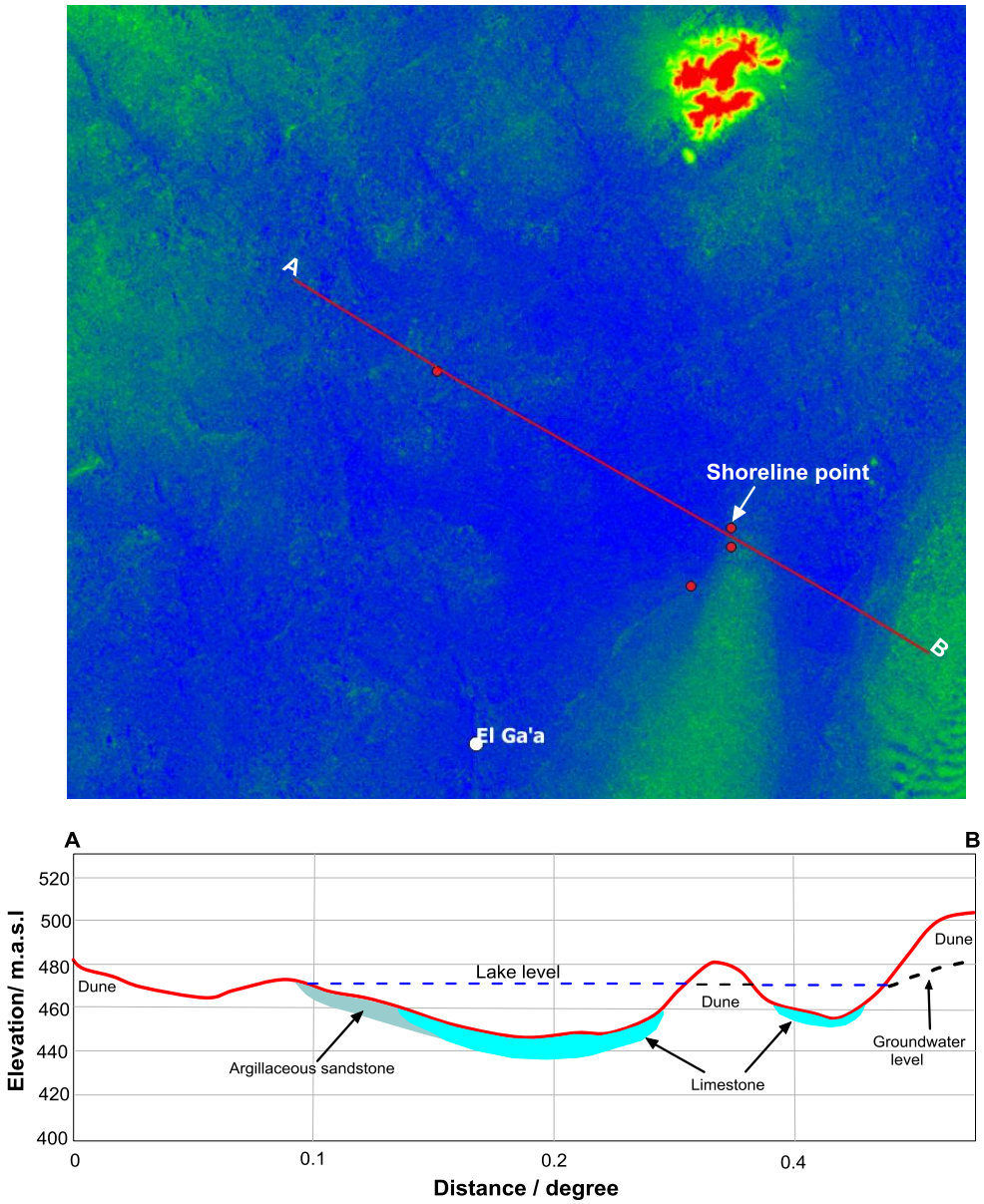


*Fig. 4.33: Profile showing the maximum level of the El Ga'ah paleolake.*

### 4.6.2. Interpretation

The sand dunes that controlled the development of the northern lakes indicate that these lakes were closed lakes. Thus, the maximum lake levels were relatively stable for a long time (possibly thousands of years). The 22 m maximum depth of the El Ga'ah paleolake indicates that precipitations were abundant enough to allow the presence of a permanent lake, even during the dry season, and that the mean annual evaporation was lower than the mean annual rainfall.

The geomorphology of the central area indicates that the El Khowei swamp developed along the wadies. These wadies were truly runny, slowly running or standing. The deposition of palustrine limestone and the preservation gastropod shells in the palustrine limestone provide evidence that water of these wadies were semi-permanent standing water.

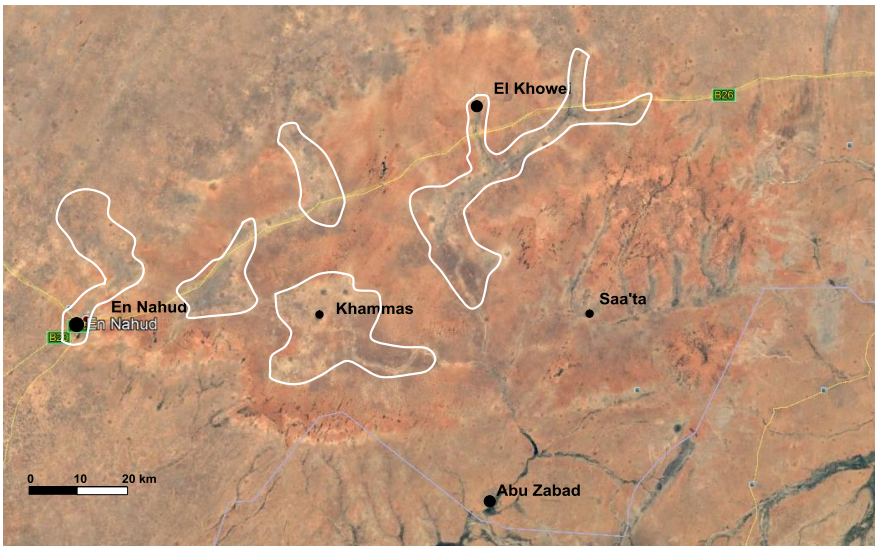


*Fig. 4.34: Location of swamps in the central area.*

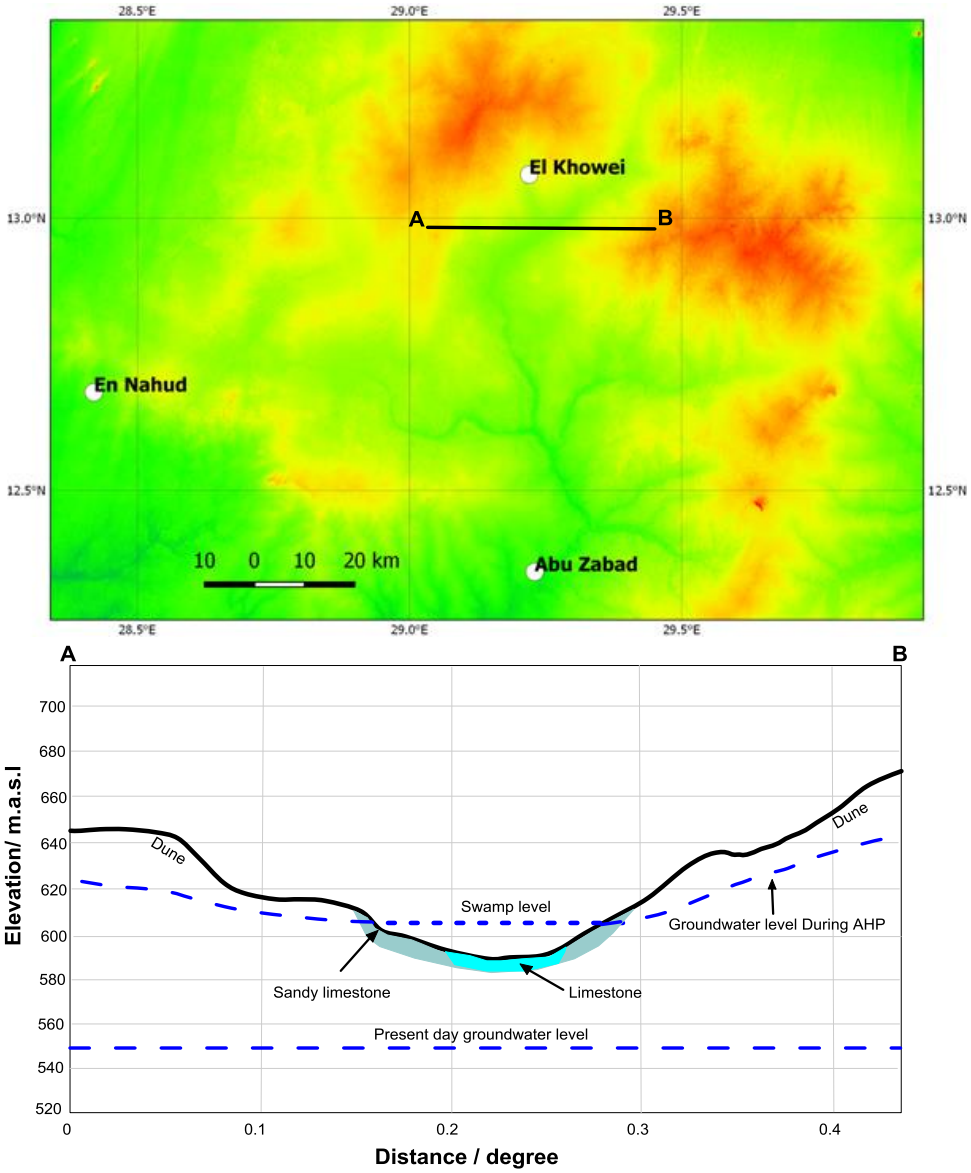


*Fig. 4.35: Topographic profile showing the maximum level of the El Khowei paleoswamp. Note the difference between the present day groundwater table and the one during the African Humid Period.*

On the other hand, deposition of sandy limestone away from the main channel of the wadi, may indicate that the water level of the swamp or wadi was not stable, and fluctuated between two levels; a temporary high level depositing sandy limestone, and a permanent low level where limestone were laid down.

During high water level, the sandy limestone was deposited as a result of the reworking of the pre-existing sediments, or of mixed, aeolian and palustrine deposits. This temporary water level may have lowered down rapidly due to the southward surficial runoff, and to direct infiltration to recharge the groundwater aquifer in the underlying Cretaceous-Paleogene "Nubian sandstone". Since the El Khowei-En Nahud area is a high plateau without feeding river, the groundwater table that controlled the development of swamps was close to the land surface. The present day groundwater level in the En Nahud-El Khowei aquifer ranges between 550 m asl to the North and 470 m asl to the South (Elmansour, 2017), which indicate a southward general flow direction, similar to the surficial flow.

# V. DISCUSSION

## 5.1. Stratigraphy, sedimentology and paleoclimate

The sedimentological and stratigraphic study in the Kordofan region enabled us to reconstruct the following sedimentological and climatic evolution during the terminal Pleistocene-Holocene period, which correlates with the other regional sedimentological and climatic records for the same interval.

### 5.1.1. Period prior to ≈ 10 ka BP

Aeolian deposition took place prior to ≈ 10 ka BP and covered most of the studied area except the southern part. This deposits represent the lower stratigraphic unit in the studied succession. During deposition of this unit, climate was probably dry with intensive aeolian deposition in the central and northern parts of the study area. Due to non-deposition in the southern part, it can be assumed that either the depositional environment was dry associated with aeolian erosion, or it was wet compared to the northern part, the aeolian sediments being removed out by rivers. We correlate this dry, windy period with the 20-12 ka BP time-span, which is known as a period of dune building in the central Sahara, Eastern Sahara, the Nile basin and East Africa (Nicholson and Flohn, 1980; Woodward et al., 2007; Tierney et al., 2011b; Williams et al., 2000; Williams, 2014). Globally, this arid period coincides with the Last Glacial Maximum (LGM) (Woodward et al., 2007). Some hydrological proxies suggest that during most of the LGM, moisture transport from the Indian Ocean was enhanced to easternmost Africa and that wet conditions prevailed in the Challa region (Tierney et al., 2011b). But elsewhere on the African continent, the LGM was typically dry (Gasse, 2000; Gasse et al., 2008). The maximum aridity was probably achieved between 18,000 and 14,000 B.P. when the Sahara invaded the Sahel and moved 400-800 km southward (Bakker and Maley, 1977; Pachur and Kröpelin, 1987; Gasse, 2000). This aeolian activity formed various dune types in Eastern Sahara. Accordingly, barchans and linear dunes are recognized in the Western Desert of Egypt (Hamdan et al., 2014), and longitudinal ridges and transverse dunes are known in the Kordofan region and the Libyan Desert (Edmond, 1942). These longitudinal or linear dunes reflect strong wind energy resulting in widespread dune fields in northern Sudan, extending from latitude 10° N to the South to the Egyptian border the North (Abdu, 1976). During this dry period, the Sahara extended southward over time before most of these dunes were stabilized by vegetation (Warren, 1970).

### 5.1.2. Period between ≈ 10 and ≈ 6 ka BP

Lacustrine, palustrine and fluviatile deposits were recognized in most parts of the study area, dated between ≈ 10 and ≈ 6 ka BP in the northern and central part, and from ≈ 8 to ≈ 3 ka BP in the southern part. During this period, the environment was wet, vegetated across the study area, and locally swampy. This kind of depositional environment have already been reported in several sites across the African continent during the well-known "African Humid Period" (AHP) (DeMenocal and Tierney, 2012) or "lacustrine period" (Williams, 2014). Although much of the references indicate that the AHP lasted from ≈ 12 to 6 ka BP, Shanahan et al. (2015) reported that the real start of this wet conditions began almost everywhere at about 14-15 ka

BP, although maximum humidity was not achieved until the early Holocene because of a return to more arid conditions during the so-called "Younger Dryas" event, which is well recorded in Eastern Africa between 12.8 - 11.6 ka cal BP (Tierney et al., 2011b; Shanahan et al., 2015).

According to previous works, the age of the wet phase varies from one site to another. It has been dated between 11 and 5 ka in North and East Africa (Tierney et al., 2011a), between 9.5 and 4.5 ka BP in NW Sudan (Pachur and Kropelin, 1987; Abell and Hoelzmann, 2000; Pachur and Hoelzmann, 1991), between 9 and 6 ka BP across North Africa (DeMenocal and Tierney, 2012), and between 6.5 and 4.5 ka BP as a second lacustrine phase in the Nile Valley and part of Eastern Sahara (Nicholson and Flohan, 1980). During this period, the present-day hyperarid Saharan desert was vegetated and covered with numerous scattered lakes (Cole et al., 2009) and many development stages of these lakes are generally of the same age (Bakker and Maley, 1977). Most of the lacustrine lakes in northern and northwestern Sudan were dated as early as mid-Holocene: Dry Selima Lake deposits range from 8 820 ± 80 to 5 570 ± 60 yr BP (Abell and Hoelzmann, 2000), West Nubian Palaeolake sediments range from 9 400 to at least 3 800 yr BP (Hoelzmann et al., 2001), and paleolakes formed along the Wadi Howar are dated between 9 500 and 4 500 yr BP (Kröpelin, 1993, *in* Abell and Hoelzmann, 2000).

According to our data, this wet phase lasted in Kordofan at least from ≈ 10 to 6 ka BP in the North and up to 3 ka BP in the South of the studied region. However, the dated samples may not represent the base and top of the palustrine/lacustrine carbonate. In El Ga'ah, the well caved near the village may not have reached the base of the lacustrine deposits, and in the En Nahud area, the erosional surface that caps the palustrine carbonate suggests that the upper part of this limestone has been eroded. Therefore, the ≈ 10 ka BP and ≈ 6 ka BP dates obtained in palustrine limestones near En Nahud do not accurately represent the base and top of the palustrine limestone and therefore, the wet period may have started earlier than ≈ 10 ka BP and may have come to an end after 6 ka BP. Moreover, the lacustrine deposits dated north of the study area at Dry Selima, West Nubian Palaeolake, and Wadi Howar lake, not only support continuity of the wet phase in the central and northern parts of the study area after 6 ka BP, but also according to the starting dates, they provide other evidence that this wet period had started earlier in the Kordofan region than in north-central, northwestern, and northern Sudan. According to the indicated ages, the wet period started in the Kordofan region ≈ 500 year earlier than in Wadi Howar (north-central Sudan), ≈ 600 year earlier than in the West Nubia Palaeolake (NW Sudan), and ≈ 1200 year earlier than in the Dry Selima Paleolake. This information suggests that the AHP did not occur abruptly, neither across the continent nor across the Eastern Sahara, but it occurred gradually through a gradual northward shift of the Inter Tropical Convergence Zone (ITCZ).

Taking in consideration that the lakes of northern Kordofan and those previously studied (Wadi Howar, West Nubia, Selima) are latitudinally arranged. The northern end of the Kordofan lakes is observed up to latitude 14°30′N, Wadi Howar flows from the west to the east between latitudes 16°30′N and 18°30′N, but its greatest part "which contains the lakes" fall at latitude 17°30′N. The center of the West Nubian Paleolake is located approximately at 18°30′N. The dry Selima paleolake is located at 21°23′N. The latitudinal position of these lakes and the known starting time of the wet phase in these lakes will help in the determination of four approximate positions of the northern limit of the northern end of the ITCZ (Fig. 5.1).

The first position of the ITCZ was located between the northern end of the Kordofan lakes and Wadi Howar lakes. The wet phase started in Kordofan at ≈ 10 000 yr BP, and started ≈ 500 yr later in Wadi Howar. That means that at about 9 750 yr BP, the ITCZ was fluctuating around latitude 16°N.

The second position of the ITCZ was between Wadi Howar and the West Nubian Paleolake, since the wet phase occurred at ≈ 9 500 and ≈ 9 400 year BP, respectively, at these two sites. This suggests that at about 9450 yr BP the ITCZ was fluctuating around latitude 17°N.

The third position of the ITCZ was between the West Nubia and the Selima paleolake. The wet phase began at ≈ 9 400 and ≈ 8 800 year BP, respectively, at these two sites. This suggests that at about 9 100 yr BP, the ITCZ was fluctuating around latitude 20°N (Fig. 5.1).

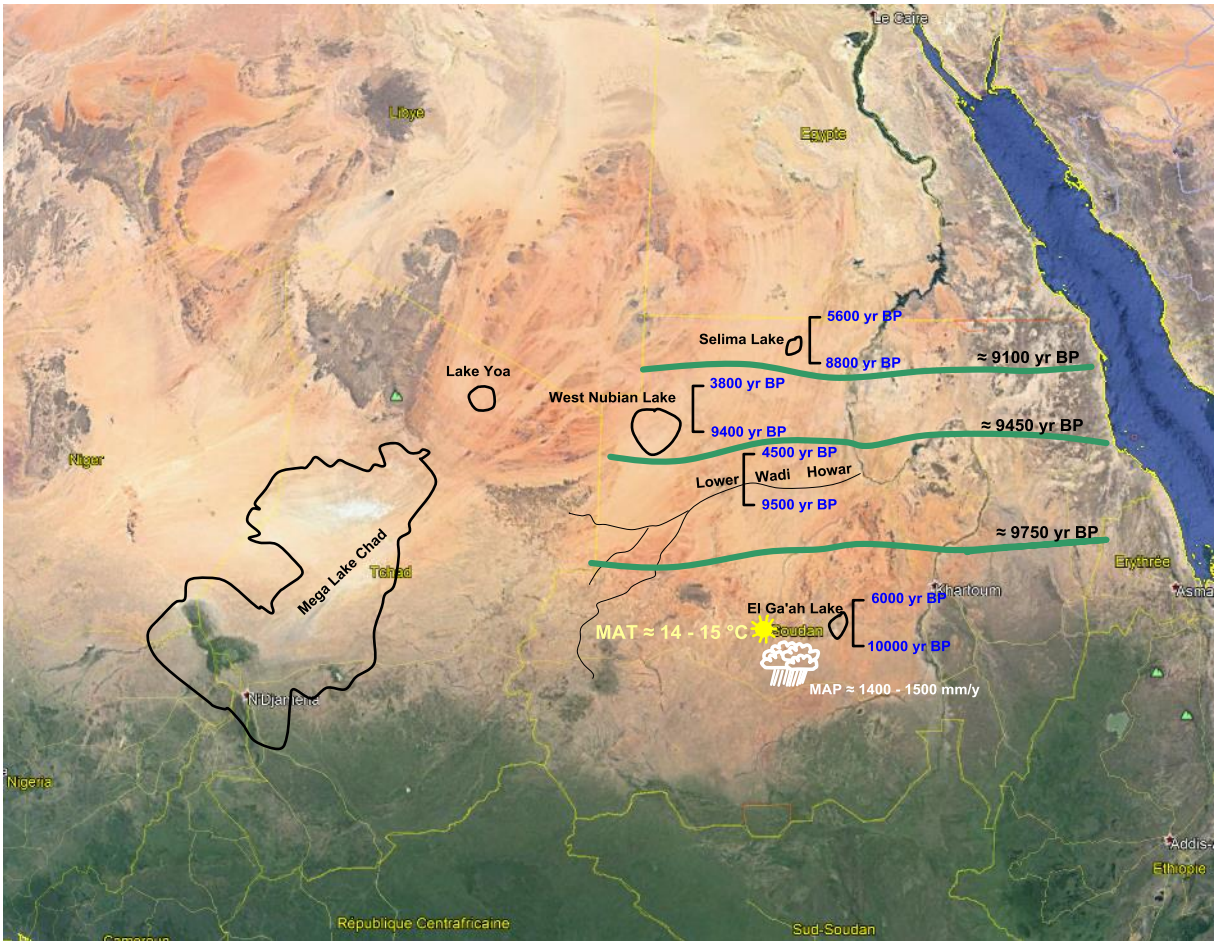


*Fig. 5.1:* ***The northern limit of the rainy belt for different intervals during the African humid period****. The positions of the northern limit of the rainy bilt are based on ages of lacustrine lake sediments of El Ga'ah, Wadi Howar, West Nubia, and Selima Lake. Remark the gradual northward enlargement of the rainy belt. The lower and upper numbers in each lake represent the beginning and the end of AHP, respectively. The estimated mean annual precipitation (MAP) and mean annual temperature (MAT) for the AHP are based on Climofunctions of major elements geochemistry.*

Fluviatile sediments recorded in abundance in the southern part of the study area, and locally as either conglomeratic lenses or as very local delta sediments (El Ga'ah) in other areas, can be correlated with similar deposits or flood events reported throughout the central Sahara during the early Holocene until 6 500 yr BP (Bakker and Maley, 1977). Fluviatile sediments in the

Western Nubian Paleolake are formed of coarse sand to fine-grained gravels mostly of aeolian origin and redeposited by local fluvial transport ≈ 9 000 year BP ago (Hoelzmann et al., 2001). Fluvial sediment input in the northern Red Sea suggests substantially higher rainfall and freshwater runoff in this area between 9.25 and 7.25 ka BP (Arz et al., 2003).

They can be correlated with a series of flood events well documented in the White and Blue Nile Rivers, either as flood, or high water levels during the early to mid-Holocene, which recorded high White Nile levels around 14.7–13.1 ka, 9.7–9.0 ka, 7.9–7.6 ka, 6.3 ka and 3.2–2.8 ka (Williams, 2009). Additionally, peak floods are evident toward 9 500 yr BP and again at 8 500–7 000 yr BP, with less extensive flooding at about 7 000, 5 500, 3 000, 2 700, and 2000–1500 yr BP (Williams and Adamson, 1980).

Since the White Nile is a river originating from lakes Lakes Victoria and Albert, the flood events or high level along the White Nile reflect intensive rainfall around the equator, which leads to an overflow at Lakes Victoria and Albert. Such overflows of Lakes Victoria and Albert are recorded soon after 12 500 BP and brought dramatic and enduring changes to the lower White Nile valley. By 11 500–11 000 BP, the White Nile was up to 5 m higher and 20–40 km wider than today (Williams and Adamson, 1974; 1980). During the flood events in the White Nile, the previously mobile desert dunes became vegetated, and many dunes became wholly or partly buried beneath the fluvio-lacustrine clays (Williams et al., 2000). In the Blue Nile, high flood levels are recorded around 13.9–13.2 ka, 8.6 ka, 7.7 ka and 6.3 ka (Williams, 2009). As a result of overflow between 12 000 and 8 000 yr BP, the White Nile remained high and formed an extensive lake up to 30 km wide or more in addition to other small lakes west of the White Nile (20 km northwest of Jebel Aulia, south of Khartoum) (Williams and Adamson, 1974). This lake dammed by a former sand dune developed during the LGM between 20 and 18 ka ago (Williams et al., 2000). However, such lakes formed close to the White Nile as a result of flooding will not provide the real climate of their sites in Sudan, but instead, they can provide climatic proxies for the equatorial Africa in particular Lakes Victoria and Albert. In contrast the lakes of Northern Kordofan and flood events in Southern Kordofan provide the climatic proxies for Kordofan region itself, due to the local origin of these and of the flooding wadies or seasonal rivers.

North of the Kordofan region, fluviatile and/or alluvial sediments distributed along the lower part of Wadi Howar exhibit gravelly sand, silty fine sand and alluvial sand in addition to local lacustrine marl and chalk (Kröpelin and Soulié-Märsche, 1991). These deposits were laid down between about 9 500 and 4 500 years ago, when the lower Wadi Howar flowed through an environment characterized by numerous ground water outlets and freshwater lakes (Pachur and Kröpelin, 1987). Wadi Howar constituted the largest tributary to the Nile from the Sahara between the Mediterranean Sea and the Atbara River, and it drained a 400 km wide area with present rainfall of 25 mm/year (Pachur and Kröpelin, 1987). Nowadays, Wadi Howar is defunct and its course is only marked by linear tree vegetation, sustained by a ground water table some 6 to 10 m below the surface (Pachur and Kröpelin, 1987).

In some sites in lower Wadi Howar (jebel Rahib), the former river bed is blocked by a 15 m high and 5 km wide dune barrier. Pachur and Kröpelin (1987) reported some flooding events between ≈ 5600 and 7000 yr BP in the eastern part of lower Wadi Howar. Such wadi floods or

overflows also have been reported in some wadies in West Nubia: Wadi Fesh-Fesh in Western Nubia was surrounded by numerous scattered swamps (Pachur and Hoelzmann, 1991).

In the Kordofan region the paleowadi activity, represented by either fluviatile, or palustrine depositional environments, has been recorded in several sites mostly coeval to Wadi Howar and Wadi Fesh-Fesh. This similarity of depositional environment between Kordofan, northern Sudan and Eastern Sahara in general, suggests that the same wet climatic condition was prevailing at the same time, although according to the carbon dating, this wet phase started earlier in the South (older than 10 ka BP.), while in Eastern Sahara this wet phase started around 9.5 ka BP (Pachur and Kröpelin, 1987).

### 5.1.3. Period after ≈ 6 ka BP

Although incomplete, the sedimentary record in the study area, allows to distinguish three main peridos between 6 ky BP and Present times (see Figs. 3.18 and 6.1): a transitional, aridification period (6-3 ky BP), a hiatus corresponding to non deposition or erosion due to strong aeolian activity (3-1 ky BP), and a dry period dominated by aeolian deposits (1-0 ky BP). As a whole, the prolonged hiatus (≈ 6 to ≈ 1 ka BP in the North, ≈ 3 to ≈ 1 ka BP in the South) and the generally dry, windy environment recorded after 1000 yr BP result from the aridification of the climate in the northern part of the study area, the southern parts remaining wetter.

The erosional surface at the top of the palustrine limestone in the En Nahud-El Khowei area suggests that sedimentation did not come to an end at ≈ 6 ka BP. Instead, the apparently 5000 yr lasting hiatus has been probably amplified by significant wind erosion that removed part, or all, sediments deposited between 6 and 3 ka BP in this area. As a matter of fact, considering the relatively narrow latitudinal extension of the study area (about 3.5 latitudinal degrees), it is difficult to consider that in the northern/central part of the study area, the wet phase ended 3000 year age earlier than in the southern parts. Therefore, we shall consider that the trasitional, aridification period occurred between 6 and 3 ky BP in the study area.

This aridification period is correlated with the well-documented aridity that already considerably advanced farther North, in Eastern Sahara by 6 ka BP (Manning and Timpson, 2014; Tierney and deMenocal, 2013). Such aridification is evidenced by (1) the desertification and aeolian deflation during the Middle and Late Holocene (≈ 5.4 ka BP) recorded in Egypt and northern Sudan (Nicoll, 2004); (2) deflation and erosional surfaces recorded in the Western Nubia Paleolake at ≈ 4 ka BP (Pachur and Hoelzmann, 1991); (3) aridification that began in NE Africa at ≈ 6 kyr BP (Jung et al., 2004), and (4) a shift from an earlier predominantly monsoonal climate regime, to one dominated by northern Mediterranean fluxes recorded after 4000 cal yr BP at Lake Yao in Chad (Lézine et al., 2011). Nevertheless, the timing and amplitude of the transition between the "green Sahara" and the present day hyper-arid desert at the end of the AHP is still a matter of debate (Lézine et al., 2011). The drying events stated elsewhere in the Sahara may be explained by fading rainfall at a specific latitudinal position at a certain moment, or by local dropping of groundwater (Kuper and Kropelin, 2006). According to Lézine et al. (2011), the shift from the wet monsoonal climate to the dry one occurred gradually through transitional climatic conditions that lasted from ≈ 5.5 to 2.7 ka BP.

Therefore, the aridification period appears to have occurred earlier at northern latitudes than in southern ones, since it is recorded at ≈ 5.4 ka BP in southern Egypt and northern Sudan, ≈ 4 ka

BP at the West Nubia Paleolake, and ≈ 3 k BP in central-southern Kordofan. Taking in consideration that aeolian erosion removed part of the sediments deposited during the wet or transition periods in Kordofan and West Nubia, this indicates that aridity in these areas was achieved later than these dates. However, this remarkable southward shift of aridity suggests a southward migration of ITCZ, that was moving northward during the AHP. This southward shift of the ITCZ resulted in the narrowing of the tropical rainy belt. The available dates of the aridification period can help in the determination of an approximate positon of the ITCZ (or northern end of the equatorial rainy belt) during the transitional period. The ITCZ was approximately fluctuating around latitude 21°N at ≈ 5.4 ka BP, around latitudes 18 - 19°N (west Nubia) at ≈ 4 ka BP, and around latitudes 13 – 13.5°N at ≈ 3 ka BP.

A period of strong aeolian activity is well recorded in NE Africa between ≈ 5.4 and 2.7 ky BP (see above). In the study area, the beginning of aeolian related hiatus likely did not occur exactly at ≈ 3 ka BP, since part of the former deposits may have been removed. Therefore, the wind erosion may have begun after 3 ka BP. In any case, the wind erosion was stronger in the North than in the South of the study area (Figs. 3.18 and 6.1). Several causes may be invoked to explain this feature : (1) the northern areas are closer to the Saharan wind storms, and thus more exposed to aeolian erosion; (2) assuming that winds were blowing from the North, as indicating by the grain size analysis (section 3.5), the southern areas (South of El Obeid-En Nahud) are located leeward, while the northern areas are located windward (see Fig. 3.39) and are, therefore, more exposed to the wind action; and (3) the southern areas being wetter than the northern ones, the vegetal cover may have limited the erosion.

After the recorded wind-related hiatus (≈ 3-1 ka BP), the climate seems to have been comparable to that of today.

## 5.2. Discussion of the isotopic results

The isotopic composition of the analyzed samples can be correlated with some previous isotopic investigations carried out in Sudan and surrounding areas.

Oxygen isotope values for gastropod shells from the Esh Shawal area (Central Sudan between latitudes 13.5 and 14°N, western bank of the White Nile) range from -0.927‰ to +6.537‰ (PDB) (Williams et al., 2000). These shells were collected at 100-110 cm below the surface and accumulated during the peak of the White Nile palaeolake transgression, at 11 500–11 000 BP (Williams et al., 2000). The isotope results of Esh Shawal gastropods generally tend toward positive values when compared to our isotopic values. The positive isotopic values from the Esh Shawal site suggest that the AHP did not occur in central Sudan before 11 ka BP and consequently, that the arid period known as the period of dune building, was still dominating the climate of Central Sudan west of the White Nile around latitude 13.5°N. This provides more evidences that the wet lacustrine period have started in northern Kordofan between the proposed 10 ka BP (age of our palustrine and lacustrine carbonates) and 11 ka BP (according to oxygen isotope of the Esh Shawal gastropods). However, the entire White Nile flood plain may reflect the climatic conditions of the source area rather than the local climate, therefore, the enriched $\delta^{18}O$ of Esh Shawal area reflect drier condition at the source area (Lake Victoria and Albert)

taking in consideration the evaporation effect along the course of the White Nile, which reduces the lighter oxygen ($^{16}O$).

On the other hand, oxygen stable isotope analysis of 8500 to 7000 yr old gastropods from shallow claypans near Wadi Mansurab in north-central Sudan reveals that the shell carbonate is highly depleted in $\delta^{18}O$ (-5.3‰ to -12.7‰ PDB), with extreme variability up to 6-7‰ PDB (Ayliffe et al., 1996). These variability is interpreted as due to seasonal rainfall regime, characterized by a high degree of inter-annual variability.

Isotope values from shells of the bivalve *Etheria elliptica* (dated 6653 ± 110 yr BP) from Wadi Howar yielded highly depleted $\delta^{18}O$ values (-10‰ to -12‰ PDB) with some variations (Rodrigues et al., 2000). This high depletion and variations in $\delta^{18}O$ are interpreted as due to high seasonality of monsoonal rains (Rodrigues et al., 2000). Such depleted gastropod shells oxygen isotope were also reported by Abell and Hoelzmann (2000) in Selima, North Sudan, and in some paleolakes along Wadi Howar. Moreover, these depleted $\delta^{18}O$ values suggest that north-central and northwestern Sudan (Wadi Mansurab and Wadi Howar) were located within the tropical rain belt, but the variability in these depleted $\delta^{18}O$ values evidences that the seasonal fluctuation of the ITCZ was more erratic, as this period corresponds the late phase of the AHP. In our study, coeval gastropod shells from En Nahud and El Khowei recorded depleted but less variable $\delta^{18}O$ values, compared to those recorded from Wadi Mansurab and from Wadi Howar bivalve shells. This may indicate that the Kordofan region was affected by the ITCZ seasonal fluctuations later than the Wadi Mansurab and Wadi Howar areas, located farther north.

In the Afar region in Ethiopia, freshwater gastropods of early to mid-Holocene age (11 070 ± 160 to 6 670 ± 110 yr BP) recorded $\delta^{18}O$ between -4 to -6 ‰, while modern shells of the same area yielded $\delta^{18}O$ values between -1.5 and + 6 ‰ along the spiral growth (from the aperture to the apex), with most values around -1.5‰ (Abell and Williams, 1989). The depleted $\delta^{18}O$ values of the early to mid-Holocene are interpreted as due to episodes of high rainfall in the Ethiopian highlands, while arid spells produced enriched $\delta^{18}O$ values in the modern shells (Abell and Williams, 1989). Compared to isotopic values of the Ethiopian shells of early to mid-Holocene age, our results suggest that the meteoric water of the Kordofan region was more depleted in $\delta^{18}O$ than that of the Afar region in East Africa. This variation suggests that during the early to mid-Holocene period, either the Kordofan region was wetter than eastern Africa, or, more probably, the latter region received rainfall from a different source. As a matter of fact, the East African rainfalls are mostly influenced by Indian Ocean sea surface temperature variations, while those of West and Central Africa (Shanahan et al., 2015) are mostly of Atlantic origin with probably some influences of the Congo Air Basin. These complex rainfall sources may explain isotopic variations at the same time in different regions, even though the regional climate is comparable.

Studying the isotopic composition of modern African freshwater gastropods, Abell (1985) evidenced variable oxygen isotopic ratios across the continent. Among these samples, those from the surrounding regions of Sudan and the Sahara can help in this discussion. According to Abell (1985), the Congo samples recorded $\delta^{18}O$ values between +2.77 and +2.62‰, Uganda from +4.0 to +1.73‰, and Kenya +3.67 and -3.57‰. To the East, in samples from Ethiopia, $\delta^{18}O$ ranges between -3.58 and -4.4 ‰. One sample from Sudan recorded $\delta^{18}O$ of -3.54 ‰. In

North Africa samples from northeast Egypt range between -6.39 and +2.15‰, around -9.87‰ in Libya, and about -8.38‰ in Algeria. To the west, samples of Nigeria recorded $\delta^{18}O$ between -4.00 and +4.07 ‰. Although samples of Ethiopia, Sudan and Nigeria are approximately from the same latitudinal zone, those from Sudan and Ethiopia are more negative than those of Nigeria. This variation may be due to the variation of the water vapor source, since the Indian Ocean represent the main source of the rainfall in the Ethiopian highland, while in Sudan and Nigeria the rainfall source is from the Atlantic Ocean. However, assuming that the Sudanese and Nigerian rainfall come from the same source, why $\delta^{18}O$ values are negative in Sudan and positive in Nigeria and in other Sahelian countries of West Africa ? These variations may be due the continental or latitude effect, which decreases $\delta^{18}O$ values with increasing distance from the source. Northern Nigeria is about 1500 km from the Atlantic Ocean, while Sudan is more than 3500 km apart from the same ocean. Therefore, the water vapor form the Atlantic Ocean will travel along large distances to reach Sudan, will be precipitated and evaporated repeatedly crossing the Congo Basin, thus depleting the rainfall in the heavier $^{18}O$ isotope. For instance, the meteoric water in Uganda and Southern Sudan has a present-day $\delta^{18}O$ value of about -2‰, while the corresponding value for present-day gastropods in Lake Victoria is +1.5‰ (Williams et al., 2000). On the other hand, the highly depleted North African shells are due to different climate and water rain source, as North Africa is dominated by the Mediterranean Sea climate.

In our case, the variation in $\delta^{18}O$ between the highly depleted values in the shells from the carbonate horizon (Second unit), and the less depleted values of the shells from the upper unit of red sand sediments, may be due the combination of evaporative and temperature effects. Since the gastropod shells analyzed in this study are from the same latitudinal zone, the vertical variation in $\delta^{18}O$ for the same site is only due to climatic changes (evaporation and temperature) through time.

Abell (1985) summarized some problems in the use of stable isotope ratios of gastropod shells as environmental indicators: (1) the shells of most freshwater molluscs are generally aragonite. The aragonite crystal structure is thermodynamically unstable compared to calcite under most ambient conditions (Folk, 1965). Therefore, recrystallization may occur with concomitant isotopic reequilibration with the new environment. (2) Modern gastropods can usually be collected alive, so there is no question of their age, but ancient gastropod shells are often quite robust and can be preserved for millions of years. Reworking of the sediments in which the shells were embedded can produce a mixture of shells of different ages and environments. It is essential to use gastropod shells that give every evidence of being *in situ* (Abell, 1985). (3) The isotopic content of a body of water do not reflect necessarily accurately the local environment as a whole. For example, some species of gastropods can aestivate successfully, and their isotope ratios can reflect highly evaporative conditions such as in temporary irrigation ditches or ephemeral lakes and streams. Such gastropods will have isotope ratios significantly different from gastropods growing in the same locality but in permanent rivers and lakes. In the present study, some anomalies in gastropod shells oxygen isotope may be due to some of these problems. Very negative $\delta^{18}O$ values have been recorded in the East El Khowei section, among less depleted values from the upper unit (aeolian red sand sediments). An acceptable explanation is that the analyzed shell may have been reworked from underlying palustrine unit, which is marked by such depleted value.

Concerning the isotopic composition of the calcareous nodules, our interpretation proposed that the calcareous nodules of the lower unit of the mottled sand sediments and those formed within the second unit in the southern part, were mostly developed during the AHP. Although these nodules formed during this wet phase, their $\delta^{18}O$ values are less depleted than gastropod shells of the same period. Ground water composition has probably a major influence in the development of these calcareous nodules. If so, the isotopic composition of the nodules results from a combination of different isotopic sources that include the initial groundwater, the recharged water during the wet phase, and the evaporative condition during formation of the nodules, which may modify the isotopic composition of the newly recharged water. According to this, the subsurface isotopic composition will differ from the surficial one, in spite of similar climatic condition.

## 5.3. Paleohydrology

The most important and already investigated hydrological features are paleolakes of the Mega Chad Lake (Bouchette et al., 2010), Western Nubia in NW Sudan (Pachur and Hoelzmann, 1991; Hoelzmann et al., 2001), Selima in north Sudan (Abell and Hoelzmann, 2000), some small lakes along Wadi Howar in NW Sudan (Pachur and Kröpelin, 1987) and the 400 km long Wadi Howar paleohydrological network in northwestern Sudan, which linked the mountains of Western Sudan to the Nile (Pachur and Kröpelin, 1987).

Gasse (2000) concluded that the hydrological history of Africa appears to have been a complex alternation of wet and dry episodes with abrupt transitions and sometimes these fluctuations recorded short fluctuation events rapidly followed by a return to initial conditions (Gasse, 2000). Such fluctuations of the water level have been evidenced through structural characteristics of the sediment in the West Nubian Paleolake; temporarily the lake dried up and desiccation cracks formed in the calcareous muds are filled with fragments of lake chalk and carbonate mud (Pachur and Hoelzmann, 1991). In the El Ga'ah Lake (this study), water level fluctuations have been evidenced through two observations: (1) the alternating lacustrine limestone and argillaceous sand sediments beds, which indicate environmental changes (Fig. 3.6); (2) the desiccation features on top of each lacustrine limestone horizon, which indicate drying up of the lake and subaerial exposure of the deposited carbonate mud. Because of dating scarcity, it is difficult to determine correctly the periods of El Ga'ah Lake low level, but two drying up event prior the last drying phase have been observed through the alternation of these sediments.

Although the paleolakes of the Northern Kordofan and the Central Kordofan swamps, and those previously investigated (West Nubian paleolake, Wadi Howar lakes, Maegalake Chad), are all approximately of early-Holocene age, they are marked by some hydrologic variations. The most important variation represent the type or the mechanisms of the precipitation and the kind of the infilling water of these lakes. The West Nubian, Wadi Howar and Megalake Chad are filled up by meteoric water precipitated over mountainous areas of Jebl Marra, Ennedi Mountains and Tibesti Mountain, and their catchment areas are marked by extensive drainage areas, gathering many tributaries. In contrast, the source water of the Kordofan lakes or swamps is only from local precipitation over the surrounding catchment areas of normal reliefs (no mountainous

areas). Mountains usually attract clouds and rains (topographic effect), which is only very partially the case of the North Kordofan lakes. Due to this topographic effect, the high level periods of the West Nubian, Wadi Howar and Chad lakes may have started before, and ended after, the Kordofan lakes. For instance, in spite of subsequent aeolian erosion in Kordofan and West Nubia, the youngest recorded ages of the lakes are ≈ 6 ka BP in Kordofan (14°30'N) and ≈ 3800 yr BP in West Nubia (18-19°N).

Much of the groundwater of the West Nubian paleolake is fossil water and was accumulated during different geological times much wetter than the present-day hyper-arid climate of Eastern Sahara. This basin has an area of ≈ 13 160 $km^2$ and a 1.6 km thick Paleozoic and Mesozoic sedimentary section capable of holding ≈ 1 120 $km^3$ of groundwater if the sediments are completely saturated (Elsheikh et al., 2011). Nowadays, the water table in West Nubia is estimated to be ≈ 50 m deep (Gossel et al., 2004), while in Wadi Howar the groundwater table lays 6 to 10 m below the surface (Pachur and Kröpelin, 1987). Gossel et al. (2004) proposed that groundwater of the Eastern Sahara aquifers was infiltrated during the wet periods 20 000 and 5 000 yr BP ago.

The existence of megalakes in Chad, West Nubia and Selima, of small lakes in Wadi Howar and of the recently discovered lakes in the Kordofan region, all of early to mid-Holocene age, reflect that the hydrological situation was comparable across this region in spite of the previously mentioned topographic effect. The lacustrine-palustrine carbonates deposited in these lakes provide evidences for mostly permanent surficial water bodies and provide an indicator that groundwater table was very shallow (few meters below the surface) in areas surrounding the lakes, and was in direct contact with the water bodies. Since some evidences indicate that the lake levels was fluctuating, the groundwater table was fluctuating too. These fluctuations probably constitute a normal response to the ITCZ fluctuations. Such fluctuations have already been documented in the West Nubian paleolake between 9400 and 3800 $^{14}C$ yr BP (Hoelzmann et al., 2001). Later on, Hoelzmann et al. (2010) recognized that between 10.9 and 8.9 ka BP, the lake was shallow with fluctuating salinity. After about 8.7 ka BP, the lake level rose, water became fresh to oligo-saline, and the lake had a minimum depth of at least 8 m. This record shows that lakes in Eastern Sahara registered short-term climatic events, as long as they were isolated from large-scale artesian groundwater systems (Hoelzmann et al., 2010).

The deepest depression of megalake Chad is less than 200 m in elevation (Bouchette et al., 2010). Four distinct paleo-lake levels have been identified in megalake Chad at 290 m, 300 m, 320 m and 330 m. The water depth, derived from present-day topography of Lake Chad, exceeded 150 m at its deepest part in the central northern sub-basin (Bouchette et al., 2010). The maximum water depth estimated in the West Nubian paleolake between 9400 and 7500 $^{14}C$ yr BP is 15 m (Hoelzmann et al., 2001), while the present groundwater in West Nubia is ≈ 50 m deep (Gossel and Wycisk, 2004; Elsheikh et al., 2011) and its central part is relatively flat with a mean elevation of ≈ 550 m (Elsheikh et al., 2011). In the western part of the lower Wadi Howar, Pachur and Kröpelin (1987) mention a paleolake ("2" in their Fig. 1a, 17°N) about 40 km to the south of the channel of Wadi Howar and of its tributaries, indicating that the water table was there at the surface (545 m asl).

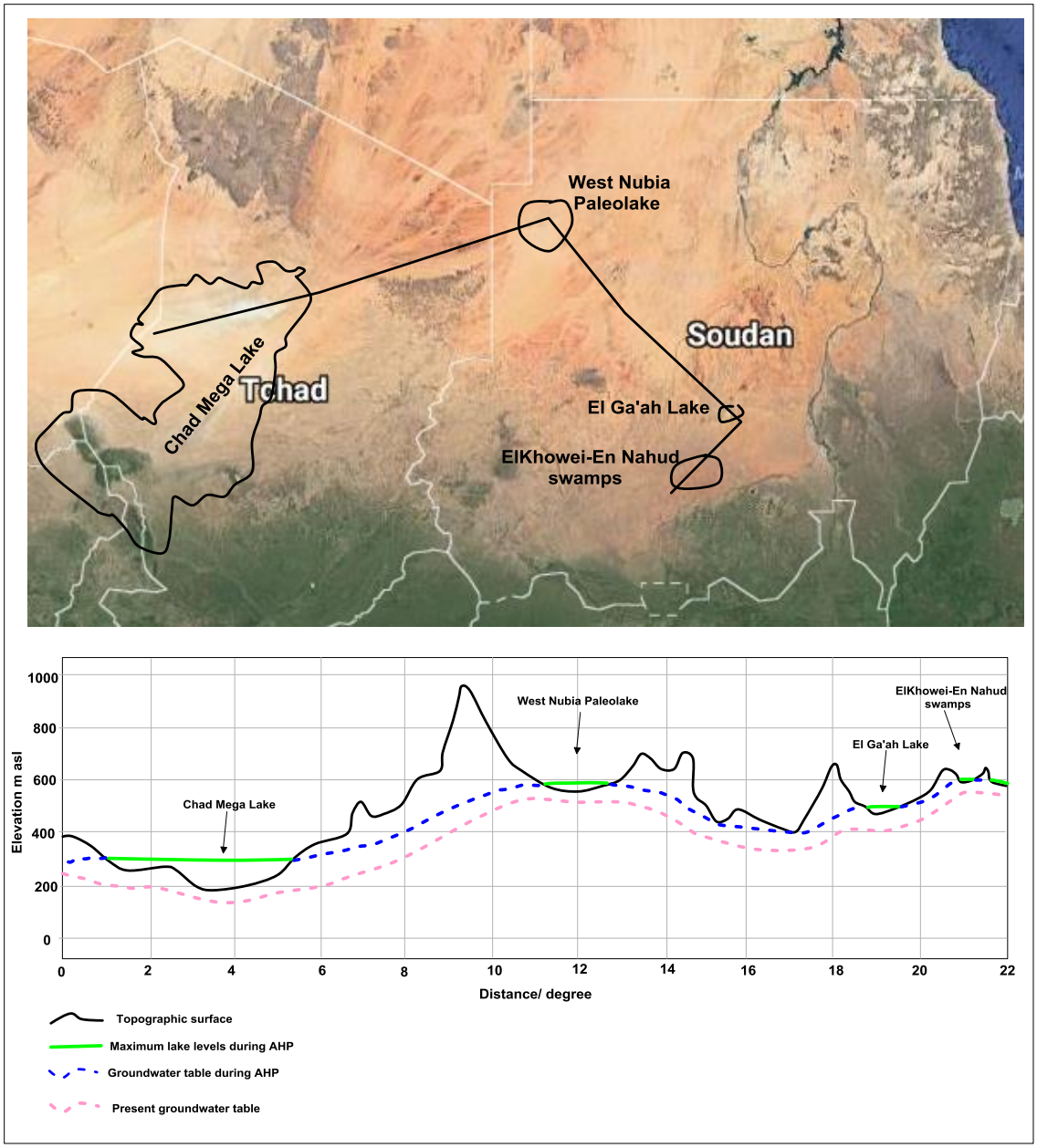


*Fig. 5.2: Profile of Eastern Sahara, showing the reconstructed hydrological situation during the AHP and the present water table.*

The elevation of the deepest part in El Ga'ah Lake is ≈ 450 m asl. Since the only measured maximum shoreline is ≈ 472 m asl, the maximum water depth estimated is about 22 m, and according to a hand-dug well drilled by the local citizens in El Ga'ah, the groundwater table in weathered basement aquifer is about 80 m deep (i.e. 400 m asl). In the El Khowei-En Nahud swamps, the deepest depression is ≈ 590 m asl and the shoreline is estimated at ≈ 610 m asl. According to Elmansour (2017), the present elevation of the groundwater table in En Nahud-El Khowei basin ranges between 550 and 500 m asl. For the latter area, it is noteworthy that they are located on a plateau that dominates surrounding areas and do not receive any significant river. Therefore, the presence, there, of swamps indicates that, at least during the wet season, rainfall were sufficient to allow semi-permanent water bodies to occur.

Hydrological information about these lakes would be very powerful for a paleohydrological reconstruction of Eastern Sahara taking into account megalake Chad, West Nubia, El Ga'ah-Sodari lakes and the El Khowei-En Nahud swamps. A topographic profile has been drawn from Digital Elevation Model along a total distance of ≈ 2200 km, showing the maximum lake levels, the groundwater table during the AHP, and the present groundwater table (Fig. 5.2.). The very high lake level at Megalake Chad, the relatively high lake level in the West Nubia and El Ga'ah lakes, and the remarkable groundwater table raise during the AHP provide clear evidence that Eastern Sahara experienced abundant rainfall during the AHP, and that the region may have remained during about 4000 year (10-6 ka BP) within the tropical rainy belt.

## 5.4. Archeology

The lake stages and environmental condition in the Western Nubian Paleolake correlate well with the distribution of early human settlements, characterized by dotted wavy-lines pottery dated between 6300 and 3500 $^{14}C$ yr BP (Hoelzmann et al., 2001). Such dotted wavy line potteries have a wide distribution west of the Nile across the Sahara-Sahel Belt (Mohammed-Ali, 2003) and have been observed in several sites along Wadi Howar (Jesse, 2007). In the present study, the existence of some archeological remnants (potteries, grinding stones, cutting tools, etc) on the northwestern shoreline of El Ga'ah Lake and El Firja depression lake (North of Sodari), provides good evidences that these lakes developed at the same time as the West Nubian and Wadi Howar paleolakes, and that they experienced similar human settlements. The latter are controlled by several factors, but hydrology and climate are the most important controlling factors on the distribution these archeological sites, since the density of human population in Africa is primarily regulated by the availability of water (Gasse, 2000). Moreover, we found historic potteries (Merowetic and Islamic eras) associated with the Neolithic dotted wavy-lines potteries around the El Ga'ah and El Firja lakes. The fact that such historic potteries are not reported from the Western Nubia and Wadi Howar lakes, suggests that these lakes dried up before the beginning of these historic era. On the other hand, this may provide evidence of the southward human migration as a dynamic response to the southward shift of the rainy belt after the late AHP, as documented by Kuper and Kröpelin (2006).

## 5.4. Grain size and Major elements geochemistry

As presented in the results of major elements geochemistry (4.4.1), the ratio of $SiO_2$ to $Al_2O_3$ is modrately high in both sections of North Bara3 and West El Obeid, with little variability along both the Lower unit (mottled sand facies) and the Upper unit (red sand facies). This moderately high ratio is interpreted as due to the domination of silicate minerals. Figs. 5.3 and 5.4 represent a comparison between the mean grain size and the $SiO_2$ /$Al_2O_3$ ratio for the two sections. It appears that the mean grain size is within the range of sand : medium sand and fine sand at North Bara3 and West El Obeid, respectively. The sandy nature of the Lower and Upper units is in good agreement with the $SiO_2$/$Al_2O_3$ ratio, which evidences a high $SiO_2$ content. These data strongly suggest aeolian deposition in an arid environment for both units.

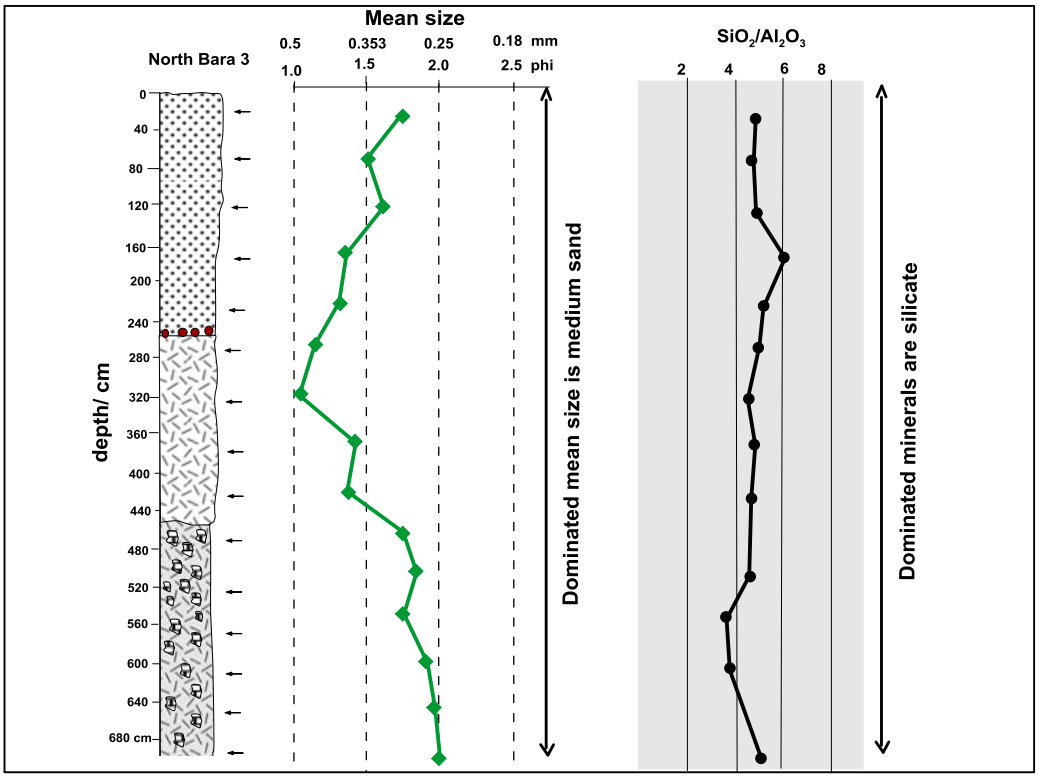


*Fig. 5.3: Mean grain size and $SiO_2/Al_2O_3$ plots for the North Bara3 section.*

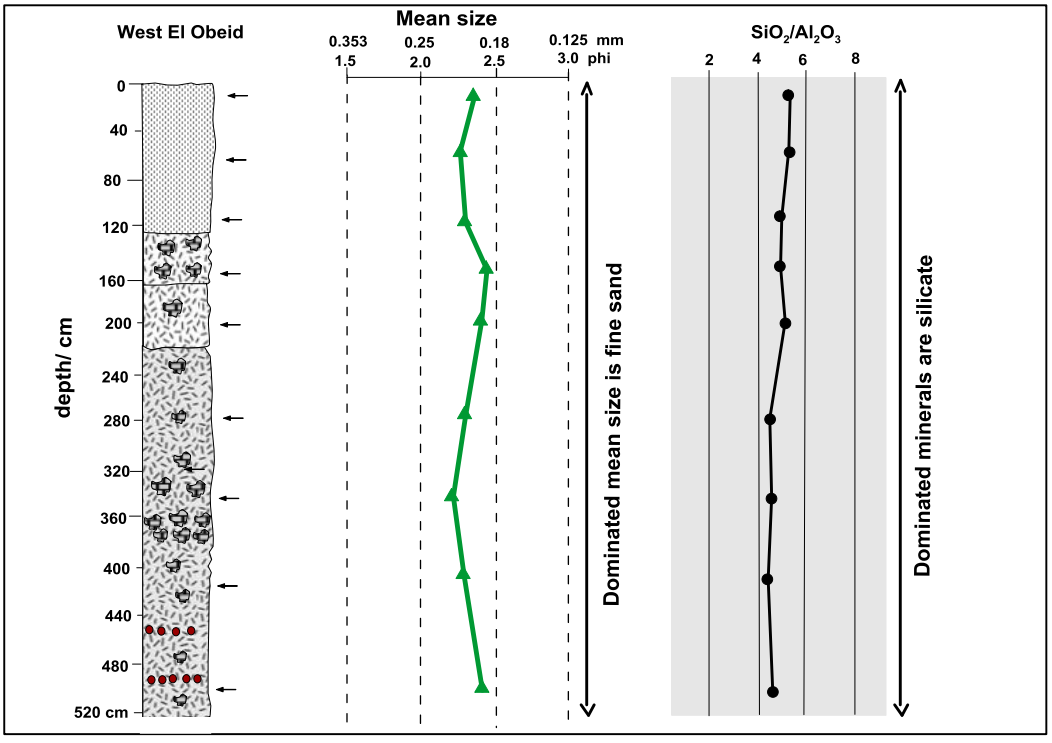


*Fig. 5.4: Mean grain size and $SiO_2/Al_2O_3$ plots for the West El Obeid section.*

# VI. CONCLUSION

## 6.1. Summary

Primary observations on temporal and spatial variations of the sedimentological records in the study area suggest that the Kordofan region has been submitted to significant climatic and environmental fluctuations.

The sedimentological and stratigraphic investigations allowed to distinguish eight different sedimentological facies belonging to four stratigraphic units. The identified facies are: mottled sand or silty sand, lens shaped conglomerate, alternating sand and silts, sandy carbonate, carbonate, argillaceous sand, red sand facies, and clinoform bearing, coarse clastic facies.

Carbon dating permitted to date the stratigraphic units and therefore, to correlate them and to establish the succession of sedimentological and climatic events that occurred in the terminal Pleistocene to Holocene period.

Sedimentological variations, sub-fossil contents, sedimentary and pedogenetic features were used to reconstruct the depositional environments, sedimentary evolution and the evolving paleogeography in the study area.

The sedimentology, palynology, gastropod sub-fossil shells paleontology, stable isotopes, major elements geochemistry, and clay mineralogy were used as proxies to reconstruct the paleoclimatic evolution of the study area throughout the latest Pleistocene-Holocene period.

These studies made it possible to place the resulting paleoclimatic reconstruction in the context of the climatic evolution of the East Saharan Region.

## 6.2. Main results

The sedimentological and paleoclimate results are summarized in figure (6.1). The main findings of this study are:

- Prior to ≈ 10 ka BP, the depositional environment was dominated by aeolian activities, and the climate seems to have been arid to hyper-arid.
- Between ≈ 10 and ≈ 6 ka BP, the northern part of the study area was marked by lacustrine/palustrine depositional environment and the climate was humid. In the southern part of the area, this humid period may have extended until ≈ 3 ka BP and the sedimentation was dominated by fluviatile deposits.
- Between ≈ 6 and ≈ 1 ka BP, the northern part of the area was marked by a non-deposition period, interpreted as a hiatus due to strong aeolian activity preventing deposition and causing erosion, associated with an arid climate. Meanwhile, the southern area was wetter than the northern one, and the hiatus lasted from ≈ 3 ka BP to ≈ 1 ka BP.
- After ≈ 1 ka BP, the depositional environment was dominated by aeolian activity in the North, while the southern part was dominated by both aeolian and fluviatile processes. Consequently, the climate was generally dry but wetter to the South.

- The correlation of this results with some similar climatic studies in the Eastern Sahara indicates that these climatic changes resulted in gradual northward movement of the northern limit of the tropical rainy belt during the AHP.
- During the aridification period that followed the AHP, the climatic change resulted in the gradual southward shift of the rainy belt and of the ITCZ.

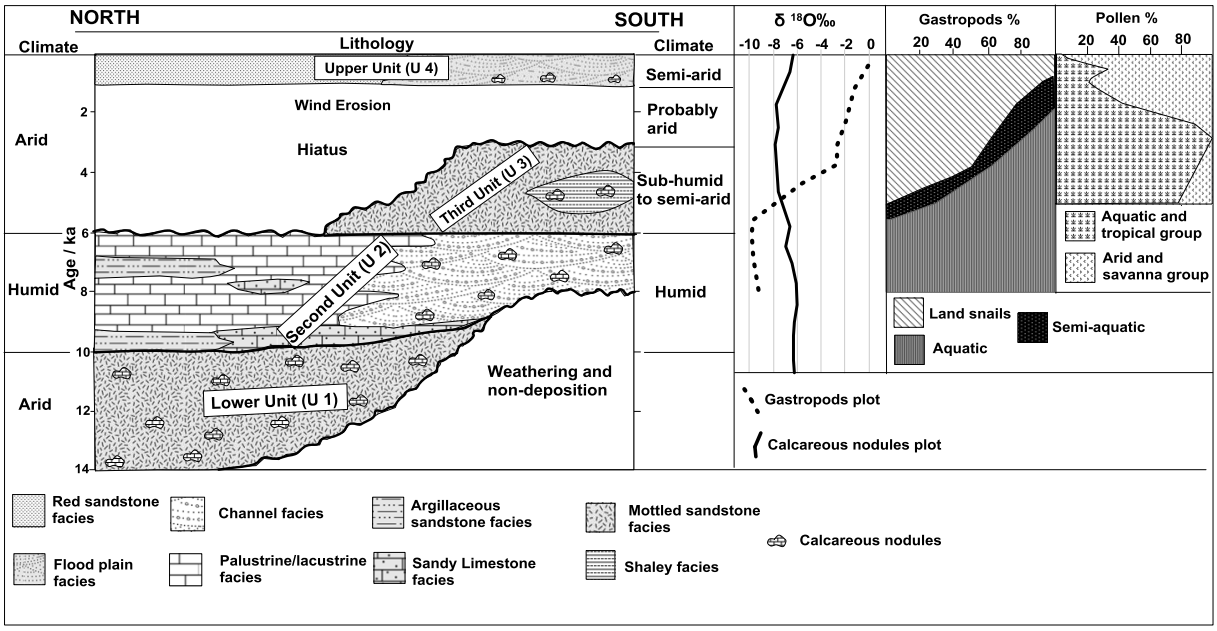


*Figure 6.1: Synthesis of the sedimentary and climatic evolution of the study area since 14 ky BP.*

## 6.3. Perspectives

The reconstruction of the sedimentary and paleoclimatic evolution of the Kordofan region in late Pleistocene-Holocene times is the first attempt in this area. Despite the fact that the final output of this study provided very valuable information about the sedimentary and climatic evolution in this region in particular and Eastern Sahara in general, there is great potential for further work to be conducted in this region and its surroundings for a better understanding of this evolution. The future work that may be done include the following points:

- The actual dates and duration of the African Humid period should be specified, in order to reconstruct the movements of the ITCZ. This requires more dating of the base and top of the lacustrine/palustrine facies, and more survey of the overlying deposits, in order to specify the age of the wind-related hiatus that followed the AHP.
- In spite of the lack of organic matter in the red sand facies, dating the base of this facies would help specifying the age of the end of the preceding hiatus. An alternating dating method, such as Luminescence dating will provide some clues to fix the dating problems of such kind of oxidized sediments.
- Since this study mainly dealt with pollens of the southern areas, additional palynological investigation might be carried out in other parts of the Kordofan region to build a wider palynological record and, combined with chronological dates, to refine the paleoenvironmental and paleoclimatic reconstructions.

- Paleobiology of gastropods combined with the Chemical Index of Alteration (CIA), seems to be a promising and effective tool to assess the mean annual rainfalls experienced by a region, and thus to constrain the paleohydrological regime of the area.
- Systematic analysis of oxygen isotope should be done on individual gastropod shells along the spiral growth line (from the apex to aperture) to determine whether the wet and dry episodes, are due to mere seasonality or to ITCZ fluctuations.
- Intensive archeological investigations are very important to be achieved across the region, particularly around the shorelines of the northern lakes of El Ga'ah and Sodari and around the En Nahud – El Khowei swamps. Such investigations will improve the understanding of the climate-human settlement relations.
- More regionally, climatic studies in the eastern Sudan will help to determine whether the Eastern monsoon of the Indian Ocean hade any influences on the precipitation pattern in this part of Sudan, or if the Ethiopian highlands prevent moisture to cross further West, the Kordofan region remaining dominated by the southwesterly moisture from the Atlantic Ocean and the Congo Basin.

## REFERENCES


Abdel Galil, M. Y., 2008. Geology and Mineralization related to anorogenic igneous complex of Northern Nuba Mountains and Northern Kordofan, Sudan. PhD Thesis, Al Neelain University, Sudan.

Abdu, A., 1976. The Crescentic dunes of northern Sudan. East African Geographical Review 14, 61-71.

Abell, P., Williams, M. 1989. Oxygen and carbon isotope ratios in gastropod shells as indicators of paleoenvironments in Afar region of Ethiopia. *Palaeogeography, Palaeoclimatology, Palaeo-ecology, 74, 265-278.*

Abell, P.I., 1985. Oxygen isotope ratios in modern African gastropod shells: A data base for paleoclimatology. Chemical Geology (Isotope Geoscience Section) 58, 183-193.

Abell, P.I., Hoelzmann, P., 2000. Holocene palaeoclimates in northwestern Sudan: stable isotope studies on molluscs. Global and Planetary Change, 26, 1–12.

Adams, J.S., Kraus, M.J., Wing, S.L., 2011. Evaluating the use of weathering indices for determining mean annual precipitation in the ancient stratigraphic record. Palaeogeography, Palaeo-climatology, Palaeoecology 309, 358–366.

Alonso-Zarza, A.J., Jones, B.J., 2007. Root calcrete formation on Quaternary karstic surfaces of Grand Cayman. Geologica Acta 5, 77–88.

Alonso-Zarza, A.M., 2003. Palaeoenvironmental significance of palustrine carbonates and calcretes in the geological record. Earth Science Reviews 60, 261–298.

Alonso-Zarza, A.M., Genise, J.F., Verde, M., 2011. Sedimentology, diagenesis and ichnology of Cretaceous and Palaeogene calcretes and palustrine carbonates from Uruguay. Sedimentary Geology 236, 45–61.

Alonso-Zarza, A.M., Wright, V.P., 2010. Calcretes. In: Alonso-Zarza, A.M., Genise, J.F., Verde, M., 2011. Sedimentology, diagenesis and ichnology of Cretaceous and Palaeogene calcretes and palustrine carbonates from Uruguay. Sedimentary Geology 236, 45–61.

Al-Safadi, M.M., 1990. Freshwater molluscs of Yemen Arab Republic. In: IUCN, 2017. *The IUCN Red List of Threatened Species: Radix natalensis.*

Arakel, A.V., 1996. Quaternary vadose Calcretes revisited. Journal of Australian Geology & Geophysics, 16 (3), 223- 229.

Arz, H.W., Frank Lamy F., Pätzold, J., Müller, P.J., Prins M., 2003. Mediterranean Moisture Source for an Early-Holocene Humid Period in the Northern Red Sea. Science 300, 118-121.

Ayliffe, D., Williams, M., Sheldon, F. 1996. Stable carbon and oxygen isotopic composition of early-Holocene gastropods from Wadi Mansurab, north-central Sudan. The Holocene 6, 157-169.

Bagnold, R.A., 1956. In: Visher, G., 1969. Grain size distributions and depositional processes. *Journal of Sedimentary Petrology, 39, 3*, 1074 – 1106.

Bakker, E. M., Maley, J., 1977. Late Quaternary Palaeoenvironments of the Sahara Region. A.A. Balkema-Rotterdam, Orstom Fond Documentaire, Palaeoclimatology of Africa and the surrounding Islands, Vol. 11.

Berke, M. A., Johnson, T. C., Werne, J. P., Schouten, S., Sinninghe Damsté J.S., 2012. A mid-Holocene thermal maximum at the end of the African Humid Period. Earth and Planetary Science Letters 351–352, 95 –104.

Bishop, M.J. 1979. A new species of *Caracolus* (Pulmonata: Camaenidae) from the Oligocene of Nebraska and the biotic history of the American camaenid land snails. *Zoological Journal of the Linnean Society*, 67, 269-284.

Boggs, S., 2006. Principle of Sedimentology and Stratigraphy (4th ed.), Prentice-Hall, New Jersey, 662 p.

Bolaji, D.A, Edokpayi, C.A., Samuel, O. B., Akinnigbagbe, R.O., Ajulo, A.A., 2011. Morphological characteristics and Salinity tolerance of *Melanoides tuberculatus* (Muller, 1774). *World Journal of Biological Research 4(2)*, 1-11.

Bouchette, F., Schuster, M., Ghienne, J., Denamiel, C., Roquin, C., Moussa, A., Marsaleix, P., Duringer, P., 2010. Hydrodynamics in Holocene Lake Mega-Chad. Quaternary Research 73, 226–236.

Bradley, R.S., 1989. Recent Developments in Quaternary Paleoclimatology. Kluwer Academic Publisher, Climate and Geoscience, 165-171.

Brown, D. S., Fison, T., Southgate, V. R., Wright, C. A., 1984. Aquatic snails of the Jonglei region, southern Sudan, and transmission of trematode parasites. *Hydrobiologia 110*, 247-271.

Brown, D. S., Rollinson, D., 1982. The southern distribution of the freshwater snail *Bulinus truncatus.* In Brown, D. S., Fison, T., Southgate, V. R., Wright, C. A., 1984. Aquatic snails of the Jonglei region, southern Sudan, and transmission of trematode parasites. *Hydrobiologia 110*, 247-271.

Brown, D.S., Gallagher, M.D. 1985. Freshwater snails of Oman, South Eastern Arabia. In: IUCN, 2017. *The IUCN Red List of Threatened Species: Radix natalensis.* Assessment by: Van Damme, D.

Brown, D.S., Wright, C.A. 1980. Molluscs of Saudi Arabia, freshwater molluscs. In: IUCN, 2017. *The IUCN Red List of Threatened Species: Radix natalensis.* Assessment by: Van Damme, D.

Chambers, F.M., van Geel, B., van der Linden, M., 2014. Considerations for the preparation of peat samples for palynology, and for the counting of pollen and non-pollen palynomorphs. *Mires and Peat* 7, 1 – 14.

Chen, X.Y., Lintern, M.J., Roach I.C., 2002 (eds.), Calcrete characteristics, distribution and use in mineral exploration. Cooperative Research Centre for Landscape Environments and Mineral Exploration, Perth, Western Australia, 160 p.

Chiaghanam, O.I., Chiadikobi, K.C., Ikegwuonu, O.N. Omoboriowo, A.O, 2014. Palynology, Source Rock Potential and Thermal Maturity of Eocene Nanka Formation (Ameki Group) In Anambra Basin: An Investigation of Agulu Lake, South-Eastern Nigeria. Journal of Applied Geology and Geophysics 2/5, 87-97.

Ciolkosz, E.J., Dobos, R.R., 1990. Color and mottling in Pennsylvania soil. Agronomy series number 108. The Pennsylvania state university.

Cole, J.M., Goldstein, S.L., deMenocal, P.B., Hemming, S.R., Grousset, F.E., 2009. Contrasting compositions of Saharan dust in the eastern Atlantic Ocean during the last deglaciation and African Humid Period. Earth and Planetary Science Letters 278, 257-266.

Collier, P., Conway, G., Venables, T., 2008. Climate change and Africa. Oxford Review of Economic Policy 24 (2), 337–353.

Creese, A., Pokam, W., 2016. Central Africa's climate system. In: Future Climate for Africa - Africa's climate: Helping decision-makers make sense of climate information. Report of a project funded by the UK Department for International Development (DFID) and the Natural Environment Research Council (NERC) for the developing countries and the advance of scientific research.

Dávalos-Álvarez, O.G., Nieto-Samaniego, Á.F., Alaniz-Álvarez, S.A., Martínez-Hernández, E., Ramírez-Arriaga, Y.E., 2007. Estratigrafía cenozoica de la región de Tehuacán y su relación con el sector norte de la falla de Oaxaca. *Revista Mexicana de Ciencias Geológicas 24 (2), 197-215.*

Dawelbeit, A., 2010, Hydrogeological Evaluation of Sug'a El Jamal Basin, North Kordofan State, Sudan. M.Sc. Thesis, University of Kordofan, Sudan.

de Kock, K.N., Wolmarans, C.T., 2009. Distribution and habitats of *Melanoides tuberculata* (Müller, 1774) and *M. victoriae* (Dohrn, 1865) (Mollusca: Prosobranchia: Thiaridae) in South Africa. *Water SA 35(5)*, 713-720.

de Kock, K.N., Wolmarans, C.T., Bornman, M., 2004. Distribution and habitats of *Biomphalaria pfeifferi*, snail intermediate host of *Schistosoma mansoni*, in South Africa. *Water SA 30*, 29 -36.

Dehghani, M., Akhani, H., 2009. Pollen morphological studies in subfamily Suaedoideae (Chenopodiaceae). *Grana 48*, 79 – 101.

deMenocal, P. B., Tierney J. E., 2012. Green Sahara: African Humid Periods paced by Earth's orbital changes. Nature Education, Knowledge 3.

deMenocal, P., Ortiz, J., Guilderson, T., Adkins, J., Sarnthein, M., Baker, L., Yarusinsky M., 2000. Abrupt onset and termination of the African Humid Period: rapid climate responses to gradual insolation forcing. Quaternary Science Reviews, 19, 347-361.

Demske, D., Tarasov, P.E., Nakagawa, T., Suigetsu 2006. Project Members, 2013. Atlas of pollen, spores and further non-pollen palynomorphs recorded in the glacial-interg laciallate Quaternary sediments of Lake Suigetsu, central Japan. *Quaternary International 290-291*, 164-238.

Dobos, R.R., Ciolkosz, E.J., Waltman, W.J., 1990. The effect of organic carbon, temperature, time, and redox conditions on soil color. In Ciolkosz, E.J., and Dobos, R.R., 1990. Color and mottling in Pennsylvania soil. Agronomy series number 108. The Pennsylvania state university.

Dupouy, J., Rousseau, D., Dussart, G., Liaud, M.V., Nassi, H., 1993. Correspondence analysis of shell morphology in the African freshwater snail *Bkomphalaria pfeiierk* (Kraus 1848) (Pulmonata: Gastropoda. *Biological Journal of the Linnean Society 50,* 329-338.

Edmond J. M. (1942). The Distribution of the Kordofan Sands "Anglo-Egyptian Sudan". Geol. Magazine, 79 (1), 18-30.

Edwards, D.N., 2007. The archeology of Sudan and Nubia. *Annual Review of Anthropology* 36, 211-28.

Eisawi, A., Schrank, E., 2008. Upper Cretaceous to Neogene palynology of the Melut basin, southeast Sudan. *Palunology 32,* 101 – 129.

El Ghazali, G.E.B., 1993. A study of pollen flora of Sudan. *Review of Palaeobotany and Palynology* 76, 99-345.

El Shafie, A. A. I., Zeinelabdein, K. A. E., Eisawi, A. A. M., 2011. Paleoclimatic evolution of central Sudan during the Late Miocene to Pleistocene. Saudi Society for Geosciences, Arab J Geosci, DOI 10.1007/s12517-011-0435-z.

El-Amier, Y.A., 2015. Morphological studies of the pollen grains for some hydrophytes in coastal Mediterranean lakes, Egypt. *Egyptian Journal of basic and applied Sciences 2*, 132-138.

Elhadi, M., 2012. Assessment and evaluation of the Water-bearing formations in central-north Kordofan and West White Nile States, Sudan. PhD thesis. El Neelain University.

Elhag, A.B., Elzien, S.M., 2013. Structures controls on groundwater occurrence and flow in crystalline bedrocks: a case study of the El Obeid area, Western Sudan. Global Advanced Research Journal of Environmental Science and Toxicology, 2, 37-46 (ISSN: 2315-5140).

Elmansour, A.A., 2017, Assessment of the groundwater of En Nuhud basin, West Kordofan State-Sudan. Doctoral thesis, University of West Kordofan.

Elmansour, A.A., Omer, O.A., 2017. Crustal architecture, geodynamics and evolution of En Nuhud basin area, Kordofan region, Sudan. International Jurnal of advanced Geoscience 5 (2), 121 – 132.

Elsheikh, A., Abdelsalam, M.G., Mickus, K., 2011. Geology and geophysics of the West Nubian Paleolake and the Northern Darfur Megalake (WNPL–NDML): Implication for groundwater resources in Darfur, northwestern Sudan. Journal of African Earth Sciences, 61, 82–93.

Fact sheet no. 3. 2009. Organic matter decline. Sustainable agriculture and soil conservation (SoCo). European Communities.

Fadipe, O.A., Carey, P.F., Adekola, S.A., 2011. Provenance, diagenesis and reservoir quality of the lower Cretaceous sandstone of the Orange basin, South Africa. South African Journal of Geology 114 (3-4), 433-448.

Faegri, K., Iversen, J., 1989. Textbook of Pollen Analysis, 4th ed. John Wiley & Sons, Chichester. In Quick, L.J., 2013. Late Quaternary palaeoenvironments of the southern Cape, South Africa: palynological evidence from three coastal wetlands. PhD thesis. University of Cape Town, South Africa.

Fairbanks, R.G., Mortlock, R.A., Chiu, T.-C., Cao, L., Kaplan, A., Guilderson, T.P., Fairbanks, T.W., Bloom, A.L., Grootes, P.M., Nadeau, M.-J., 2005. Radiocarbon calibration curve spanning 0 to

50,000 years BP based on paired $^{230}Th/^{234}U/^{238}U$ and $^{14}C$ dates on pristine corals. Quaternary Science Reviews 24, 1781-1796.

Faure, G., Mensing, T.M., 2005. Isotopes: principles and applications (3rd edition). John Wiley & Sons, Inc., Hoboken, New Jersey, 897 p.

Ferry, B., Eglin, T., Bispo, A., Dambrine, É., Chenu, C., 2014. Soil organic matter of forests and climate and atmosphere changes (*English translation of: « Matières organiques des sols forestiers et changements climatique et atmosphérique »).*

Filatoff, J., 1975. Jurassic palynology of the Perth Basin, Western Australia. Palaeontographica Bd. 154 Abt. B.

Foerster, V., Junginger, A., Langkamp, O., Gebru, T., Asrat, A., Umer, M., Lamb, H.F., Wennrich, V., Rethemeyer, J., Nowaczyk, N., Trauth, M.H., Schaebitz, F., 2012. Climatic change recorded in the sediments of the Chew Bahir basin, southern Ethiopia, during the last 45,000 years. Quaternary International 274, 25 – 37.

Folk, R. L., Ward, W. C., 1957. Brazos River Bar: a study in the significance of grain size parameters. *J. Sediment. Petrol.,* 27, 3-26.

Folk, R., 1974. Longitudinal dunes of the northwestern edge of the Simpson Desert, northern Territory, Australia, 1. Geomorphology and grain size relationships. Sedimentology 16, 5-54.

Freytet, P., 1973. Petrography and paleo-environment of continental carbonate deposits with particular reference to the Upper Cretaceous and Lower Eocene of Languedoc (Southern France). Sedimentary Geology 10, 25 – 60.

Freytet, P., Plaziat, J., Verrecchia, E.P., 1997. A classification of rhizogenic (root-formed) calcretes, with examples from the Upper Jurassic-Lower Cretaceous of Spain and Upper Cretaceous of southern France – Discussion. Sedimentary geology 110, 299 – 303.

Freytet, P., Verrecchia, E.P., 2002. Lacustrine and palustrine carbonate petrography: an overview. *Journal of Paleolimnology* 27, 221–237.

Gasse, F., 2000. Hydrological changes in the African tropics since the Last Glacial Maximum. Quaternary Science Reviews, 19, 189-211.

Gasse, F., Chalié, F., Vincens, A., Williams, M.A.J., Williamson, D., 2008. Climatic patterns in equatorial and southern Africa from 30,000 to 10,000 years ago reconstructed from terrestrial and nearshore proxy data. Quaternary Science Reviews, 27, 2316–2340.

Geotechnica, 1985. Elobeid Water Supply Project, Feasibility study of Groundwater Resources, Master Report. National water Administration, Ministry of Energy and Mining. Khartoum, Sudan.

Gilmore, S., Hill, K.D., 1997. Relationships of the Wollemi Pine (*Wollemia nobilis*) and a molecular phylogeny of the Araucariaceae. *Telopea 7(3)*, 275 – 291.

Ginaya, M. A., Elkrail, A., Farawa. A., 2013. Numerical Modelling of the Groundwater flow in Ennahud Basin, Northern Kordofan – Sudan. Research and Applications (IJERA), 3, 217-222.

Ginaya, M.A., 2011. Updating of Groundwater Conditions of Ennahud Basin - North Kordofan, Sudan. Ph.D. Thesis, Institute for Energy & Earth Sciences, Ministry of Sciences & Technology, Sudan.

Goji, T.C., Ayodele, A.E., 2005. Foliar epidermal and Pollen Characters in the genus *Cola* Schott. & Endl. in Nigeria. *Acta Satech 2*, 57 – 63.

Goodfriend, G.A., Magaritz, M., Gat, J.R., 1989. Stable isotope composition of land snail body water and its relation to environmental waters and shell carbonate. *Geochimica et Cosmochimica Acta 53*, 3215-3221.

Gosling, W.D., Miller, C.S., Livingstone, D.A., 2013. Atlas of the tropical West African pollen flora. Review of Palaeobotany and Palynology 199, 1–135.

Gossel, W., Ebraheem, A.M., Wycisk, P., 2004. A very large scale GIS-based groundwater flow model for the Nubian sandstone aquifer in Eastern Sahara (Egypt, northern Sudan and eastern Libya). Hydrogeology Journal12, 698–713.

Hamann, Y., Ehrmann, W., Gerhard Schmiedl, G., Kuhnt, T., 2009. Modern and late Quaternary clay mineral distribution in the area of the SE Mediterranean Sea. Quaternary Research 71, 453–464.

Hamdan, M.A., Refaat, A.A., Abu Anwar, E., Shallaly, N.A., 2014. Source of the aeolian dune sand of Toshka area, southeastern Western Desert, Egypt. Aeolian Research 17, 275– 289.

Hassan, F., 1986. Chronology of the Khartoum 'Mesolithic' and 'Neolithic' and related sites in the Sudan: statistical analysis and comparisons with Egypt. *The African Archaeological Review* 4, 83-102.

Hesse, M., Zetter, R., 2007. The fossil pollen record of Araceae. Plant Systematics and Evolution 263, 93-115.

Hewaidy, A., Elshahat, O.R., Kamal, S., 2018. Stratigraphy, facies analysis and depositional environments of the Upper Unit of Abu Roash "E" member in the Abu Gharadig field, Western Desert, Egypt. Journal of African Earth Sciences 139, 26-37.

Hill, C.L., 2001. Geologic Contexts of the Acheulian (Middle Pleistocene) in the Eastern Sahara. Geoarchaeology: An International Journal, 16, 1, 65–94.

Hoelzmann, P., Keding, B., Berke, H., Kröpelin, S., Kruse, H., 2001. Environmental change and archeology: lake evaluation and human occupation in the Eastern Sahara during the Holocene. Palaeogeography, Palaeoclimatology, Palaeoecology 169, 193-217.

Hoelzmann, P., Schwalb, A., Roberts, N., Cooper, P., Burgess, A., 2010. Hydrological response of an east-Saharan palaeolake (NW Sudan) to early-Holocene climate. The Holocene 20 (4), 537-549.

Hong, H., Wang, C., Zeng, K., Gu, Y., Wu, Y., Yin, K., Li, Z., 2013. Geochemical constraints on provenance of the mid-Pleistocene red earth sediments in subtropical China. Sedimentary Geology 290, 97–108.

Idohou, R., Djagoun, C.A. Kassa, B., Assogbadjo, A.E., Claude Codjia, J.T., 2013. Soil factors affecting density of three giant land snail species in different habitats of Dassa-Zoume` district (Central Benin). Qatar Foundation Journals, open access.

IUCN, 2010. *The IUCN Red List of Threatened Species: Pila wernei.* Assessment by: Jorgensen, A., Kristensen, T.K., Stensgaard, A-S. and Van Damme, D.

IUCN, 2012. *The IUCN Red List of Threatened Species: Bulinus truncatus.* Assessment by: Van Damme, D., Jorgensen, A., Kristensen, T.K., Lange, C., Stensgaard, A.-S. and Garcia, N.

IUCN, 2017. *The IUCN Red List of Threatened Species: Radix natalensis.* Assessment by: Van Damme, D.

Jesse 2000**,** JESSE F., Early Khartoum ceramics in the Wadi Howar (Northwest Sudan), *in : Recent research into the Stone Age of northeastern Africa*, Krzyzaniak L., Kroeper K., Kobusiewicz M. Eds., Poznan, Archaeological Museum, 2000, p. 77-87 (Studies in African Archaeology ; 7).

Jung, S.J.A., Davies, G.R., Ganssen, G.M., Kroon, D., 2004. Stepwise Holocene aridifcation in NE Africa deduced from dust-borne radiogenic isotope records. Earth and Planetary Science Letters 221, 27 – 37.

Karkanis, B.G., 1966. Hydrochemical Facies of Grounwater in the Western Provinces of Sudan. MSc. Thesis, Graduate College, University of Arizona.

Kemp, S.J., Ellis, M.A., Mouteney, I., Kender, S., 2016. Palaeoclimatic implications of high resolution clay mineral assemblages preceding and across the onset of the Palaeocene-Eocene Thermal Maximum, North Sea Basin. Clay Minerals, 51, 793–813.

Kershaw, P., Wagstaff, B., 2001. The southern conifer family Araucariaeacae: History, Status, and Value for Paleoenvironmental Reconstruction. Annu. Rev. Ecol. Syst., 32, 397–414.

Klappa, C.F., 1980. Rhizoliths in terrestrial carbonates: classification, recognition, genesis and significance. Sedimentology 27, 611-627.

Köhler, F., Glaubrecht, M., 2006. The Types of Ampullariidae Gray, 1824 (Mollusca, Gastropoda) in the Malacological Collection of the Natural History Museum, Berlin: an annotated catalogue with lectotype designations. *Mitt. Mus. Nat. kd. Berlin, Zool. Reihe 82(1)*, 198–215.

Kröpelin, S., Soulié-Märche, I., 1991. Charophyte remains from Wadi Howar as evidence for deep Mid-Holocene freshwater lakes in the Eastern Sahara of Northwest Sudan. Quaternary research 36, 210 – 223.

Kröpelin, S., Verschuren, D., Lézine, A.-M., Eggermont, H., Cocquyt, C., Francus, P., Cazet, J.-P., Fagot, M., Rumes, B., Russell, J. M., Darius, F., Conley, D. J., Schuster, M., von Suchodoletz, H., Engstrom, D. R. 2008. Climate-Driven Ecosystem Succession in the Sahara: The Past 6000 Years. Science 320, 765-768.

Kumar, A., 2016. New palynological evidence for the age of the Beda Formation, Sirte Basin, Libya. *Palaeontologia Electronica* 19.3, 43A: 1-14.

Kuper, R., Kröpelin, S., 2006. Climate-Controlled Holocene Occupation in the Sahara: Motor of Africa's Evolution. Science 313, 803-807.

Lario, J., Sanshez-Moral, S., Fernandez, V., Jimeno, A., Menendez, M., 1997. Paleoenvironmental Evolution of the Blue Nile (central Sudan) During the Early and Mid-Holocene (Mesolithic-Neolithic Transition). Quaternary Science Reviews, 16, 583-588.

Larsson, L.M., Vajda, V., Rasmussen, E.S. 2006. Early Miocene pollen and spores from western Jylland, Denmark – environmental and climatic implications. *GFF 128*, 261-272.

Lézine, A.-M., Zheng, W., Braconnot, P., Krinner G., 2011. A late Holocene pollen and climate record from Lake Yoa, northern Chad. Clim. Past Discuss, 7, 2413–2444.

Lotfy, W., Lotfy, L.M., 2015. Synopsis of the Egyptian freshwater snail fauna. *Folia Malacol. 23(1)*, 19–40.

Lu, Y., Hautevelle, Y., Michels, R., 2012. Determination of the molecular signature of fossil conifers by experimental palaeochemotaxonomy – Part 1: The Araucariaceae family. Biogeosciences Discuss. 9, 10513–10550.

Lukavský, J., 2009. Algae, Cyanobacteria and Chytridiales of Èerné Lake inthe Bohemian Forest (Šumava, Czech Republic). *Silva Gabreta 15(1)*, 1 – 48.

Madhavaraju, J., Ramasamy, S., Ruffell, A., Mohan, S. P., 2002. Clay mineralogy of the Late Cretaceous and early Tertiary successions of the Cauvery Basin (southeastern India): implications for sediment source and palaeoclimates at the K/T boundary. *Cretaceous Research* 23, 153–163.

Madhavaraju, J., Ramírez-Montoya, E., Monreal, R., González–León, C.M., Pi-Puig, T., Espinoza-Maldonado, I.G., Grijalva–Noriega, F.J., 2016, Paleoclimate, paleoweathering and paleoredox conditions of Lower Cretaceous shales from the Mural Limestone, Tuape section, northern Sonora, Mexico: Constraints from clay mineralogy and geochemistry: Revista Mexicana de Ciencias Geológicas, 33/1, 34-48.

Madukwe, H. Y. and Obasi, R. A., 2016. Geochemistry, Classification and maturity of the Sandstone facies of the Abeokuta Formation, south west Nigeria. *European Journal of Basic and Applied Sciences 3 (2), 2059-3058.*

Magendantz, M., 1972. The biology of *Biomphalaria choanomphala* and *B. sudanica* in relation to their role in the transmission of Schistosoma mansoni in Lake Victoria at Mwanza, Tanzania. *Bull. Org. mond. Santé (Bull. Wld. Hlth Org.) 47*, 331-342.

Malek, E. A., 1958. Distribution of the intermediate hosts of bilharziasis in relation to hydrography. With special reference to the Nile basin and the Sudan. In: Brown, D. S., Fison, T., Southgate, V. R., Wright, C. A., 1984. Aquatic snails of the Jonglei region, southern Sudan, and transmission of trematode parasites. *Hydrobiologia 110*, 247-271.

Mann, A.W., Horwitz, R.C., 1979. Grmmdwater calcrete deposits in Australia: some observations from Western Australia. In: Alonso-Zarza, A.M., 2003. Palaeoenvironmental significance of palustrine carbonates and calcretes in the geological record. Earth Science Reviews 60, 261–298.

Manning, K., Timpson, A., 2014. The demographic response to Holocene climate change in the Sahara. Quaternary Science Reviews 101, 28 – 35.

Marks, A. E., 1991. Shaqadud and the 1981/83 excavations. In: Mohammed-Ali, A.S., Khabir, A.M., 2003. The Wavy Line and the Dotted Wavy Line Pottery in the Prehistory of the Central Nile and the Sahara-Sahel Belt. *African Archaeological Review, 20(1)*, 25-58.

Mohammed-Ali, A.S., 1991. The Mesolithic and Neolithic ceramics from Shaqadud Midden. In: Mohammed-Ali, A.S., Khabir, A.M., 2003. The Wavy Line and the Dotted Wavy Line Pottery in

the Prehistory of the Central Nile and the Sahara-Sahel Belt. *African Archaeological Review, 20(1),* 25-58.

Mohammed-Ali, A.S., Khabir, A.M., 2003. The Wavy Line and the Dotted Wavy Line Pottery in the Prehistory of the Central Nile and the Sahara-Sahel Belt. *African Archaeological Review, 20(1),* 25 – 58.

Monga, P., Kumar, M., Prasad, V., Joshi, Y., Palynostratigraphy, palynofacies and depositional environment of a lignite-bearing succession at Surkha Mine, Cambay Basin, north-western India. Acta Palaeobotanica 55(2), 183–207.

Muscheler, R., Beer, J., Wagner, G., Laj, C., Kissel, C., Raisbeck, G.M., Yiou, F., Kubik, P.W., 2004. Changes in the carbon cycle during the last deglaciation as indicated by the comparison of $^{10}$Be and $^{14}$C records. Earth and Planetary Science Letters 219, 325-340.

Nawari, O., Schetelig, K., 1992. Chemical, mineralogical and fabric properties of Kordofan tropical black soils (Sudan). Journal of Aft-lean Earth Sciences, Vol. 14, No. 4, 545-55.

Ndifon, G.T., Ukoli, F.M., 1989. Ecology of freshwater snails in south-western Nigeria. I: Distribution and habitat preferences. *Hydrobiologia 171,* 231-253.

Nesbitt, H.W., Young, G.M., 1982. Early Proterozoic climates and plate motions inferred from major elements chemistry of lutites. Nature 299, 715 – 717.

Netterberg, p., 1969. The interpretation of some basin calcrete types. In: Alonso-Zarza, A.M., 2003. Palaeoenvironmental significance of palustrine carbonates and calcretes in the geological record. Earth Science Reviews 60, 261–298.

Neubert, E. 1998. Annotated checklist of the terrestrial and freshwater molluscs of the Arabian Peninsula with descriptions of new species. In: IUCN, 2017. *The IUCN Red List of Threatened Species: Radix natalensis.* Assessment by: Van Damme, D.

Ngaira. J.K.W., 2007. Impact of climate change on agriculture in Africa by 2030. Scientific Research and Essays 2 (7), 238-243.

Nicholson, S., Flohn, H., 1980. African Environmental and Climatic changes and the general atmospheric circulation in Late Pleistocene and Holocene. Climatic Change 2, 313-348.

Nicoll, K., 2004. Recent environmental change and prehistoric human activity in Egypt and Northern Sudan. Quaternary Science Reviews 23, 561–580.

Offord C.A., 2011. Pushed to the limit: consequences of climate change for the Araucariaceae: a relictual rain forest family. *Annals of Botany 108,* 347–357.

Oloto, I.N., Yikarebogha, Y., Omoboriowo, A.O., 2013. Palynological studies of Upper Cretaceous succession of Herwa-1 well, central Chad Basin, Nigeria. *International Journal of Innovative Research in Science, Engineering and Technology 2(4),* 880– 889.

Oni, S.O. and Olatuji, A.S., 2017. Depositional environments signatures, maturity and source weathering of Niger ddelta sediments from an oil well in southeastern Delta State, Nigeria. *Eurasian Journal of Soil Scince 6 (3), 259 – 274.*

Onoduku U.S., Okosun E.A, 2014. Palynology, Palynostratigraphy and Paleoenvironmental Analysis of Maiganga Coal Mine, Gombe Formation, Nigeria. Universal Journal of Geoscience 2(3), 93-103.

Pachur H. J., 1974. In: Pachur, H. J., Kröpelin, S., 1987. Wadi Howar: Paleoclimatic Evidence from an Extinct River System in the Southeastern Sahara. SCIENCE, VOL. 237, 298-300.

Pachur, H. J., Hoelzmann, P., 1991. Paleoclimatic Implications of Late Quaternary Lacustrine Sediments in Western Nubia, Sudan. Quaternary Research 36, 257-216.

Pachur, H. J., Kröpelin, S., 1987. Wadi Howar: Paleoclimatic Evidence from an Extinct River System in the Southeastern Sahara. SCIENCE, VOL. 237, 298-300.

Pacific, J. Veg. Sci., 10, 793–804, 1999.

Perveen, A., 1999. A Palynological Survey of Aquatic Flora of Karachi-Pakistan. Tr. J. of Botany 23, 309 – 317.

Peters, J., 1991. The faunal remains from Shaqadud. In: Marks, A.E., Mohammed-Ali, A., 1991. The Late Prehistory of the Eastern Sahel-the Mesolithic and Neolithic of Shaqadod, Sudan. *Southern Methodist University Press*, USA.

Petersen, H.I. Lindström, S., Nytoft, H.P., Rosenberg, P., 2009. Composition, peat-forming vegetation and kerogen paraffinicity of Cenozoic coals: Relationship to variations in the petroleum generation potential (Hydrogen Index). International Journal of Coal Geology 78, 119–134.

Pilsbry, H.A., Bequaert, J., 1927. The aquatic molluscs of the Belgian Congo, with a geographical and ecological account of Congo malacology. In: de Kock, K.N., Wolmarans, C.T., 2009. Distribution and habitats of *Melanoides tuberculata* (Müller, 1774) and *M. victoriae* (Dohrn, 1865) (Mollusca: Prosobranchia: Thiaridae) in South Africa. *Water SA 35(5)*, 713 -720.

Potter, P.E. (1978) Petrology and chemistry of modern big river sands. *The Journal of Geology*, 86(4): 423–449. In: Madukwe, H. Y. and Obasi, R. A., 2016. Geochemistry, Classification and maturity of the Sandstone facies of the Abeokuta Formation, south west Nigeria. *European Journal of Basic and Applied Sciences 3 (2), 2059-3058.*

Priene, S., Lavee, H., 2015. Soil organic matter and degradation. Soil conservation and protection for Europe (SCOPE).

Qamar, S., Saif, A., Altaf, J., 2017. Identification of the species of genus *Zootecus* on the basis of morphology. *Journal of Biodiversity and Environmental Sciences 11(3)*, 122 – 127.

Quick, L.J., 2013. Late Quaternary palaeoenvironments of the southern Cape, South Africa: palynological evidence from three coastal wetlands. PhD thesis. University of Cape Town, South Africa.

Rao, M.R., Sahni, A., Rana, R.S., Verma, P., 2013. Palynostratigraphy and depositional environment of Vastan Lignite Mine (Early Eocene), Gujarat, western India. *J. Earth Syst. Sci.* 122, No. 2, 289 – 307.

Raut, S. K., Barker, G.M., 2002. *Achatina fulica* Bowdich and other Achatinidae as pests in tropical agriculture. In: Tan, S.K., Low, M.E., 2011. An update on the West African *Limicolaria flammea* (Müller, 1774) in Singapore, and its distinction from the confamilial *Achatina fulica* Bowdich, 1822 (Mollusca: Grastropoda: Achatinidae). *Nature in Singapore 4*, 311 – 317.

Riding, J.B., Leng, M.J., Kender, S., Hesselbo, S.P., Feist-Burkhardt, S., 2013. Isotopic and palynological evidence for a new Early Jurassic environmental perturbation. Palaeogeography, Palaeoclimatology, Palaeoecology 374, 16–27.

Rodis, H.G., Hassan, A., Wahadan, L., 1968. Groundwater Geology of Kordofan Province-Sudan, Contribution to the hydrology of Africa and Mediterranean Region. United State government printing office. Washington.

Rodrigues, D, Abell, P.I., Kröpelin, S., 2000. Seasonality in the early Holocene climate of Northwest Sudan: interpretation of *Etheria elliptica* shell isotopic data. Global and Planetary Change 26, 181–187.

Rozanski, K., Araguás-Araguás, L., Gonfiantini, R., 1993. Isotopic patterns in modern global precipitation. Geophysical Monograph 78, 1 – 36.

Rull, V., 2001. A quantitative palynological record from the Early Miocene of western Venezuela, with emphasis on mangroves. Palynology 25, 109 – 126.

Salama, R., 1976. Groundwater Resources of Sudan. Technical report, Directorate for groundwater and Wadi water resources, Ministry of irrigation and water resources, Khartoum., Sudan.

Salard-Cheboldaeff, M., 1990. Intertropical African Palynostratigraphy from Cretaceous to Late Quaternary times. *Journal of African Earth Sciences*, 11, 1-24, pl. 1-9.

Scavati, L., Melendi, D.L., Volkheimer, W., 2009. A Danian subtropical lacustrine palynobiota from South America (Bororó Formation, San Jorge Basin, Patagonia - Argentina). *Geologica Acta 7(1-2)*, 35 – 61.

Schrank, E., 1994. Nonmarine Cretaceous palynology of northern Kordofan, Sudan, with notes on fossil Salviniales (water ferns). *Geol. Rundschau 83*, 773-786.

Schultheiß, R., Ndeo, O.W., Malikwisha, M., Marek, C., Bößneck, U., Albrecht, C., 2011. Freshwater molluscs of the Eastern Congo: notes on taxonomy, biogeography and conservation. *African Invertebrates 52(2)*, 265 – 284.

Scott, L., Cooremans, B., de Wet, J.S., Vogel, J.C., 1991. Holocene environmental changes in Namibia inferred from pollen analysis of swamp and lake deposits. Holocene 1, 8-13.

Shanahan, T., McKay, N.P., Hughen, K.A., Overpeck, J.T., Otto-Bliesner, B., Heil, C.W., King, J., Scholz, C. A., Peck, J., 2015. The time-transgressive termination of the African Humid Period. Nature Geoscience 8, 140 – 144.

Sheldon, N.D., Retallack, G.J., Tanaka, S., 2002. Geochemical climofunctions from North American soils and application to paleosols across the Eocene–Oligocene boundary in Oregon. Journal of Geology 110, 687–696.

Sheldon, N.D., Tabor, N.J., 2009. Quantitative paleoenvironmental and paleoclimatic reconstruction using paleosols. Earth-Science Reviews 95, 1–52.

Smith, N.D., 1970. The Braided Stream Depositional Environment: Comparison of the Platte River with Some Silurian Clastic Rocks, North-Central Appalachians. Geological Society of America Bulletin, 81, 2993-3014.

Smythe, K.R., Gallagher, M.D. 1977. Land and Freshwater Mollusca. In: IUCN, 2017. *The IUCN Red List of Threatened Species: Radix natalensis.* Assessment by: Van Damme, D.

Soares, E.A., Dino, R., Soares, D.P., Antonioli, L., da Silva, M.A.L., 2015. New sedimentological and palynological data from surface Miocene strata in the central Amazonas Basin area. *Brazilian Journal of Geology 45(3)*, 337-357.

Strojexport, 1976. Geophysical Investigations of Groundwater Structures, Western of Kordofan Province and Eastern part of Darfur Province, Fourth stage. Ministry of Agriculture food and Natural Resources, Rural Water Corporation, Khartoum, Sudan.

Stukins, S., Jolley, D.W., McIlroy, D., Hartley, A.J., 2013. Middle Jurassic vegetation dynamics from allochthonous palynological assemblages: An example from a marginal marine depositional setting; Lajas Formation, Neuquén Basin, Argentina. Palaeogeography, Palaeoclimatology, Palaeoecology 392, 117–127.

Szabo, B.I., Haynes Jr, C.V., Maxwell, T.A., 1995. Ages of Quaternary pluvial episodes determined by uranium-series and radiocarbon dating of lacustrine deposits of Eastern Sahara. Palaeogeography, Palaeoclimatology, Palaeoecology 113, 227 – 242.

Tan, S.K., Clements, G.R., 2011. *Limicolaria flammea* (Müller, 1774), another potentially invasive African land snail in tropical Asia. *Tropical Conservation Science* Vol. 4 (1), 97-102.

Tan, S.K., Low, M.E., 2011. An update on the West African *Limicolaria flammea* (Müller, 1774) in Singapore, and its distinction from the confamilial *Achatina fulica* Bowdich, 1822 (Mollusca: Grastropoda: Achatinidae). *Nature in Singapore 4*, 311 – 317.

Tchouatcha, S.M., Ricard, N., M.M., Said, D.A., Ekodeck, E.G., 2010. Existence of "late continental" deposits in the Mbere and Djerem sedimentary basins (North Cameroon): Palynologic and stratigraphic evidence. Journal of Geology and Mining Research Vol. 2(6), 159-169.

Telford, R.J., Lamb, H.F., 1999. Groundwater-Mediated response to Holocene climatic change recorded by the Diatom Stratigraphy of an Ethiopian Crater Lake. Quaternary Research 52**,** 63–75.

Tierney, J.E., Lewis, S.C., Cook, B.I., LeGrande, A.N., Schmidt, G.A., 2011a. Model, proxy and isotopic perspectives on the East African Humid Period. Earth and Planetary Science Letters 307, 103 – 112.

Tierney, J.E., Russell, J.M., Sinninghe Damsté, J.S., Huang Y., Verschuren, D., 2011b. Late Quaternary behavior of the East African monsoon and the importance of the Congo Air Boundary. Quaternary Science Reviews 30, 798 – 807.

Tóth, J.A., Lajtha, K., Kotroczó, Z., Krakomperger, Z., Caldwell, B., Bowden, R., Papp, M., 2007. The effect of climate change on soil Organic Matter decomposition. Acta Silv. Lign. Hung. 3, 75- 85.

Traverse, A., 2008. Paleopalynology, Second ed., Springer.

Tripathi, S.K.M., Kumar, M., Srivastava, D., 2009. Palynology of Lower Palaeogene (Thanetian-Ypresian) coastal deposits from the Barmer Basin (Akli Formation, Western Rajasthan, India): Palaeoenvironmental and palaeoclimatic implications. *Geologica Acta Vol.7, N$^{os}$ 1-2*, 147 – 160.

Tucker, M.E., 2003. Sedimentary rocks in the field (3$^{rd}$ edition). John Wiley & Sons Ltd. Englad. 234p.

Tucker, M.E., Wright, V.P., 1990, Carbonate sedimentology. Blackwell Science, Oxford, 482 p.

Uzodimma, D.E., 2013. Palynostratigraphy, Age Determination and Depositional Environments of the Imo Shale Exposures at the Okigwe/Port Harcourt Express Road Junction Okigwe, Southeastern Nigeria. Greener Journal of Physical Sciences 3 (7), 255–272.

Van der Schalie, H., 1948. The land and fresh-water mollusks of Puerto Rico. In: Bishop, M.J. 1979. A new species of *Caracolus* (Pulmonata: Camaenidae) from the Oligocene of Nebraska and the biotic history of the American camaenid land snails. *Zoological Journal of the Linnean Society*, 67, 269-284.

Visher, G., 1969. Grain size distributions and depositional processes. *Journal of Sedimentary Petrology 39, 3*, 1074 – 1106.

Volkhemer, W., Rauhut, O.W.M., Quattrocchio, M.E., Martinez, M.A., 2008. Jurasic paleoclimate in Argentina, a review. *Revista de la Asociación Geológica Argentina 63 (4)*, 549- 556.

Volkoff, B. 1988, Red and lateritic soils: World scenario. In: Managing Red and Lateritic Soils for Sustainable Agriculture, vol. 1 (J. Sehagal, W. E. H. Blum, K. S. Gajbhiya, eds). Oxford and IBH Publishing Co., New Delhi, India, pp. 57–74.

Walker, M., 2005. Quaternary dating methods. John Wiley & Sons Ltd. England. 286p.

Warren, M. J., 2009. Tectonic Inversion and Petroleum System Implications in the Rifts of Central Africa. Frontiers + Innovation CSPG CSEG CWLS Convention, pp, 461-464.

Webbe, G., 1962. In: Magendantz, M., 1972. The biology of *Biomphalaria choanomphala* and *B. sudanica* in relation to their role in the transmission of Schistosoma mansoni in Lake Victoria at Mwanza, Tanzania. *Bull. Org. mond. Santé (Bull. Wld. Hlth Org.) 47*, 331-342.

Whiteman, A.J., 1971. The Geology of the Sudan Republic. Oxford University press, London.

Williams, M. A. J., Talbot, M., Aharon, P., Abdl Salaam, Y., Williams, F., Brendeland, K. L., 2006. Abrupt return of the summer monsoon 15,000 years ago: new supporting evidence from the lower White Nile valley and Lake Albert. Elsevier, Quaternary Science Reviews 25, 2651–2665.

Williams, M., 2014. Climate Change in Deserts (past, present and future). Cambridge University Press, New York, USA.

Williams, M.A.J., 2009. Late Pleistocene and Holocene environments in the Nile basin. Global and Planetary Change 69, 1–15.

Williams, M.A.J., Adamson, D., Cock, B., McEvedy, R., 2000. Late Quaternary environments in the White Nile region, Sudan. Elsevier, Global and Planetary Change 26, 305–316.

Williams, M.A.J., Adamson, D.A., 1974. Late Pleistocene desiccation along the White Nile. Nature 248, 584–586.

Williams, S. N., Hunter, P. J., 1968. The distribution of *Bulinus* and *Biomphalaria* in Khartoum and Blue Nile provinces, Sudan. In: Brown, D. S., Fison, T., Southgate, V. R., Wright, C. A., 1984. Aquatic snails of the Jonglei region, southern Sudan, and transmission of trematode parasites. *Hydrobiologia 110*, 247-271.

Wilson, M.J., 1999. The origin and formation of clay minerals in soils: past, present, and feature prospectives. Clay minerals 34, 7 – 25.

Woodward, J.C., Macklin, M.G., Michael, D. Krom, D., Williams, M.A., 2007. The Nile: Evolution, Quaternary River Environments and Material Fluxes. John Wiley & Sons Ltd. Large Rivers: Geomorphology and Management.

Worobiec, E., 2014. Fossil zygospores of Zygnemataceae and other microremains of freshwater algae from two Miocene palaeosinkholes in the Opole region, SW Poland. Acta Palaeobotanica 54, 113–157.

Worobiec, E., Gedl, P., 2010. Spore-pollen and phytoplankton analysis of the Upper Miocene deposits from Józefina (Kraków–Silesia Upland, Poland). *Geological Quarterly 54 (1)*, 41–54.

Worobiec, E., Worobiec, G., 2016. Miocene palynoflora from the KRAM-P 218 leaf assemblage from the Bełchatów Lignite Mine (Central Poland). *Acta Palaeobotanica* 56(2), 499–517.

Ybert. J.P., 1979. Atlas de pollen de Côte D'Ivoire. Initiations – Documentations Techniques No 40. *Office de la Recherche Scientifique et Technique Outre-Mer. Paris.*

Zetter, R., Hesse, M., Frosch-Radivo, A., 2011.Early Eocene zona-aperturate pollen grains of the Proxapertites type with affinity to Araceae. Review of Paleaobotany and Palynology 117, 267-279.